AWARD NUMBER:	W81XWH-11-1-0106
TITLE:	"Molecular Mechanisms Underlying Genomic Instability in Brca-Deficient Cells"
PRINCIPAL INVESTIGATOR:	Dr. Andre Nussenzweig, NCI
RECIPIENT:	The Geneva Foundation Tacoma, WA 98402
REPORT DATE:	November 2014
TYPE OF REPORT:	FINAL
PREPARED FOR:	U.S. Army Medical Research and Materiel Command Fort Detrick, Maryland 21702-5012

DISTRIBUTION STATEMENT:

X Approved for public release; distribution unlimited

REPORT DOCUMENTATION PAGE

Form Approved
OMB No. 0704-0188

1. REPORT DATE *(DD-MM-YYYY)*	2. REPORT TYPE	3. DATES COVERED *(From - To)*
November 2014	**Final**	1 Mar 2011 - 31 Aug 2014

4. TITLE AND SUBTITLE
Molecular Mechanisms Underlying Genomic Instability in

BRCA- Deficient Cells

5a. CONTRACT NUMBER

5b. GRANT NUMBER
W81XWH-11-1-0106

5c. PROGRAM ELEMENT NUMBER

6. AUTHOR(S)

Dr. Andre Nussenzweig – Principal Investigator
email: andre_nussenzweig@nih.gov

5d. PROJECT NUMBER

5e. TASK NUMBER

5f. WORK UNIT NUMBER

7. PERFORMING ORGANIZATION NAME(S) AND ADDRESS(ES)

National Cancer Institute
Bethesda, MD 20892
The Geneva Foundation
917 Pacific Ave, Suite 600
Tacoma, WA 98402

8. PERFORMING ORGANIZATION REPORT NUMBER

9. SPONSORING / MONITORING AGENCY NAME(S) AND ADDRESS(ES)
U.S. Army Medical Research and Materiel Command
Ft Detrick, MD 21702-5012

10. SPONSOR/MONITOR'S ACRONYM(S)

11. SPONSOR/MONITOR'S REPORT NUMBER(S)

12. DISTRIBUTION / AVAILABILITY STATEMENT

Approved for public release; distribution unlimited

13. SUPPLEMENTARY NOTES

14. ABSTRACT

Our proposal is to explore the novel notion that it may be possible to restore near normal HR activity in Brcal cells and tissues. We believe that this phenomenon will lead to targeted therapies to reduce lifetime risk of tumor formation in BRCA1 and potentially BRCA2 carriers.

15. SUBJECT TERMS
BRCA1, 53BP1, cancer biology, DNA repair, tumorigenesis

16. SECURITY CLASSIFICATION OF:			17. LIMITATION OF ABSTRACT	18. NUMBER OF PAGES	19a. NAME OF RESPONSIBLE PERSON
a. REPORT	b. ABSTRACT	c. THIS PAGE			USAMRMC
U	U	U	UU	82	19b. TELEPHONE NUMBER *(include area code)*

Table of Contents

1. INTRODUCTION:

The objective of the DOD Idea Award was to examine the cellular processes involved in the selection of DNA repair pathways and to understand how the choice of pathways determined whether repair is error free or error-prone. The choice of pathways, in the end, will have major implications for overall genome stability and disease onset. A hallmark feature of cancer cells lacking the tumor suppressor genes BRCA1/2 is their inability to repair DNA through a complex repair mechanism known as homologous recombination (HR). The BRCA1 gene is required for normal embryonic development and DNA repair by the error-free HR pathway. The 53BP1 protein promotes ligation and facilitates repair by error-prone end joining (Non-Homologous End Joining, NHEJ). In previous studies and experiments performed under the aegis of the Idea Award, we have demonstrated that BRCA1 and 53BP1 can compete for the processing of DSBs and 53BP1 can promote genomic instability in the absence of BRCA1. Our studies as part of the Idea Award focused on establishing genetic states that shifted the balance between these two repair pathways (HR and NHEJ) to restore error free repair and genomic stability. We believe that a better understanding of mechanisms of DSB repair pathway choice may have important therapeutic implications for prevention or treatment of BRCA1/2 germline mutation-associated cancers. These studies will be continued with the support of the DOD Idea Expansion award where we will use genetic and computational approaches to further define interactions between NHEJ and HR effectors. This, we expect, will help in our understanding of chemoresistance and sensitivity in BRCA1- and BRCA2 mutated cancers.

2. KEYWORDS:

BRCA1/2, 53BP1, Rif1, Ptip, Ku, Phospho-proteins, Homologous Recombination, Non-Homologous End Joining, Breast Cancer, Ovarian Cancer, Molecular Inhibitors, Chemoresistance/Chemosensitivity, H2AX, PARP inhibitors, Ionizing radiation, Genomic instability, Small molecule inhibitors, Drug screens, ERFS

3. OVERALL PROJECT SUMMARY:

The Idea Award comprised three major aims. They are outlined below, as originally stated.

Aim 1: Determine the capacity of NHEJ deficiency to rescue defects in homologous recombination (HR). Using various established mouse models where there is a clearly described defect in HR, we will test the role of the NHEJ proteins 53BP1 and Ku in subverting HR.
Aim 2: Determine the domain of 53BP1 that inhibits HR in BRCA1-deficient mice. We will use a combined *in vitro* and *in vivo* reconstitution approach to define the functional domains of 53BP1 that regulate the observed HR defects seen in BRCA1-deficient cells.
Aim3: Develop small molecule inhibitors of 53BP1 as possible lead compounds to inhibit BRCA- mediated tumor formation.

Each proposed aim was comprised of multiple individual tasks (as highlighted in the original statement of work and previous annual reports). Each of these tasks have been completed or are work in progress. Specifically, **Aim 1**, **Tasks 1-7** (6 Tasks since there is no Task 4) focused on generating mice containing floxed alleles of various HR factors and either 53BP1$^{-/-}$ or 53BP1$^{+/+}$ to determine whether these various genetic combinations could rescue embryonic lethality and homologous recombination. These tasks have been completed. The work proposed in **Aim 1** has been published in several papers, most notably in Molecular Cell (***Bunting, S.F., Callen, E., et. al., 2012***). See expanded **Reference** section for complete bibliography.

A brief summary of the salient results from **Aim 1** (also see **Key Research Accomplishments**), have determined that a rescue of embryonic lethality and HR as seen with the hypomorphic exon 11 BRCA1 deletion can be recapitulated and validated in the complete absence of BRCA1 (**Task 1**) (**Table 1**).

Table 1. Impact of Deletion of Ku or 53BP1 on the Survival of Brca1$^{\Delta 11/\Delta 11}$ and Brca1-Null Embryos

Brca1$^{\Delta 11/+}$ Ku80$^{+/-}$ × Brca1 $^{\Delta 11/+}$ Ku80$^{+/-}$ Intercross:					
		Brca1$^{\Delta 11/\Delta 11}$Ku80$^{+/+}$ or Brca1$^{\Delta 11/\Delta 11}$Ku80$^{+/-}$	Brca1$^{+/+}$Ku80$^{-/-}$ or Brca1$^{\Delta 11/+}$Ku80$^{-/-}$	Brca1$^{\Delta 11/\Delta 11}$Ku80$^{-/-}$	Other Genotypes
E13.5 embryos	Expected:	9	9	3	27
(48 screened)	Observed:	4	12	0	32
Live pups	Expected:	30	30	10	90
(160 screened)	Observed:	0	13	0	147
Brca1$^{+/-}$ 53BP1$^{+/-}$ × Brca1$^{+/-}$ 53BP1$^{+/-}$ Intercross:					
		Brca1$^{-/-}$ 53BP1$^{+/+}$ or Brca1$^{-/-}$ 53BP1$^{+/-}$	Brca1$^{+/+}$ 53BP1$^{-/-}$ or Brca1$^{+/-}$ 53BP1$^{-/-}$	Brca1$^{-/-}$ 53BP1$^{-/-}$	Other Genotypes
Live pups	Expected:	21.75	21.75	7.25	65.25
(116 screened)	Observed:	0	22	4	90
Brca1$^{+/-}$ 53BP1$^{-/-}$ × Brca1$^{+/-}$ 53BP1$^{-/-}$ Intercross:					
		Brca1$^{-/-}$ 53BP1$^{+/+}$ or Brca1$^{-/-}$ 53BP1$^{+/-}$	Brca1$^{+/+}$ 53BP1$^{-/-}$ or Brca1$^{+/-}$ 53BP1$^{-/-}$	Brca1$^{-/-}$ 53BP1$^{-/-}$	Other Genotypes
Live pups	Expected:	0	66	22	0
(88 screened)	Observed:	0	72	16	0

Frequency of embryos at day E13.5 and live-born pups of the indicated genotypes is shown. See also Table S1.

Table1. **Impact of deletion of Ku or 53BP1 on the survival of Brca1D11/D11 and Brca1-Null Embryos**. 53BP1 deletion is able to rescue embryonic lethality in mice that are null for Brca1 while Ku80 deletions do not.

Tasks 2 &3 involved the breeding of various HR knockouts with 53BP1 nulls. These mice have been generated and drug sensitivity data with these crosses have been included in the aforementioned Molecular Cell paper. In the case of some HR factor deletions (such as PALB2), the additional loss of 53BP1 does not rescue the genomic instability associated with PALB2 deletions (**Fig. 1**). This work has been published in Proc. Natl. Acad. Sci (***Bowman-Colin, C., et. al., 2013***).

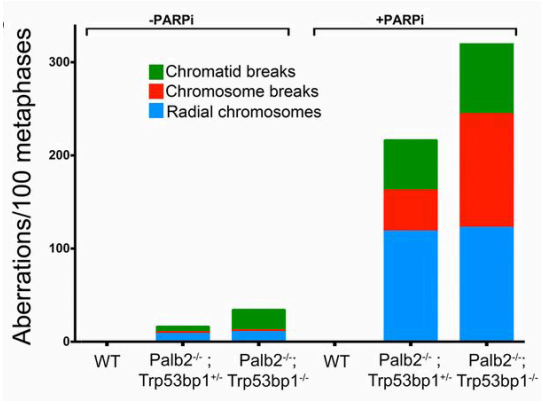

Fig.1. The HR defect in Palb2-deficient cells and tumors. Acute chromosomal damage and genome instability observed in chromosome spreads following PARPi treatment are not rescued by Trp53bp1 deletion in Palb2fl/fl;CD19-Cre B lymphocytes.

Tasks 5 & 6 centered around the rescue of FANCD2-, and BRCA2-deficient phenotypes with 53BP1 null animals (using a variety of cellular, molecular and genetic assays). FANCD2 and BRCA2 have distinct and important roles in in the repair of DNA double-strand breaks by homologous recombination. Our results indicate that 53BP1 deletion did not rescues FANCD2 phenotypes (**Task 5**) or the HR defect in BRCA2-deficient mice (**Task 6**) (**Fig. 2**). Interestingly, Ku which binds directly to double strand breaks and facilitates DNA end-joining via the NHEJ pathway, does not rescue the embryonic lethality in BRCA1-deficient mice (**Task 7**) (**Table 1**). It does, however, afford some rescue of genomic instability (data published in ***Bunting, S.F., Callen, E., et. al., 2012,*** Molecular Cell) (**Fig. 3**).

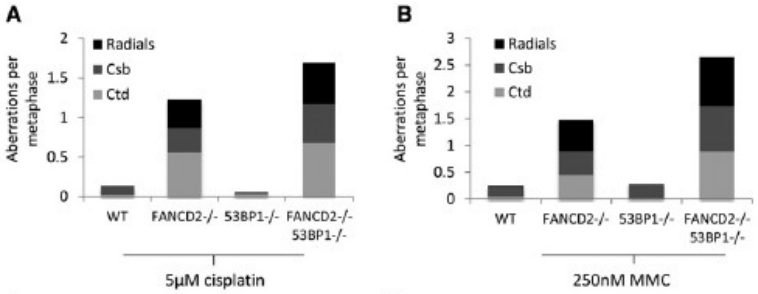

Fig.2. Genomic Instability in Metaphases from Cells Treated Overnight with Drugs to Induce DNA Interstrand Crosslinks (A) Genomic instability in B cells from WT, FANCD2/, and FANCD2/53BP1/ mice treated overnight with 5 mM cisplatin. (B) Genomic instability in B cells from WT, FANCD2/, and FANCD2/53BP1/ mice treated overnight with 250 nM mitomyin C (MMC).

As part of **Aim 1**, we have discovered new proteins that influence DNA repair pathway selection. Specifically, we have identified a new NHEJ factor Rif1 that acts downstream of 53BP1 in blocking re-section. This work has been published in Science (***Di Virgilio, M., et. al., 2013***) (**model in Fig. 4**). Another novel observation and published in Cell (***Callen, E., et. al.,* 2013**) demonstrated that the ablation of PTIP phenocopies the 53BP1 deletion, in that it promotes genome stability and survival in BRCA1 mutant B cells (**Fig. 5**). Loss of PTIP increased HR in BRCA1 mutant cells by promoting DSB resection, increasing Rad51 foci formation and decreasing sensitivity to DNA damaging agents such as PARP inhibitors (PARPi).

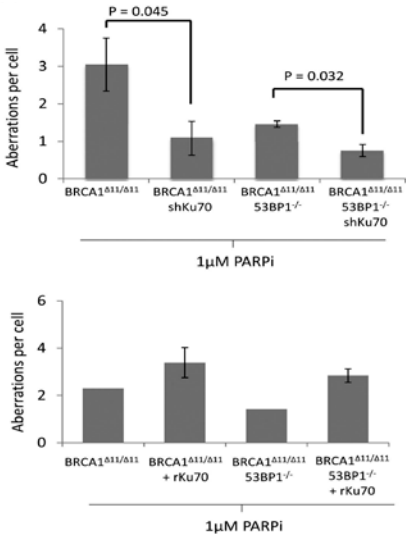

Fig.3. Ku Expression Correlates with Genomic Instability and Reduced Proliferation in Brca1-Deficient Cells Treated with PARP Inhibitor. (Top Panel) Average genomic instability observed in metaphase spreads from MEF cells treated overnight with 1 mM PARP inhibitor (PARPi) and (Bottom Panel) Genomic instability in metaphases from MEFs overexpressing rat Ku70. These results suggest that Ku sensitizes WT or Brca1 deficient cells to the cytotoxic effects of cisplatin.

In **work in progress**, we have examined the sensitivity of BRCA1/PTIP deficient cells to cisplatin. While BRCA1/53BP1 deficient cells are sensitive to cisplatin (described in our previous annual report and in ***Bunting et al., 2012***), we have found that BRCA1/PTIP-mutant cells are resistant as measured by metaphase analysis. While BRCA1 is implicated in an upstream role in homology-directed repair, which is counteracted by 53BP1, BRCA2 functions later by promoting RAD51 filament formation. We have generated BRCA2/PTIP-doubly deficient B cells (CD19 CRE BRCA2f/fPTIPf/f) and measured their sensitivity to PARPi and cisplatin. Strikingly, in contrast to BRCA2/53BP1 mutants, which are hypersensitive to both DNA damaging agents, BRCA2/PTIP deficient cells are resistant (**Fig. 6**). Based on these results, we hypothesize that in addition to its role in modulating 53BP1-dependent DSB resection, PTIP could also function independently of 53BP1 in regulating DNA repair choice.

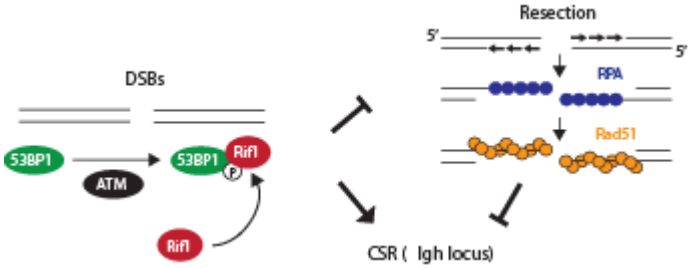

Fig.4. Model: DNA damage activates ATM, which phosphorylates multiple targets, including 53BP1. This event recruits Rif1 to 53BP1 at the DSB, where it inhibits DNA resection. The extensive resection in the absence of Rif1 impairs class-switch recombination, for example at the Igh locus.

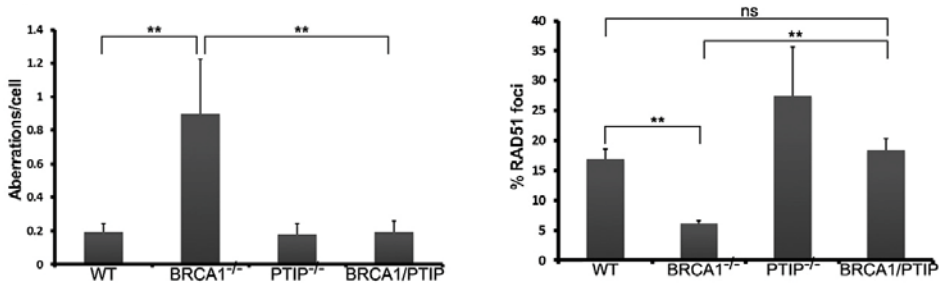

Fig.5. Ablation of PTIP rescues homologous recombination in BRCA1-deficient cells, as measured by reduced genome instability in the presence of PARPi (left panel) and increased Rad51 foci formation (right panel).

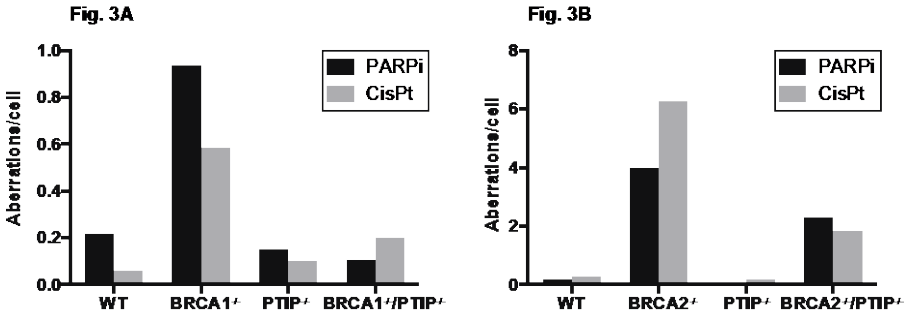

Fig.6. PTIP ablation confers PARPi and cis-platin resistance in BRCA1/2-deficient cells.

In **Aim 2**, an *in vivo* genetic approach was employed to determine the specific domains in 53BP1 that regulated HR activity. This task was completed and resulted in publications in Molecular Cell (***Bothmer A., Robbiani D., et. al., 2011***) and Cell (***Callen, E., et. al., 2013***). The plan (**Task 1**) to generate 53BP1 knock-in mice harboring specific mutants have been generated. Specifically, the four 53BP1 mutants generated included a deletion of the BRCT domain, an inactivating mutation within the Tudor domain, a deletion of the H2AX interacting region and a combined H2AX+Tudor mutation (**Fig. 7**). All lines were crossed with BRCA1 null mice to assess whether they could recapitulate the phenotypic rescue observed in the complete absence of 53BP1 ($53BP1^{-/-}$). In **Task 2** of **Aim 2**, these studies were complemented and extended by reconstituting 53BP1 mutants into BRCA1 null B cells by using PARPi sensitivity as a screen for determining which domain of 53BP1 was necessary for the inhibition of HR activity. The major outcome of these studies revealed that the Tudor domain, and not the BRCT domain, of 53BP1 was essential for the promotion of genomic instability in BRCA1 deficient cells (**model in Fig. 8**). Related to **Task 2** and published in Cell, (***Callen, E., et. al., 2013***), has shown that a 53BP1 phosphomutant, 53BP18A, comprising alanine substitutions of the eight most N-terminal S/TQ phosphorylation sites, mimics 53BP1 deficiency by restoring genome stability in BRCA1-deficient cells yet behaves like wild-type 53BP1 with respect to immunoglobulin class switch recombination (CSR). 53BP18A recruits RIF1 but fails to recruit the DDR protein PTIP to DSBs, and disruption of PTIP phenocopies 53BP18A. The work from this paper has allowed us to conclude that 53BP1 promotes productive CSR and suppresses mutagenic DNA repair through distinct phospho-dependent interactions with RIF1 and PTIP.

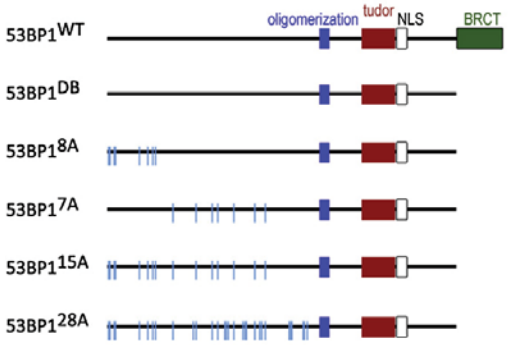

Fig.7. Various 53BP1 constructs were generated to identify specific 53BP1 domains involved in homologous recombination.

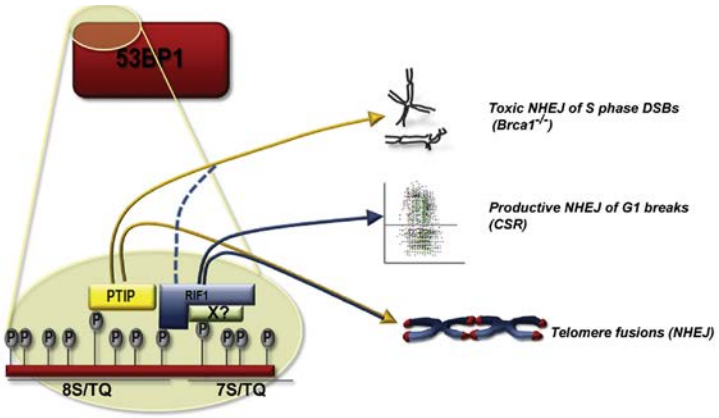

Fig.8. A clear separation of function can be ascribed to 53BP1 and is illustrated in the model figure. Data supporting this model demonstrates that PTIP and RIF1 association with DSBs is dependent on distinct phosphorylation sites within 53BP1.

In the context of this proposal, we have also discovered a novel type of "fragile" site that contributes to genome instability. These sites (coined "ERFS", for Early Replication Fragile Sites, are broken spontaneously during replication, and their fragility is increased by hydroxyurea, ATR inhibition, deregulated c-Myc expression and by PARPi treatment of BRCA1 deficient cells. This work was recently published in Cell (***Barlow , J. et. al., 2013***) (**Fig. 9**).

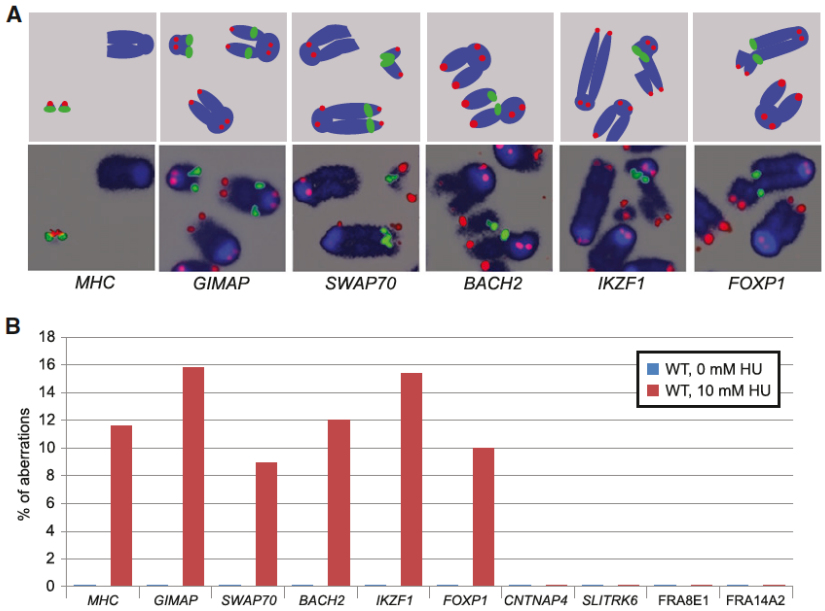

Fig.9. ERFS break in response to HU. (A) Upper panel, diagram of FISH probes. Lower panel, representative DNA aberrations identified by FISH. Blue is DAPI-stained DNA, green represents the BAC probe (MHC, GIMAP, SWAP70, BACH2, IKZF1 or FOXP1) and red marks telomeric DNA. (B) HU induced aberrations were found at ERFSs but not at "cold sites" (CNTNAP4, SLITRK6) or CFSs (FRA16D, FRA3B). Quantitation of abnormalities from FISH analysis of untreated cells (blue bars) or cells treated with 10 mM HU (red bars). The percent aberrations specifically at the BAC probes relative to the total damage is plotted.

In **Aim 3**, imaging systems have been established to screen large-scale compound libraries targeting the 53BP1 protein. Specifically, we have obtained a GFP-53BP1 containing cell line (Stephen Kron, University of Chicago) that conditionally (dox inducible)

expresses a minimal domain within 53BP1. This truncated form of 53BP1 forms robust foci following DNA damage and appears to recapitulate biological features observed with endogenous 53BP1 (**Fig. 10**). We have determined conditions for measuring 53BP1 foci using a GFP-based approach that elicits robust foci formation following treatment with the radiomimetic drug, neocarzinostatin (NCS). This highly ambitious project is still ***ongoing***. In collaboration with Dr. Marc Ferrer of the National Center for Advancing Translational Science and Jim McMahon of the Molecular targets Lab at NCI, we hope to visualize foci using automated high-throughput imaging platforms. This will enable screening of the NCI Diversity Set of compounds and other small molecule libraries. Lead compounds will be categorized as those that suppress the appearance of 53BP1 foci or enhance the chromatin association of 53BP1 following DNA damage. Currently we are optimizing this system with appropriate positive and negative controls.

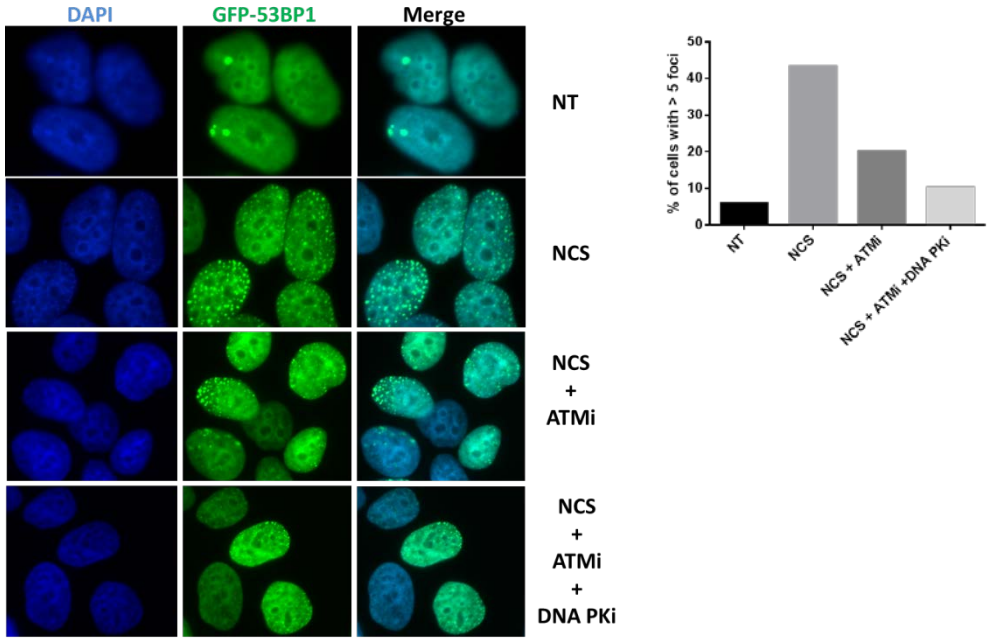

Fig.10. **A robust, cell-based foci-forming assay for screening 53BP1 inhibitors**. GFP-53BP1 was induced with doxycycline for 48 hours followed by treatment (15 min) with the DNA double strand break inducing drug, neocarzinostatin (NCS). Short treatments with NCS induce the formation of numerous GFP-53BP1 foci (left panel, 2nd row). Foci formation is dramatically reduced by a 2hr pre-treatment with ATM inhibitors (ATMi) or the combined action of ATM and DNA PK inhibitors (left panel). A quantitation of the effect of inhibitors on foci formation is shown in the right panel.

4. KEY RESEARCH ACCOMPLISHMENTS:

Bullet points of **major research highlights** during the duration of the Idea Grant

- Deletion of the DNA damage response gene, 53BP1, allows survival of BRCA1-nullizygous mice.
- Genomic instability and hypersensitivity of BRCA1-deficient cells to inhibitors of polyADP- ribose polymerase (PARP inhibitors, PARPi) is suppressed by deletion of 53BP1.
- 53BP1 deletion does not rescue genomic instability in BRCA2-null cells.
- Association of 53BP1 with chromatin through the Tudor domain is essential for the role of 53BP1 in promoting genomic instability in BRCA1-deficient cells
- Association of 53BP1 with p53 through the 53BP1 BRCT domain has no impact on the effect of 53BP1 in causing genomic instability in BRCA1-deficient cells.
- Deletion of the DNA damage response gene, RIF1, mimics 53BP1 deficiency with respect to increased resection and defective class switching.
- Genomic instability and hypersensitivity of BRCA1-deficient cells to inhibitors of polyADP-ribose polymerase (PARP inhibitors, PARPi) is not suppressed by deletion of PALB2.
- Phosphorylation of the N-terminus of 53BP1 is essential for the role of 53BP1 in promoting genomic instability in BRCA1-deficient cells but is dispensable for class switching.
- PARPi treatment leads to genome instability at preferred genomic sites.
- Deletion of the DNA damage response gene RIF1 mimics 53BP1 deficiency with respect to increased resection and defective class switching.
- Deletion of the DNA damage response gene PTIP rescues homologous recombination in BRCA1-deficient cells.
- PTIP ablation confers PARPi and cis-platin resistance in BRCA1 and BRCA2-deficient cells.
- A systematic mutational analysis of phosphorylation sites within 53BP1 allows for functional segregation of domains within 53BP1 that interact with RIF1 and PTIP.
- We have conducted preliminary characterization of a DNA damage-inducible GFP-53BP1 foci forming cell line for high throughput screening of small molecule libraries.
- Discovery of a novel type of “fragile” site that contributes to genome instability. These sites (coined “ERFS” are broken spontaneously during replication, and their fragility is increased by replication stress and inhibitors to DNA damage responding proteins.

5. CONCLUSIONS:

This work has revealed for the first time that deletion of 53BP1 prevents genomic instability in cells lacking the tumor suppressor, BRCA1. 53BP1 therefore plays a key role in cellular changes leading to cancer in individuals with BRCA1 mutations. This validates the targeting of 53BP1 as a chemopreventive measure to avert the appearance of cancer in women with mutations in BRCA1, which accounts for ~5% of all annual cases of breast cancer and a higher proportion of ovarian cancers. This work further suggests that 53BP1 inactivation is a potential pathway leading to resistance of BRCA1-deficient tumors to chemotherapeutic regimens involving PARP inhibitors. In addition to providing new mechanistic insight, this study has important therapeutic implications because loss of 53BP1 may be a mechanism by which BRCA1-mutant tumors develop resistance to chemotherapy. Consistent with this, we found that loss of 53BP1 alleviates hypersensitivity of BRCA1- mutant cells to PARP inhibition. We have also begun to map the pathways that acts downstream of 53BP1 to inhibit HR: we discovered that the effector proteins RIF1 (M. Di Virgilio et al. Science 2013) and PTIP (Callen et al. Cell 2013) are recruited to sites of DNA damage via interactions with phosphorylated 53BP1, where they facilitate DNA repair in part by protecting DNA ends from resection.

These studies will be continued with the support of the DOD Idea Expansion award where we will use genetic and computational approaches to further define interactions between NHEJ and HR effectors. This, we expect, will help in our understanding of chemoresistance and sensitivity in BRCA1- and BRCA2 mutated cancers.

6. PUBLICATIONS, ABSTRACTS AND PRESENTATIONS:

A. Invited Reviews and Commentaries

1: Ira G, Nussenzweig A. A new Riff: Rif1 eats its cake and has it too. EMBO Rep. 2014 Jun;15(6):622-4.

2: Fernandez-Capetillo O, Nussenzweig A. Naked replication forks break apRPArt. Cell. 2013 Nov 21;155(5):979-80.

3: Bunting SF, Nussenzweig A. End-joining, translocations and cancer. Nat Rev Cancer. 2013 Jul;13(7):443-54.

4: Daniel JA, Nussenzweig A. The AID-induced DNA damage response in chromatin. Mol Cell. 2013 May 9;50(3):309-21.

Peer Reviewed Articles: Directly Related to Goals of the DOD Idea Award

5: Callen E, Di Virgilio M, Kruhlak MJ, Nieto-Soler M, Wong N, Chen HT, Faryabi RB, Polato F, Santos M, Starnes LM, Wesemann DR, Lee JE, Tubbs A, Sleckman BP, Daniel JA, Ge K, Alt FW, Fernandez-Capetillo O, Nussenzweig MC, Nussenzweig A. 53BP1 mediates productive and mutagenic DNA repair through distinct phosphoprotein interactions. Cell. 2013 Jun 6;153(6):1266-80.

6: Bowman-Colin C, Xia B, Bunting S, Klijn C, Drost R, Bouwman P, Fineman L, Chen X, Culhane AC, Cai H, Rodig SJ, Bronson RT, Jonkers J, Nussenzweig A, Kanellopoulou C, Livingston DM. Palb2 synergizes with Trp53 to suppress mammary tumor formation in a model of inherited breast cancer. Proc Natl Acad Sci U S A. 2013 May 21;110(21):8632-7.

7: Barlow JH, Faryabi RB, Callén E, Wong N, Malhowski A, Chen HT, Gutierrez-Cruz G, Sun HW, McKinnon P, Wright G, Casellas R, Robbiani DF, Staudt L, Fernandez-Capetillo O, Nussenzweig A. Identification of early replicating fragile sites that contribute to genome instability. Cell. 2013 Jan 31;152(3):620-32.

8: Di Virgilio M, Callen E, Yamane A, Zhang W, Jankovic M, Gitlin AD, Feldhahn N, Resch W, Oliveira TY, Chait BT, Nussenzweig A, Casellas R, Robbiani DF, Nussenzweig MC. Rif1 prevents resection of DNA breaks and promotes immunoglobulin class switching. Science. 2013 Feb 8;339(6120):711-5.

9: Bunting SF, Callén E, Kozak ML, Kim JM, Wong N, López-Contreras AJ, Ludwig T, Baer R, Faryabi RB, Malhowski A, Chen HT, Fernandez-Capetillo O, D'Andrea A, Nussenzweig A. BRCA1 functions independently of homologous recombination in DNA interstrand crosslink repair. Mol Cell. 2012 Apr 27;46(2):125-35.

10: Bothmer A, Robbiani DF, Di Virgilio M, Bunting SF, Klein IA, Feldhahn N, Barlow J, Chen HT, Bosque D, Callen E, Nussenzweig A, Nussenzweig MC. Regulation of DNA end joining, resection, and immunoglobulin class switch recombination by 53BP1. Mol Cell. 2011 May 6;42(3):319-29.

Peer Reviewed Articles: Inspired by Work from the DOD Idea Award

11: Santos MA, Faryabi RB, Ergen AV, Day AM, Malhowski A, Canela A, Onozawa M, Lee JE, Callen E, Gutierrez-Martinez P, Chen HT, Wong N, Finkel N, Deshpande A, Sharrow S, Rossi DJ, Ito K, Ge K, Aplan PD, Armstrong SA, Nussenzweig A. DNA-damage-induced differentiation of leukaemic cells as an anti-cancer barrier. Nature. 2014 Jul 27.

12: Polato F, Callen E, Wong N, Faryabi R, Bunting S, Chen HT, Kozak M, Kruhlak MJ, Reczek CR, Lee WH, Ludwig T, Baer R, Feigenbaum L, Jackson S, Nussenzweig A.

CtIP-mediated resection is essential for viability and can operate independently of BRCA1. J Exp Med. 2014 Jun 2;211(6):1027-36.

13: Lee BS, Gapud EJ, Zhang S, Dorsett Y, Bredemeyer A, George R, Callen E, Daniel JA, Osipovich O, Oltz EM, Bassing CH, Nussenzweig A, Lees-Miller S, Hammel M, Chen BP, Sleckman BP. Functional intersection of ATM and DNA-dependent protein kinase catalytic subunit in coding end joining during V(D)J recombination. Mol Cell Biol. 2013 Sep;33(18):3568-79.

14: Yamane A, Robbiani DF, Resch W, Bothmer A, Nakahashi H, Oliveira T, Rommel PC, Brown EJ, Nussenzweig A, Nussenzweig MC, Casellas R. RPA accumulation during class switch recombination represents 5'-3' DNA-end resection during the S-G2/M phase of the cell cycle. Cell Rep. 2013 Jan 31;3(1):138-47.

15: Bothmer A, Rommel PC, Gazumyan A, Polato F, Reczek CR, Muellenbeck MF, Schaetzlein S, Edelmann W, Chen PL, Brosh RM Jr, Casellas R, Ludwig T, Baer R, Nussenzweig A, Nussenzweig MC, Robbiani DF. Mechanism of DNA resection during intrachromosomal recombination and immunoglobulin class switching. J Exp Med. 2013 Jan 14;210(1):115-23.

16: Sin HS, Barski A, Zhang F, Kartashov AV, Nussenzweig A, Chen J, Andreassen PR, Namekawa SH. RNF8 regulates active epigenetic modifications and escape gene activation from inactive sex chromosomes in post-meiotic spermatids. Genes Dev. 2012 Dec 15;26(24):2737-48.

17: Callen E, Faryabi RB, Luckey M, Hao B, Daniel JA, Yang W, Sun HW, Dressler G, Peng W, Chi H, Ge K, Krangel MS, Park JH, Nussenzweig A. The DNA damage- and transcription-associated protein paxip1 controls thymocyte development and emigration. Immunity. 2012 Dec 14;37(6):971-85.

18: Muñoz MC, Laulier C, Gunn A, Cheng A, Robbiani DF, Nussenzweig A, Stark JM. RING finger nuclear factor RNF168 is important for defects in homologous recombination caused by loss of the breast cancer susceptibility factor BRCA1. J Biol Chem. 2012 Nov 23;287(48):40618-28.

19: Feldhahn N, Ferretti E, Robbiani DF, Callen E, Deroubaix S, Selleri L, Nussenzweig A, Nussenzweig MC. The hSSB1 orthologue Obfc2b is essential for skeletogenesis but dispensable for the DNA damage response in vivo. EMBO J. 2012 Oct 17;31(20):4045-56.

20: Daniel JA, Pellegrini M, Lee BS, Guo Z, Filsuf D, Belkina NV, You Z, Paull TT, Sleckman BP, Feigenbaum L, Nussenzweig A. Loss of ATM kinase activity leads to embryonic lethality in mice. J Cell Biol. 2012 Aug 6;198(3):295-304.

21: Daniel JA, Nussenzweig A. Roles for histone H3K4 methyltransferase activities during immunoglobulin class-switch recombination. Biochim Biophys Acta. 2012 Jul;1819(7):733-8

22: Hakim O, Resch W, Yamane A, Klein I, Kieffer-Kwon KR, Jankovic M, Oliveira T, Bothmer A, Voss TC, Ansarah-Sobrinho C, Mathe E, Liang G, Cobell J, Nakahashi H, Robbiani DF, Nussenzweig A, Hager GL, Nussenzweig MC, Casellas R. DNA damage defines sites of recurrent chromosomal translocations in B lymphocytes. Nature. 2012 Feb 7;484(7392):69-74.

23: Klein IA, Resch W, Jankovic M, Oliveira T, Yamane A, Nakahashi H, Di Virgilio M, Bothmer A, Nussenzweig A, Robbiani DF, Casellas R, Nussenzweig MC. Translocation-capture sequencing reveals the extent and nature of chromosomal rearrangements in B lymphocytes. Cell. 2011 Sep 30;147(1):95-106.

24: Ichijima Y, Ichijima M, Lou Z, Nussenzweig A, Camerini-Otero RD, Chen J, Andreassen PR, Namekawa SH. MDC1 directs chromosome-wide silencing of the sex chromosomes in male germ cells. Genes Dev. 2011 May 1;25(9):959-71.

25: Zhang S, Yajima H, Huynh H, Zheng J, Callen E, Chen HT, Wong N, Bunting S, Lin YF, Li M, Lee KJ, Story M, Gapud E, Sleckman BP, Nussenzweig A, Zhang CC, Chen DJ, Chen BP. Congenital bone marrow failure in DNA-PKcs mutant mice associated with deficiencies in DNA repair. J Cell Biol. 2011 Apr 18;193(2):295-305.

26: Fernando RN, Eleuteri B, Abdelhady S, Nussenzweig A, Andäng M, Ernfors P. Cell cycle restriction by histone H2AX limits proliferation of adult neural stem cells. Proc Natl Acad Sci U S A. 2011 Apr 5;108(14):5837-42.

27: Gapud EJ, Dorsett Y, Yin B, Callen E, Bredemeyer A, Mahowald GK, Omi KQ, Walker LM, Bednarski JJ, McKinnon PJ, Bassing CH, Nussenzweig A, Sleckman BP. Ataxia telangiectasia mutated (Atm) and DNA-PKcs kinases have overlapping activities during chromosomal signal joint formation. Proc Natl Acad Sci U S A. 2011 Feb 1;108(5):2022-7.

28: Pellegrini M, Claps G, Orlova VV, Barrios F, Dolci S, Geremia R, Rossi P, Rossi G, Arnold B, Chavakis T, Feigenbaum L, Sharan SK, Nussenzweig A. Targeted JAM-C deletion in germ cells by Spo11-controlled Cre recombinase. J Cell Sci. 2011 Jan 1;124(Pt 1):91-9.

Abstracts

1. Poster presentation by Dr. Elsa Callen at the international ‘Mechanisms of Genomic Instability’, meeting in Bahamas, March 2012.

B. **National and International Presentations (Invited Talks)**

1: March 3-6, 2014-Maintenance of Genome Stability Conference in St. Kitts- “Genome Stability during DNA Replication”

2: January 29-31, 2014- AACR Conference on Cancer Susceptibility and Cancer Susceptibility Syndromes in San Diego, CA-"Role of BRCA1 in genome stability"

3: December 10-14, 2013-CTRC-AACR- San Antonio Breast Cancer Symposium in Texas-“Mechanisms that maintain genome stability”

4: November 14, 2013-Fox Chase Cancer Center Distinguished Lecture Series – Philadelphia, PA- "Mechanisms that maintain genome stability."

5: June 12, 2013- 2012-2013 Samuel Lunenfeld Research Institute Seminar Series in Toronto, Canada-"Maintenance of Genome Stability."

6: May 27, 2013-Collaborative Research Center 655 from Cells to Tissues seminar series at the Max-Planck-Institute in Dresden, Germany-“Genome Stability during DNA Replication”

7: May 25, 2013- 5th Else Kroner-Fresenius Symposium on Adult Stem Cells in Aging, Diseases & Cancer in Eisenach, Germany-“Genome Stability during DNA Replication”

8: May 3, 2013- Chemical and Systems Biology Department Seminar Series at Stanford University-“Genome Stability during DNA Replication”

9: April 15, 2013- Spanish National Cancer Research Centre (CNIO) in Madrid, Spain- "Genome Instability during DNA Replication."

10: April 12, 2013-University of Zurich Cancer Mini-Symposium in Grindelwald, Switzerland- “Genome Stability during DNA Replication”

11: March 3-8, 2013- Keystone Symposia: Genetic Instability and DNA Repair in Fairmont Banff Springs, Alberta- “Identification of a novel class of early replicating fragile sites that contribute to genomic instability in B cell lymphomas”

12: Invited keynote presentation by Dr. Andre Nussenzweig at the international ‘Mechanisms of Genomic Instability’ meeting in Bahamas, March 2012.

7. INVENTIONS, PATENTS AND LICENSES:

No inventions, patents or licenses have been generated as a result of this work.

8. REPORTABLE OUTCOMES:

4 reviews and commentaries, **6 peer-reviewed articles** in high-impact journals and **18 peer-reviewed articles** that are tangentially related but stimulated by ideas related to the DOD Award have been published in the funding years 2011-2014. Additionally, the principal investigator and members of his laboratory have presented **abstracts** and delivered **talks** at numerous national and international scientific conferences.

9. OTHER ACHIEVEMENTS: Numerous mouse strains and many retroviral expression constructs have been generated that provide a new resource for testing the molecular functions of homologous recombination and non-homologous end-joining effector proteins.

10. REFERENCES:

1: Ira G, Nussenzweig A. A new Riff: Rif1 eats its cake and has it too. EMBO Rep. 2014 Jun;15(6):622-4.

2: Fernandez-Capetillo O, Nussenzweig A. Naked replication forks break apRPArt. Cell. 2013 Nov 21;155(5):979-80.

3: Bunting SF, Nussenzweig A. End-joining, translocations and cancer. Nat Rev Cancer. 2013 Jul;13(7):443-54.

4: Daniel JA, Nussenzweig A. The AID-induced DNA damage response in chromatin. Mol Cell. 2013 May 9;50(3):309-21.

5: Callen E, Di Virgilio M, Kruhlak MJ, Nieto-Soler M, Wong N, Chen HT, Faryabi RB, Polato F, Santos M, Starnes LM, Wesemann DR, Lee JE, Tubbs A, Sleckman BP, Daniel JA, Ge K, Alt FW, Fernandez-Capetillo O, Nussenzweig MC, Nussenzweig A. 53BP1 mediates productive and mutagenic DNA repair through distinct phosphoprotein interactions. Cell. 2013 Jun 6;153(6):1266-80.

6: Bowman-Colin C, Xia B, Bunting S, Klijn C, Drost R, Bouwman P, Fineman L, Chen X, Culhane AC, Cai H, Rodig SJ, Bronson RT, Jonkers J, Nussenzweig A, Kanellopoulou C, Livingston DM. Palb2 synergizes with Trp53 to suppress mammary tumor formation in a model of inherited breast cancer. Proc Natl Acad Sci U S A. 2013 May 21;110(21):8632-7.

7: Barlow JH, Faryabi RB, Callén E, Wong N, Malhowski A, Chen HT, Gutierrez-Cruz G, Sun HW, McKinnon P, Wright G, Casellas R, Robbiani DF, Staudt L, Fernandez-Capetillo O, Nussenzweig A. Identification of early replicating fragile sites that contribute to genome instability. Cell. 2013 Jan 31;152(3):620-32.

8: Di Virgilio M, Callen E, Yamane A, Zhang W, Jankovic M, Gitlin AD, Feldhahn N, Resch W, Oliveira TY, Chait BT, Nussenzweig A, Casellas R, Robbiani DF, Nussenzweig MC. Rif1 prevents resection of DNA breaks and promotes immunoglobulin class switching. Science. 2013 Feb 8;339(6120):711-5.

9: Bunting SF, Callén E, Kozak ML, Kim JM, Wong N, López-Contreras AJ, Ludwig T, Baer R, Faryabi RB, Malhowski A, Chen HT, Fernandez-Capetillo O, D'Andrea A,

Nussenzweig A. BRCA1 functions independently of homologous recombination in DNA interstrand crosslink repair. Mol Cell. 2012 Apr 27;46(2):125-35.

10: Bothmer A, Robbiani DF, Di Virgilio M, Bunting SF, Klein IA, Feldhahn N, Barlow J, Chen HT, Bosque D, Callen E, Nussenzweig A, Nussenzweig MC. Regulation of DNA end joining, resection, and immunoglobulin class switch recombination by 53BP1. Mol Cell. 2011 May 6;42(3):319-29.

11: Santos MA, Faryabi RB, Ergen AV, Day AM, Malhowski A, Canela A, Onozawa M, Lee JE, Callen E, Gutierrez-Martinez P, Chen HT, Wong N, Finkel N, Deshpande A, Sharrow S, Rossi DJ, Ito K, Ge K, Aplan PD, Armstrong SA, Nussenzweig A. DNA-damage-induced differentiation of leukaemic cells as an anti-cancer barrier. Nature. 2014 Jul 27.

12: Polato F, Callen E, Wong N, Faryabi R, Bunting S, Chen HT, Kozak M, Kruhlak MJ, Reczek CR, Lee WH, Ludwig T, Baer R, Feigenbaum L, Jackson S, Nussenzweig A. CtIP-mediated resection is essential for viability and can operate independently of BRCA1. J Exp Med. 2014 Jun 2;211(6):1027-36.

13: Lee BS, Gapud EJ, Zhang S, Dorsett Y, Bredemeyer A, George R, Callen E, Daniel JA, Osipovich O, Oltz EM, Bassing CH, Nussenzweig A, Lees-Miller S, Hammel M, Chen BP, Sleckman BP. Functional intersection of ATM and DNA-dependent protein kinase catalytic subunit in coding end joining during V(D)J recombination. Mol Cell Biol. 2013 Sep;33(18):3568-79.

14: Yamane A, Robbiani DF, Resch W, Bothmer A, Nakahashi H, Oliveira T, Rommel PC, Brown EJ, Nussenzweig A, Nussenzweig MC, Casellas R. RPA accumulation during class switch recombination represents 5'-3' DNA-end resection during the S-G2/M phase of the cell cycle. Cell Rep. 2013 Jan 31;3(1):138-47.

15: Bothmer A, Rommel PC, Gazumyan A, Polato F, Reczek CR, Muellenbeck MF, Schaetzlein S, Edelmann W, Chen PL, Brosh RM Jr, Casellas R, Ludwig T, Baer R, Nussenzweig A, Nussenzweig MC, Robbiani DF. Mechanism of DNA resection during intrachromosomal recombination and immunoglobulin class switching. J Exp Med. 2013 Jan 14;210(1):115-23.

16: Sin HS, Barski A, Zhang F, Kartashov AV, Nussenzweig A, Chen J, Andreassen PR, Namekawa SH. RNF8 regulates active epigenetic modifications and escape gene activation from inactive sex chromosomes in post-meiotic spermatids. Genes Dev. 2012 Dec 15;26(24):2737-48.

17: Callen E, Faryabi RB, Luckey M, Hao B, Daniel JA, Yang W, Sun HW, Dressler G, Peng W, Chi H, Ge K, Krangel MS, Park JH, Nussenzweig A. The DNA damage- and transcription-associated protein paxip1 controls thymocyte development and

emigration. Immunity. 2012 Dec 14;37(6):971-85.

18: Muñoz MC, Laulier C, Gunn A, Cheng A, Robbiani DF, Nussenzweig A, Stark JM. RING finger nuclear factor RNF168 is important for defects in homologous recombination caused by loss of the breast cancer susceptibility factor BRCA1. J Biol Chem. 2012 Nov 23;287(48):40618-28.

19: Feldhahn N, Ferretti E, Robbiani DF, Callen E, Deroubaix S, Selleri L, Nussenzweig A, Nussenzweig MC. The hSSB1 orthologue Obfc2b is essential for skeletogenesis but dispensable for the DNA damage response in vivo. EMBO J. 2012 Oct 17;31(20):4045-56.

20: Daniel JA, Pellegrini M, Lee BS, Guo Z, Filsuf D, Belkina NV, You Z, Paull TT, Sleckman BP, Feigenbaum L, Nussenzweig A. Loss of ATM kinase activity leads to embryonic lethality in mice. J Cell Biol. 2012 Aug 6;198(3):295-304.

21: Daniel JA, Nussenzweig A. Roles for histone H3K4 methyltransferase activities during immunoglobulin class-switch recombination. Biochim Biophys Acta. 2012 Jul;1819(7):733-8

22: Hakim O, Resch W, Yamane A, Klein I, Kieffer-Kwon KR, Jankovic M, Oliveira T, Bothmer A, Voss TC, Ansarah-Sobrinho C, Mathe E, Liang G, Cobell J, Nakahashi H, Robbiani DF, Nussenzweig A, Hager GL, Nussenzweig MC, Casellas R. DNA damage defines sites of recurrent chromosomal translocations in B lymphocytes. Nature. 2012 Feb 7;484(7392):69-74.

23: Klein IA, Resch W, Jankovic M, Oliveira T, Yamane A, Nakahashi H, Di Virgilio M, Bothmer A, Nussenzweig A, Robbiani DF, Casellas R, Nussenzweig MC. Translocation-capture sequencing reveals the extent and nature of chromosomal rearrangements in B lymphocytes. Cell. 2011 Sep 30;147(1):95-106.

24: Ichijima Y, Ichijima M, Lou Z, Nussenzweig A, Camerini-Otero RD, Chen J, Andreassen PR, Namekawa SH. MDC1 directs chromosome-wide silencing of the sex chromosomes in male germ cells. Genes Dev. 2011 May 1;25(9):959-71.

25: Zhang S, Yajima H, Huynh H, Zheng J, Callen E, Chen HT, Wong N, Bunting S, Lin YF, Li M, Lee KJ, Story M, Gapud E, Sleckman BP, Nussenzweig A, Zhang CC, Chen DJ, Chen BP. Congenital bone marrow failure in DNA-PKcs mutant mice associated with deficiencies in DNA repair. J Cell Biol. 2011 Apr 18;193(2):295-305.

26: Fernando RN, Eleuteri B, Abdelhady S, Nussenzweig A, Andäng M, Ernfors P. Cell cycle restriction by histone H2AX limits proliferation of adult neural stem cells. Proc Natl Acad Sci U S A. 2011 Apr 5;108(14):5837-42.

27: Gapud EJ, Dorsett Y, Yin B, Callen E, Bredemeyer A, Mahowald GK, Omi KQ, Walker LM, Bednarski JJ, McKinnon PJ, Bassing CH, Nussenzweig A, Sleckman BP. Ataxia telangiectasia mutated (Atm) and DNA-PKcs kinases have overlapping activities during chromosomal signal joint formation. Proc Natl Acad Sci U S A. 2011 Feb 1;108(5):2022-7.

28: Pellegrini M, Claps G, Orlova VV, Barrios F, Dolci S, Geremia R, Rossi P, Rossi G, Arnold B, Chavakis T, Feigenbaum L, Sharan SK, Nussenzweig A. Targeted JAM-C deletion in germ cells by Spo11-controlled Cre recombinase. J Cell Sci. 2011 Jan 1;124(Pt 1):91-9.

11. APPENDICES:

Appendix of relevant journal articles is attached (in Pdf)

Cell

53BP1 Mediates Productive and Mutagenic DNA Repair through Distinct Phosphoprotein Interactions

Elsa Callen,[1] Michela Di Virgilio,[3] Michael J. Kruhlak,[2] Maria Nieto-Soler,[4] Nancy Wong,[1] Hua-Tang Chen,[1] Robert B. Faryabi,[1] Federica Polato,[1] Margarida Santos,[1] Linda M. Starnes,[5] Duane R. Wesemann,[6] Ji-Eun Lee,[7] Anthony Tubbs,[8] Barry P. Sleckman,[8] Jeremy A. Daniel,[5] Kai Ge,[7] Frederick W. Alt,[6] Oscar Fernandez-Capetillo,[4] Michel C. Nussenzweig,[3] and André Nussenzweig[1,*]

[1]Laboratory of Genome Integrity
[2]Experimental Immunology Branch
National Cancer Institute, NIH, Bethesda, MD 20892, USA
[3]Laboratory of Molecular Immunology and Howard Hughes Medical institute, Rockefeller University, New York, NY 10065, USA
[4]Genomic Instability Group, Spanish National Cancer Research Centre (CNIO), Madrid 28029, Spain
[5]The Novo Nordisk Foundation Center for Protein Research, Faculty of Health and Medical Sciences, University of Copenhagen, Copenhagen, Denmark
[6]Program in Cellular and Molecular Medicine, Immune Disease Institute and Howard Hughes Medical Institute, Children's Hospital, Boston, MA 02115, USA
[7]Laboratory of Endocrinology and Receptor Biology, National Institute of Diabetes and Digestive and Kidney Diseases, NIH, Bethesda, MD 20892, USA
[8]Department of Pathology and Immunology, Washington University School of Medicine, St. Louis, MO 63110, USA
*Correspondence: andre_nussenzweig@nih.gov
http://dx.doi.org/10.1016/j.cell.2013.05.023

SUMMARY

The DNA damage response (DDR) protein 53BP1 protects DNA ends from excessive resection in G1, and thereby favors repair by nonhomologous end-joining (NHEJ) as opposed to homologous recombination (HR). During S phase, BRCA1 antagonizes 53BP1 to promote HR. The pro-NHEJ and antirecombinase functions of 53BP1 are mediated in part by RIF1, the only known factor that requires 53BP1 phosphorylation for its recruitment to double-strand breaks (DSBs). Here, we show that a 53BP1 phosphomutant, 53BP1^{8A}, comprising alanine substitutions of the eight most N-terminal S/TQ phosphorylation sites, mimics 53BP1 deficiency by restoring genome stability in BRCA1-deficient cells yet behaves like wild-type 53BP1 with respect to immunoglobulin class switch recombination (CSR). 53BP1^{8A} recruits RIF1 but fails to recruit the DDR protein PTIP to DSBs, and disruption of PTIP phenocopies 53BP1^{8A}. We conclude that 53BP1 promotes productive CSR and suppresses mutagenic DNA repair through distinct phosphodependent interactions with RIF1 and PTIP.

INTRODUCTION

Class switch recombination (CSR) is initiated by activation-induced cytidine deaminase (AID), which generates multiple double-strand breaks (DSBs) at highly repetitive immunoglobulin (Ig) switch regions. Paired distal DSBs are then rejoined by nonhomologous end-joining (NHEJ), thereby replacing Igμ by a downstream constant region (Igγ, Igε, or Igα). Alternatively, if DSBs persist, a homology-driven pathway that involves resection of repetitive switch regions, can repair DSBs locally. Such abortive "intraswitch" recombination events are increased at the expense of CSR in the absence of 53BP1(Reina-San-Martin et al., 2007), a key suppressor of end resection (Bothmer et al., 2010; Bouwman et al., 2010; Bunting et al., 2010; Cao et al., 2009; Difilippantonio et al., 2008).

In addition to its productive effect on CSR, 53BP1 blocks DNA ends from resection in BRCA1-deficient cells, leading to toxic radial chromosomes that arise from NHEJ (Bouwman et al., 2010; Bunting et al., 2010, 2012; Cao et al., 2009). Deletion of 53BP1 leads to deposition of homologous recombination (HR) factors RPA and RAD51 on single-strand DNA, which, in the case of recombining switch regions, promotes intraswitch recombination (Yamane et al., 2013) and, in the setting of BRCA1 deficiency, restores HR (Bouwman et al., 2010; Bunting et al., 2010; Cao et al., 2009). Thus, DNA end protection by 53BP1 is critical for CSR in G1 but can unleash genome instability in S phase.

In addition to DNA end-blocking activities that disfavor HR and thereby promote NHEJ, 53BP1 has been suggested to directly mediate long-range chromosomal interactions and DSB mobility that facilitates the juxtaposition of distal DNA ends. These activities are believed to be responsible for 53BP1's ability to support recombination of DSB ends that are far apart during V(D)J recombination and class switch recombination (Callén et al., 2007b; Difilippantonio et al., 2008) and to fuse uncapped telomeric DNA ends (Dimitrova et al., 2008). Both pro-NHEJ and

anti-HR functions require the direct physical association of 53BP1 with DNA ends but also necessitate the DSB-induced phosphorylation of its N-terminal ATM/ATR kinase sites (Bothmer et al., 2011; Ward et al., 2006).

The DNA damage response (DDR) protein RIF1 was recently identified as an essential factor recruited by phosphorylated 53BP1 to promote NHEJ and block HR (Chapman et al., 2013; Di Virgilio et al., 2013; Escribano-Díaz et al., 2013; Feng et al., 2013; Zimmermann et al., 2013). Like 53BP1, RIF1 is required for CSR (Chapman et al., 2013; Di Virgilio et al., 2013; Escribano-Díaz et al., 2013). Although the NHEJ of dysfunctional telomeres is abrogated in cells lacking 53BP1 or in cells expressing $53BP1^{28A}$(Lottersberger et al., 2013), an allele harboring alanine substitutions at all 28 N-terminal ATM/ATR kinase phosphorylation targets sites, loss of RIF1 has considerably milder defect (Zimmermann et al., 2013). Moreover, although the generation of toxic radial chromosomes in BRCA1-deficient cells is prevented in *53BP1*$^{-/-}$ or in $53BP1^{28A}$ mutant cells (Bothmer et al., 2011; Bouwman et al., 2010; Bunting et al., 2012; Bunting et al., 2010), the loss of RIF1 only partially rescues HR in BRCA1-deficient cells (Escribano-Díaz et al., 2013; Feng et al., 2013; Zimmermann et al., 2013). This suggests that additional phosphorylation-dependent but RIF1-independent activities of 53BP1 might regulate the balance between HR and NHEJ.

PTIP is a ubiquitously expressed nuclear protein that associates constitutively with two of the known histone methyltransferases that catalyze trimethylation of histone H3 at lysine 4 (H3K4me3), MLL3, and MLL4 (Cho et al., 2007; Patel et al., 2007). In addition to its well-established role in transcription initiation, a separate pool of PTIP functions in an unknown capacity in the DDR (Gong et al., 2009). Indeed, PTIP has been implicated in both HR (Wang et al., 2010) and NHEJ (Callen et al., 2012). PTIP is recruited to DSBs by its tandem BRCT (BRCA1 carboxyl-terminal) domains (Manke et al., 2003; Yu et al., 2003), which associate with the serine 25 phosphorylation site within the N terminus of 53BP1 (Munoz et al., 2007). In contrast to RIF1, PTIP recruitment to DSBs was reported to be 53BP1 and ATM independent (Gong et al., 2009; Jowsey et al., 2004; Munoz et al., 2007). Thus, the mechanism by which PTIP is recruited to DSBs, its role in DSB repair, and the physiological significance of PTIP interaction with 53BP1 remain unclear. Here, we show that PTIP is required for 53BP1-mediated inhibition of HR in BRCA1-deficient cells but is dispensable for 53BP1-initiated DSB repair during productive CSR. Thus, RIF1 and PTIP separate 53BP1 functions in productive and pathologic DSB repair.

RESULTS

A Separation of Function Mutation in 53BP1

To determine whether 53BP1's activities in NHEJ and HR are distinct, we compared $53BP1^{8A}$, which disrupts phosphorylation of the eight N-terminal ATM/ATR target sites (Figure 1A), to the $53BP1^{DB}$ allele, which is indistinguishable from WT 53BP1 in all functional aspects (Bothmer et al., 2011). To assay for CSR, BRCA1/53BP1-deficient B cells were transduced with wild-type and 53BP1 mutant proteins by retroviral infection after activation with lipopolysaccharide (LPS) and interleukin-4 (IL4). As expected, $53BP1^{DB}$ fully complemented the CSR defects (Figure 1B) and produced high levels of genome instability in PARPi-treated BRCA1/53BP1-deficient cells (Figure 1C) (Bothmer et al., 2011). Surprisingly, despite rescuing CSR, the $53BP1^{8A}$ allele failed to promote genome instability in PARPi-treated BRCA1/53BP1-deficient cells above the levels observed in controls (Figure 1C). This effect was not due to differences in the expression levels of 53BP1 (Figure 1D) or in the recruitment of 53BP1 and RIF1 to DSBs (Figure 1E). Similar to B cells, BRCA1/53BP1-deficient MEFs complemented with $53BP1^{DB}$ were hypersensitive to PARPi, whereas $53BP1^{8A}$ transduced MEFs were not (Figure S1 available online). Thus, the mechanism by which 53BP1 promotes CSR and blocks HR in BRCA1-deficient cells is distinct. Moreover, the recruitment of RIF1 is insufficient to induce genome instability in PARPi-treated BRCA1-deficient cells.

Role of PTIP in the DNA Damage Response

Upon DNA damage, PTIP binds to the serine 25 residue within the N terminus of 53BP1(Munoz et al., 2007), which is located within the eight N-terminal sites mutated in $53BP1^{8A}$. Consistent with this, immunoprecipitation analysis revealed that PTIP association with 53BP1 after irradiation was abrogated in cells expressing S25A-harboring mutants $53BP1^{8A}$, $53BP1^{15A}$, or $53BP1^{28A}$ (Figures 2A and S2A). In contrast, the damage-induced 53BP1/PTIP interaction was maintained in the $53BP1^{7A}$ mutant, comprising alanine substitutions of 7 S/TQ phosphorylation sites C terminus of those mutated in $53BP1^{8A}$ (Figures 1A and S2A).

To explore the function of PTIP in the DDR, we asked whether PTIP-deficient cells are sensitive to DNA damaging agents that are predominantly repaired by HR (Sonoda et al., 2006). WT and *PTIP*$^{-/-}$ MEFs were exposed to either cisplatin, camptothecin, or PARPi, all of which sensitize HR-deficient cells (Bryant et al., 2005; Farmer et al., 2005). Each of these agents induced a similar level of chromosomal aberrations and reduction in cell survival in WT and *PTIP*$^{-/-}$ MEFs (Figures 2B, 2C, and S2B). In contrast, *PTIP*$^{-/-}$ MEFs were sensitive to irradiation (IR) (Figures 2B, 2C, and S2B) (Gong et al., 2009; Jowsey et al., 2004; Munoz et al., 2007). Moreover, $53BP1^{8A}$ MEFs exhibited increased genome instability and reduced cell survival following IR (Figures S2C and S2D). To examine the recruitment of HR proteins to DSBs, we evaluated BRCA1, RAD51, and γ-H2AX foci formation after IR in WT and *PTIP*$^{-/-}$ MEFs. All of these factors were normally recruited to DSBs in PTIP-deficient cells (Figure S2E). Moreover, 53BP1 also formed robust foci in the absence of PTIP (Figure S2E). Thus, *PTIP*$^{-/-}$ MEFs are tolerant to agents that are highly toxic to HR-deficient cells and the recruitment of several factors implicated in DSB repair is intact in the absence of PTIP. Nevertheless, both *PTIP*$^{-/-}$ and $53BP1^{8A}$ MEFs are sensitive to IR.

PTIP Is Dispensable for NHEJ during CSR but Is Required for NHEJ of Dysfunctional Telomeres

To explore the role of PTIP in NHEJ, we first assayed CSR. Deletion of PTIP in B cells leads to a defect in class switching to IgG3, IgG2b, and IgG1 (Daniel et al., 2010; Schwab et al., 2011). By recruiting an MLL-like methyltransferase complex to the switch regions of these isotypes, PTIP promotes histone modifications

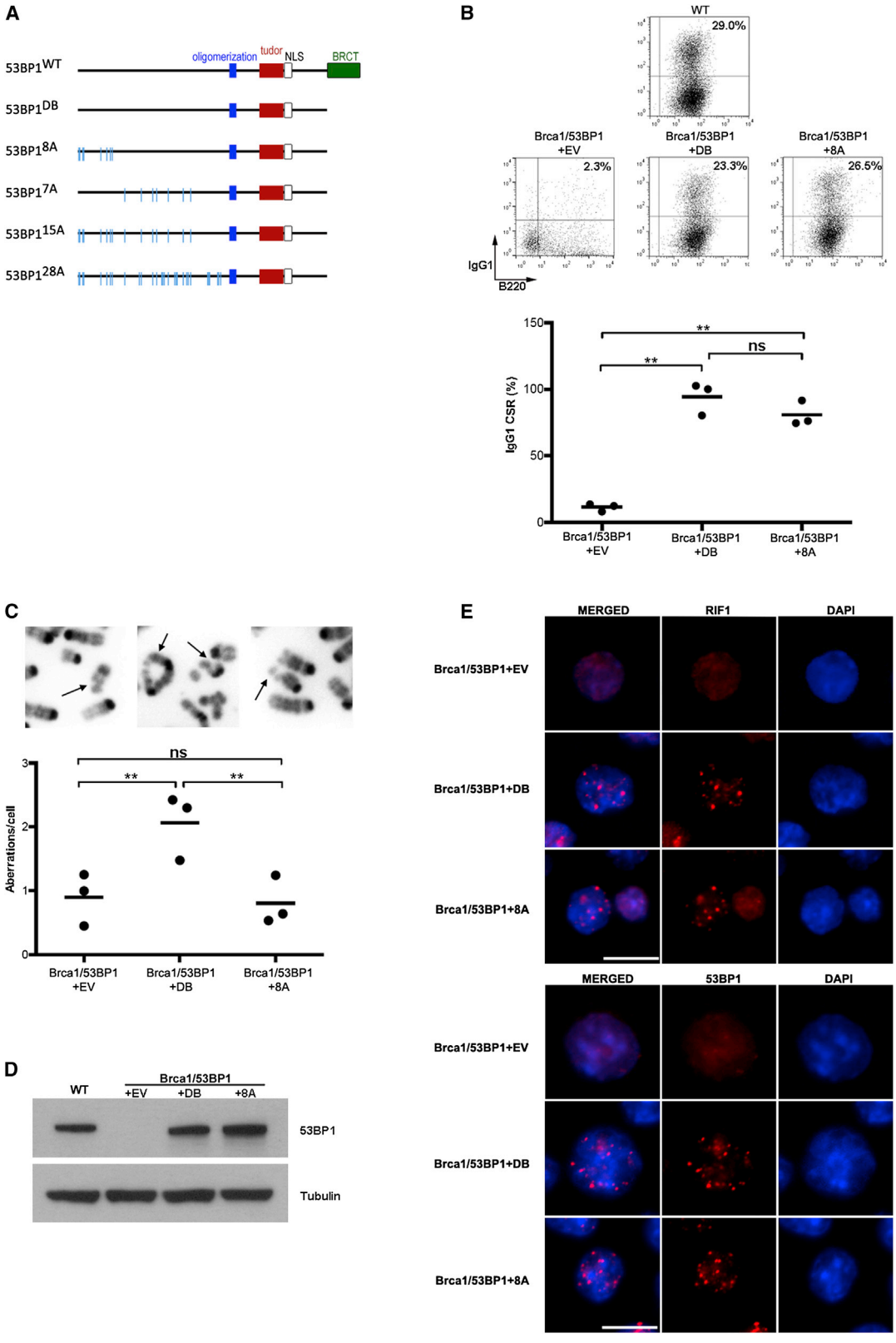

(legend on next page)

and transcription initiation of IgG3/IgG2b/IgG1 germline switch regions, which are necessary for AID targeting (Daniel et al., 2010; Schwab et al., 2011). However, PTIP does not affect transcription at Igμ and Igε (Daniel et al., 2010), indicating that PTIP-associated methyltransferase complex promotes the accessibility of some but not all switch loci. To distinguish between PTIP's effects on transcription versus DSB repair, we compared CSR to IgG1 and IgE on day 5 after stimulation with αCD40+IL4 as described (Wesemann et al., 2011). As expected *PTIP*$^{f/f}$ *CD19*^{CRE} (*PTIP*$^{-/-}$) B cells displayed a defect in switching to IgG1 (Figures 3A and 3B), which is consistent with decreased *Igγ1* germline transcription (Daniel et al., 2010; Schwab et al., 2011). However, there was no defect in IgE germline transcription (Daniel et al., 2010) or IgE CSR in PTIP-deficient cells (Figures 3A and 3B). Indeed, IgE CSR was consistently higher in the absence of PTIP, likely because Sγ1 is no longer a target for AID. In contrast to *PTIP*$^{-/-}$, ablation of RIF1 in *Rif1*$^{f/f}$ CD19^{CRE} (*RIF1*$^{-/-}$) B cells impaired CSR to both IgG1 and IgE (Figures 3A and 3B). We conclude that loss of PTIP phenocopies the 53BP1^{8A} mutant allele in that neither has a significant impact on NHEJ during CSR.

An alternative end-joining pathway can catalyze substantial CSR end-joining to IgG1 and IgE even in the absence of classical NHEJ (Boboila et al., 2010). Loss of PTIP leads to IR sensitivity but tolerance to agents that are repaired by HR. We therefore speculated that PTIP might function in other reactions besides CSR that might rely on classical NHEJ, such as the fusion of dysfunctional telomeres. When the shelterin factor TRF2 is removed, deprotected telomeres trigger ATM-dependent phosphorylation of 53BP1, and the ends are processed by NHEJ to generate chromosome fusions (Celli et al., 2006; Rai et al., 2010; Zimmermann et al., 2013). Because ATM-dependent phosphorylation of 53BP1 is also required for interaction between 53BP1 and PTIP (Figures 2A and S2A) (Jowsey et al., 2004; Manke et al., 2003), we asked whether PTIP promotes NHEJ-mediated fusion of deprotected telomeres. To address this, we uncapped telomeres in SV40-immortalized WT and *PTIP*$^{-/-}$ MEFs by removing TRF2 with short hairpin RNA against TRF2 (Rai et al., 2010). Upon TRF2 depletion we observed a similar level of phosphorylation of the ATM target KAP-1 in WT and *PTIP*$^{-/-}$ MEFs, as measured by quantitative flow cytometry (Figure 4A). Consistent with this, there was an accumulation of cytologically discernable telomere-induced DNA damage foci (TIFs) containing γ-H2AX in WT and *PTIP*$^{-/-}$ cells (Figure 4B). Despite a robust DNA damage response and activation of ATM, the frequency of end-end chromosomal fusions was reduced by 2.8-fold in *PTIP*$^{-/-}$ MEFs relative to WT (Figures 4C and 4D). Whereas 42% of WT cells bearing fusions had more than 30% of their chromosome ends fused, only 13% of PTIP KO cells had greater than 30% of their ends fused (Figure 4E). Thus, PTIP deficiency results in a reduction in the number of long-chain telomere fusions when telomeres are deprotected. We conclude that PTIP contributes to the NHEJ of dysfunctional telomeres.

PTIP Promotes Genome Instability in BRCA1-Deficient Cells

In contrast to 53BP1, loss of RIF1 only partially reverses the chromosomal aberrations and hypersensitivity produced by PARPi treatment of BRCA1-deficient cells (Escribano-Díaz et al., 2013; Zimmermann et al., 2013). To determine whether PTIP could overcome the HR defects in BRCA1-deficient cells, we crossed *PTIP*$^{f/f}$ and *BRCA1*$^{f(Δ11)/f(Δ11)}$ mice with CD19 CRE transgenic mice to simultaneously delete PTIP and exon 11 of BRCA1 in primary B lymphocytes. When unchallenged, *BRCA1*$^{+/+}$*PTIP*$^{+/+}$ CD19^{CRE} (WT), *BRCA1*$^{f(Δ11)/f(Δ11)}$ CD19^{CRE} (*BRCA1*$^{-/-}$), *PTIP*$^{f/f}$ CD19^{CRE} (*PTIP*$^{-/-}$), and *BRCA1*$^{f(Δ11)/f(Δ11)}$*PTIP*$^{f/f}$ CD19^{CRE} (*BRCA1*$^{-/-}$*PTIP*$^{-/-}$) doubly deficient B cells divided normally as determined by carboxyfluorescein succinimidyl ester (CFSE) dye dilution (Figure 5A) and cell-cycle distribution (Figure 5B). Treatment with PARPi did not impair the proliferation of WT or *PTIP*$^{-/-}$ B cells (see also Figures 2B and 2C); however, *BRCA1*$^{-/-}$ cells underwent fewer divisions over the course of 72 hr (Figure 5A). In contrast, loss of PTIP completely reversed the *BRCA1*$^{-/-}$ growth defect (Figure 5A). Strikingly, although PARPi treatment generated chromatid breaks, chromosome breaks, and radial chromosomes in BRCA1-deficient cells (Bunting et al., 2010), *BRCA1*$^{-/-}$*PTIP*$^{-/-}$ B cells were insensitive to PARPi (Figure 5C). Thus, ablation of PTIP phenocopies both the 53BP1^{8A} mutation (Figure 1C) and 53BP1 deficiency (Bouwman et al., 2010; Bunting et al., 2010; Cao et al., 2009) in that it promotes genome stability and survival in BRCA1 mutant cells.

Loss of PTIP Increases HR in BRCA1 Mutant Cells by Promoting DSB Resection

BRCA1 and RAD51 function in a common HR pathway that promotes RAD51-mediated DNA strand exchange (Bhattacharyya et al., 2000; Moynahan et al., 1999; Scully et al., 1997). Loss of 53BP1 rescues RAD51 foci formation and HR in

Figure 1. Characterization of a Separation of Function Mutant 53BP1

(A) Diagram of the 53BP1 retroviral constructs used. Hash marks indicate location of substituted S/TQ sites.

(B) Top: Representative flow cytometry plots measuring CSR after stimulation of WT and *BRCA1*$^{-/-}$*53BP1*$^{-/-}$ B cells infected with retroviruses expressing 53BP1^{DB} (amino acids 1–1710), the N-terminal mutant 53BP1^{8A} or empty vector (EV). Numbers represent the percentages of IgG1 switched cells. B220 is a B cell marker. Bottom: Dot plot indicating IgG1 CSR as a percentage of WT value in the same experiment. Three independent experiments are shown. **$p < 0.001$ (two-tailed unpaired t test); BRCA1/53BP1+DB versus BRCA1/53BP1+8A, $p > 0.1$, which is not significant (ns).

(C) *BRCA1*$^{-/-}$*53BP1*$^{-/-}$ B cells were reconstituted with empty vector, 53BP1^{DB} and 53BP1^{8A} retroviruses and treated with PARPi. The arrows indicate representative images of aberrant chromosomes. Dot plot indicates the total aberrations per cell in three independent experiments. At least 50 metaphases were analyzed for each genotype in each experiment. **$p < 0.01$ (two-tailed unpaired t test); ns: not significant.

(D) Western blot analysis of 53BP1 expression in WT B cells and *BRCA1*$^{-/-}$*53BP1*$^{-/-}$ B cells stimulated and infected with empty vector, 53BP1^{DB}, or 53BP1^{8A}.

(E) *BRCA1*$^{-/-}$*53BP1*$^{-/-}$ B cells infected with EV, 53BP1^{DB} or 53BP1^{8A} retroviruses were assayed for IRIF (10 Gy, 2 hr recovery) for RIF1 (red, top), and 53BP1 (red, bottom). Cells were counterstained with DAPI (blue). Scale bar, 10 μm.

See also Figure S1.

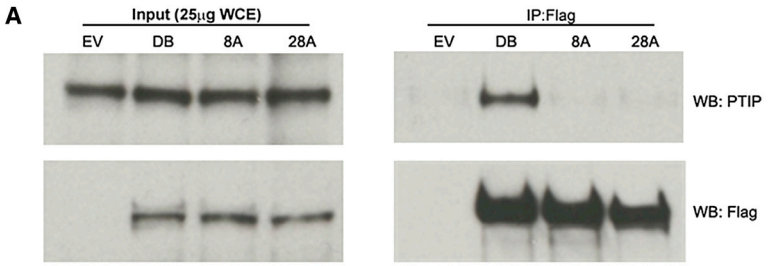

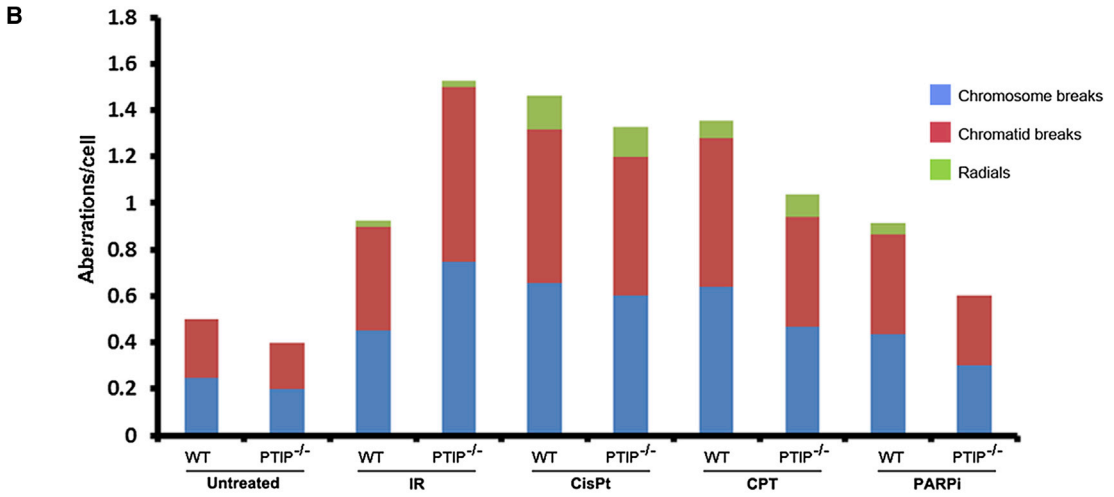

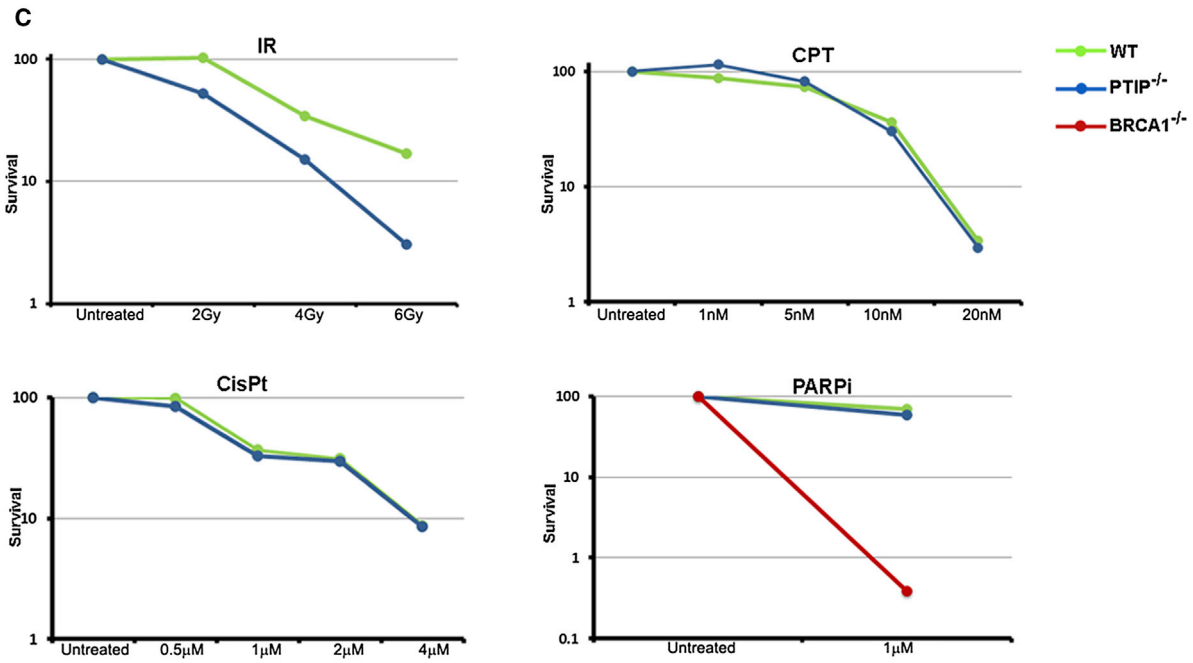

(legend on next page)

BRCA1-deficient cells (Bouwman et al., 2010; Bunting et al., 2010). To explore whether PTIP deficiency also promotes HR in BRCA1-deficient cells, we irradiated WT, *BRCA1*$^{-/-}$, *PTIP*$^{-/-}$, and *BRCA1*$^{-/-}$*PTIP*$^{-/-}$B cells and measured the frequency of immunofluorescent RAD51 foci. All mutant cells proliferated similarly to WT over the course of 3 days (Figure 5A), and as expected, RAD51 foci were reduced in IR-treated *BRCA1*$^{-/-}$ cells (Figure 5D). However, in *PTIP*$^{-/-}$ cells, the frequency of RAD51 foci was greater than WT, and RAD51 foci were normalized to WT levels in *BRCA1*$^{-/-}$*PTIP*$^{-/-}$ B cells (Figure 5D). These results suggest that loss of PTIP reverses the HR defect in BRCA1-deficient cells, thereby explaining the insensitivity of *BRCA1*$^{-/-}$ *PTIP*$^{-/-}$ B cells to PARPi.

Loss of PTIP might promote RAD51 foci formation by allowing increased resection of DSBs; this is similar to what happens with the loss of 53BP1 (Bunting et al., 2010; Difilippantonio et al., 2008). Because 5′→3′ DSB end resection produces RPA-coated single-strand DNA, we monitored RPA foci formation by high content microscopy. Irradiated *PTIP*$^{-/-}$ cells exhibited a significant increase in the mean number of RPA foci per cell relative to WT (Figure 5E); moreover, the fraction of *PTIP*$^{-/-}$ cells that had more than 15 RPA foci following IR was approximately 2-fold greater than WT (Figure 5E). Thus, PTIP limits the amount of chromatin bound RPA at IR-induced DSBs.

PTIP Recruitment to DSBs Promotes Radial Chromosomes in BRCA1-Deficient Cells

PTIP is a subunit of the MLL3/4 methyltransferase complex and promotes histone H3 lysine 4 trimethylation and transcription initiation at specific promoters, such as the Sγ3/Sγ1 switch regions of the *Igh* locus (Daniel et al., 2010) (Figure S3A). To determine whether transcription of DDR genes is altered by PTIP ablation, we profiled the transcriptome of WT and *PTIP*$^{-/-}$ B cells. Overall, there were 471 RefSeq annotated genes that were deregulated by more than 5-fold in *PTIP*$^{-/-}$ versus WT (Figure S3B). However, HR and NHEJ DNA damage response genes were not among deregulated pathways (Figures S3B and S3C). This suggests that the functions of PTIP in suppressing HR might be unrelated to its role in transcriptional regulation.

To determine whether PTIP recruitment to DSBs is essential for its effects on HR, we made use of a point mutation in the BRCT domain 3 (W663R) of PTIP that selectively blocks its interaction with 53BP1 (Gong et al., 2009; Munoz et al., 2007) and is unable to form foci (Figure S4A) (Daniel et al., 2010) but retains PTIP association with the MLL3/4 complex, which is dependent on BRCT (domains 5 and 6) (Patel et al., 2007). *BRCA1*$^{-/-}$ *PTIP*$^{-/-}$ B cells were infected with PTIP^{WT} and PTIP^{W663R} encoding retroviruses, treated with PARPi, and monitored for chromosomal damage (Figures 5F and S4B). Whereas PTIP^{WT} expression in *BRCA1*$^{-/-}$*PTIP*$^{-/-}$ cells led to an increase in the number of chromosomal radials relative to uninfected cells, *BRCA1*$^{-/-}$*PTIP*$^{-/-}$ cells transduced with PTIP^{W663R} remained insensitive (Figures 5F and S4B). Thus, PTIP recruitment to DSBs is necessary to block HR in BRCA1-deficient cells.

Recruitment of PTIP to DSBs Is Dependent on the Eight Most N-Terminal S/TQ Phosphorylation Sites of 53BP1

To explore the mechanism of PTIP recruitment to DSBs, we expressed FLAG-tagged PTIP in WT, *53BP1*$^{-/-}$, and *ATM*$^{-/-}$ MEFs and irradiated them with 10 Gy (Figure 6A). Although PTIP ionizing-irradiation-induced foci (IRIF) were detectable in nearly all WT cells, PTIP IRIF formation was impaired in the absence of 53BP1 or ATM (Figure 6A). Measurements of colocalization coefficients of γ-H2AX (a marker of the DNA breaks) with PTIP in irradiated WT, *53BP1*$^{-/-}$, and *ATM*$^{-/-}$ MEFs revealed that 80% of γ-H2AX foci in WT cells contained PTIP, whereas less than 15% and 10% of γ-H2AX foci in the *53BP1*$^{-/-}$ and *ATM*$^{-/-}$ cells, respectively, contained PTIP. Consistent with these findings, PTIP IRIF was highly sensitive to pharmacological inhibition of ATM (ATMi), less sensitive to ATRi treatment, and insensitive to DNA-PKi. (Figure S5). These findings contrast with previous reports suggesting that PTIP, 53BP1, and ATM are independently recruited to DSBs (Gong et al., 2009; Jowsey et al., 2004; Munoz et al., 2007). Because available PTIP antibodies are unable to detect endogenous PTIP foci, we used laser microirradiation to generate DSBs in WT, *53BP1*$^{-/-}$, and *ATM*$^{-/-}$ MEFs. In WT cells, PTIP was recruited to laser scissors-induced DSBs, which colocalized with γ-H2AX (Figure 6B). Consistent with our analysis of IRIF, PTIP recruitment to DNA damage sites was 53BP1 and ATM dependent (Figure 6B). Moreover, PTIP failed to be recruited to DSBs in *53BP1*$^{-/-}$ MEFs reconstituted with a mutant protein lacking all 28 N-terminal S/TQ phosphorylation sites of 53BP1, 53BP1^{28A} (Figure 6B). We conclude that ATM-dependent phosphorylation of 53BP1 is necessary for PTIP recruitment to DSBs.

Given that RIF1 is also recruited to DSBs in a 53BP1- and ATM-dependent manner (Chapman et al., 2013; Di Virgilio et al., 2013; Escribano-Díaz et al., 2013; Feng et al., 2013; Silverman et al., 2004; Zimmermann et al., 2013), we next monitored the codependency of PTIP and RIF1 for localization to DNA damage foci (Figure 6C). We found that 82% of PTIP IRIF colocalized

Figure 2. Response of PTIP to Different DNA Damaging Agents

(A) *53BP1*$^{-/-}$ B cells were reconstituted with empty vector, 53BP1^{DB}, 53BP1^{8A}, or 53BP1^{28A} retroviruses that were FLAG-tagged. Cells were irradiated (10 Gy, 45 min recovery) and immunoprecipitation was performed with anti-FLAG antibodies. Western blot analysis of PTIP and FLAG are shown for input (left) and immunoprecipitated protein (right).

(B) Isogenic immortalized WT and *PTIP*$^{-/-}$ MEFs were either untreated or treated with irradiation (IR, 2 Gy), cisplatin (CisPt, 0.5 μM), camptothecin (CPT, 10 nM) or PARP inhibitor (PARPi, 1 μM) and chromosomal aberrations (chromatid breaks, chromosome breaks, and radials) were quantified in at least 50 metaphase spreads for each genotype and each treatment. Data from an independent experiment is shown in Figure S2B.

(C) WT (green lines) and *PTIP*$^{-/-}$ (blue line) MEFs were treated with different doses of the above drugs, and colony formation was quantified relative to colonies formed in untreated cells from the same genotype. An experiment performed in parallel demonstrated that 1 μM PARPi treatment is toxic for BRCA1 mutant MEFs (red line).

See also Figure S2.

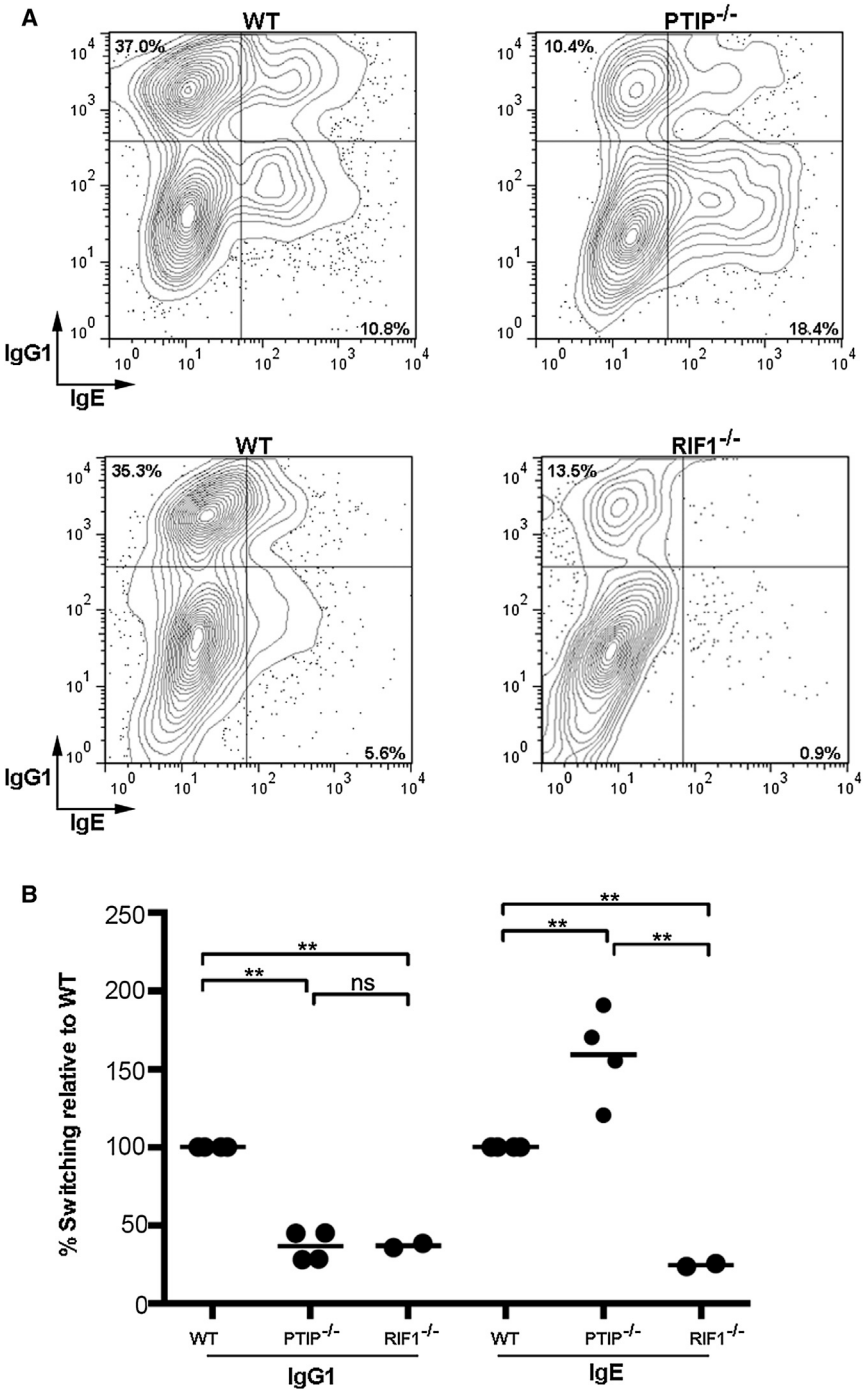

Figure 3. PTIP Is Dispensable for CSR to IgE

PTIP$^{f/f}$*CD19*^{CRE} (*PTIP*$^{-/-}$), (*Rif1*$^{f/f}$*CD19*^{CRE}) *RIF1*$^{-/-}$ and littermate WT B cells were stimulated with αCD40 plus IL-4 and analyzed for IgG1 and IgE CSR on day 5.

(A) Representative flow cytometry plots. The percentages of IgG1 switched cells (upper-left quadrant) and IgE switched cells (lower-right quadrant) is indicated.

(B) Dot plot indicates IgG1 and IgE CSR in *PTIP*$^{-/-}$ and *RIF1*$^{-/-}$ as a percentage of the WT value in the same experiment. **p < 0.01 (two-tailed unpaired t test); ns: not significant.

with RIF1 foci and 78% of RIF1 colocalized with PTIP foci (Figure 6C, n > 800 foci). However, RIF1 was recruited to DNA damage sites in *PTIP*$^{-/-}$ MEFs (Figure 6D) and vice versa (Figure 6E). Thus, RIF1 and PTIP are independently recruited to IRIF in a phospho-53BP1-dependent manner.

To further define the residues required for recruitment to phospho-53BP1, we examined PTIP and RIF1 recruitment in 53BP1^{DB}, 53BP1^{8A}, and 53BP1^{7A} mutant MEFs (Figures 2A and S2A). Whereas expression of 53BP1^{DB} in *53BP1*$^{-/-}$ MEFs reconstituted PTIP IRIF (Figures 7A and S6A), PTIP recruitment to DSBs was abrogated in 53BP1^{8A} MEFs (Figures 7A and S6A). By contrast, RIF1 recruitment was independent of these eight most N terminus phosphorylation sites on 53BP1, partially dependent on the seven S/TQ phosphorylation sites C terminus to 53BP1^{8A}, and abrogated in 53BP1^{15A} mutant cells that lack all 8S/TQ and 7S/TQ phosphorylation sites (Figures 7A–7C and S6B). Thus, PTIP and RIF1 exhibit distinct phosphorylation-dependent interactions with 53BP1 that guide them to DSBs. The association of PTIP with the 8S/TQ sites on 53BP1 upon DNA damage (Figures 2A, 7, and S6A) likely explains why loss of PTIP phenocopies 53BP1^{8A} with respect to CSR, irradiation sensitivity, and reversal of genome instability in BRCA1-deficient cells.

DISCUSSION

Regulation of DSB Repair Choice

53BP1 and BRCA1 play a critical role in channeling DSBs into either NHEJ or HR. 53BP1 promotes NHEJ in G1 by tethering DSBs together and by protecting these ends from exonuclease processing (Bothmer et al., 2010; Difilippantonio et al., 2008). In S phase, the inhibitory effect of 53BP1 on resection is antagonized by BRCA1 (Bouwman et al., 2010; Bunting et al., 2010). Loss of BRCA1 results in a shift toward a mutagenic NHEJ pathway that results in chromosomal abnormalities, tumorigenesis, and embryonic lethality, but all of these phenotypes are relieved by 53BP1 deletion (Bouwman et al., 2010; Bunting et al., 2010; Cao et al., 2009). In contrast, loss of classical NHEJ proteins (e.g., Ku, Ligase IV, DNA-PKcs) does not overcome the HR defects associated with BRCA1 deficiency (Bunting et al., 2012; Bunting et al., 2010), perhaps because these factors play a more limited role

in repressing 5′-3′ resection (Bunting et al., 2012; Sfeir and de Lange, 2012). Despite the striking rescue of BRCA1 deficiency, disrupting 53BP1 does not reverse the DNA repair defects associated with downstream mediators of the HR reaction (e.g., XRCC2, BRCA2, or PALB2) (Bouwman et al., 2010; Bowman-Colin et al., 2013; Bunting et al., 2010). Thus, 53BP1 and BRCA1 oppose each other during critical initial stages of DSB repair before commitment to repair the ends by NHEJ or HR.

Mechanism of PTIP and RIF1 Association with 53BP1

The molecular events that are required for 53BP1 to promote the ligation of DNA ends during CSR and the aberrant chromosomal rearrangements in BRCA1 mutant cells were previously thought to be identical. Surprisingly our data suggest that the pro-NHEJ and anti-HR functions of 53BP1 are in fact distinct and separable activities that nevertheless require 53BP1 phosphorylation. These complementary aspects of 53BP1's activities are mediated by the independent recruitment of RIF1 and PTIP, respectively, to phosphorylated 53BP1.

PTIP contains BRCT domains that interact directly with phosphorylated 53BP1 (Manke et al., 2003; Munoz et al., 2007). In contrast, RIF1 does not contain a known phosphorecognition motif, and it remains unclear how ATM-dependent phosphorylation facilitates RIF1 association with 53BP1. RIF1 may associate with 53BP1 directly or through interactions with effector molecules that contain BRCT phosphobinding modules (Figure 7D). Based on the observation that there is no detectable defect in RIF1 foci in 53BP1^{8A} cells (Figures 7A and S6B), we suspected that a major RIF1-interaction motif would reside C terminus of the 8S/TQ PTIP interaction sites. Consistent with this, the 53BP1^{7A} C-terminal mutant exhibits a reduction in RIF1 IRIF (Figures 7A–7C) and CSR (Bothmer et al., 2011). RIF1 IRIF and CSR are further reduced in 53BP1^{15A} mutant cells that lack 8S/TQ and 7S/TQ sites (Figures 7A and 7B) (Bothmer et al., 2011), suggesting that both regions contribute to RIF1 interactions with 53BP1 (Figure 7D). If so, we would predict some degree of competition between PTIP and RIF1 binding to 53BP1. Consistent with this, we have found an increased association between PTIP and 53BP1 in response to DNA damage in RIF1-deficient cells (Figure S6C). Thus, distinct from PTIP, RIF1 association with 53BP1 occurs via multidomain interactions (Figure 7D).

Role of PTIP and RIF1 in DSB Resection

Deletion of either PTIP or RIF1 leads to increased resection (Figure 5E) (Chapman et al., 2013; Di Virgilio et al., 2013; Escribano-Díaz et al., 2013; Feng et al., 2013; Zimmermann et al., 2013). However, whereas PTIP ablation rescues HR in BRCA1-deficient cells and is largely dispensable for NHEJ during CSR, RIF1 is essential for CSR and only partially contributes to the HR defects in BRCA1-deficient cells (Di Virgilio et al., 2013; Escribano-Díaz et al., 2013; Feng et al., 2013; Zimmermann et al., 2013). How can these observations be reconciled? One possibility is that distinct S/TQ kinase target sites in 53BP1 are phosphorylated during CSR in G1 and during replication fork collapse in S, resulting in independent recruitment of the two factors to DNA ends in distinct phases of the cell cycle. Consistent with this idea, it was reported that the localization of RIF1 to DSBs is mainly restricted to G1 and is suppressed by BRCA1 in S/G2 (Chapman et al., 2013; Escribano-Díaz et al., 2013; Feng et al., 2013). However, our finding that PTIP and RIF1 colocalize in the majority of irradiated cells and that both proteins form IRIF during G1 and S/G2 (Figure S7) indicates that PTIP and RIF1 are not recruited to DSBs in distinct cell-cycle phases.

Another possibility is that PTIP and RIF1 sites on 53BP1 are equally phosphorylated during the cell cycle but that these proteins might make the DSB-proximal chromatin refractory to a distinct set of nucleases. For example, initial DNA end resection is mediated by MRE11/RAD50/NBS1 and CTIP, whereas DNA2, EXO1, and BLM carry out more extensive resection (Symington and Gautier, 2011), and RIF1 appears to be involved in protection against initial but not sustained resection (Feng et al., 2013). In this model, the level of resection supported by loss of RIF1 would be insufficient for complete rescue of HR in *BRCA1*-deficient cells, which might require more extensive 3′ single-strand tails. In contrast, ablation of PTIP supports the sustained resection required for the rescue of HR in *BRCA1*-deficient cells. Thus, RIF1 and PTIP may block different steps in resection or distinct nucleases that mediate HR.

Role of PTIP and RIF1 in Telomeric End-Joining

Depending on the nature of the break, RIF1 and PTIP might cooperate to promote NHEJ. For example, PTIP and RIF1 deficiency both result in IR sensitivity (Figures 2B and 2C) (Feng et al., 2013), and defective NHEJ of dysfunctional telomeres (Figure 4) (Chapman et al., 2013; Zimmermann et al., 2013). It has been demonstrated that 53BP1 has RIF1-independent roles in promoting telomeric end-joining, evidenced by the considerably higher frequency of telomeric fusions in *RIF1*$^{-/-}$*TRF2*$^{-/-}$ versus *53BP1*$^{-/-}$*TRF2*$^{-/-}$ or *53BP1*^{28A}*TRF2*$^{-/-}$ MEFs (Lottersberger et al., 2013; Zimmermann et al., 2013). This RIF1-independent but phospho-53BP1-dependent function at telomeres has been linked to the induction of chromosome mobility (Zimmermann et al., 2013), which increases the probability that DNA ends fuse. Because PTIP binds to DSBs in a 53BP1-dependent but RIF1-independent manner, it is possible that this 53BP1-dependent/RIF1-independent increase in telomere mobility is mediated by PTIP.

Implications for Cancer Therapy

The identification of separation of function mutations that selectively disrupt antirecombination functions of 53BP1 during replication fork collapse and CSR may open up new therapeutic opportunities. Breast cancers arising in BRCA1 mutation carriers frequently show low levels of 53BP1 expression (Bouwman et al., 2010), which might result in resistance to PARPi therapy, a promising strategy for treating HR-deficient tumors (Bryant et al., 2005; Farmer et al., 2005). Consistent with this, 53BP1 was lost in a fraction of BRCA1-deficient mouse mammary tumors that acquired PARPi resistance in vivo (Jaspers et al., 2013). Interestingly, a fraction of PARPi-resistant tumors restored HR yet did not lose 53BP1. We speculate that PTIP mutation might emerge as a novel causal factor in PARPi resistance of BRCA1-deficient mammary tumors that restore HR. With respect to intervention, our study also suggests that it might be possible to increase HR in BRCA1 heterozygous carriers

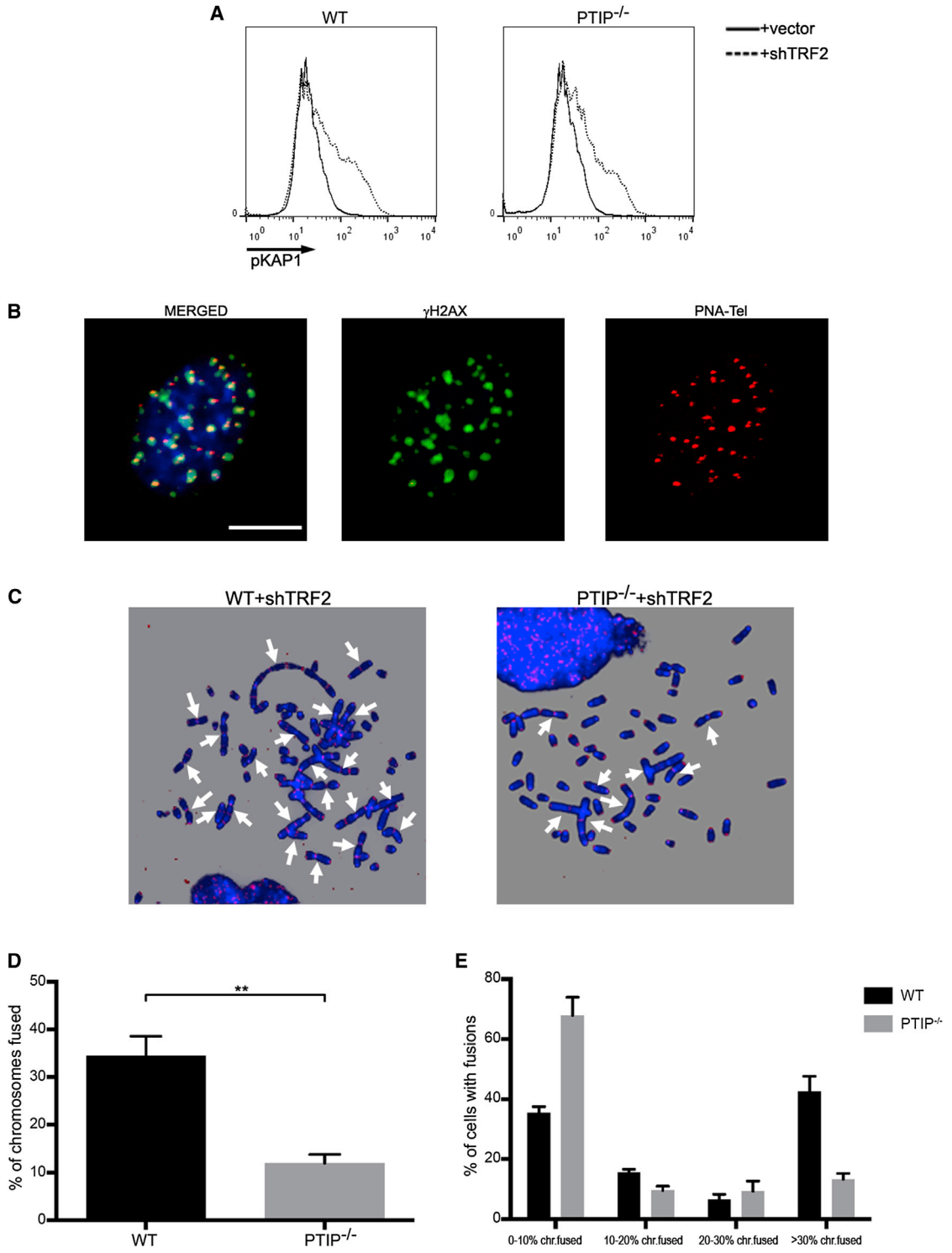

Figure 4. PTIP Is Required for NHEJ of Dysfunctional Telomeres

(A) WT and *PTIP*$^{-/-}$ MEFs were infected with a retrovirus expressing either an empty vector or shRNA against TRF2 (shTRF2), and phosphorylated KAP1 (pKAP1) levels were measured by flow cytometry.

(B) γ-H2AX (green) in telomere-dysfunction-induced foci (TIF) generated in shTRF2-infected WT cells. PNA probe is shown in red, and images are merged on top of DAPI (blue). Scale bar, 10 μm.

(C) Representative images of a metaphase spread from WT and *PTIP*$^{-/-}$ MEFs infected with shTRF2. Telomere fusions are visualized by a telomeric PNA probe (red) and DAPI (blue). Arrows point to representative telomeric fusions.

(legend continued on next page)

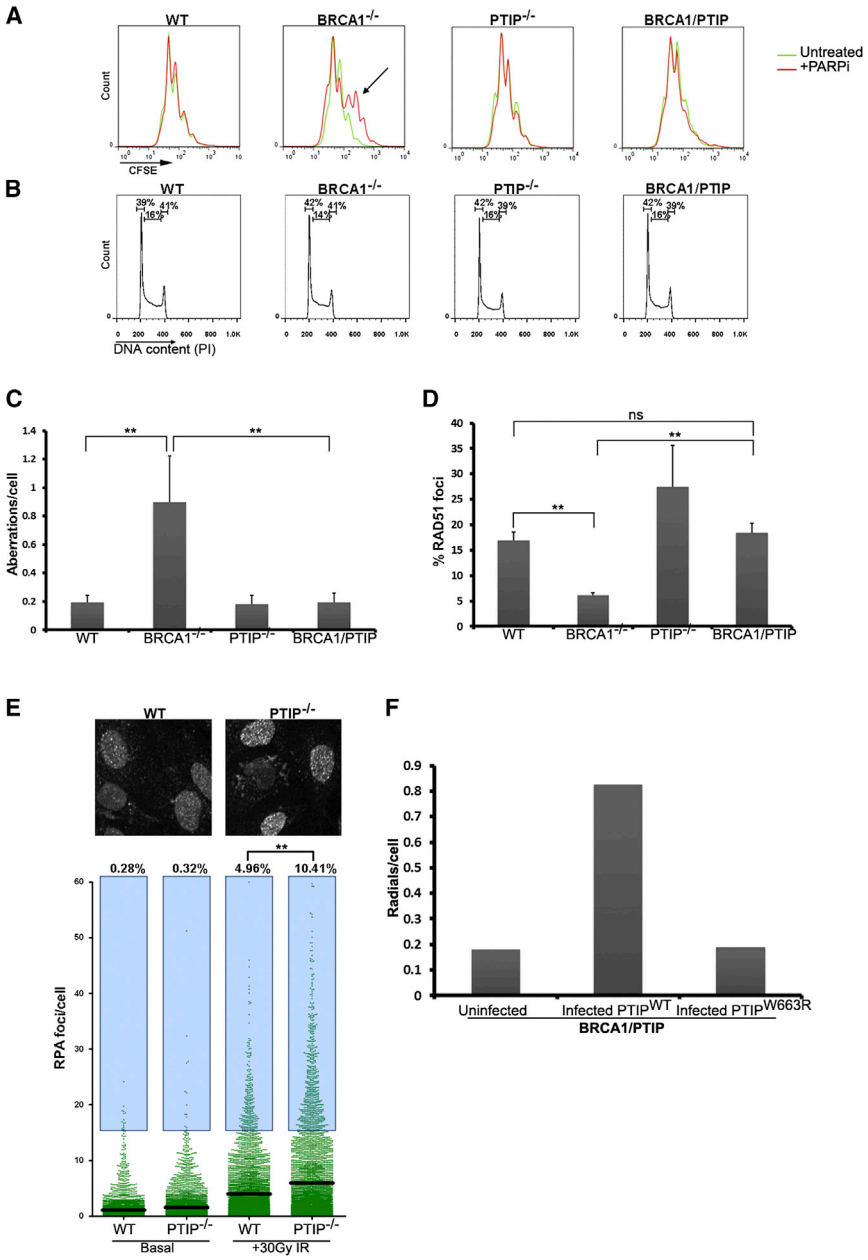

Figure 5. Ablation of PTIP Rescues Homologous Recombination in BRCA1-Deficient Cells

(A) WT, *BRCA1*$^{-/-}$, *PTIP*$^{-/-}$, and *BRCA1*$^{-/-}$ *PTIP*$^{-/-}$ B cells were pulsed with CFSE and stimulated with (red) or without (green) PARPi. CFSE signal diminishes with increasing division. *BRCA1*$^{-/-}$ cells are sensitive to PARPi (arrow indicates sluggish cells) but loss of PTIP in BRCA1-deficient cells rescues the proliferation defect.

(B) WT, *BRCA1*$^{-/-}$, *PTIP*$^{-/-}$, and *BRCA1*$^{-/-}$ *PTIP*$^{-/-}$ B cells were stimulated with LPS+IL4 and cell-cycle distribution was monitored by propidum iodide (PI) staining. Percentage of cells in G1, S, and G2/M is indicated.

(C) Analysis of genomic instability (radial chromosomes, chromatid breaks, and chromosome breaks) in metaphases from B cells treated with 1 μM PARPi. At least 50 metaphases were analyzed for each genotype.

(D) B cells were stimulated for 2 days, irradiated with 10 Gy, and the percentage of cells with immunofluorescent RAD51 foci were quantified (at least 400 cells counted for each genotype).

Data in (B) and (C) represent mean of three experiments ± standard deviations. **p < 0.05 (two-tailed unpaired t test), ns, not significant.

(E) High-throughput microscopy quantification of RPA foci per cell in WT and *PTIP*$^{-/-}$ MEFs that were either untreated or treated with 30 Gy IR. Top: representative image of chromatin bound RPA in irradiated WT and *PTIP*$^{-/-}$ cells. Bottom: quantitation of RPA foci. Bar indicates the mean number of RPA foci per cell, and the blue box designates cells with more than 15 foci, whose percentage is indicated above each box. **p < 0.001.

(F) *BRCA1*$^{-/-}$*PTIP*$^{-/-}$ B cells were reconstituted with PTIP^{WT} or PTIP^{W663R} retroviruses (expressing a GFP marker driven by an internal ribosome entry site) and treated with PARPi. Cells were sorted (GFP^{positive} = infected and GFP^{negative} = uninfected) and metaphases were analyzed for radial chromosomes (n = 50 metaphases analyzed in each case).

See also Figures S3 and S4.

without compromising B cell immunoglobulin class switching by inhibiting the recruitment of PTIP to DSBs.

EXPERIMENTAL PROCEDURES

Mice, MEFs, B Cell Culture, and Infections

53BP1$^{-/-}$ (Ward et al., 2004), *BRCA1*$^{f(\Delta 11)/f(\Delta 11)}$ (NCI mouse repository), *RIF1*$^{f/f}$ (Buonomo et al., 2009; Di Virgilio et al., 2013), and *PTIP*$^{f/f}$ (Daniel et al., 2010) mice have been described. Resting splenic B cells were isolated from 8- to 12-week-old WT or mutant spleen with anti-CD43 microbeads (anti-Ly48; Miltenyi Biotech) and were cultured with LPS (25 μg/ml; Sigma) and IL-4 (5 ng/ml; Sigma) or αCD40 (1 μg/ml; eBiosciences) and IL4 as described (Barlow et al., 2013; Wesemann et al., 2011). WT, 53BP1$^{-/-}$, and ATM$^{-/-}$ MEFs were immortalized by SV40. SV40T immortalized *PTIP*$^{f/f}$ (Cho et al., 2009) and *RIF1*$^{f/f}$ MEFs were infected with CRE viruses to delete PTIP and RIF1, respectively. PMX-PIE-based retroviruses encoding 53BP1^{DB} and 53BP1^{8A} were previously described (Bothmer et al., 2011). Coding sequences

(D) Quantitation of telomeric fusion frequencies. At least 1,800 chromosomes from each genotype were analyzed. Mean value derived from three independent experiments. **p < 0.01 (two-tailed unpaired t test). Error bars represent SEM.

(E) Distribution of telomeric fusions per metaphase in WT and *PTIP*$^{-/-}$ MEFs. At least 30 cells were examined in each of three independent experiments. p(chi-square) < 1 × 10^{-5}. Error bars represent SEM.

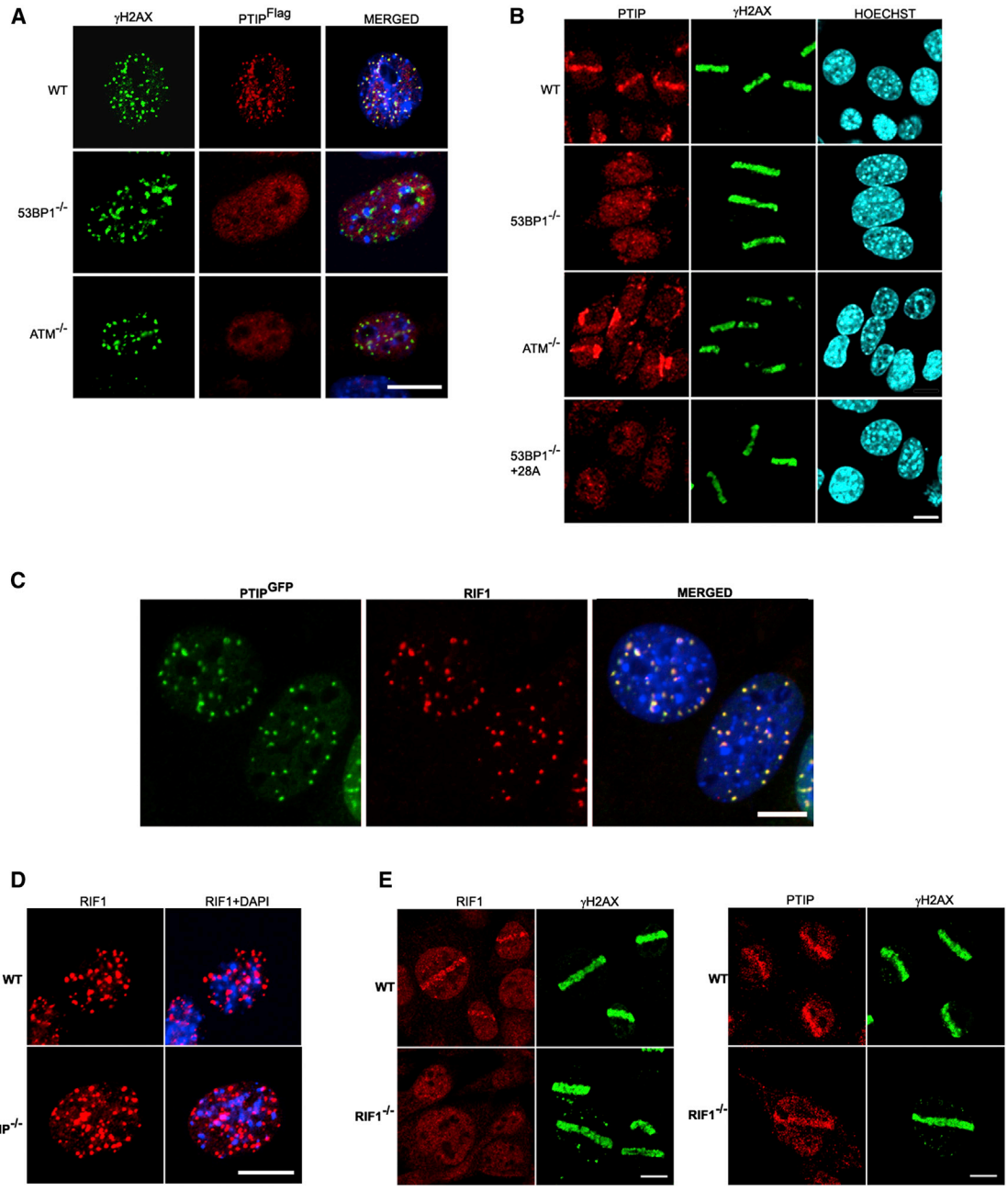

Figure 6. Recruitment of PTIP to DSBs Is ATM and Phospho-53BP1-Dependent but RIF1-Independent

(A) WT, *53BP1*$^{-/-}$, and *ATM*$^{-/-}$ MEFs were infected with a FLAG-tagged WT PTIP retrovirus. Cells were irradiated with 10 Gy, and FLAG (red) IRIF together with γ-H2AX (green) were assessed 4 hr post-IR. DAPI is indicated in blue.

(B) WT, *53BP1*$^{-/-}$, *ATM*$^{-/-}$, and *53BP1*$^{-/-}$ MEFs reconstituted with 53BP1^{28A} were treated with Hoecsht 33342 and then irradiated with a 364 nm laser line. Cells were allowed to recover for 15 min before processing for immunfluorescence analysis of PTIP and γ-H2AX. Hoechst counterstain is indicated in blue.

(C) Cells expressing GFP-PTIP were irradiated with 10 Gy, and PTIP^{GFP} (green) and RIF1 (red) IRIF were assessed 4 hr later. A representative image is shown; 82% of PTIP IRIF colocalized with RIF1 foci and 78% of RIF1 colocalized with PTIP foci (n ≥ 800 foci examined; cells had on average 28 foci).

(D) RIF1 IRIF (red) in irradiated WT and *PTIP*$^{-/-}$ MEFs.

(E) RIF1 (red) and PTIP (red) recruitment to laser scissors damage in WT and *RIF1*$^{-/-}$ MEFs. Damaged cells are indicated by γ-H2AX tracks (green). Scale bars, 10 μm.

See also Figure S5.

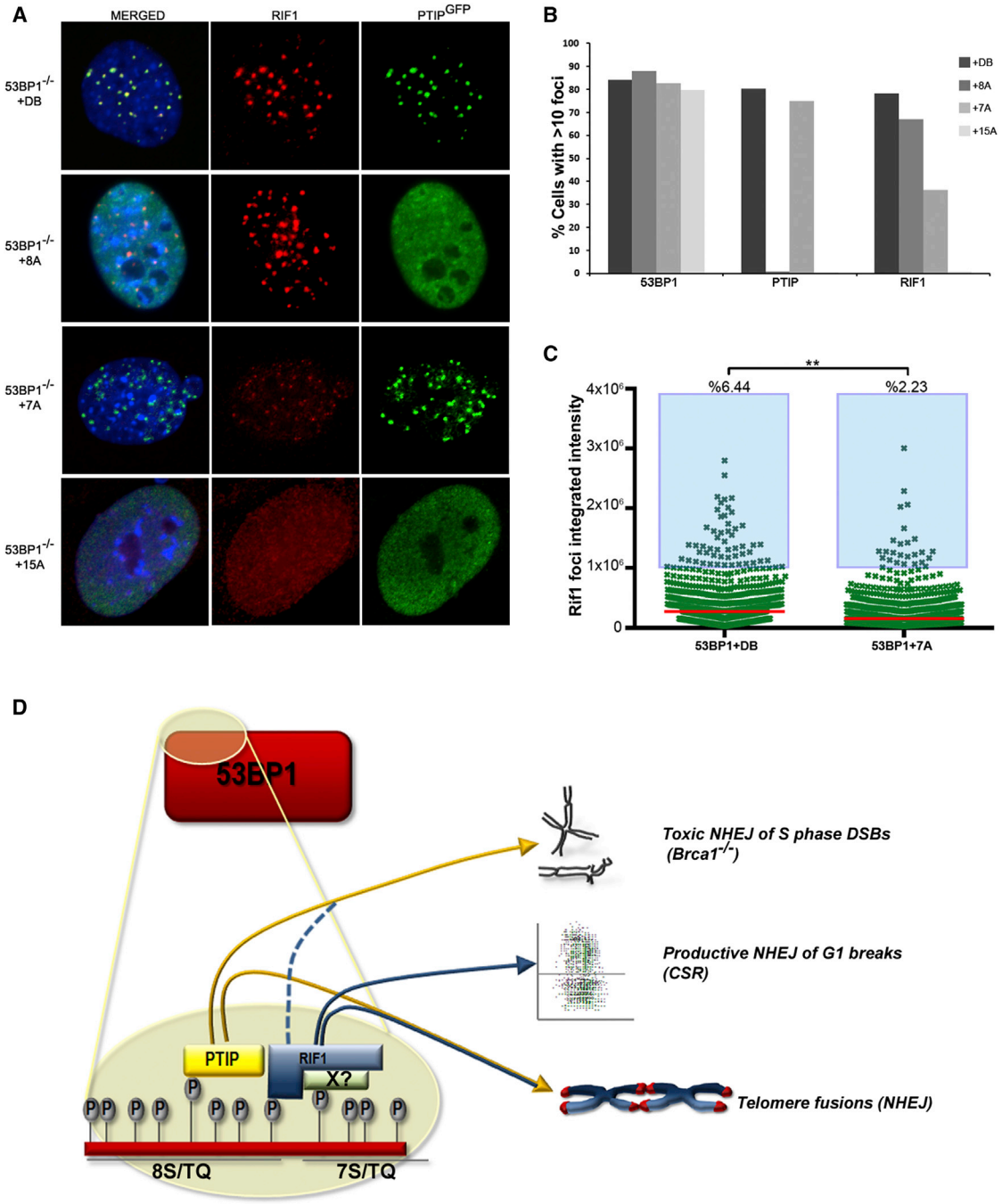

Figure 7. PTIP and RIF1 Association with DSBs Is Dependent on Distinct Phosphorylation Sites on 53BP1

(A) *53BP1*$^{-/-}$ MEFs (reconstituted with 53BP1^{DB}, 53BP1^{8A}, 53BP1^{7A}, or 53BP1^{15A}) were costained with RIF1 (red) and PTIP (green).

(B) Quantitation of percent 53BP1^{DB}, 53BP1^{8A}, 53BP1^{7A}, or 53BP1^{15A} cells with greater than ten 53BP1, PTIP, or RIF1 foci. At least 100 cells were analyzed for each genotype.

(C) Integrated intensity of individual RIF1 IRIF in *53BP1*$^{-/-}$ MEFs reconstituted with DB or 7A. Average RIF1 foci intensity (red line) is 1.6-fold greater in DB versus 7A (**$p < 0.001$, one-tailed unpaired t test), and a greater percentage of very intense foci (z score > 3) are generated in 53BP1^{DB} compared to 53BP1^{7A} (blue box).

(D) Model for regulation of 53BP1 pro-NHEJ and anti-HR activities by distinct phosphointeractions with RIF1 and PTIP, respectively. PTIP binds to the 8S/TQ sites. RIF1 recruitment is largely dependent on C-terminal 7S/TQ sites, but RIF1 may also be stabilized by interactions with 8S/TQ. An unknown factor (X) may bind directly to phosphorylated 53BP1 and mediate RIF1 recruitment, whereas PTIP interaction with 53BP1 is direct (Munoz et al., 2007).

See also Figures S6 and S7.

for mouse PTIP^{WT}/PTIP^{W663R} and PTIP-GFP were cloned into the PMX-IRES-GFP and MIG-IRES-mCherry retroviral vectors, respectively. PARP (KU58948), ATM (Ku55933), and DNA-PK (NU7026) inhibitors were obtained from Astra Zeneca and ATRi has recently been described (Toledo et al., 2011).

Flow Cytometry, Metaphase Analysis, and Telomere FISH

For FACs analysis, splenic B cells were stained with fluorochrome-conjugated anti-B220, anti-igG1, and anti-igE antibodies (PharMingen) as described (Wesemann et al., 2011). Carboxyfluorescein succinimidyl esther (CFSE) labeling was performed to track cell division. Samples were acquired on a FACSCalibur (Becton Dickinson), and cell sorting was preformed on a FACsAria (Becton Dickinson). Cells were harvested for metaphase analysis as described (Callén et al., 2007a). The murine TRF2 shRNA-targeting construct and MEF retroviral infection have been described (Rai et al., 2010). Telomere-induced foci were visualized by hybrization with anti-mouse γ-H2AX antibody (Upstate Biotechnology) together with PNA probe (Applied Biosystems). Phosphorylated Kap-1 was detected by flow cytometry after intracellular staining using the BD Cytofix/Cytoperm kit (BD Biosciences).

DNA Damage, Laser Microirradiation, Immunoprecipitation, and RNA-Sequencing

Cells were treated with different DNA damaging agents (IR, CPT, CisPt, and PARPi), and colony survival was assessed after 14 days, or metaphase analysis was performed 24 hr after treatment. For immunofluorescent staining, cells were irradiated with indicated doses of ionizing radiation, allowed to recover, and then fixed and processed as described (Celeste et al., 2003). For microirradiation, cells were presensitized in DMEM media containing 0.1 μg/ml of Hoechst 33342 for 60 min before replacing with phenol red free media containing 5 mM HEPES, and then irradiated with the 364 nm laser line on a LSM510 confocal microscope (Zeiss) equipped with a heated stage. Cells were allowed to recover for 15 min prior to processing for immunofluorescence. Analysis of RPA foci was performed using an Opera High-Content Screening system as described (López-Contreras et al., 2012). Primary antibodies for immunofluorescence were rabbit anti-53BP1 (Novus), mouse anti-γ-H2AX (Upstate Biotechnology), mouse or rabbit anti-FLAG-M2 (Sigma), mouse anti-AIM1 (Becton Dickinson), mouse anti-GFP (Roche), rabbit anti-RAD51 (Santa Cruz), rat anti-RPA (Cell Signaling), rabbit-anti-PTIP (Cho et al., 2009), and rabbit-anti-RIF1(Di Virgilio et al., 2013). DNA was counterstained with DAPI. For immunoprecipitation, primary *53BP1*$^{-/-}$ B cells were infected with retroviral constructs. Ninety-six hours postactivation, cells were irradiated (10 Gy), left to recover for 45 min, and collected by centrifugation. Cells were lysed, sonicated, and cell lysates were incubated with magnetic beads (M-270 epoxy beads, Invitrogen) conjugated with anti-Flag M2 antibody (Di Virgilio et al., 2013). 53BP1-associated proteins were eluted by incubation in NuPAGE LDS sample buffer (Invitrogen) supplemented with 45 mM DTT for 10 min at 72°C. For RNA sequencing, reads from each cDNA library were mapped onto the Build 37 assembly of the National Center for Biotechnology Information mouse genome data (July 2007; NCBI37/mm9) using TopHat. Bioconductor (Gentleman et al., 2004) was used to calculate the RPKM (reads per kilobase exon model per million mapped reads) of the RefSeq annotated genes.

SUPPLEMENTAL INFORMATION

Supplemental Information includes seven figures and can be found with this article online at http://dx.doi.org/10.1016/j.cell.2013.05.023.

ACKNOWLEDGMENTS

We thank all members of the A. Nussenzweig lab and Davide Robbiani for discussions; Titia de Lange for RIF1f/f mice; Susan Sharrow for flow cytometry; and Sandy Chang for the TRF2 shRNA construct. M.C.N., F.W.A and O.F.-C. are HHMI investigators. D.R.W. was supported by NIH grants AI89972, the American Association of Allergy Asthma and Immunology and CSL Behring, and a Career Award for Medical Scientists (Burroughs Wellcome Fund). This work was supported by the Intramural Research Program of the NIH, the National Cancer Institute, and the Center for Cancer Research, and by a Department of Defense grant to A.N. (BC102335).

Received: March 20, 2013
Revised: April 9, 2013
Accepted: May 10, 2013
Published: May 30, 2013

REFERENCES

Barlow, J.H., Faryabi, R.B., Callén, E., Wong, N., Malhowski, A., Chen, H.T., Gutierrez-Cruz, G., Sun, H.W., McKinnon, P., Wright, G., et al. (2013). Identification of early replicating fragile sites that contribute to genome instability. Cell *152*, 620–632.

Bhattacharyya, A., Ear, U.S., Koller, B.H., Weichselbaum, R.R., and Bishop, D.K. (2000). The breast cancer susceptibility gene BRCA1 is required for subnuclear assembly of Rad51 and survival following treatment with the DNA cross-linking agent cisplatin. J. Biol. Chem. *275*, 23899–23903.

Boboila, C., Jankovic, M., Yan, C.T., Wang, J.H., Wesemann, D.R., Zhang, T., Fazeli, A., Feldman, L., Nussenzweig, A., Nussenzweig, M., and Alt, F.W. (2010). Alternative end-joining catalyzes robust IgH locus deletions and translocations in the combined absence of ligase 4 and Ku70. Proc. Natl. Acad. Sci. USA *107*, 3034–3039.

Bothmer, A., Robbiani, D.F., Feldhahn, N., Gazumyan, A., Nussenzweig, A., and Nussenzweig, M.C. (2010). 53BP1 regulates DNA resection and the choice between classical and alternative end joining during class switch recombination. J. Exp. Med. *207*, 855–865.

Bothmer, A., Robbiani, D.F., Di Virgilio, M., Bunting, S.F., Klein, I.A., Feldhahn, N., Barlow, J., Chen, H.T., Bosque, D., Callen, E., et al. (2011). Regulation of DNA end joining, resection, and immunoglobulin class switch recombination by 53BP1. Mol. Cell *42*, 319–329.

Bouwman, P., Aly, A., Escandell, J.M., Pieterse, M., Bartkova, J., van der Gulden, H., Hiddingh, S., Thanasoula, M., Kulkarni, A., Yang, Q., et al. (2010). 53BP1 loss rescues BRCA1 deficiency and is associated with triple-negative and BRCA-mutated breast cancers. Nat. Struct. Mol. Biol. *17*, 688–695.

Bowman-Colin, C., Xia, B., Bunting, S., Klijn, C., Drost, R., Bouwman, P., Fineman, L., Chen, X., Culhane, A.C., Cai, H., et al. (2013). Palb2 synergizes with Trp53 to suppress mammary tumor formation in a model of inherited breast cancer. Proc. Natl. Acad. Sci. USA. Published online May 8, 2013. http://dx.doi.org/10.1073/pnas.1305362110.

Bryant, H.E., Schultz, N., Thomas, H.D., Parker, K.M., Flower, D., Lopez, E., Kyle, S., Meuth, M., Curtin, N.J., and Helleday, T. (2005). Specific killing of BRCA2-deficient tumours with inhibitors of poly(ADP-ribose) polymerase. Nature *434*, 913–917.

Bunting, S.F., Callén, E., Wong, N., Chen, H.T., Polato, F., Gunn, A., Bothmer, A., Feldhahn, N., Fernandez-Capetillo, O., Cao, L., et al. (2010). 53BP1 inhibits homologous recombination in Brca1-deficient cells by blocking resection of DNA breaks. Cell *141*, 243–254.

Bunting, S.F., Callén, E., Kozak, M.L., Kim, J.M., Wong, N., López-Contreras, A.J., Ludwig, T., Baer, R., Faryabi, R.B., Malhowski, A., et al. (2012). BRCA1 functions independently of homologous recombination in DNA interstrand crosslink repair. Mol. Cell *46*, 125–135.

Buonomo, S.B., Wu, Y., Ferguson, D., and de Lange, T. (2009). Mammalian Rif1 contributes to replication stress survival and homology-directed repair. J. Cell Biol. *187*, 385–398.

Callén, E., Jankovic, M., Difilippantonio, S., Daniel, J.A., Chen, H.T., Celeste, A., Pellegrini, M., McBride, K., Wangsa, D., Bredemeyer, A.L., et al. (2007a). ATM prevents the persistence and propagation of chromosome breaks in lymphocytes. Cell *130*, 63–75.

Callén, E., Nussenzweig, M.C., and Nussenzweig, A. (2007b). Breaking down cell cycle checkpoints and DNA repair during antigen receptor gene assembly. Oncogene *26*, 7759–7764.

Callen, E., Faryabi, R.B., Luckey, M., Hao, B., Daniel, J.A., Yang, W., Sun, H.W., Dressler, G., Peng, W., Chi, H., et al. (2012). The DNA damage- and transcription-associated protein paxip1 controls thymocyte development and emigration. Immunity *37*, 971–985.

Cao, L., Xu, X., Bunting, S.F., Liu, J., Wang, R.H., Cao, L.L., Wu, J.J., Peng, T.N., Chen, J., Nussenzweig, A., et al. (2009). A selective requirement for 53BP1 in the biological response to genomic instability induced by Brca1 deficiency. Mol. Cell *35*, 534–541.

Celeste, A., Fernandez-Capetillo, O., Kruhlak, M.J., Pilch, D.R., Staudt, D.W., Lee, A., Bonner, R.F., Bonner, W.M., and Nussenzweig, A. (2003). Histone H2AX phosphorylation is dispensable for the initial recognition of DNA breaks. Nat. Cell Biol. *5*, 675–679.

Celli, G.B., Denchi, E.L., and de Lange, T. (2006). Ku70 stimulates fusion of dysfunctional telomeres yet protects chromosome ends from homologous recombination. Nat. Cell Biol. *8*, 885–890.

Chapman, J.R., Barral, P., Vannier, J.B., Borel, V., Steger, M., Tomas-Loba, A., Sartori, A.A., Adams, I.R., Batista, F.D., and Boulton, S.J. (2013). RIF1 is essential for 53BP1-dependent nonhomologous end joining and suppression of DNA double-strand break resection. Mol. Cell *49*, 858–871.

Cho, Y.W., Hong, T., Hong, S., Guo, H., Yu, H., Kim, D., Guszczynski, T., Dressler, G.R., Copeland, T.D., Kalkum, M., and Ge, K. (2007). PTIP associates with MLL3- and MLL4-containing histone H3 lysine 4 methyltransferase complex. J. Biol. Chem. *282*, 20395–20406.

Cho, Y.W., Hong, S., Jin, Q., Wang, L., Lee, J.E., Gavrilova, O., and Ge, K. (2009). Histone methylation regulator PTIP is required for PPARgamma and C/EBPalpha expression and adipogenesis. Cell Metab. *10*, 27–39.

Daniel, J.A., Santos, M.A., Wang, Z., Zang, C., Schwab, K.R., Jankovic, M., Filsuf, D., Chen, H.T., Gazumyan, A., Yamane, A., et al. (2010). PTIP promotes chromatin changes critical for immunoglobulin class switch recombination. Science *329*, 917–923.

Di Virgilio, M., Callen, E., Yamane, A., Zhang, W., Jankovic, M., Gitlin, A.D., Feldhahn, N., Resch, W., Oliveira, T.Y., Chait, B.T., et al. (2013). Rif1 prevents resection of DNA breaks and promotes immunoglobulin class switching. Science *339*, 711–715.

Difilippantonio, S., Gapud, E., Wong, N., Huang, C.Y., Mahowald, G., Chen, H.T., Kruhlak, M.J., Callen, E., Livak, F., Nussenzweig, M.C., et al. (2008). 53BP1 facilitates long-range DNA end-joining during V(D)J recombination. Nature *456*, 529–533.

Dimitrova, N., Chen, Y.C., Spector, D.L., and de Lange, T. (2008). 53BP1 promotes non-homologous end joining of telomeres by increasing chromatin mobility. Nature *456*, 524–528.

Escribano-Díaz, C., Orthwein, A., Fradet-Turcotte, A., Xing, M., Young, J.T., Tkáč, J., Cook, M.A., Rosebrock, A.P., Munro, M., Canny, M.D., et al. (2013). A cell cycle-dependent regulatory circuit composed of 53BP1-RIF1 and BRCA1-CtIP controls DNA repair pathway choice. Mol. Cell *49*, 872–883.

Farmer, H., McCabe, N., Lord, C.J., Tutt, A.N., Johnson, D.A., Richardson, T.B., Santarosa, M., Dillon, K.J., Hickson, I., Knights, C., et al. (2005). Targeting the DNA repair defect in BRCA mutant cells as a therapeutic strategy. Nature *434*, 917–921.

Feng, L., Fong, K.W., Wang, J., Wang, W., and Chen, J. (2013). RIF1 counteracts BRCA1-mediated end resection during DNA repair. J. Biol. Chem. *288*, 11135–11143.

Gentleman, R.C., Carey, V.J., Bates, D.M., Bolstad, B., Dettling, M., Dudoit, S., Ellis, B., Gautier, L., Ge, Y., Gentry, J., et al. (2004). Bioconductor: open software development for computational biology and bioinformatics. Genome Biol. *5*, R80.

Gong, Z., Cho, Y.W., Kim, J.E., Ge, K., and Chen, J. (2009). Accumulation of Pax2 transactivation domain interaction protein (PTIP) at sites of DNA breaks via RNF8-dependent pathway is required for cell survival after DNA damage. J. Biol. Chem. *284*, 7284–7293.

Jaspers, J.E., Kersbergen, A., Boon, U., Sol, W., van Deemter, L., Zander, S.A., Drost, R., Wientjens, E., Ji, J., Aly, A., et al. (2013). Loss of 53BP1 causes PARP inhibitor resistance in Brca1-mutated mouse mammary tumors. Cancer Discov *3*, 68–81.

Jowsey, P.A., Doherty, A.J., and Rouse, J. (2004). Human PTIP facilitates ATM-mediated activation of p53 and promotes cellular resistance to ionizing radiation. J. Biol. Chem. *279*, 55562–55569.

López-Contreras, A.J., Gutierrez-Martinez, P., Specks, J., Rodrigo-Perez, S., and Fernandez-Capetillo, O. (2012). An extra allele of Chk1 limits oncogene-induced replicative stress and promotes transformation. J. Exp. Med. *209*, 455–461.

Lottersberger, F., Bothmer, A., Robbiani, D.F., Nussenzweig, M.C., and de Lange, T. (2013). Role of 53BP1 oligomerization in regulating double-strand break repair. Proceedings of the National Academy of Sciences of the United States of America.

Manke, I.A., Lowery, D.M., Nguyen, A., and Yaffe, M.B. (2003). BRCT repeats as phosphopeptide-binding modules involved in protein targeting. Science *302*, 636–639.

Moynahan, M.E., Chiu, J.W., Koller, B.H., and Jasin, M. (1999). Brca1 controls homology-directed DNA repair. Mol. Cell *4*, 511–518.

Munoz, I.M., Jowsey, P.A., Toth, R., and Rouse, J. (2007). Phospho-epitope binding by the BRCT domains of hPTIP controls multiple aspects of the cellular response to DNA damage. Nucleic Acids Res. *35*, 5312–5322.

Patel, S.R., Kim, D., Levitan, I., and Dressler, G.R. (2007). The BRCT-domain containing protein PTIP links PAX2 to a histone H3, lysine 4 methyltransferase complex. Dev. Cell *13*, 580–592.

Rai, R., Zheng, H., He, H., Luo, Y., Multani, A., Carpenter, P.B., and Chang, S. (2010). The function of classical and alternative non-homologous end-joining pathways in the fusion of dysfunctional telomeres. EMBO J. *29*, 2598–2610.

Reina-San-Martin, B., Chen, J., Nussenzweig, A., and Nussenzweig, M.C. (2007). Enhanced intra-switch region recombination during immunoglobulin class switch recombination in 53BP1-/- B cells. Eur. J. Immunol. *37*, 235–239.

Schwab, K.R., Patel, S.R., and Dressler, G.R. (2011). Role of PTIP in class switch recombination and long-range chromatin interactions at the immunoglobulin heavy chain locus. Mol. Cell. Biol. *31*, 1503–1511.

Scully, R., Chen, J., Plug, A., Xiao, Y., Weaver, D., Feunteun, J., Ashley, T., and Livingston, D.M. (1997). Association of BRCA1 with Rad51 in mitotic and meiotic cells. Cell *88*, 265–275.

Sfeir, A., and de Lange, T. (2012). Removal of shelterin reveals the telomere end-protection problem. Science *336*, 593–597.

Silverman, J., Takai, H., Buonomo, S.B., Eisenhaber, F., and de Lange, T. (2004). Human Rif1, ortholog of a yeast telomeric protein, is regulated by ATM and 53BP1 and functions in the S-phase checkpoint. Genes Dev. *18*, 2108–2119.

Sonoda, E., Hochegger, H., Saberi, A., Taniguchi, Y., and Takeda, S. (2006). Differential usage of non-homologous end-joining and homologous recombination in double strand break repair. DNA Repair (Amst.) *5*, 1021–1029.

Symington, L.S., and Gautier, J. (2011). Double-strand break end resection and repair pathway choice. Annu. Rev. Genet. *45*, 247–271.

Toledo, L.I., Murga, M., Zur, R., Soria, R., Rodriguez, A., Martinez, S., Oyarzabal, J., Pastor, J., Bischoff, J.R., and Fernandez-Capetillo, O. (2011). A cell-based screen identifies ATR inhibitors with synthetic lethal properties for cancer-associated mutations. Nat. Struct. Mol. Biol. *18*, 721–727.

Wang, X., Takenaka, K., and Takeda, S. (2010). PTIP promotes DNA double-strand break repair through homologous recombination. Genes Cells. Published online January 19, 2013. http://dx.doi.org/10.1111/j.1365-2443.2009.01379.x.

Ward, I.M., Reina-San-Martin, B., Olaru, A., Minn, K., Tamada, K., Lau, J.S., Cascalho, M., Chen, L., Nussenzweig, A., Livak, F., et al. (2004). 53BP1 is required for class switch recombination. J. Cell Biol. *165*, 459–464.

Ward, I., Kim, J.E., Minn, K., Chini, C.C., Mer, G., and Chen, J. (2006). The tandem BRCT domain of 53BP1 is not required for its repair function. J. Biol. Chem. *281*, 38472–38477.

Wesemann, D.R., Magee, J.M., Boboila, C., Calado, D.P., Gallagher, M.P., Portuguese, A.J., Manis, J.P., Zhou, X., Recher, M., Rajewsky, K., et al. (2011). Immature B cells preferentially switch to IgE with increased direct Sμ to Sε recombination. J. Exp. Med. *208*, 2733–2746.

Yamane, A., Robbiani, D.F., Resch, W., Bothmer, A., Nakahashi, H., Oliveira, T., Rommel, P.C., Brown, E.J., Nussenzweig, A., Nussenzweig, M.C., and Casellas, R. (2013). RPA accumulation during class switch recombination represents 5′-3′ DNA-end resection during the S-G2/M phase of the cell cycle. Cell Rep *3*, 138–147.

Yu, X., Chini, C.C., He, M., Mer, G., and Chen, J. (2003). The BRCT domain is a phospho-protein binding domain. Science *302*, 639–642.

Zimmermann, M., Lottersberger, F., Buonomo, S.B., Sfeir, A., and de Lange, T. (2013). 53BP1 regulates DSB repair using Rif1 to control 5′ end resection. Science *339*, 700–704.

Palb2 synergizes with *Trp53* to suppress mammary tumor formation in a model of inherited breast cancer

Christian Bowman-Colin[a], Bing Xia[b], Samuel Bunting[c], Christiaan Klijn[d,1], Rinske Drost[d], Peter Bouwman[d], Laura Fineman[a], Xixi Chen[a], Aedin C. Culhane[e,f], Hong Cai[b], Scott J. Rodig[g], Roderick T. Bronson[h], Jos Jonkers[d], Andre Nussenzweig[i], Chryssa Kanellopoulou[a,2,3], and David M. Livingston[a,3]

[a]Department of Cancer Biology, and [e]Biostatistics and Computational Biology, Dana-Farber Cancer Institute, Boston, MA 02215; [b]Cancer Institute of New Jersey, New Brunswick, NJ 08901; [c]Department of Molecular Biology and Biochemistry, Rutgers University, Piscataway, NJ 08854; [d]Division of Molecular Pathology, The Netherlands Cancer Institute, 1066 CX Amsterdam, The Netherlands; [f]Biostatistics, Harvard School of Public Health, Boston, MA 02115; [g]Department of Pathology, Brigham and Women's Hospital, Boston, MA 02115; [h]Rodent Histology Core, Dana-Farber/Harvard Cancer Center, Harvard Medical School, Boston, MA 02115; and [i]Laboratory of Genome Integrity, National Cancer Institute, National Institutes of Health, Bethesda, MD 20892

Contributed by David M. Livingston, March 21, 2013 (sent for review February 20, 2013)

Germ-line mutations in *PALB2* lead to a familial predisposition to breast and pancreatic cancer or to Fanconi Anemia subtype N. PALB2 performs its tumor suppressor role, at least in part, by supporting homologous recombination-type double strand break repair (HR-DSBR) through physical interactions with BRCA1, BRCA2, and RAD51. To further understand the mechanisms underlying PALB2-mediated DNA repair and tumor suppression functions, we targeted *Palb2* in the mouse. *Palb2*-deficient murine ES cells recapitulated DNA damage defects caused by PALB2 depletion in human cells, and germline deletion of *Palb2* led to early embryonic lethality. Somatic deletion of *Palb2* driven by *K14*-Cre led to mammary tumor formation with long latency. Codeletion of both *Palb2* and Tumor protein 53 (*Trp53*) accelerated mammary tumor formation. Like *BRCA1* and *BRCA2* mutant breast cancers, these tumors were defective in RAD51 focus formation, reflecting a defect in *Palb2* HR-DSBR function, a strongly suspected contributor to *Brca1, Brca2*, and *Palb2* mammary tumor development. However, unlike the case of *Brca1*-mutant cells, *Trp53bp1* deletion failed to rescue the genomic instability of *Palb2*- or *Brca2*-mutant primary lymphocytes. Therefore, *Palb2*-driven DNA damage control is, in part, distinct from that executed by *Brca1* and more similar to that of *Brca2*. The mechanisms underlying *Palb2* mammary tumor suppression functions can now be explored genetically in vivo.

mouse model | familial breast cancer

Partner and Localizer of BRCA2 (*PALB2*) is a breast cancer susceptibility gene. Its product was identified as a major interacting protein of the BReast CAncer susceptibility gene product 2, BRCA2 (1). This interaction is required for the repair of DNA double strand breaks (DSBs) by homologous recombination (HR) because PALB2 is necessary for the chromatin association of BRCA2 and its partner, RAD51 (1). RAD51 is the central recombinase in HR, and it participates in D-loop formation and strand displacement (2). PALB2 also plays a BRCA2-independent role in the HR process by enhancing RAD51 function (3, 4).

PALB2 interacts with both BRCA1 and BRCA2 and mediates the long-known interaction between these proteins (5, 6). Loss of PALB2 does not affect BRCA1 recruitment to irradiation-induced foci (IRIF) but abrogates colocalization of BRCA2 and RAD51 at these structures (1, 5). Genetic analyses have shown that, like BRCA2, a member of Fanconi anemia complementation group D1, PALB2 is also the Fanconi anemia complementation group N protein (FANCN) (7, 8). PALB2 is also a breast cancer suppressor protein in its own right (9–12). Unlike *BRCA1* and *BRCA2* mutant tumors, only some *PALB2*-associated breast cancers have undergone loss of *PALB2* heterozygosity (LOH) (9, 10). This finding implies that a reduction of *PALB2* gene copy number might be sufficient to allow breast cancer development in some, but not all, settings. Why this difference exists is an open question.

Breast cancer in *PALB2*-mutated families is of intermediate penetrance, unlike that in *BRCA1/2* families (10, 12). Although *PALB2* mutations are rarer than *BRCA1/2* mutations, available clinical data suggest that heterozygous, germ-line *PALB2* mutations do not precisely phenocopy either *BRCA1* or *BRCA2* cancer predisposition syndromes (9, 10). This finding is consistent with the notion that PALB2 biological functions extend beyond simply enabling BRCA1–BRCA2 complex formation. PALB2 also interacts with MRG15 (also known as MORF4L1) (13), a subunit of histone acetyl transferase/deacetylase complexes, and with KEAP1, a major regulator of the antioxidant transcription factor NRF2 (also known as NFE2L2) (14). In addition, PALB2 contains a highly conserved, chromatin-associated domain (ChAM) for which no binding partners are known (15). The contribution of these PALB2 binding partners and of the ChAM domain to the BRCA1-PALB2-BRCA2 HR machinery and/or to PALB2's cancer suppression function is unclear. Thus, it is conceivable that PALB2 exerts multiple functions that extend beyond its known role in HR-mediated double strand break repair.

To date, it has been difficult to study the molecular pathogenesis of *PALB2* breast cancer in detail because of the lack of a genetically engineered mouse model that recapitulates the human disease. Thus, we have generated a model of *Palb2* breast cancer in the mouse and have documented its most salient properties. An analogous model was recently generated by others (16).

Results and Discussion

Targeting the Mouse *Palb2* Gene and Generation of *Palb2*-Deficient ES Cells. To generate a *Palb2* allele that could be conditionally inactivated upon Cre recombinase expression, we inserted *loxP* sites flanking exons 2 and 3 of the *Palb2* gene (Fig. S1 *A* and *B*). These exons encode a putative nuclear localization signal sequence and the PALB2 coiled-coil domain (Fig. 1*A*, Fig. S1*A*). The latter mediates the PALB2 interaction with BRCA1 (5, 6). Deletion of these exons would result in out-of-frame reading of exon 4 and premature termination of the PALB2 translation before the BRCA2-interacting, seven-bladed WD40-type β-propeller domain (Fig. 1*A*, Fig. S1*A*). Due to premature truncation

Author contributions: C.B.-C., B.X., S.B., A.N., C. Kanellopoulou, and D.M.L. designed research; C.B.-C., B.X., S.B., C. Klijn, L.F., X.C., H.C., S.J.R., J.J., and C. Kanellopoulou performed research; C.B.-C., B.X., R.D., P.B., J.J., and D.M.L. contributed new reagents/analytic tools; C.B.-C., S.B., C. Klijn, L.F., A.C.C., S.J.R., R.T.B., A.N., C. Kanellopoulou, and D.M.L. analyzed data; and C.B.-C., B.X., C. Kanellopoulou, and D.M.L. wrote the paper.

The authors declare no conflict of interest.

[1]Present address: Department of Bioinformatics and Computational Biology, Genentech, South San Francisco, CA 94080.

[2]Present address: Laboratory of Immunology, National Institute of Allergy and Infectious Diseases, National Institutes of Health, Bethesda, MD 20892.

[3]To whom correspondence may be addressed. E-mail: chrysi.kanellopoulou@nih.gov or david_livingston@dfci.harvard.edu.

This article contains supporting information online at www.pnas.org/lookup/suppl/doi:10.1073/pnas.1305362110/-/DCSupplemental.

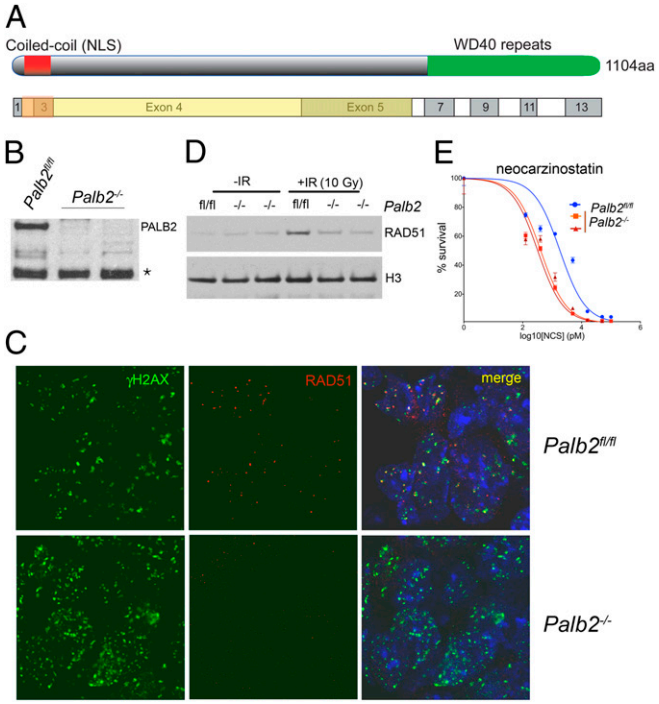

Fig. 1. Conditional gene targeting of mouse *Palb2*. (*A*) Schematic representation of *Palb2* domains and the exons from which they are encoded. The yellow area corresponds to the frameshifted ORF that results from recombination of the inserted *loxP* recombination sites. (*B*) Western blot analysis for PALB2 isolated in chromatin-enriched extracts (S420) of three independent ES cell lines. The full-length mouse PALB2 protein is ~120 kDa. A nonspecific background band is indicated by an asterisk and can be used as an internal loading control. (*C*) Recruitment of RAD51 to DSBs marked by γH2AX IRIF 2 h after exposure of $Palb2^{fl/fl}$ and $Palb2^{-/-}$ ES cells to to 5 Gy of ionizing radiation (IR). (*D*) Western blot analysis of chromatin-bound (S420) RAD51 in $Palb2^{fl/fl}$ and $Palb2^{-/-}$ ES cells that received 10 Gy of IR and the respective unirradiated control cells. Histone H3 was used as a loading control. (*E*) Dose–response curves of $Palb2^{fl/fl}$ and $Palb2^{-/-}$ ES cells after exposure to increasing concentrations of neocarzinostatin.

of the *Palb2* ORF, the resulting transcript is also a candidate for degradation via nonsense-mediated decay.

Targeting of the *Palb2* locus and integration of both *loxP* recombination sites was confirmed by Southern blot analysis (Fig. S1*C*). Heterozygous ES cells ($Palb2^{neo/+}$) were injected into blastocysts, and the resulting chimeras from two individual clones were bred to either *Flp*-deleter mice (to eliminate the Frt-flanked neomycin resistance cassette and generate a conditional allele) or *Cre*-deleter mice (to generate a conventional *Palb2* KO allele). Germ-line transmission of the $Palb2^{neo}$ allele occurred from nearly all chimeras, and mice were successfully genotyped for the Flp- and the Cre-recombined alleles ($Palb2^{fl}$ or $Palb2^{-}$, respectively).

We attempted to derive ES cells from the $Palb2^{-}$ allele. Three, independent *Palb2* ES cell lines were derived from a single, heterozygous $Palb2^{fl/-}$ cross. Expression analysis of *Palb2* mRNA by quantitative real-time RT-PCR (qRT-PCR) confirmed that one of these ES lines was $Palb2^{fl/fl}$ and the other two were $Palb2^{-/-}$ (Fig. S1*D*). The loss of full-length Palb2 expression from these lines was further confirmed by Western blotting, using a polyclonal anti-mouse PALB2 antibody raised against the N-terminal 200 residues of the mouse PALB2 protein (Fig. 1*B*). Therefore, *Palb2* loss did not prevent ES cell derivation and subsequent survival. The three ES cell lines we derived were morphologically comparable, proliferated at the same rate as wild-type (WT) ES cells and were capable of differentiation into embryoid bodies.

ES cells that are deficient for *Brca1* or *Brca2* have been notoriously difficult to isolate and are severely compromised in their proliferation (17, 18). In keeping with these findings, $Palb2^{-/-}$ ES cells could not be derived from embryos carrying a conventional PALB2 gene-trap allele (19). Because PALB2 operates immediately upstream of BRCA2 and is required for BRCA2 localization at DNA double strand breaks, it is possible that the viability and robustness of our $Palb2^{-/-}$ ES cells were due to residual expression of a truncated PALB2 species. Such a polypeptide could, in theory, result from translation initiation downstream of the engineered *Palb2* genomic deletion. No such truncated protein was detected with our polyclonal antibody (Fig. 1*B*).

To test whether the conditional gene targeting approach that was used had generated an allele that would be rendered null after Cre action, the response of $Palb2^{fl/fl}$ and $Palb2^{-/-}$ ES cells to DNA damaging agents that cause double strand breaks was analyzed. Normally, exposure of *PALB2*-proficient cells to ionizing radiation (IR) leads to the formation of phosphorylated histone H2A.X (γH2AX) nuclear foci and subsequent recruitment of BRCA1, BRCA2, and RAD51 to these structures. As expected, after exposure to IR, γH2AX and BRCA1 IRIF formation was unaffected in $Palb2^{-/-}$ cells (Fig. 1*C*, Fig. S2*A*). However, the recruitment of RAD51 was severely compromised (Fig. 1*C*). This defect was also evident at the biochemical level because no increase in chromatin loading of RAD51 after IR could be detected in nuclear extracts of IR-treated $Palb2^{-/-}$ cells (Fig. 1*D*).

Because biallelic PALB2 mutations in humans cause Fanconi anemia, a hallmark of which is increased sensitivity to DNA cross-linking agents such as mitomycin C (MMC), the sensitivity of $Palb2^{-/-}$ ES cells to MMC as well other DNA damaging agents was assayed. Both $Palb2^{-/-}$ ES lines displayed increased sensitivity to MMC, IR, and the radiomimetic drug, neocarzinostatin (Fig. 1*E*, Fig. S2 *B* and *C*). These findings further imply that these $Palb2^{-/-}$ cells are functional KOs for *Palb2* because they are compromised in multiple, known *Palb2*-associated functions. Thus, upon Cre-mediated recombination in vivo, the aforementioned conditional *Palb2* allele appears to be converted to a *Palb2*-null allele.

Loss of *Palb2* in the Germ Line Results in Early Embryonic Lethality. Germ-line deletion of *Brca1* or *Brca2* results in early embryonic lethality (17, 20, 21). Although $Palb2^{-/-}$ ES cells displayed no apparent growth defects compared with $Palb2^{fl/fl}$ controls, *Palb2* loss could still be deleterious in differentiated progeny cells, and thereby negatively affect mouse development. Indeed, we were unable to obtain $Palb2^{-/-}$ mice from heterozygous crosses (Fig. S3*A*), consistent with previous reports (19, 22). Dissection of embryos from timed pregnancies revealed that *Palb2*-null embryos could be recovered only up to E12.5, but even then at sub-Mendelian ratios. These embryos repeatedly exhibited severe malformations. At earlier time points, morphological aberrations of $Palb2^{-/-}$ embryos were less obvious. However, these mutant embryos were clearly smaller than WT or heterozygous littermate embryos (Fig. S3*B*), and some displayed exencephaly as well as malformations of the placental labyrinth and yolk sac-associated blood islets (Fig. S3 *C*–*F*). The fact that *Palb2* nullizygosity resulted in embryonic lethality detectable at E8.5–E10.5 is consistent with earlier reports showing that homozygous *Palb2*-deficient mice also die during embryogenesis at ~E8.5 (19, 22).

Embryonic lethality due to loss of *Brca1* or *Brca2* can be delayed by concomitant loss of P53 (encoded by *Trp53*) or the CDK inhibitor p21 (encoded by the *Cdkn1a* gene) (23), (24). *Trp53* loss also delayed the lethality of *Palb2* KO embryos, which otherwise exhibited increased p21 abundance (22). We therefore tested whether loss of p21 expression affects $Palb2^{-/-}$ embryonic lethality by generating *Palb2*; $Cdkn1a^{-/-}$ embryos. As expected, loss of p21 expression did delay embryonic lethality of *Palb2* KO embryos by 2–3 d (Fig. S3*A*). However, all *Palb2*/*Cdkn1a* double KO embryos still displayed multiple malformations and impaired growth compared with *Palb2* heterozygous or WT littermates

and were eventually resorbed. Therefore, these *Palb2*$^{-/-}$ embryonic rescue effects were incomplete and failed to suppress embryonic lethality.

Because the establishment of the placenta and onset of embryonic hematopoiesis are critical steps in development that take place around the time of lethality of *Palb2* embryos, we asked whether the lethality of *Palb2* KO embryos could be bypassed by a WT placenta. To this end, we used the *Palb2*$^{fl/fl}$ and *Palb2*$^{-/-}$ ES cells we had generated to perform tetraploid complementation assays. In this assay, diploid KO ES cells are aggregated to tetraploid WT blastocysts to generate KO embryos that are supported by a WT placenta because the tetraploid WT blastomeres are still capable of forming a placenta but cannot contribute to the embryo.

We found that embryos derived from the *Palb2*$^{-/-}$ ES cells were already underdeveloped and malformed at E9.5 compared with their *Palb2*$^{fl/fl}$ counterparts (Fig. S3 *I* and *J*). At E12.5, embryos derived from *Palb2*$^{fl/fl}$ ES cells appeared normal whereas embryos from *Palb2*$^{-/-}$ ES cells had been resorbed (Fig. S3 *K* and *L*). Likewise, breeding of the *Palb2*$^{fl/fl}$ conditional allele to *Meox2-Cre* knock-in (KI) mice (in which Cre is expressed from the endogenous *Meox2* locus only in the embryo proper and not in the placenta or extraembryonic tissues) (25) only yielded viable mice in which the *Palb2* deletion was incomplete. Collectively, these findings indicate that *Palb2* is an essential gene during development, and its deficiency in the embryo proper is incompatible with life. These findings are analogous to previous results showing that the lethality of *Brca1*$^{-/-}$ embryos could not be rescued by tetraploid complementation assay (20).

***Palb2* Is a Breast Tumor Suppressor in Mice.** To assess the effect of *Palb2* loss-of-function on mammary tumorigenesis, we crossed *Palb2*$^{fl/fl}$ mice with keratin 14 promoter-driven *Cre* (*K14-Cre*) transgenic mice (26). *K14-Cre* transgenic animals preferentially express Cre recombinase in the basal epithelium of the mammary ducts, as well as in skin and oral mucosa. *K14-Cre* has previously been used to model murine *Brca1* and *Brca2* mammary tumorigenesis (27).

PALB2, like BRCA1 and -2, appears to be a breast cancer suppressor in humans (9, 10, 28). Therefore, in an effort to develop a tractable system for studying how *Palb2* operates in this regard, we set out to develop a *Palb2* mouse breast cancer model. Mammary tumor formation initiated by BRCA1 or BRCA2 loss requires concomitant loss of functional p53 (encoded by *Trp53* in mice) (27, 29). This observation was considered in efforts to establish a *Palb2* model.

We first generated *Palb2*/*Trp53* double conditional mice by crossing *Palb2*$^{fl/fl}$; *K14-Cre* transgenic mice with *Trp53* conditional mice. All mice that harbored the conditional alleles for *Palb2* and/or *Trp53* in the absence of *K14-Cre* were phenotypically normal, fertile, and capable of nursing their litters. During the period of tumor monitoring (up to 600 d after birth), *Trp53*$^{fl/fl}$; *K14-Cre* female mice developed spontaneous mammary tumors with a frequency of ~80% and a mean tumor-free interval ($T_{1/2}$) of 320 d. By contrast, *Palb2*$^{fl/fl}$; *Trp53*$^{fl/fl}$; *K14-Cre* double conditional mice developed tumors much faster ($T_{1/2}$ = 192 d, $P = 2.4 \times 10^{-5}$), indicating that *Palb2* loss accelerates tumor formation on a *Trp53*-null background (Fig. 2*A*). These latencies are comparable with *Brca2*$^{fl/f}$; *Trp53*$^{fl/fl}$; *K14-Cre* and *Brca1*$^{fl/fl}$; *Trp53*$^{fl/fl}$; *K14-Cre* mice ($T_{1/2}$ = 181 and 213 d, respectively) (27, 30).

Somatic loss of one *Trp53* allele displayed, as expected, a haploinsufficient tumor suppressor phenotype (27, 30), given that *Palb2*$^{fl/fl}$; *Trp53*$^{fl/+}$; *K14-Cre* mice developed tumors significantly faster than *Palb2*$^{fl/fl}$; *Trp53*$^{+/+}$; *K14-Cre* mice ($T_{1/2}$ = 225 d vs. 420 d, respectively, $P = 2.5 \times 10^{-12}$, Fig. S4*C*). *Palb2* loss of function also accelerated tumor formation on a *Trp53* heterozygous (fl/+) background, again reflecting the genetic interaction of these two genes (Fig. 2*B*).

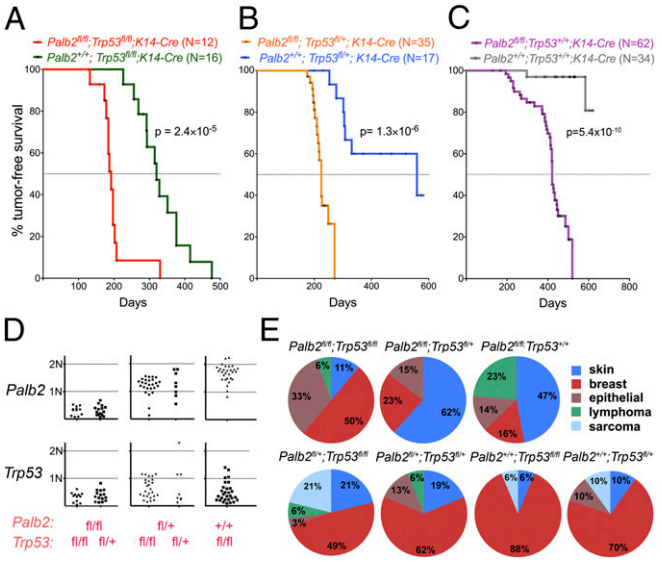

Fig. 2. Tumor formation in *Palb2*$^{fl/fl}$ conditional mice. (*A*–*C*) Kaplan–Meier curves display that *Palb2* loss accelerates tumor formation both on a *Trp53*-conditional null background (*A*), on a *Trp53*-conditional heterozygous background (*B*), and on a *Trp53* WT background (*C*). (*D*) Gene dosages of *Palb2* (*Upper*) and *Trp53* (*Lower*) in mammary tumors derived from *Palb2*/*Trp53* double conditional mouse cohorts. The germ-line *Palb2* and *Trp53* genotypes of the mice are indicated in red below the graphs. (*E*) Spectrum of tumors arising in mouse cohorts with different combinations of *Palb2* and *Trp53* alleles. The genotypes of the mice are shown above the graphs.

K14-Cre-mediated loss of *Palb2* and *Trp53* led, predominantly, to tumor formation in breast, skin, and oral mucosa (Fig. 2*E*), as previously reported for *K14-Cre*-driven *Brca1* and *Brca2* cancers (27, 30–32). All of the mammary cancers were estrogen and progesterone receptor (ER/PR)-negative, basal-like (Fig. S4 *D*–*F*), much like the BRCA1 and -2 tumors generated by *K14-Cre* (30, 32). Although most of the tumors found in *Palb2*$^{+/+}$;*Trp53*$^{fl/fl}$; *K14-Cre* mice were breast carcinomas, *Palb2*/*Trp53* compound KO mice displayed an expanded spectrum of tissues affected by tumors (Fig. 2*E*), suggesting that combined loss of PALB2 and P53, possibly due to some expression of Cre in other tissues, also results in tumor formation that is not restricted to the mammary gland.

Mice harboring conditional alleles for *Palb2* and *Trp53,* but no *K14-Cre* transgene, and *Palb2*$^{+/+}$; *Trp53*$^{+/+}$; *K14-Cre* mice did not display overt tumor formation during the observation period (Fig. 2*C*), despite the intrinsic mutagenic activity of Cre in mammalian cells (31, 33). Therefore, tumor formation in the above-noted experiments is a product of targeted gene deletion.

All tumors from *Palb2*$^{fl/fl}$; *Trp53*$^{fl/fl}$; *K14-Cre* mice (n = 12) had lost both copies of *Palb2* and *Trp53* (Fig. 2*D*). Similarly, in all tumors from *Palb2*$^{fl/fl}$; *Trp53*$^{fl/+}$; *K14-Cre* mice (n = 15), the conditional *Palb2* and *Trp53* alleles were recombined. The WT copy of *Trp53* was also lost in most tumors, probably through LOH.

Early reports describing a lack of *PALB2* LOH in clinical tumor samples from heterozygous patients suggested that PALB2 could be a haploinsufficient tumor suppressor in humans whereas other reports showed that multiple *PALB2* tumors revealed *PALB2* LOH, implying that the *PALB2* tumor formation process is not uniform (9, 34, 35). In our experimental setting, no haploinsufficiency for tumor suppression was observed for *Palb2*, as indicated by the comparable latency in *Palb2*$^{fl/+}$; *Trp53*$^{fl/fl}$; *K14-Cre* and *Palb2*$^{+/+}$; *Trp53*$^{fl/fl}$; *K14-Cre* tumor development (P = 0.46, Fig. S4*A*). Similarly, when compared on a *Trp53*$^{fl/+}$; *K14-Cre* background, cohorts of *Palb2*$^{+/+}$ and *Palb2*$^{fl/+}$ mice developed tumors with similar latency and frequency (P =

0.96, Fig. S4*B*), implying that heterozygous *Palb2* loss of function did not contribute to tumor formation.

Moreover, *Palb2* heterozygous mouse breast tumor lines displayed proper RAD51 localization at IRIF, consistent with preserved HR function (see Fig. 4*C*). By contrast, *Palb2*$^{-/-}$ breast tumor cell lines displayed the same defect in RAD51 accumulation observed in *Palb2*-null primary cells (see Fig. 4*C*). These findings suggest a role for HR deficiency in the genesis of *Palb2* tumors, a state that is not compatible with retention of a functional copy of the gene. Moreover, an analysis of tumors that arose in *Palb2*$^{fl/+}$; *Trp53*$^{fl/fl}$; *K14-Cre* mice implies that a significant fraction of these tumors retained at least one copy of *PALB2*, suggesting that loss of one copy of the gene did not contribute to tumor formation in this model (Fig. 2*D*).

Although we observed long latency tumors only in *Palb2*$^{fl/fl}$; *K14-Cre* mice on a WT *Trp53* background ($T_{1/2}$ = 420 d), tumor formation was nonetheless highly significant compared with *Palb2*$^{+/+}$; *Trp53*$^{+/+}$; *K14-Cre* controls ($P = 5.4 \times 10^{-10}$, Fig. 2*C*). The majority of these tumors were small lesions in the head and neck, and a few were mammary tumors. All of these mammary tumors were *Palb2*$^{-/-}$, and all displayed either mutations in or loss of *Trp53* by LOH.

The finding that loss of *Palb2* alone is sufficient to induce long latency tumor formation contrasts with most *Brca1* and *Brca2* mouse models in which significant numbers of these tumors could not be detected, unless *Trp53* was codeleted (27, 30, 36, 37). One explanation for this finding is that somatic *Palb2* loss might be better tolerated than somatic *Brca1/2* loss on a *Trp53* WT background. This hypothesis fits with the finding that *Palb2* nullizygosity gives rise to a less severe phenotype in ES cells than biallelic *Brca1* or *Brca2* loss (17, 18, 27, 38).

Genomic Features of *Palb2/Trp53*-Deficient Mammary Tumors. Genomic instability is a hallmark of human cancer, and it promotes tumor initiation and progression. Experimental mouse tumor models have recapitulated this aspect of human tumorigenesis (39). To gain insight into the genomic structures of the tumors that arose due to the loss of *Palb2*, we performed high-resolution comparative genomic hybridization (CGH) (40) analysis of *Palb2/Trp53, Brca1/Trp53, Brca2/Trp53*, and *Trp53* only-deficient mammary tumors that arose in *K14-Cre* mice (Fig. 3 *A–C*).

Segmentation analysis of the CGH data was performed for each tumor to assess the number of genomic segments with deviating copy number changes (aka genomic segmentation), as a readout of genomic instability (41). *Palb2/Trp53* and *Brca1/Trp53* tumors displayed apparently greater genomic instability (genomic segmentation) compared with *Brca2/Trp53* and *Trp53*-only tumors, but the difference was not statistically significant. However, when the relative dose of amplified segments ($\log_2$ dose ≥ 0.5) was analyzed, *Palb2/Trp53* mammary tumors ($n = 8$) displayed a significantly higher average dose of amplified segments than either *Brca1/Trp53* ($n = 4$; $P < 0.0001$, Fig. 3*C*) or *Brca2/Trp53* tumors ($n = 5$; $P = 0.0014$, Fig. 3*C*). The low numbers of deletions ($\log_2$ dose $\leq$ -0.5) detected in *Brca2/Trp53* and *Trp53*-only tumors precluded further analysis of this aspect of genomic instability (Fig. 3*B*).

No significant difference in focal genome amplification appeared when *Palb2/Trp53* tumors were compared with *Trp53*-only tumors, indicating that *Palb2/Trp53* tumors share a similar amplification-prone genomic profile with *Trp53*-only tumors, despite their marked difference in tumor formation kinetics. The inability of *Palb2* loss to suppress focal genomic amplifications (unlike what was observed in *Brca1/Trp53* and *Brca2/Trp53* tumors) could be accounted for by three, alternative explanations.

First, these differences could be due to residual activity of the conditional *Palb2* allele we generated, and other *Palb2* loss of function mutations might trigger the formation of true *Brca2* tumor phenocopies. Second, our allele is a functional null, as our

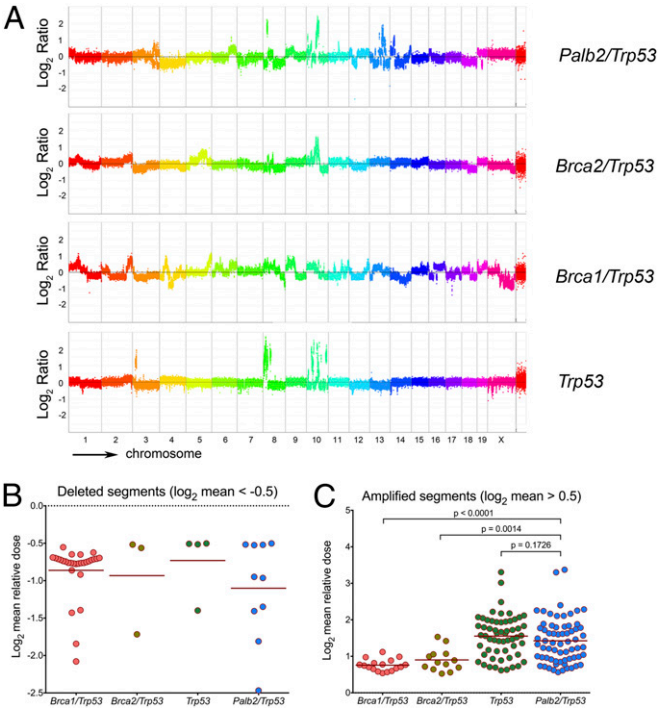

Fig. 3. CGH analysis of *Palb2* tumors. (*A*) Control (spleen) and tumor DNAs were hybridized to whole genome arrays to determine regions of loss or gains in mouse breast tumor samples. Representative rainbow graphs for each tumor genotype showing $\log_2$ mean DNA relative dose ratio (tumor/spleen) across the entire genome are presented. Each dot represents the average signal from 10 or more consecutive probes (or a segment of ~40 kb of genomic DNA). The amplitude of the data points above or below the midline indicates the extent of loss/gain in each segment, respectively. (*B* and *C*) Scatter plot graphs indicating the relative dose of the deleted segments ($\log_2 < -0.5$, *B*) and amplified segments ($\log_2 > 0.5$, *C*), each dot representing one segment. The number of dots represents the number of segments for all tumors of the relevant genotype, and the number of tumors analyzed (*n*) for *Brca1/Trp53*, *Brca2/Trp53*, *Trp53*-only, and *Palb2/Trp53* tumors were 4, 5, 7, and 8, respectively. The horizontal lines are the average segment dose per genotype, and the *P* values displayed correspond to the result of the nonparametric Mann–Whitney–Wilcoxon signed-rank test, which followed the Kruskal–Wallis one-way analysis of variance ($P < 0.0001$).

studies suggest, but complete loss of *Palb2* is similar to a BRCA2 hypomorphic phenotype rather than a complete loss of BRCA2 function. Alternatively, there are PALB2 functions that are, at least in part, nonoverlapping with the tumor suppressing functions of its BRCA2 partner protein. New experiments with additional *Palb2* and *Brca2* mutant mouse strains would be required to distinguish between these possibilities.

Finally, tumor heterogeneity likely affected the CGH profiles (Fig. S5) in ways that make it difficult to identify regions of chromosomal imbalances that were unique to *Palb2/Trp53* tumors. Conceivably, a more comprehensive analysis with a much larger collection of tumor samples would reveal such regions.

Loss of 53BP1 Fails to Rescue the HR Defect Caused by PALB2 Deficiency. Loss of 53BP1 can rescue the HR defect and lethality observed in either *Brca1*$^{\Delta 11/\Delta 11}$ or *Brca1*-null cells and mice (42–45). Similarly, decreased expression of the P53 binding protein 1 (53BP1) was detected in triple negative breast cancers as well as human *BRCA1* tumors (45). Therefore, we asked whether *Trp53bp1* (which encodes mouse 53BP1) expression is reduced in *Palb2/Trp53* KO tumors, and whether its absence rescues the HR defect associated with *Palb2* loss. Quantitative RT-PCR analysis of *Trp53bp1* mRNA in freshly isolated *Palb2* breast tumor samples

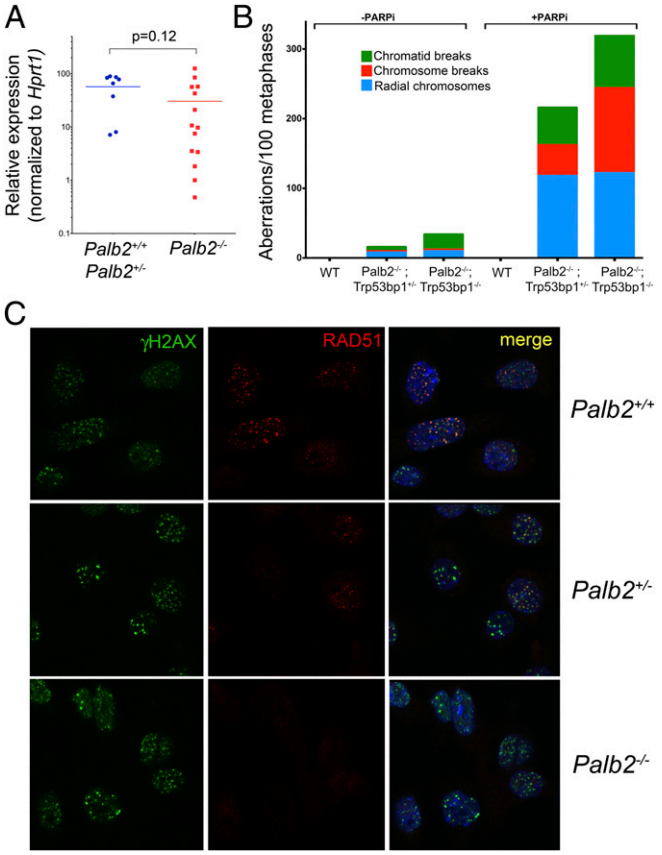

Fig. 4. The HR defect in *Palb2*-deficient cells and tumors. (*A*) qRT-PCR for *Trp53bp1* mRNA in freshly isolated tumor samples that are either *Palb2*-proficient (+/+ and +/–, $n = 8$) or *Palb2*-deficient (–/–, $n = 14$). Horizontal lines represent the average relative expression value and the *P* value associated to this comparison (Mann–Whitney *U* test) is indicated. (*B*) Acute chromosomal damage and genome instability observed in chromosome spreads following PARPi treatment that are not rescued by *Trp53bp1* deletion in *Palb2*$^{fl/fl}$;*CD19-Cre* B lymphocytes. (*C*) Established *Palb2*/*Trp53*-deficient breast tumor cell lines (example shown in the *Bottom* panels) reveal a defect in the recruitment of RAD51 to IRIF whereas *Palb2* heterozygosity does not impair the proper IRIF localization of RAD51 in breast tumor lines (*Middle* panels). Both should be compared with a *Palb2* WT control breast tumor line (*Top* panels).

showed that levels of *Trp53bp1* messenger varied considerably among the tumors that were analyzed. However, overall *Trp53bp1* mRNA levels were not significantly different in *Palb2*-deficient and *Palb2*-proficient tumors (Fig. 4*A*).

To determine whether HR deficiency due to *Palb2* loss is complemented by *Trp53bp1* loss in primary cells (cultured primary splenic B cells), we generated *Palb2*$^{fl/fl}$; *CD19-Cre* mice that were or were not deficient in *Trp53bp1*. Cultured primary splenocytes from these mice were then assayed for HR competence upon treatment with PARP inhibitors (PARPi), which selectively induces DNA damage and chromosomal aberrations in HR-deficient cells (46). Treatment with KU0058948 (PARPi) led to an accumulation of chromosomal and chromatid breaks, and radial structures were evident in chromosomal spreads from cultured *Palb2*$^{fl/fl}$; *Trp53bp1*$^{+/-}$; *CD19-Cre* primary splenocytes (Fig. 4*B*). The number of chromosomal aberrations observed was not reduced in *Palb2*$^{fl/fl}$; *Trp53bp1*$^{-/-}$; *CD19-Cre* splenocytes, implying that *Trp53bp1* deletion did not complement the HR defect caused by *Palb2* deficiency (Fig. 4*B*). *Trp53bp1* deletion also failed to rescue the chromosomal aberrations found in spreads from PARPi-treated *Brca2*$^{fl/fl}$; *Trp53bp1*$^{-/-}$; *CD19-Cre* splenocytes (Fig. S6*A*), which appeared to be even more extensive than those observed in PARPi-treated *Palb2*$^{fl/fl}$; *Trp53bp1*$^{-/-}$; *CD19-Cre* cells (Fig. 4*B*). As has been previously described (43, 45), complete rescue of the DNA repair deficiency in *Brca1*$^{fl/fl}$; *Trp53bp1*$^{-/-}$; *CD19-Cre* splenocytes was observed (Fig. S6*B*).

Of note, both *Palb2*/*Trp53bp1* and *Brca2*/*Trp53bp1* compound KO cells displayed more chromosomal aberrations after PARPi exposure than *Palb2* or *Brca2* single mutants (Fig. 4*B*, Fig. S6*A*). Thus, whereas *Brca1, Palb2, and Brca2* manifest closely related, even overlapping functions, loss of *Palb2* or *Brca2* also resulted in a different DNA damage response after *Trp53bp1* elimination from that manifested by *Brca1* KO cells, in which *Trp53bp1* codeletion rescued the genomic instability observed after PARP inhibition.

These observations suggest that the contributions of PALB2 and BRCA2 to HR-based DSB repair are distinct from those of BRCA1 and cannot be complemented by 53BP1 loss. In keeping with existing evidence, PALB2 and BRCA2 may be de facto HR effectors that cannot be replaced or bypassed, except by artificially forcing the loading of RAD51 onto chromatin at/near DSB, which 53BP1 loss has not yet been shown to promote (45, 47–49). These observations, along with earlier results (4), also suggest that PARP inhibition might be a potential therapeutic regimen in PALB2-deficient tumors, as it is in BRCA1- and BRCA2-associated tumors (46).

Conclusions

In summary, we have shown that *Palb2* is a breast tumor suppressor gene in mice as it is in humans and that it synergizes with *Trp53* to suppress tumor formation. The outcome of dual *Palb2*/*Trp53* nullizygosity in the mouse mammary gland is highly penetrant breast cancer. In keeping with the fact that *PALB2* is also a breast tumor suppressor in humans, *PALB2* might be viewed as a *BRCA3*-like allele. Moreover, tumorigenesis driven by *Palb2* loss in the mouse is not entirely suppressed on a *Trp53* WT germline background, unlike most *Brca1* and *Brca2* mouse models of breast tumorigenesis (50).

Despite many similarities to *Brca2*/*Trp53* and *Brca1*/*Trp53* breast tumors, *Palb2* tumors displayed certain divergent genomic features that might be viewed as separating them from BRCA1 and -2 cancers. Specifically, we observed patterns of genomic aberrations that were different in *Palb2*/*Trp53*-derived tumors from those detected in *Brca1*/*Trp53*- or *Brca2*/*Trp53*-derived tumors. These data are consistent with the hypothesis that PALB2 possesses biological functions that extend beyond those of its major interactors, BRCA1 and BRCA2. Alternatively, the effect of *Palb2* deletion may mimic a phenotype akin to partial loss of BRCA2, resulting in a less dramatic genomic instability profile in the relevant tumor cells.

Although the genomic instability of *Brca1*-deficient cells can be rescued by loss of *Trp53bp1*, deletion of the latter had, if anything, an adverse effect in *Palb2* KO cells. In that context, *Palb2* is more similar to *Brca2*, the absence of which leads to an HR defect that also cannot be rescued by *Trp53bp1* deletion.

Haploinsufficiency for *Palb2* tumor suppression was not detected in this model although one cannot rule out the possibility that it would be manifest in a different model system and/or with enlarged cohorts of experimental mice. For example, the tumors in this mouse model driven by *K14-Cre* were uniformly of the triple negative phenotype. This characteristic might well contribute to the absence of haploinsufficiency in our system, in the same way that BRCA1 mammary tumors derived from distinct cell populations display preferential patterns of consecutive LOH events along the tumorigenesis pathway (32, 51).

We believe that this mouse model will be useful in understanding how *Palb2* serves its breast cancer suppression function.

Materials and Methods

ES Cell Derivation, Embryo Harvesting, and Tetraploid Complementation Assay. Generation of the conditional allele for *Palb2* and additional experimental details are described in *SI Material and Methods.* Oligo sequences used are described in Table S1. ES cell derivation was performed according to standard protocols (52). Pregnant mice from timed matings were killed at indicated time points by CO_2 asphyxiation following institutional guidelines. Uterine horns and embryos were dissected under the microscope, and isolated embryos were directly used for digestion, DNA extraction, and genotyping. Negative selection of *Palb2* KO embryos was analyzed according to the Hardy–Weinberg equilibrium model, using an online tool (http://ihg.gsf.de/cgi-bin/hw/hwa1.pl). Tetraploid complementation assays were performed as described (53). All experimental procedures involving mouse work were approved by the Dana-Farber Cancer Institute Institutional Care and Use Committee under Animal Protocol 07–011.

Tumorigenesis Studies. Mouse cohorts were monitored for tumor formation biweekly. Mammary tumor formation was scored when a palpable tumor of 1.0 cm in its greatest diameter could be detected, as previously described (27, 30). Mice harboring tumors were humanely killed when the tumor diameter reached 2.0 cm in its greatest dimension. Mice that were otherwise severely diseased/distressed were also killed according to institutional guidelines. Mantel–Cox logrank test was applied for comparison of tumor-free survival of mouse cohorts.

ACKNOWLEDGMENTS. We thank Drs. Ron DePinho and William Kaelin for *Trp53*$^{fl/fl}$ mice and Dr. Bing Xia for openly exchanging information on *PALB2* KO mice with our laboratory. We also thank Drs. Kristine McKinney, Nana Naetar-Kerenyi, Patricia Dahia, and Stefan Muljo for critical reading of this manuscript; Dvora Ghitza and Dr. Klaus Rajewsky for help with the tetraploid complementation assays; Dr. Rene Maehr for V6.5 ES cells; Dr. Ronny Drapkin for the antibody developed against mouse BRCA1; and James Horner for ES cell microinjections. We also thank all members of the D.M.L. laboratory for cooperation, expertise, and reagent sharing, as well as fruitful discussions. Finally, we thank the staff from the Dana-Farber Cancer Institute Animal Resources Facility for excellent technical support and Anuradha Kohli and Nancy Gerard for outstanding administrative support. This work was supported by National Cancer Institute Grant P01CA80111, by a Specialized Program of Research Excellence grant in breast cancer research (2P50CA089393 to the Dana-Farber/Harvard Cancer Center), by the Susan G. Komen Foundation for the Cure (SAC110022), and grants from the Breast Cancer Research Foundation.

1. Xia B, et al. (2006) Control of BRCA2 cellular and clinical functions by a nuclear partner, PALB2. *Mol Cell* 22(6):719–729.
2. West SC (2003) Molecular views of recombination proteins and their control. *Nat Rev Mol Cell Biol* 4(6):435–445.
3. Dray E, et al. (2010) Enhancement of RAD51 recombinase activity by the tumor suppressor PALB2. *Nat Struct Mol Biol* 17(10):1255–1259.
4. Buisson R, et al. (2010) Cooperation of breast cancer proteins PALB2 and piccolo BRCA2 in stimulating homologous recombination. *Nat Struct Mol Biol* 17(10):1247–1254.
5. Sy SM, Huen MS, Chen J (2009) PALB2 is an integral component of the BRCA complex required for homologous recombination repair. *Proc Natl Acad Sci USA* 106(17):7155–7160.
6. Zhang F, et al. (2009) PALB2 links BRCA1 and BRCA2 in the DNA-damage response. *Curr Biol* 19(6):524–529.
7. Reid S, et al. (2007) Biallelic mutations in PALB2 cause Fanconi anemia subtype FA-N and predispose to childhood cancer. *Nat Genet* 39(2):162–164.
8. Xia B, et al. (2007) Fanconi anemia is associated with a defect in the BRCA2 partner PALB2. *Nat Genet* 39(2):159–161.
9. Tischkowitz M, et al. (2007) Analysis of PALB2/FANCN-associated breast cancer families. *Proc Natl Acad Sci USA* 104(16):6788–6793.
10. Erkko H, et al. (2007) A recurrent mutation in PALB2 in Finnish cancer families. *Nature* 446(7133):316–319.
11. Jones S, et al. (2009) Exomic sequencing identifies PALB2 as a pancreatic cancer susceptibility gene. *Science* 324(5924):217.
12. Rahman N, et al.; Breast Cancer Susceptibility Collaboration (UK) (2007) PALB2, which encodes a BRCA2-interacting protein, is a breast cancer susceptibility gene. *Nat Genet* 39(2):165–167.
13. Sy SM, Huen MS, Chen J (2009) MRG15 is a novel PALB2-interacting factor involved in homologous recombination. *J Biol Chem* 284(32):21127–21131.
14. Albertson DG, Collins C, McCormick F, Gray JW (2003) Chromosome aberrations in solid tumors. *Nat Genet* 34(4):369–376.
15. Bleuyard JY, Buisson R, Masson JY, Esashi F (2012) ChAM, a novel motif that mediates PALB2 intrinsic chromatin binding and facilitates DNA repair. *EMBO Rep* 13(2):135–141.
16. Huo Y, et al. (2013) Autophagy opposes p53-mediated tumor barrier to facilitate tumorigenesis in a model of PALB2-associated hereditary breast cancer. *Cancer Discovery*, in press.
17. Liu CY, Flesken-Nikitin A, Li S, Zeng Y, Lee WH (1996) Inactivation of the mouse Brca1 gene leads to failure in the morphogenesis of the egg cylinder in early post-implantation development. *Genes Dev* 10(14):1835–1843.
18. Sharan SK, et al. (1997) Embryonic lethality and radiation hypersensitivity mediated by Rad51 in mice lacking Brca2. *Nature* 386(6627):804–810.
19. Rantakari P, et al. (2010) Inactivation of Palb2 gene leads to mesoderm differentiation defect and early embryonic lethality in mice. *Hum Mol Genet* 19(15):3021–3029.
20. Hakem R, et al. (1996) The tumor suppressor gene Brca1 is required for embryonic cellular proliferation in the mouse. *Cell* 85(7):1009–1023.
21. Suzuki A, et al. (1997) Brca2 is required for embryonic cellular proliferation in the mouse. *Genes Dev* 11(10):1242–1252.
22. Bouwman P, et al. (2011) Loss of p53 partially rescues embryonic development of Palb2 knockout mice but does not foster haploinsufficiency of Palb2 in tumour suppression. *J Pathol* 224(1):10–21.
23. Ludwig T, Chapman DL, Papaioannou VE, Efstratiadis A (1997) Targeted mutations of breast cancer susceptibility gene homologs in mice: Lethal phenotypes of Brca1, Brca2, Brca1/Brca2, Brca1/p53, and Brca2/p53 nullizygous embryos. *Genes Dev* 11(10):1226–1241.
24. Hakem R, de la Pompa JL, Elia A, Potter J, Mak TW (1997) Partial rescue of Brca1 (5-6) early embryonic lethality by p53 or p21 null mutation. *Nat Genet* 16(3):298–302.
25. Tallquist MD, Soriano P (2000) Epiblast-restricted Cre expression in MORE mice: A tool to distinguish embryonic vs. extra-embryonic gene function. *Genesis* 26(2):113–115.
26. Dassule HR, Lewis P, Bei M, Maas R, McMahon AP (2000) Sonic hedgehog regulates growth and morphogenesis of the tooth. *Development* 127(22):4775–4785.
27. Jonkers J, et al. (2001) Synergistic tumor suppressor activity of BRCA2 and p53 in a conditional mouse model for breast cancer. *Nat Genet* 29(4):418–425.
28. Erkko H, et al. (2008) Penetrance analysis of the PALB2 c.1592delT founder mutation. *Clin Cancer Res* 14(14):4667–4671.
29. Holstege H, et al. (2009) High incidence of protein-truncating TP53 mutations in BRCA1-related breast cancer. *Cancer Res* 69(8):3625–3633.
30. Liu X, et al. (2007) Somatic loss of BRCA1 and p53 in mice induces mammary tumors with features of human BRCA1-mutated basal-like breast cancer. *Proc Natl Acad Sci USA* 104(29):12111–12116.
31. Loonstra A, et al. (2001) Growth inhibition and DNA damage induced by Cre recombinase in mammalian cells. *Proc Natl Acad Sci USA* 98(16):9209–9214.
32. Molyneux G, et al. (2010) BRCA1 basal-like breast cancers originate from luminal epithelial progenitors and not from basal stem cells. *Cell Stem Cell* 7(3):403–417.
33. Silver DP, Livingston DM (2001) Self-excising retroviral vectors encoding the Cre recombinase overcome Cre-mediated cellular toxicity. *Mol Cell* 8(1):233–243.
34. García MJ, et al. (2009) Analysis of FANCB and FANCN/PALB2 fanconi anemia genes in BRCA1/2-negative Spanish breast cancer families. *Breast Cancer Res Treat* 113(3):545–551.
35. Casadei S, et al. (2011) Contribution of inherited mutations in the BRCA2-interacting protein PALB2 to familial breast cancer. *Cancer Res* 71(6):2222–2229.
36. Xu X, et al. (1999) Conditional mutation of Brca1 in mammary epithelial cells results in blunted ductal morphogenesis and tumour formation. *Nat Genet* 22(1):37–43.
37. Ludwig T, Fisher P, Ganesan S, Efstratiadis A (2001) Tumorigenesis in mice carrying a truncating Brca1 mutation. *Genes Dev* 15(10):1188–1193.
38. Gowen LC, Johnson BL, Latour AM, Sulik KK, Koller BH (1996) Brca1 deficiency results in early embryonic lethality characterized by neuroepithelial abnormalities. *Nat Genet* 12(2):191–194.
39. Cheon DJ, Orsulic S (2011) Mouse models of cancer. *Annu Rev Pathol* 6:95–119.
40. Kallioniemi A, et al. (1992) Comparative genomic hybridization for molecular cytogenetic analysis of solid tumors. *Science* 258(5083):818–821.
41. de Ronde JJ, et al. (2010) KC-SMARTR: An R package for detection of statistically significant aberrations in multi-experiment aCGH data. *BMC Res Notes* 3:298.
42. Cao L, et al. (2009) A selective requirement for 53BP1 in the biological response to genomic instability induced by Brca1 deficiency. *Mol Cell* 35(4):534–541.
43. Bunting SF, et al. (2010) 53BP1 inhibits homologous recombination in Brca1-deficient cells by blocking resection of DNA breaks. *Cell* 141(2):243–254.
44. Bunting SF, et al. (2012) BRCA1 functions independently of homologous recombination in DNA interstrand crosslink repair. *Mol Cell* 46(2):125–135.
45. Bouwman P, et al. (2010) 53BP1 loss rescues BRCA1 deficiency and is associated with triple-negative and BRCA-mutated breast cancers. *Nat Struct Mol Biol* 17(6):688–695.
46. Farmer H, et al. (2005) Targeting the DNA repair defect in BRCA mutant cells as a therapeutic strategy. *Nature* 434(7035):917–921.
47. Brown ET, Holt JT (2009) Rad51 overexpression rescues radiation resistance in BRCA2-defective cancer cells. *Mol Carcinog* 48(2):105–109.
48. Martin RW, et al. (2007) RAD51 up-regulation bypasses BRCA1 function and is a common feature of BRCA1-deficient breast tumors. *Cancer Res* 67(20):9658–9665.
49. Schild D, Wiese C (2010) Overexpression of RAD51 suppresses recombination defects: A possible mechanism to reverse genomic instability. *Nucleic Acids Res* 38(4):1061–1070.
50. Evers B, Jonkers J (2006) Mouse models of BRCA1 and BRCA2 deficiency: Past lessons, current understanding and future prospects. *Oncogene* 25(43):5885–5897.
51. Martins FC, et al. (2012) Evolutionary pathways in BRCA1-associated breast tumors. *Cancer Discov* 2(6):503–511.
52. Kanellopoulou C, et al. (2009) X chromosome inactivation in the absence of Dicer. *Proc Natl Acad Sci USA* 106(4):1122–1127.
53. Nagy A, et al. (1990) Embryonic stem cells alone are able to support fetal development in the mouse. *Development* 110(3):815–821.

Cell

Identification of Early Replicating Fragile Sites that Contribute to Genome Instability

Jacqueline H. Barlow,[1,9] Robert B. Faryabi,[1,9] Elsa Callén,[1] Nancy Wong,[1] Amy Malhowski,[1] Hua Tang Chen,[1] Gustavo Gutierrez-Cruz,[3] Hong-Wei Sun,[4] Peter McKinnon,[6] George Wright,[2] Rafael Casellas,[5] Davide F. Robbiani,[7] Louis Staudt,[2] Oscar Fernandez-Capetillo,[8] and André Nussenzweig[1,*]

[1]Laboratory of Genome Integrity
[2]Metabolism Branch Center for Cancer Research
National Cancer Institute, NIH, Bethesda, Maryland 20892, USA
[3]Laboratory of Muscle Stem Cells and Gene Regulation
[4]Biodata Mining and Discovery Section, Office of Science and Technology
[5]Laboratory of Immunogenetics
National Institute of Arthritis and Musculoskeletal and Skin Diseases, NIH, Bethesda, MD 20892, USA
[6]Department of Genetics, St. Jude Children's Research Hospital, Memphis, TN 38105, USA
[7]Laboratory of Molecular Immunology, The Rockefeller University, New York, NY 10065, USA
[8]Genomic Instability Group, Spanish National Cancer Research Centre (CNIO), E-28029 Madrid, Spain
[9]These authors contributed equally to this work
*Correspondence: andre_nussenzweig@nih.gov
http://dx.doi.org/10.1016/j.cell.2013.01.006

SUMMARY

DNA double-strand breaks (DSBs) in B lymphocytes arise stochastically during replication or as a result of targeted DNA damage by activation-induced cytidine deaminase (AID). Here we identify recurrent, early replicating, and AID-independent DNA lesions, termed early replication fragile sites (ERFSs), by genome-wide localization of DNA repair proteins in B cells subjected to replication stress. ERFSs colocalize with highly expressed gene clusters and are enriched for repetitive elements and CpG dinucleotides. Although distinct from late-replicating common fragile sites (CFS), the stability of ERFSs and CFSs is similarly dependent on the replication-stress response kinase ATR. ERFSs break spontaneously during replication, but their fragility is increased by hydroxyurea, ATR inhibition, or deregulated c-Myc expression. Moreover, greater than 50% of recurrent amplifications/deletions in human diffuse large B cell lymphoma map to ERFSs. In summary, we have identified a source of spontaneous DNA lesions that drives instability at preferred genomic sites.

INTRODUCTION

Double-strand breaks (DSBs) arise spontaneously during DNA replication, as a result of oncogenic stress, and as a part of the gene diversification programs in lymphocytes (Bartek et al., 2007; Callén et al., 2007; Gostissa et al., 2011; Halazonetis et al., 2008). When B lymphocytes are activated, they undergo rapid proliferation and simultaneously initiate two-genome remodeling reactions, termed somatic hypermutation (SHM) and class switch recombination (CSR). The coupling of rapid cycling and programmed DNA damage poses the B cell genome at high risk for destabilization.

SHM introduces point mutations in the variable region of immunoglobulin (Ig) genes, which can increase antibody affinity, whereas CSR is a DNA deletion event that replaces one Ig constant region gene for another. Both of these reactions are initiated by the enzyme activation-induced cytidine deaminase (AID), which deaminates cytosine residues in single-stranded DNA exposed during Ig gene transcription (Chaudhuri and Alt, 2004). In addition to Ig genes, AID causes a considerable amount of collateral genomic damage (Chiarle et al., 2011; Kato et al., 2012; Klein et al., 2011; Liu et al., 2008), including oncogenic targets such as c-Myc (Robbiani et al., 2008). Nevertheless, many recurrent mutations in B cell lymphoma are not associated with AID activity, and the mechanisms of rearrangements at these sites remain unclear.

The DNA damage response (DDR) is activated during programmed rearrangements in lymphocytes to ensure faithful DNA repair and prevent chromosomal translocation (Chen et al., 2000; Petersen et al., 2001). The DDR is also triggered by aberrant oncogene expression that induces precocious entry into S phase and perturbs replication fork progression (Bartek et al., 2007; Bester et al., 2011; Halazonetis et al., 2008). Replication fork instability can also be triggered by exogenous agents such as hydroxyurea (HU), which depletes deoxynucleotide pools, or by deficiencies in homologous recombination pathways that are needed to complete DNA replication after fork stalling or collapse (Schlacher et al., 2012).

Oncogenic stress has been shown to preferentially target genomic regions called common fragile sites (CFSs) (Bartek et al., 2007; Halazonetis et al., 2008). Historically, CFSs have been mapped in lymphocytes but are induced in all cell types under conditions that obstruct replication, such as treatment with low doses of the DNA polymerase inhibitor aphidicolin. DNA breakage within CFSs spans megabase regions. Nevertheless, CFSs share characteristic features including association with very large genes, enrichment of long stretches of AT dinucleotide-rich repeats, and incomplete DNA replication (Durkin and Glover, 2007).

Replication-stress-induced DNA damage is also observed in yeast. Similar to CFSs, sites located in "replication slow zones" (RSZs) are late replicating and breakage prone (Cha and Kleckner, 2002). In addition to late replicating areas, irreversible replication fork collapse in response to acute doses of hydroxyurea has been observed preferentially around a subset of early firing replication origins in yeast (Raveendranathan et al., 2006), which do not overlap with RSZs (Cha and Kleckner, 2002; Hashash et al., 2011). Although the molecular mechanisms governing replication initiation in yeast and mammalian cells are distinct, we wondered if fragility at early firing origins is also a feature of mammalian cells. Here, we identify highly unstable regions of the B cell genome designated as "early replicating fragile sites" (ERFSs). We propose that ERFSs are a new class of fragile sites in mammalian cells that contribute to recurrent rearrangements during lymphomagenesis.

RESULTS

Genome-wide Mapping of Replication-Induced DNA Damage

Single-strand DNA (ssDNA) mapping has been used to localize origins of replication in yeast (Feng et al., 2006). To identify potential sites of fork collapse, we first profiled the location and extent of ssDNA genome-wide using chromatin immunoprecipitation (ChIP) with an anti-replication protein A (RPA) antibody (Figure 1). RPA associates with ssDNA at stalled forks near early firing origins when fork movement is inhibited by HU (Tanaka and Nasmyth, 1998).

Freshly isolated mouse B cells are arrested in the G_0 phase of the cell cycle (Figure 1A). Upon stimulation with LPS/IL4, cells synchronously enter into the cell cycle so that by 22 hr, approximately 8% of cells have entered S phase, whereas at 28 hr over 30% are in S/G2 phases (Figure 1A). To profile early replication origins, we treated cells at 22 hr with 10 mM HU for 6 hr to fully arrest cells at G_1/S (Figures 1A and 1B). We then performed ChIP-seq of RPA in both untreated and HU-treated cells at 28 hr (Figures 1A and 1B). Two independent experiments showed reproducibility of genome-wide RPA association in HU-treated cells (Figure S1A available online). We generated profiles of RPA in untreated and treated samples, centered on individual RPA-bound sites (Figure S1B), and observed a marked increase in the intensity of RPA in HU-treated B cells relative to untreated cells where 5,939 out of 11,942 genomic regions (49.7%) displayed more than a 4-fold increase in RPA recruitment. In addition to the 53% overlap of RPA-associated regions between HU-untreated versus -treated cells, we also observed that 1,441 regions were present only in HU-treated samples (Figure S1B). These HU-dependent ssDNA regions may correspond to the firing of new replication origins to compensate for inefficient replication.

To confirm that RPA recruitment maps early replication zones, we used the Repli-Seq approach (Hansen et al., 2010) to identify replication origins in B cells during HU arrest. Approximately 12,000 early activating replication origins across the murine B cell genome were identified (Figure S1C). By comparing the distribution of BrdU incorporation relative to the individual RPA-occupied genomic regions, we observed association of BrdU incorporation with nearly 80% of RPA-bound regions (Figure S1C). Moreover, more than 86% of RPA/BrdU enriched genomic sites coincided with previously mapped early replicating regions in the mouse B cell line CH12 (Stamatoyannopoulos et al., 2012) ($p(permutation) < 1 \times 10^{-5}$, Figure S1D). Thus, HU-arrested B cells exhibited an enrichment of RPA at early replicating zones, consistent with an early S phase cell-cycle arrest (Figure 1A).

Early replicating regions are associated with accessible chromatin configuration (MacAlpine et al., 2004). In agreement with this, we found that more than 67% of RPA-bound regions in HU-arrested cells reside within intragenic sequences (Figures S1E and S1I), a frequency significantly higher than expected ($p(permutation) < 1 \times 10^{-5}$). Moreover, RPA preferentially associated with DNaseI hypersensitive sites (DHS) and euchromatic promoters marked by H3K4me3 (Figure S1F). Finally, we measured transcriptional activity in HU-treated B cells directly by genome-wide RNA sequencing. We observed high transcription activity within the RPA-occupied genomic regions as shown by the aggregated pattern of RNA-Seq centered on those regions (Figure S1G). Moreover, 6,100 RPA-bound RefSeq genes exhibited significantly higher average mRNA abundance than those that did not show RPA binding ($p < 1 \times 10^{-16}$, Figure S1H). Thus, HU-induced RPA recruitment in early S phase maps to actively transcribed genes that show the hallmarks of euchromatin.

Replisome stalling in response to HU triggers the activation of the ATR kinase (Ward and Chen, 2001), which protects forks from collapse (Cimprich and Cortez, 2008), and leads to phosphorylation of H2AX (γ-H2AX) (Ward and Chen, 2001), which colocalizes with RPA (Petermann et al., 2010). To examine the relative distribution of γ-H2AX and RPA genome-wide, we carried out ChIP-seq with an antibody that recognizes γ-H2AX (Figure S1A) and examined their profiles with respect to the center of RPA-bound sites. γ-H2AX-associated genomic regions were much broader than RPA, but these regions overlapped with 93% of RPA-bound sites marking ssDNA in HU-treated cells (Figure 1C), consistent with the finding that γ-H2AX marks stalled forks even prior to DSB formation (Petermann et al., 2010). γ-H2AX/RPA enriched loci may therefore correspond to a combination of stalled and broken replisomes.

Cells deficient in homologous recombination (HR) pathway components, such as XRCC2, often accumulate spontaneous chromosome breaks and exhibit hypersensitivity to HU (Sonoda et al., 1998). Consistent with increased spontaneous DNA damage at replication forks, untreated *XRCC2*$^{-/-}$ cells exhibited accumulation of γ-H2AX at similar genomic regions and at almost similar levels observed in HU-treated wild-type (WT)

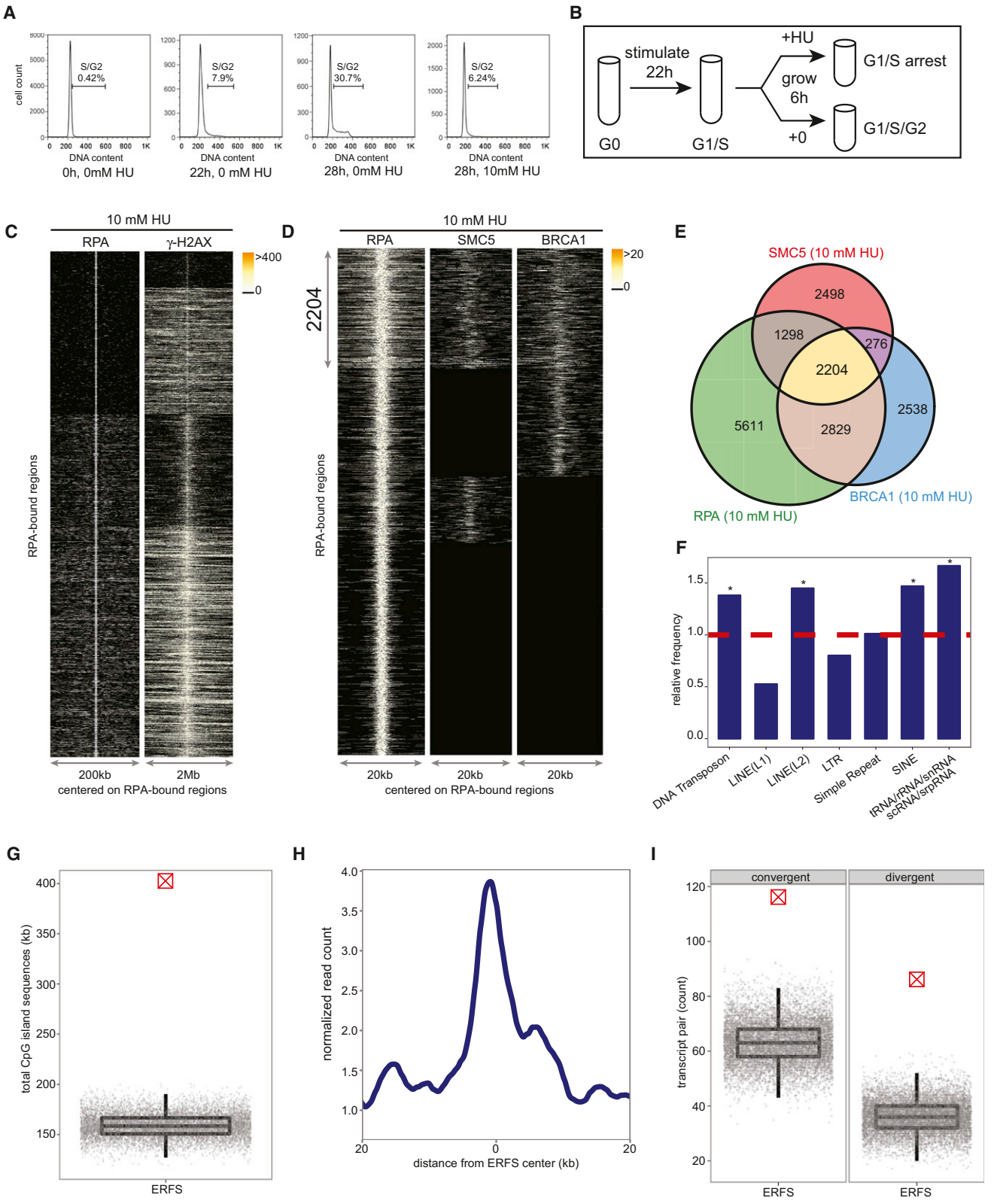

Figure 1. Mapping Replication-Induced DNA Damage in Murine B Lymphocytes

(A) FACS analysis showing DNA content of freshly isolated and ex vivo stimulated splenic murine B lymphocytes in the absence and presence of 10 mM HU.

(B) Experimental plan describing cell synchronization and isolation for samples used in ChIP-seq and RNA-Seq experiments.

(legend continued on next page)

B cells (Figures S2A–S2C). 90% of γ-H2AX-associated genomic regions in untreated *XRCC2*$^{-/-}$ cells correlate with the regions enriched for this protein in HU-treated WT B cells (Figure S2B), and nearly 80% of the regions with enriched γ-H2AX observed in HU-treated WT B cells overlapped with those seen in HU-treated *XRCC2*$^{-/-}$ cells (Figure S2C). These data indicate that XRCC2 deficiency leads to increased endogenous levels of replication stress mostly at the same loci where HU induces replication fork stalling and/or breakage in WT cells.

RPA, BRCA1, and SMC5 Colocalization Marks the Sites of Replication Stress in Early Replicating Zones

Like XRCC2, BRCA1 and members of the structural maintenance of chromosome (SMC) family have been implicated in promoting replication fork restart (Schlacher et al., 2012; Stephan et al., 2011). To determine whether HR proteins bind to a subset of stalled forks marked by RPA and γ-H2AX, we also defined the genome-wide profile of BRCA1 and SMC5. We confirmed BRCA1 and SMC5 ChIP-seq efficacy by observing their association at both Sμ and Sγ1 in *53BP1*$^{-/-}$ cells, where the breaks in IgH persist unrepaired and undergo extensive resection (Figure S3A) (Bothmer et al., 2010; Bunting et al., 2010, 2012; Yamane et al., 2011, 2013).

We then determined the localization of BRCA1 and SMC5 in HU-arrested B cells. Two independent experiments showed reproducibility of genome-wide BRCA1 and SMC5 association (Figures S3B and S3C). To identify the RPA genomic sites co-occupied by the HR proteins BRCA1 and SMC5, we plotted the distribution of their binding with respect to the center of individual RPA-bound regions. Overall, 2,204 regions spanning 10 kbp on average showed RPA/BRCA1/SMC5 triple colocalization (Figures 1D and 1E). We found that RPA was recruited to more than 88% of genomic sites exhibiting BRCA1 and SMC5 association (Figure 1E). Furthermore, genome-wide analysis of RPA/BRCA1/SMC5 profiles in untreated cells revealed more than a 21% increase in the number of genomic regions occupied by these three proteins after HU treatment (Figure S4A). Nevertheless, 48% of RPA/BRCA1/SMC5 triple colocalizations were common between the unperturbed and HU-arrested B cells (Figure S4A). Therefore, we hypothesized that chromatin with concomitant RPA, BRCA1, and SMC5 binding might correspond to regions undergoing replication fork collapse both in response to replication stress and during normal DNA replication. Given that our analysis focused on early replicating sites, which contrasts with late replicating CFSs, we designated these regions as ERFSs.

We then characterized ERFSs to determine whether they share common underlying primary sequence characteristics. Indeed, these loci were enriched at known repetitive elements, including LINE L2, SINE, DNA transposons, and tRNA elements (p(permutation) $< 1 \times 10^{-3}$, Figure 1F), which are known replication fork barriers (Mirkin and Mirkin, 2007). Furthermore, ERFSs showed significantly higher G and C nucleotide content compared to the whole mouse genome, in contrast to CFSs that are enriched in A+T sequences (p(Wilcoxon) $< 1 \times 10^{-16}$, Figure S4B). Twenty-six percent of the ERFSs regions overlapped with CpG islands, which are highly enriched at translocation breakpoints in B cell lymphoma (Tsai et al., 2008). Conversely, CpG islands covered approximately 400,000 nucleotides within these regions (p(permutation) $< 1 \times 10^{-5}$, Figure 1G). As anticipated, ERFSs clustered at early replication origins (Figure S4C), and over 66% of the loci overlapped with intragenic or promoter sequences of RefSeq annotated protein coding genes (p(permutation) $< 1 \times 10^{-3}$, Figures S4D and S4E). Moreover, ERFSs are more transcriptionally active relative to flanking genomic regions shown by relative mRNA enrichment by RNA-Seq (Figure 1H). Indeed, more than 86% of the RefSeq annotated genes with ERFSs are among the highest transcribed genes (p(binomial) $< 1 \times 10^{-16}$, Figure S4F). Finally, ERFSs were significantly enriched in gene pairs that are transcribed in converging or diverging directions (see Experimental Procedures), such as the convergent transcription pair of *IKZF1* and *FIGNL1* shown in Figure 2A. Compared to expected values, ERFSs were at least two times more likely to localize in regions containing gene pairs exhibiting convergent and/or divergent gene pairs (p(permutation) $< 1 \times 10^{-5}$, Figure 1I).

(C) For each RPA-bound site in response to 10 mM HU (y axis), each column depicts the presence of RPA (left) and γ-H2AX (right) within a window centered on the RPA-bound sites. Color map corresponds to binding intensities where "black" represents no binding. K-mean clustering algorithm was used to group the protein-bound sites.

(D) RPA, SMC5, and BRCA1 co-occupy 2,204 genomic regions in response to 10 mM HU. The plot in each column, from left to right, represents the pattern of RPA, SMC5, and BRCA1 genomic occupancy in response to HU centered on RPA-bound sites. K-mean clustering algorithm is used to group the protein-bound sites.

(E) The Venn diagram shows the overlap of sites bound by RPA, SMC5, and BRCA1 in response to 10 mM HU. The total number of bound sites is indicated for each shared and unique area.

(F) Relative frequency of ERFSs in classes of repetitive sequences is shown. Dashed line indicates the expected frequency based on the permutation model (*, enriched repetitive element classes; $p < 1 \times 10^{-3}$).

(G) ERFSs are enriched in CpG islands. Total CpG island sequences in all the 2,204 ERFSs as indicated by the crossed red point is compared to the permutation model as indicated by the gray points. Each gray point corresponds to the total CpG island sequences covered in an iteration of the permutation model. The box plot depicts the quantiles of total CpG sequences based on the permutation model ($p < 1 \times 10^{-5}$).

(H) ERFS genomic regions are transcriptionally active. The line plot represents the average RNA tag count (loess smoothed) in a genomic window around the center of the ERFSs.

(I) ERFSs are enriched in transcriptionally active convergent and divergent gene pairs. Count of divergent/convergent gene pairs coinciding with ERFSs as indicated by the crossed red point is compared to the permutation model as indicated by the gray points. Each gray point corresponds to the total number of divergent/convergent gene pairs observed in an iteration of the permutation model. The box plot depicts the quantiles of the total convergent/divergent transcript pair count based on the permutation model ($p < 1 \times 10^{-5}$). For definition of convergent/divergent gene pairs see Experimental Procedures. See also Figures S1, S3, S4.

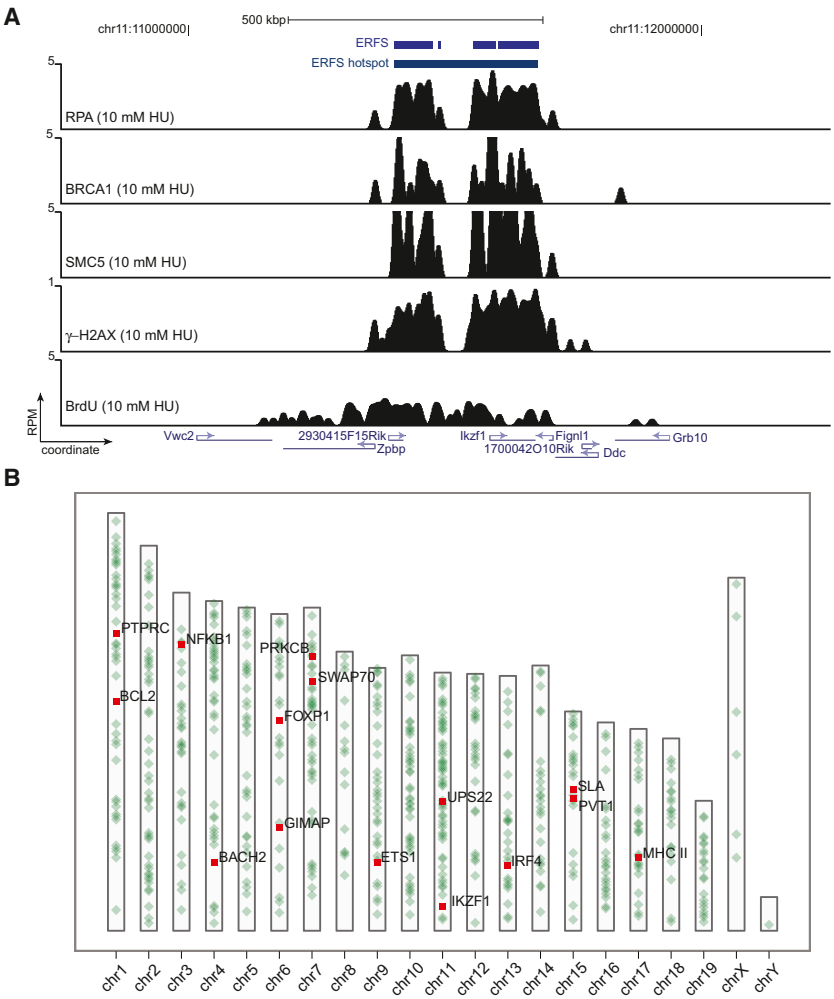

C

	ERFS Name	Chromosome	Length (Kb)	Gene Cluster	Transcribed	Convergent and/or Divergent Transcripts	Rearranged in B Cell Cancer	AID Target
1	MHCII	17	333	Yes	Yes	Yes	Yes	Yes
2	GIMAP	6	128	Yes	Yes	Yes	No	Yes
3	SWAP70	7	314.6	Yes	Yes	Yes	No	No
4	BACH2	4	419.4	No	Yes	Yes	Yes	No
5	IKZF1	11	281.4	Yes	Yes	Yes	Yes	Yes
6	FOXP1	6	431.8	No	Yes	No	Yes	No
7	PTPRC	1	1121.6	Yes	Yes	Yes	No	No
8	SLA	15	498.8	Yes	Yes	Yes	No	No
9	PVT1	15	669.8	No	Yes	Yes	Yes	Yes
10	ETS1	9	520	Yes	Yes	Yes	Yes	Yes
11	IRF4	13	283	Yes	Yes	Yes	Yes	Yes
12	BCL2	1	656.8	Yes	Yes	Yes	Yes	No
13	USP22	11	60.2	No	Yes	Yes	No	No
14	NFκB1	3	117	No	Yes	No	No	Yes
15	PRKCB	7	170.6	No	Yes	No	No	No

Figure 2. ERFS "Hot Spots" Associate with Highly Transcribed Gene Clusters

(A) Gene tracks represent, from the top, ERFS and ERFS hot spot demarcations; bindings of RPA, BRCA1, SMC5, γH2AX occupancy; and BrdU incorporation near the *IKZF1* locus. The y axis represents the total number of mapped reads per million of mapped reads (RPM) in 200 nucleotide windows (sliding-window smoothed).

(B) Genome-wide map of 619 ERFS hot spots. Each hot spot is represented by a green dot on the ideograms. The top fifteen hot spots are color-coded in red.

(C) Table of the top 15 ERFS hot spots. ERFS hot spots are ordered based on a ranked statistics of RPA/SMC5/BRCA1-binding strength (see Experimental Procedures). The first column depicts a representative gene within the hot spot. A hot spot containing at least three genes is designated as a "gene-cluster." A hot spot with a gene transcript value greater than 1 RPKM (reads per kilobase exon model per million mapped reads) is designated as transcribed. ERFS rearrangements in B cell cancers are listed in Table S2. ERFS is designated as "AID-target" according to (Chiarle et al., 2011; Klein et al., 2011). For complete definition of columns see Experimental Procedures. See also Tables S1 and S2.

Replication is organized into discrete zones (30–450 kbp in size) containing multiple replication origins that exhibit similar replication timing (Costa and Blow, 2007). Similarly, approximately 80% of the ERFSs are within 300 kbp of one another (Figures 2A and S4G). We therefore integrated these neighboring clustered ERFSs and removed those with footprints less than 10 kbp to define 619 triple colocalized hot spot regions (Figure 2B; Table S1). Interestingly, whereas these hot spots were distributed throughout the genome, the density of hot spots on autosomes was higher than on the sex chromosomes, which have a lower gene density (Figure 2B). An examination of the top 15 hot spots based on a ranked statistics of RPA/BRCA1/SMC5-binding strength showed that 9 out of the 15 regions contained gene clusters with at least three genes, and 12 out of 15 exhibited divergent/convergent gene pairs (Figures 2A and 2C; Table S1). Of note, 8 out of 15 hot spots are also rearranged in B cell lymphomas (Figure 2C; Table S2), suggesting a possible link among ERFSs, genome rearrangements, and cancer (see below).

Early S Phase Arrest by HU Induces DNA Damage at ERFSs, but Not at CFSs

DNA damage at CFSs is visualized by conventional cytogenetic analysis of metaphase chromosomes (Durkin and Glover, 2007). To investigate whether the ERFSs defined by RPA/ BRCA1/SMC5 binding are prone to actual breakage, we again treated cells with 10 mM HU, released them into fresh medium overnight, and examined metaphase spreads. Chromatid breaks, chromosome breaks, and rearrangements could be discerned in 20%–60% of WT cells after HU treatment (Figure S2D). To determine whether ERFSs are more sensitive to breakage under replication stress than regions lacking RPA/BRCA1/SMC5 binding (i.e., cold spots), we hybridized metaphases with bacterial artificial

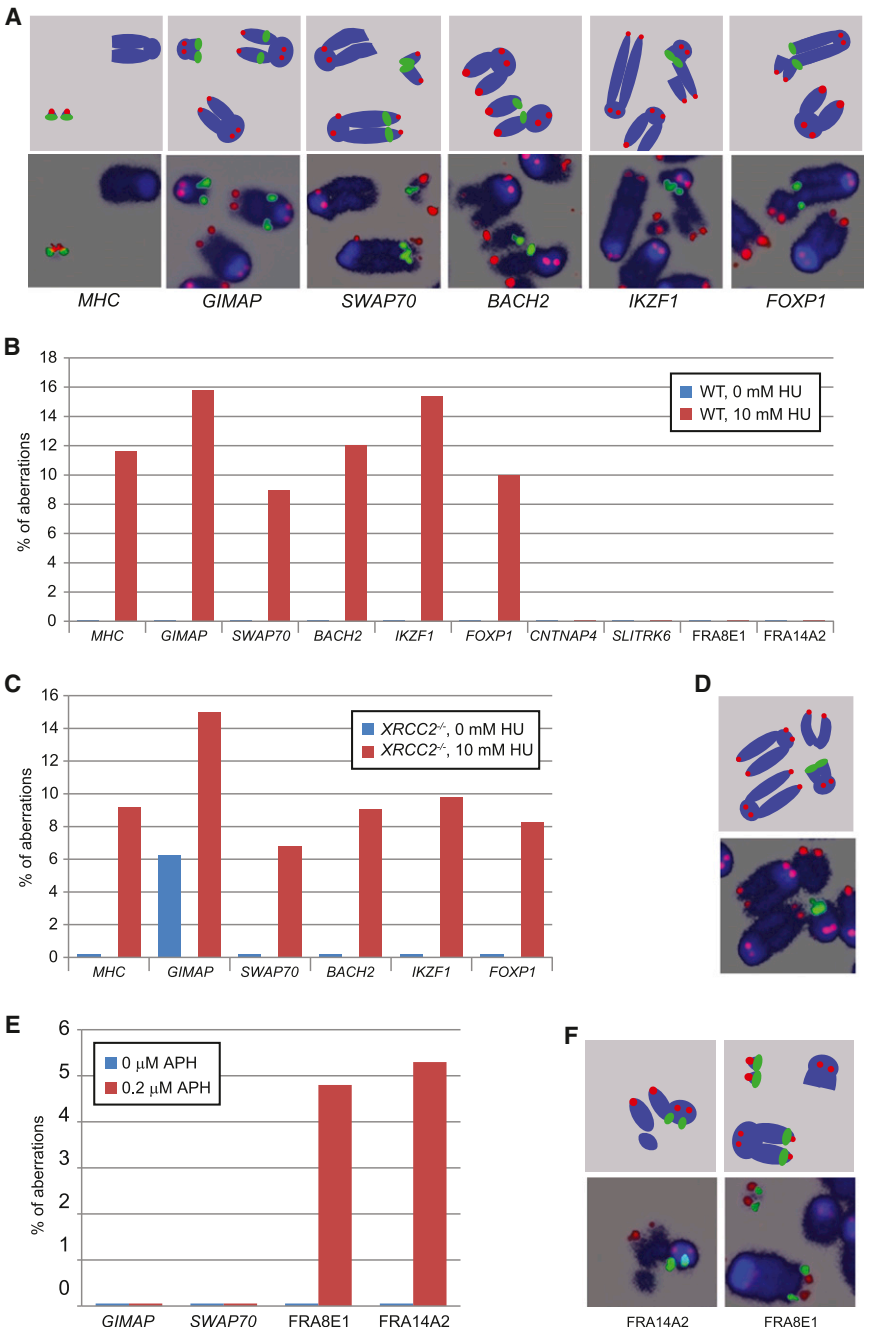

Figure 3. ERFS Break in Response to HU

(A) Upper: diagram of FISH probes. Lower: representative DNA aberrations identified by FISH. Blue is DAPI-stained DNA, green represents the BAC probe (*MHCII*, *GIMAP*, *SWAP70*, *BACH2*, *IKZF1*, or *FOXP1*) and red marks telomeric DNA.

(B) HU-induced aberrations were found at ERFSs but not at "cold sites" (*CNTNAP4*, *SLITRK6*) or CFSs (FRA8E1, FRA14A2). Quantitation of abnormalities from FISH analysis of untreated cells (blue bars) or cells treated with 10 mM HU (red bars). The percent aberrations specifically at the BAC probes relative to the total damage is plotted.

(C) Abnormalities detected by FISH in untreated (blue bars) and 10 mM HU-treated (red bars) *XRCC2*$^{-/-}$ cells.

(D) Upper: diagram of FISH probes. Lower: representative metaphase showing a spontaneous break at the *GIMAP* locus in an *XRCC2*$^{-/-}$ cell.

(E) Quantitation of abnormalities detected by FISH in untreated (blue bars) and 0.2 μM aphidicolin-treated (red bars) WT cells.

(F) Upper: diagram of FISH probes. Lower: representative metaphases showing aphidicolin-induced breaks at the FRA14A2 and FRA8E1 loci in WT cells. See also Figure S2 and Table S3.

chromosome (BAC) probes corresponding to six ERFS hot spots (*MHCII*, *GIMAP*, *SWAP70*, *BACH2*, *IKZF1*, and *FOXP1*) (Figures 3A and 3B), two cold spots (*CNTNAP4* and *SLITRK6*) and two CFSs (FRA8E1 and FRA14A2). For each of the six ERFS hot spots, a total of at least 40 chromosome aberrations were counted (Table S3). Notably, all six ERFS hot spots displayed chromosome aberrations in metaphases from HU-treated samples (Figure 3B). In contrast, neither of the cold regions or CFSs was broken under the same conditions (Figure 3B). Overall, 8%–15% of the total damage localized to individual ERFS hot spots, representing a significant fraction of the total damage (Figure 3B). DNA lesions were observed on either the centromeric or telomeric sides of ERFS-specific hybridized BAC (Figure S2E), suggesting that an ERFS represents a large fragile genomic region.

Aberrations at ERFS hot spots were also detected in *XRCC2*$^{-/-}$ cells treated with HU (Figure 3C). *XRCC2*$^{-/-}$ cells are more sensitive to HU than WT cells are, as evidenced by the higher level of total damage in these cells (Figure S2D). Breaks at *MHCII*, *GIMAP*, *SWAP70*, *BACH2*, *IKZF1*, and *FOXP1* were found in 5%–10% of HU-treated *XRCC2*$^{-/-}$ cells compared with 1%–6% of WT cells damaged in these regions (Table S3). Nevertheless, the frequency of ERFS-specific instability relative to the total damage was similar in *XRCC2*$^{-/-}$ and WT cells (Figures 3B and 3C). Interestingly, breaks in the vicinity of the *GIMAP* hot spot were detectable spontaneously in *XRCC2*$^{-/-}$ cells (Figures 3C and 3D; Table S3), which is consistent with increased γ-H2AX observed in unchallenged *XRCC2* mutant cells (Figure S2A).

None of the eight CFSs defined in mouse (Helmrich et al., 2006) were among our 619 ERFS hot spots (Table S1). Consistent with this, DNA aberrations at two of the most expressed CFSs in mouse lymphocytes, FRA14A2 and FRA8E1 (Helmrich et al., 2006) were undetectable in HU-treated WT samples

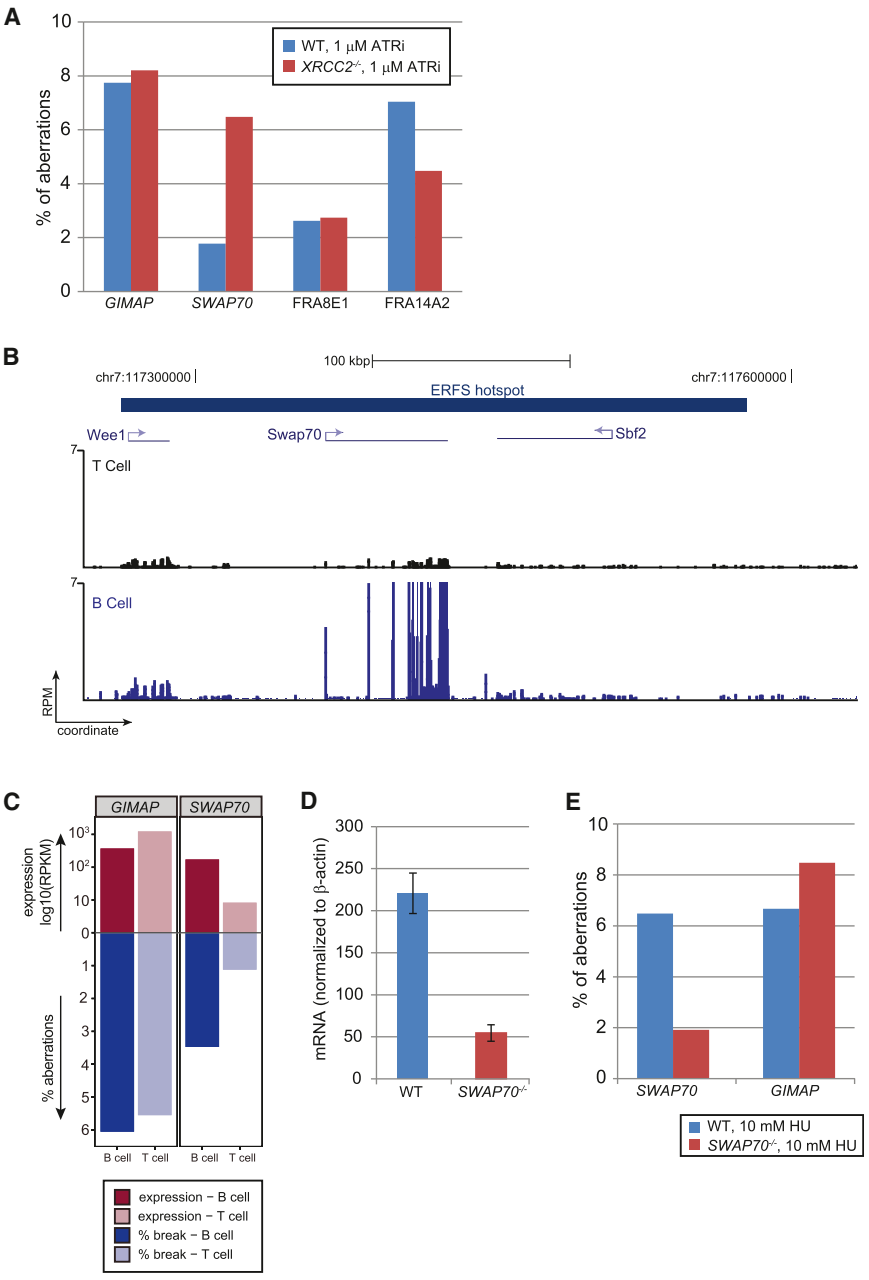

Figure 4. ERFS Break in Response to ATR Inhibition and High Transcription

(A) Quantitation of aberrations observed by FISH in response to overnight exposure to 1 μM ATRi in WT (blue bars) and *XRCC2*$^{-/-}$ cells (red bars).

(B) Gene tracks represent, from the top, ERFS demarcation and transcription measured by RNA-Seq in T and B cells at the region flanking *SWAP70* locus.

(C) Relative transcriptional activities of *GIMAP* and *SWAP70* loci in B and T cells and their relation to the ERFS fragility. *GIMAP* and SWAP70 hot spots are shown in separate facets. The x axis shows the cell lineage. The y axis upward depicts the log10(RPKM) in B and T cells by dark and light reds, respectively; the y axis downward depicts the quantitation of aberrations observed by FISH in response to overnight exposure to 1 μM ATRi in B and T cells in dark and light blue, respectively.

(D) Relative SWAP70 mRNA abundance (measured across exon 4) normalized to β-actin in WT and *SWAP70*$^{-/-}$ B cells (mean ± SD).

(E) Quantitation of aberrations in WT and *SWAP70*$^{-/-}$ cells at the *GIMAP* and *SWAP70* regions in response to 10 mM HU. See also Figure S5 and Table S3.

ATR Inhibition Promotes ERFS and CFS Expression

The ATR kinase protects the genome from chromosomal aberrations at late replicating CFSs, (Durkin and Glover, 2007) and is essential for stabilizing stalled forks and facilitates fork restart in early S phase (Cimprich and Cortez, 2008). To confirm that ATR inactivation induces CFSs and determine whether it similarly leads to damage at ERFSs, we treated asynchronous B cells on day 2 with 1 μM of a recently described ATR inhibitor (ATRi) (Toledo et al., 2011). We found that approximately 2.5% and 7.0% of the total chromosomal aberrations localized to the two CFSs, FRA8E1 and FRA14A2, respectively (Figure 4A). ATR deficiency also led to chromosomal aberrations at ERFSs at a similar frequency (Figure 4A; Table S3). Moreover, ERFSs and CFSs were both damaged in *XRCC2*$^{-/-}$ cells treated with ATRi (Figure 4A). Thus, the rupture of unreplicated regions at CFSs and fork collapse at ERFSs are similarly sensitive to ATR inhibition.

(Figure 3B). Absence of CFS expression could be explained by the fact that high concentrations of HU stall replication forks in early S phase (Figure 1A), whereas CFSs replicate late (Durkin and Glover, 2007). Conversely, we found that overnight treatment with low doses of aphidicolin (0.2 μM for 20 hr) induced damage at the CFSs FRA14A2 and FRA8E1, whereas the ERFSs *GIMAP* and *SWAP70* were largely insensitive (Figures 3E and 3F). These data are consistent with the idea that ERFS arise from fork collapse during early replication, whereas breakage at CFSs arises from a failure to replicate (Debatisse et al., 2012), and the two forms of replication stress induce distinct types of recurrent DNA lesions.

Transcriptional Activity Can Increase ERFS Fragility

As described above, ERFSs are enriched in regions with high transcriptional activity (Figures 1H, 2C, and S4F; Table S1). To determine the contribution of transcriptional activity to individual ERFSs, we focused on loci with tissue-specific transcription patterns. SWAP70 is a B-cell-specific developmental regulator, whereas genes within the *GIMAP* cluster are expressed both in

B and in T cells (Figures 4B and S5A). Treatment with ATRi led to a similar frequency of damage at *GIMAP* in B and T cells, consistent with insignificant changes in gene expression between the two cell types (Figure 4C). In contrast, damage near *SWAP70* was 3-fold lower in T than in B cells (Figure 4C; Table S3), which correlated with the decreased transcription of *SWAP70* in T cells (Figure 4B). Nevertheless, the replication timing near *SWAP70* was similar in both cell types (Figure S5B). To further delineate the role of transcription on ERFS breakage, we used *SWAP70*$^{-/-}$ mice in which 2.7 kbp, including the first exon and part of the 5′ untranslated region, is removed (Borggrefe et al., 2001), allowing us to compare the fragility of ERFSs in the same genomic region in knockout B cells. We determined that *SWAP70* mRNA in *SWAP70*$^{-/-}$ B cells was reduced by approximately 4-fold relative to levels in WT (Figure 4D). Moreover, DNA damage near *SWAP70* was approximately 2.5-fold lower in *SWAP70*$^{-/-}$ relative to levels in WT B cells (Figure 4E). In contrast, DNA damage near *GIMAP* remained at a similar level both in WT and *SWAP70*$^{-/-}$ cells (Figure 4E). Although our data indicate that high level of transcription contributes to the breakage of some ERFSs, other molecular features, including repetitive elements (Figure 1F), covalently bound protein complexes, and RNA:DNA hybrids, might also be sources of ERFS fragility.

Oncogenic Stress Can Trigger ERFS and CFS Fragility

Oncogene deregulation is thought to compromise genome integrity preferentially at CFSs (Bartek et al., 2007; Halazonetis et al., 2008), and CFS deletion has been associated with various cancers (Bignell et al., 2010). To determine whether oncogenic stress similarly induces DNA damage at ERFSs, we overexpressed *c-myc* in B cells because it has been implicated in regulating replication initiation and origin firing (Dominguez-Sola et al., 2007). *XRCC2*$^{-/-}$ cells were utilized to increase the amount of replicative stress and DNA damage as a result of decreased HR (Figure S2D). *c-myc* overexpression led to induction of p53 (Figure 5A), which correlated with an approximately 1.6-fold increase in overall DNA damage in *XRCC2*$^{-/-}$ cells overexpressing *c-myc* compared to empty vector (EV)-infected cells (Table S3). Moreover, 7.3% of the total breaks generated in *c-myc* overexpressing cells were found near *SWAP70*, compared to 2.4% of total breaks at this ERFS in EV-infected B cells (Figure 5B). Similarly, out of 43 breaks observed in *c-myc*-infected cells, 3 (7%) were found at the *GIMAP* cluster, and 3 (6.7%) were found near BACH2. *c-myc* overexpression also induced breaks at FRA8E1, showing a 2-fold relative increase in breaks relative to EV-infected cells (Figure 5B). Thus, DNA damage induced by *c-myc* overexpression can occur at ERFSs and CFSs.

ERFS Fragility Is AID Independent

Mutations and DSBs at various oncogenes, including *c-myc*, are due to AID off-target activity (Robbiani et al., 2008). Recently, a number of genome-wide studies in primary B cells mapped AID-induced DNA translocation events, and identified several novel hot spots for AID-dependent translocations at non-Ig genes (Chiarle et al., 2011; Kato et al., 2012; Klein et al., 2011). Among these translocation hot spots, *MHCII*, *GIMAP*, *IKZF1*, *PVT1*, *ETS1*, *IRF4*, and *NFkB1* were located within the top 15 ERFS hot spots in this study, whereas the *IgH* locus (the physiologic target of AID) was not ranked high on the list (Figure 2C; Table S1). To determine whether AID contributes to ERFS fragility, we stimulated WT and AID knockout B cells with LPS/IL4 for 2 days, and then treated them with ATRi overnight. These conditions induce robust AID-dependent DNA damage simultaneously with replication stress. We probed metaphases with BACs spanning the *IgH* locus, the *GIMAP* cluster, and *IKZF1*-all AID translocation hot spots—as well as *BACH2*, *SWAP70*, *FOXP1*, and *BCL2* (Figure S2E)—ERFSs that are frequently rearranged in B cell lymphoma (Figure 2C; Tables S1 and S2). In WT, the IgH locus was damaged in 3.8% of cells, but the frequency of *IgH*-specific instability did not increase with ATRi (Figure S2F), despite the fact that ATRi greatly increased overall damage (Table S3). Upon ATRi treatment, the frequency of breaks at the ERFSs *GIMAP*, *IKZF1*, *BACH2*, *SWAP70*, and *FOXP1*, and *BCL2* were elevated to the levels similar to those observed at the *IgH* in activated B cells (Figure S2F). Breaks at some ERFSs were even spontaneously detected (*FOXP1* and *GIMAP*, Figure S2F).

To determine whether AID expression contributes to aberrations observed at ERFSs, we next analyzed their breakage frequency in *AID*$^{-/-}$ cells. Unlike WT cells, *IgH* breaks were absent in *AID*$^{-/-}$ cells. In contrast, all ERFSs exhibited similar levels of breakage both in WT and *AID*$^{-/-}$ cells (Figure 5C; Table S3). Therefore, whereas *IgH* breaks in B cells are entirely AID dependent, the breakage of ERFSs is AID independent. Altogether, these data suggest that some recurrent rearrangements in B cell lymphoma are due to AID-independent replicative stress at ERFSs.

Genome Instability at ERFSs Is Observed in Mouse Models and Human Cancer

Among the top 15 ERFS hot spot that break in response to AID-independent replication stress, we have identified three partners that recurrently translocate to *IgH* in lymphomas: *BACH2*, *FOXP*1, and *BCL2* (Table S2). We hypothesized that if AID-dependent DSBs in G1 persisted into early S phase, translocations between AID-dependent breaks and ERFS might be detectable. To test this, we examined cells transgenically overexpressing AID and simultaneously deficient for 53BP1 (IgκAID/*53BP1*$^{-/-}$), thus allowing the persistence of G1 *IgH* breaks into S phase where they could be joined to ERFSs. Indeed, 26% and 7% of IgκAID/*53BP1*$^{-/-}$ B cells carried *IgH* locus and *BACH2* breaks, respectively (Figure 5D). These breaks are fusogenic because *IgH*- and *BACH2*-associated translocations to unidentified partner chromosomes were found in 7.3% and 1.2% of the metaphases, respectively (Figure 5D). Importantly, we also detected one *IgH*/*BACH2* translocation among 750 cells (Figure 5E), reminiscent of the IgH/BACH2 translocations observed in human B cell lymphoma (Kobayashi et al., 2011). Thus, AID-dependent breaks generated in G1 (Petersen et al., 2001) can join to ERFS breaks triggered in early S phase.

A hallmark of cancer genomes is widespread copy-number changes, insertions, and deletions. To determine whether deletions and/or amplifications at ERFSs are a general feature of the B cell lymphoma genome, we compared our ERFSs with

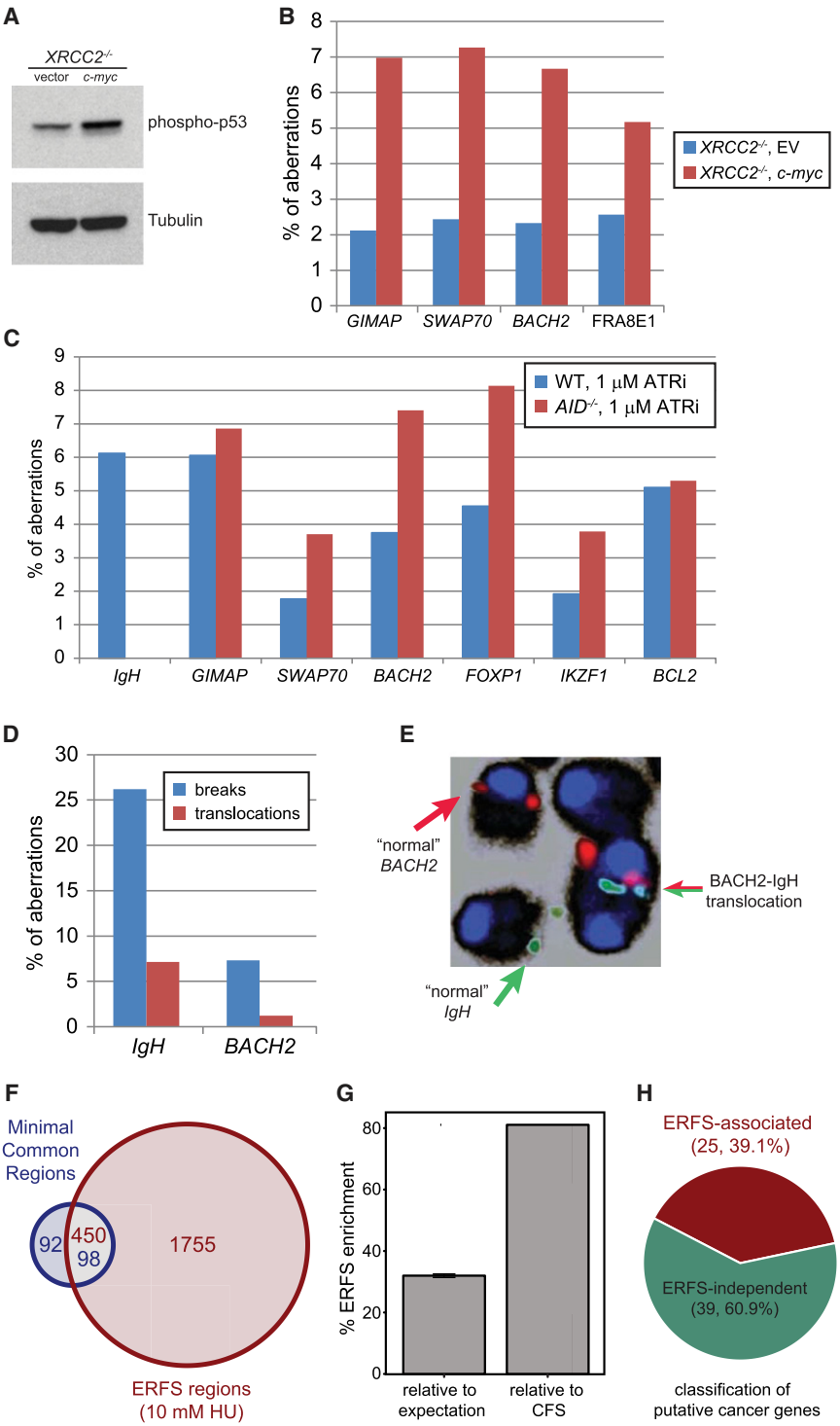

Figure 5. ERFS Fragility Is Observed in Response to Oncogenic Stress and in Human Cancer

(A) Western blot for phosphorylated p53 in *c-myc* and EV-infected *XRCC2*$^{-/-}$ B cells.

(B) Aberrations in *c-myc*-infected and EV-infected *XRCC2*$^{-/-}$ B cells.

(C) Aberrations in WT (blue bars) and *AID*$^{-/-}$ B cells (red bars) treated with 1 μM ATRi.

(D) Spontaneous chromosome breaks (blue bars) and translocations (red bars) at the *IgH* and *BACH2* locus in IgκAID/*53BP1*$^{-/-}$ B cells.

(E) Normal chromosomes and a translocation of *BACH2* ERFS (red) to the *IgH* locus (green) is shown.

(F and G) ERFSs significantly overlap with MCRs detected in DLBCL. The Venn diagram shows the overlap of ERFSs with MCR found in DLBCL. The total number of regions is indicated for each shared and unique area and color-coded based on the region's title.

(G) Significance of correlation between the ERFSs and MCRs is evaluated relative to the permutation model and CFSs. The percent increase in the overlap between the ERFSs and MCRs relative to the permutation model's expectation (mean ± SEM, $p < 1 \times 10^{-4}$) and CFSs are shown in the left and right bar graphs, respectively.

(H) ERFSs are enriched for known cancer genes. The pie chart shows the fraction of putative cancer genes (Bignell et al., 2010) associated with ERFSs ($p < 6 \times 10^{-20}$). See also Figure S6 and Tables S3 and S4.

high resolution copy-number changes detected in biopsies of patients with diffuse large B cell lymphoma (DLBCL), the most common type of non-Hodgkins lymphoma (Lenz et al., 2008). A total of 190 "minimal common regions" (MCRs) were found among 203 biopsies, carrying a gain or a loss of a chromosomal region ranging in size from 5 kbp to 21Mbp (Lenz et al., 2008). Mouse ERFS coordinates were overlaid onto the human genome using two methods, yielding 2,205 syntenic regions (Figures S6B–S6D). Notably, 51.6% of the MCRs observed in primary DLBCL overlapped with syntenic ERFS regions (p(permutation) $< 1 \times 10^{-4}$, Figure 5F). Moreover, 20.4% of ERFSs overlapped with MCRs, 32% higher than expectation (p(permutation) $< 1 \times 10^{-6}$, Figure 5G). Surprisingly, ERFS were deleted or amplified in DLBCL at least 81% more frequently as compared to CFSs, despite their cancer-specific propensity for breakage (Figure 5G). Moreover, our analysis indicated that the DLBCL copy-number alterations exhibited 2-fold higher correlation with B cell ERFSs compared to deletions and/or amplifications in T lineage acute lymphoblastic leukemia (Figure S6A) (Zhang et al., 2012a). Finally, by examining homozygous deletions in cancer genomes (Bignell et al., 2010), we found that 25 out of 64 genes known to contribute to oncogenesis coincide with ERFSs (p(hypergeometric) $< 6 \times 10^{-20}$, Figure 5H; Table S4). Based on these findings,

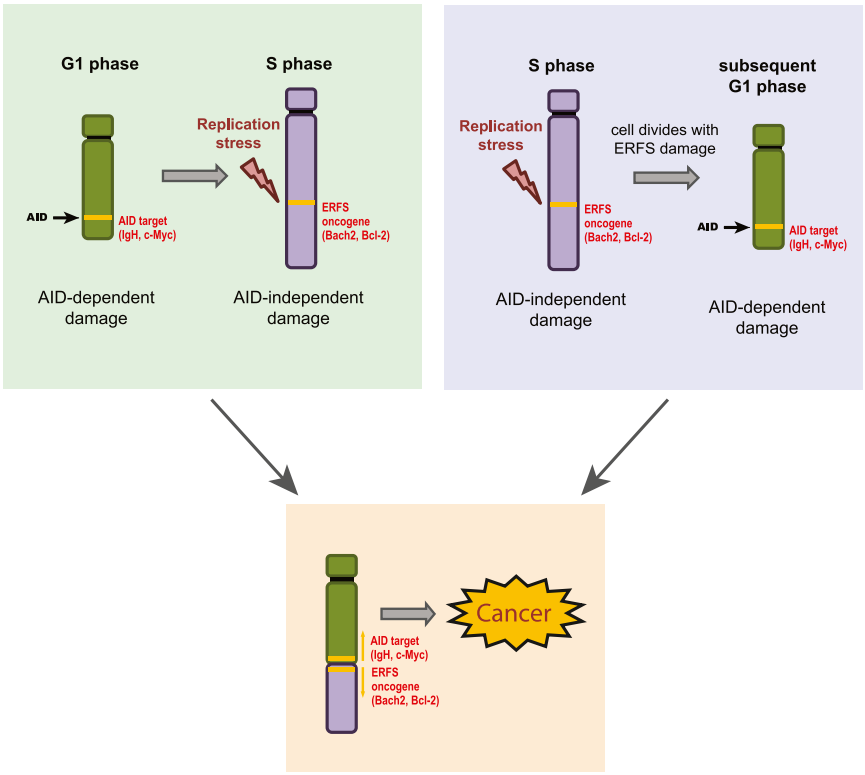

Figure 6. Model for Recurrent Rearrangements in B Cell Lymphomas

AID is active in G1 (Petersen et al., 2001) and targets IgH and various oncogenes (e.g., *c-myc*). Replication fork collapse at ERFSs in S phase occurs at preferential sites including various cancer-associated genes (e.g., *BCL2*, *BACH2*). An AID-generated break might be passed from G1 to early S, where it meets an ERFS, which may eventually result in a translocation (left). Alternatively, an ERFS (bearing unresolved a replication intermediate of under-replicated DNA) might break in mitosis and then become permissive to translocate to an AID-induced DSB in the next G1 phase of the cell cycle (right).

we conclude that ERFSs are a significant feature of the mutational landscape of diffuse large B cell lymphomas and potentially other cancers.

DISCUSSION

Replicative Stress at ERFSs Contributes to Genome Instability in B Cells

Although AID has been implicated in B cell translocations (Gostissa et al., 2011), very little is known about the mechanisms of chromosomal breakage at several *IgH*-partner loci, including *BCL2*, *BACH2*, and *FOXP1*. Besides programmed DNA damage, replication-based mechanisms are a major contributor to chromosomal instability in cancer (Liu et al., 2012). Activated B cells are among the most rapidly dividing mammalian cells (Zhang et al., 1988), which potentially exposes them to high endogenous levels of replicative stress. Here, we have used a genome-wide approach to identify a subset of early replicating regions in the B cell genome that are particularly vulnerable to fork collapse and contribute to rearrangements in B cell malignancies. In our model, ERFS breaks can occur after the generation of unrepaired AID-induced breaks in G1, and the two breaks could recombine during S or G2. Alternatively, ERFS damage might persist through mitosis resulting in DNA breaks in the subsequent G1 phase when AID is predominantly active. In either case, we suggest that AID-mediated DSBs in G1 (Petersen et al., 2001), together with replication-stress-induced damage at recurrent loci, can coordinately drive B cell lymphoma initiation and progression (Figure 6).

ERFS versus CFS

CFSs are considered to be the most replication-stress-sensitive sites in the genome (Durkin and Glover, 2007). Although no single mechanism accounts for CFS instability, it is hypothesized that a number of different characteristics may contribute to their fragility including co-occurrence with very large genes, late replication, low density of replication origins, high A-T content, and sequences prone to form secondary structures, histone hypoacetylation, and a condensed chromatin structure (Helmrich et al., 2011; Jiang et al., 2009; Letessier et al., 2011; Ozeri-Galai et al., 2011). In stark contrast to CFSs, our identified ERFSs replicate early; have an open chromatin configuration; and are origin-, gene-, and G-C-rich.

Despite these diametrically opposite properties, both CFS and ERFS fragility are increased by ATR inhibition (Figure 4A), oncogenic stress (Figure 5B), and deficiencies in HR (Figure 3C) (Bartek et al., 2007; Durkin and Glover, 2007; Halazonetis et al., 2008). These conditions decrease the rate of fork progression but concomitantly increase the density of replication initiating events (Bester et al., 2011; Daboussi et al., 2008; Dominguez-Sola et al., 2007; Shechter et al., 2004), which might contribute to the damage at both CFSs and ERFSs, respectively. The decrease in fork speed hinders the completion of replication at CFSs, either because of the scarcity of origins near CFSs (Letessier et al., 2011), the heterochromatic nature of the regions that would limit accessibility of DNA replication and/or DSB repair machineries (Jiang et al., 2009), or because of the interference between transcription and replication at very large genes (Helmrich et al., 2011). Although additional origins are not activated near CFSs upon replication stress (Letessier et al., 2011), an increase in origin activity at early replicons might paradoxically contribute to genome instability at ERFSs. For example, increasing the replication initiation events near highly transcribed gene clusters with divergent and/or convergent gene pairs could increase conflicts between DNA replication and transcription machineries. The higher density of activated origins at ERFSs would also be expected to prematurely deplete

nucleotide pools (Bester et al., 2011), thereby increasing the probability of subsequent fork stalling and collapse. These two outcomes of replication stress are likely to be linked because increased replication initiation and depletion of nucleotide supplies slows replication (Bester et al., 2011; Jones et al., 2012), whereas slow fork progression causes activation of dormant origins (Ge et al., 2007), and both incomplete replication and increased origin firing are monitored by ATR activity (Shechter et al., 2004). In conclusion, increased initiating events at ERFSs and a paucity of replication initiation at CFSs could both challenge replication fidelity.

ERFSs and Cancer

Oncogenic stress is a major driving force in the early stages of cancer development (Halazonetis et al., 2008); nevertheless, the factors that trigger replicative stress in vivo remain unclear. In the case of B cell lymphomas, oncogenic stress can be initiated by the activity of AID, which by targeting non-*Ig* genes such as *c-myc* (Robbiani et al., 2008), leads to *c-myc*/*IgH* translocations and consequent aberrant *c-myc* expression. This form of AID-induced oncogenic stress or high levels of proliferative activity in activated B cells could generate DNA damage at ERFSs (Figure 6).

Altogether, 103 AID hot spots (Chiarle et al., 2011; Klein et al., 2011)—including the *GIMAP* cluster, *MHCII* locus, and *IKZF1*—were also identified as ERFS hot spots in this study (Table S1). It is possible that the overlap observed between a subset of off-target AID sites and ERFSs is due to common underlying features of these loci. For example, AID is recruited to ssDNA regions (Chaudhuri and Alt, 2004), which are also generated during replicative stress; AID-dependent DSBs and ERFSs are also both enriched in repeat elements (Staszewski et al., 2011). In addition, chromosomal regions with the highest transcriptional activity have the highest AID-dependent translocation density (Chiarle et al., 2011; Klein et al., 2011), and early origins and translocations frequently reside near transcription start sites and RNA polymerase-II-binding sites (Chiarle et al., 2011; Klein et al., 2011). Thus, these euchromatic regions could serve both as AID targets in G1 and also be susceptible to fork collapse during early S phase.

A number of different hypotheses have been put forward about the mechanisms that promote recurrent translocations in mature B cell lymphomas. These include recurrent genomic damage by AID, random DNA damage followed by selection, and a nonrandom 3D organization of the genome (Chiarle et al., 2011; Hakim et al., 2012; Klein et al., 2011; Zhang et al., 2012b). To date, replication-stress-induced DNA damage has been associated with late-replicating CFS. By using an alternative experimental approach for the discovery of fragile site expression during early replication, we have identified a novel source of recurrent AID-independent DNA breaks that may play a mechanistic role in some of the most common genome rearrangements during B cell lymphomagenesis. Because transcriptional activity and replication timing of a genomic region vary among different cell lineages (Hansen et al., 2010), different sets of ERFSs might also account for recurrent chromosomal rearrangements in cancers of distinct cellular origins.

EXPERIMENTAL PROCEDURES

Mice

XRCC2$^{-/-}$(Frappart et al., 2009), 53BP1$^{-/-}$ (Ward et al., 2004), IgκAID (Robbiani et al., 2009), *AID*$^{-/-}$ (Muramatsu et al., 2000), and *SWAP70*$^{-/-}$ (Borggrefe et al., 2001) mice have been described. *SWAP70*$^{-/-}$ and WT control mice used in Figure 4D are C57BL/6 background; all other mice are 129/Sv x C57BL/6 background.

ChIP-Seq, Repli-Seq, RNA-Seq, DHS I Mapping, and FISH Analysis

ChIP-seq and RNA-Seq procedures were performed as in Yamane et al. (2011), Repli-Seq was performed as described in Hansen et al. (2010). DHSI mapping was performed as described (Sekimata et al., 2009), and fluorescence in situ hybridization (FISH) analysis is described in Callén et al. (2007). For detailed methods, see Extended Experimental Procedures.

BACs

Individual BACs to ERFSs were identified using NCBI clone finder and purchased from BACPAC. For complete list of BAC probes used in FISH experiments see Extended Experimental Procedures.

Retroviral Infection

Cells were infected with pMX-c-Myc-IRES-GFP or empty vector and GFP-positive cells were sorted as described (Robbiani et al., 2008).

Statistical and Computational Analyses

Detailed description is available in Extended Experimental Procedures.

ACCESSION NUMBERS

The ChIP-seq and RNA-seq data are deposited in GEO under accession number GSE43504.

SUPPLEMENTAL INFORMATION

Supplemental Information includes Extended Experimental Procedures, six figures, and four tables and can be found with this article online at http://dx.doi.org/10.1016/j.cell.2013.01.006.

ACKNOWLEDGMENTS

We thank Rolf Jessberger and Alessandra Pernis for *SWAP70*$^{-/-}$ mice, Mila Jankovic for pMX-c-Myc-IRES-GFP, Jean Gautier, Mirit Aladjem, and Toren Finkel for discussions and Lars Grontved for help with DHS mapping. This work was supported by the Intramural Research Program of the NIH, the National Cancer Institute, and the Center for Cancer Research, and by a Department of Defense grant to A.N. (BC102335). This study utilized the high-performance computational capabilities of the Biowulf Linux cluster at the NIH.

Received: November 9, 2012
Revised: December 10, 2012
Accepted: January 2, 2013
Published: January 24, 2013

REFERENCES

Bartek, J., Bartkova, J., and Lukas, J. (2007). DNA damage signalling guards against activated oncogenes and tumour progression. Oncogene *26*, 7773–7779.

Bester, A.C., Roniger, M., Oren, Y.S., Im, M.M., Sarni, D., Chaoat, M., Bensimon, A., Zamir, G., Shewach, D.S., and Kerem, B. (2011). Nucleotide deficiency promotes genomic instability in early stages of cancer development. Cell *145*, 435–446.

Bignell, G.R., Greenman, C.D., Davies, H., Butler, A.P., Edkins, S., Andrews, J.M., Buck, G., Chen, L., Beare, D., Latimer, C., et al. (2010). Signatures of mutation and selection in the cancer genome. Nature *463*, 893–898.

Borggrefe, T., Keshavarzi, S., Gross, B., Wabl, M., and Jessberger, R. (2001). Impaired IgE response in SWAP-70-deficient mice. Eur. J. Immunol. *31*, 2467–2475.

Bothmer, A., Robbiani, D.F., Feldhahn, N., Gazumyan, A., Nussenzweig, A., and Nussenzweig, M.C. (2010). 53BP1 regulates DNA resection and the choice between classical and alternative end joining during class switch recombination. J. Exp. Med. *207*, 855–865.

Bunting, S.F., Callén, E., Kozak, M.L., Kim, J.M., Wong, N., López-Contreras, A.J., Ludwig, T., Baer, R., Faryabi, R.B., Malhowski, A., et al. (2012). Mol. Cell *46*, 125–135.

Bunting, S.F., Callén, E., Wong, N., Chen, H.T., Polato, F., Gunn, A., Bothmer, A., Feldhahn, N., Fernandez-Capetillo, O., Cao, L., et al. (2010). 53BP1 inhibits homologous recombination in Brca1-deficient cells by blocking resection of DNA breaks. Cell *141*, 243–254.

Callén, E., Jankovic, M., Difilippantonio, S., Daniel, J.A., Chen, H.T., Celeste, A., Pellegrini, M., McBride, K., Wangsa, D., Bredemeyer, A.L., et al. (2007). ATM prevents the persistence and propagation of chromosome breaks in lymphocytes. Cell *130*, 63–75.

Cha, R.S., and Kleckner, N. (2002). ATR homolog Mec1 promotes fork progression, thus averting breaks in replication slow zones. Science *297*, 602–606.

Chaudhuri, J., and Alt, F.W. (2004). Class-switch recombination: interplay of transcription, DNA deamination and DNA repair. Nat. Rev. Immunol. *4*, 541–552.

Chen, H.T., Bhandoola, A., Difilippantonio, M.J., Zhu, J., Brown, M.J., Tai, X., Rogakou, E.P., Brotz, T.M., Bonner, W.M., Ried, T., and Nussenzweig, A. (2000). Response to RAG-mediated VDJ cleavage by NBS1 and gamma-H2AX. Science *290*, 1962–1965.

Chiarle, R., Zhang, Y., Frock, R.L., Lewis, S.M., Molinie, B., Ho, Y.J., Myers, D.R., Choi, V.W., Compagno, M., Malkin, D.J., et al. (2011). Genome-wide translocation sequencing reveals mechanisms of chromosome breaks and rearrangements in B cells. Cell *147*, 107–119.

Cimprich, K.A., and Cortez, D. (2008). ATR: an essential regulator of genome integrity. Nat. Rev. Mol. Cell Biol. *9*, 616–627.

Costa, S., and Blow, J.J. (2007). The elusive determinants of replication origins. EMBO Rep. *8*, 332–334.

Daboussi, F., Courbet, S., Benhamou, S., Kannouche, P., Zdzienicka, M.Z., Debatisse, M., and Lopez, B.S. (2008). A homologous recombination defect affects replication-fork progression in mammalian cells. J. Cell Sci. *121*, 162–166.

Debatisse, M., Le Tallec, B., Letessier, A., Dutrillaux, B., and Brison, O. (2012). Common fragile sites: mechanisms of instability revisited. Trends Genet. *28*, 22–32.

Dominguez-Sola, D., Ying, C.Y., Grandori, C., Ruggiero, L., Chen, B., Li, M., Galloway, D.A., Gu, W., Gautier, J., and Dalla-Favera, R. (2007). Non-transcriptional control of DNA replication by c-Myc. Nature *448*, 445–451.

Durkin, S.G., and Glover, T.W. (2007). Chromosome fragile sites. Annu. Rev. Genet. *41*, 169–192.

Feng, W., Collingwood, D., Boeck, M.E., Fox, L.A., Alvino, G.M., Fangman, W.L., Raghuraman, M.K., and Brewer, B.J. (2006). Genomic mapping of single-stranded DNA in hydroxyurea-challenged yeasts identifies origins of replication. Nat. Cell Biol. *8*, 148–155.

Frappart, P.O., Lee, Y., Russell, H.R., Chalhoub, N., Wang, Y.D., Orii, K.E., Zhao, J., Kondo, N., Baker, S.J., and McKinnon, P.J. (2009). Recurrent genomic alterations characterize medulloblastoma arising from DNA double-strand break repair deficiency. Proc. Natl. Acad. Sci. USA *106*, 1880–1885.

Ge, X.Q., Jackson, D.A., and Blow, J.J. (2007). Dormant origins licensed by excess Mcm2-7 are required for human cells to survive replicative stress. Genes Dev. *21*, 3331–3341.

Gostissa, M., Alt, F.W., and Chiarle, R. (2011). Mechanisms that promote and suppress chromosomal translocations in lymphocytes. Annu. Rev. Immunol. *29*, 319–350.

Hakim, O., Resch, W., Yamane, A., Klein, I., Kieffer-Kwon, K.R., Jankovic, M., Oliveira, T., Bothmer, A., Voss, T.C., Ansarah-Sobrinho, C., et al. (2012). DNA damage defines sites of recurrent chromosomal translocations in B lymphocytes. Nature *484*, 69–74.

Halazonetis, T.D., Gorgoulis, V.G., and Bartek, J. (2008). An oncogene-induced DNA damage model for cancer development. Science *319*, 1352–1355.

Hansen, R.S., Thomas, S., Sandstrom, R., Canfield, T.K., Thurman, R.E., Weaver, M., Dorschner, M.O., Gartler, S.M., and Stamatoyannopoulos, J.A. (2010). Sequencing newly replicated DNA reveals widespread plasticity in human replication timing. Proc. Natl. Acad. Sci. USA *107*, 139–144.

Hashash, N., Johnson, A.L., and Cha, R.S. (2011). Regulation of fragile sites expression in budding yeast by MEC1, RRM3 and hydroxyurea. J. Cell Sci. *124*, 181–185.

Helmrich, A., Stout-Weider, K., Hermann, K., Schrock, E., and Heiden, T. (2006). Common fragile sites are conserved features of human and mouse chromosomes and relate to large active genes. Genome Res. *16*, 1222–1230.

Helmrich, A., Ballarino, M., and Tora, L. (2011). Collisions between replication and transcription complexes cause common fragile site instability at the longest human genes. Mol. Cell *44*, 966–977.

Jiang, Y., Lucas, I., Young, D.J., Davis, E.M., Karrison, T., Rest, J.S., and Le Beau, M.M. (2009). Common fragile sites are characterized by histone hypoacetylation. Hum. Mol. Genet. *18*, 4501–4512.

Jones, R.M., Mortusewicz, O., Afzal, I., Lorvellec, M., García, P., Helleday, T., and Petermann, E. (2012). Increased replication initiation and conflicts with transcription underlie Cyclin E-induced replication stress. Oncogene. Published online September 3, 2012.

Kato, L., Begum, N.A., Burroughs, A.M., Doi, T., Kawai, J., Daub, C.O., Kawaguchi, T., Matsuda, F., Hayashizaki, Y., and Honjo, T. (2012). Nonimmunoglobulin target loci of activation-induced cytidine deaminase (AID) share unique features with immunoglobulin genes. Proc. Natl. Acad. Sci. USA *109*, 2479–2484.

Klein, I.A., Resch, W., Jankovic, M., Oliveira, T., Yamane, A., Nakahashi, H., Di Virgilio, M., Bothmer, A., Nussenzweig, A., Robbiani, D.F., et al. (2011). Translocation-capture sequencing reveals the extent and nature of chromosomal rearrangements in B lymphocytes. Cell *147*, 95–106.

Kobayashi, S., Taki, T., Chinen, Y., Tsutsumi, Y., Ohshiro, M., Kobayashi, T., Matsumoto, Y., Kuroda, J., Horiike, S., Nishida, K., and Taniwaki, M. (2011). Identification of IGHCδ-BACH2 fusion transcripts resulting from cryptic chromosomal rearrangements of 14q32 with 6q15 in aggressive B-cell lymphoma/leukemia. Genes Chromosomes Cancer *50*, 207–216.

Lenz, G., Wright, G.W., Emre, N.C., Kohlhammer, H., Dave, S.S., Davis, R.E., Carty, S., Lam, L.T., Shaffer, A.L., Xiao, W., et al. (2008). Molecular subtypes of diffuse large B-cell lymphoma arise by distinct genetic pathways. Proc. Natl. Acad. Sci. USA *105*, 13520–13525.

Letessier, A., Millot, G.A., Koundrioukoff, S., Lachagès, A.M., Vogt, N., Hansen, R.S., Malfoy, B., Brison, O., and Debatisse, M. (2011). Cell-type-specific replication initiation programs set fragility of the FRA3B fragile site. Nature *470*, 120–123.

Liu, M., Duke, J.L., Richter, D.J., Vinuesa, C.G., Goodnow, C.C., Kleinstein, S.H., and Schatz, D.G. (2008). Two levels of protection for the B cell genome during somatic hypermutation. Nature *451*, 841–845.

Liu, P., Carvalho, C.M., Hastings, P.J., and Lupski, J.R. (2012). Mechanisms for recurrent and complex human genomic rearrangements. Curr. Opin. Genet. Dev. *22*, 211–220.

MacAlpine, D.M., Rodríguez, H.K., and Bell, S.P. (2004). Coordination of replication and transcription along a Drosophila chromosome. Genes Dev. *18*, 3094–3105.

Mirkin, E.V., and Mirkin, S.M. (2007). Replication fork stalling at natural impediments. Microbiol. Mol. Biol. Rev. *71*, 13–35.

Muramatsu, M., Kinoshita, K., Fagarasan, S., Yamada, S., Shinkai, Y., and Honjo, T. (2000). Class switch recombination and hypermutation require activation-induced cytidine deaminase (AID), a potential RNA editing enzyme. Cell *102*, 553–563.

Ozeri-Galai, E., Lebofsky, R., Rahat, A., Bester, A.C., Bensimon, A., and Kerem, B. (2011). Failure of origin activation in response to fork stalling leads to chromosomal instability at fragile sites. Mol. Cell *43*, 122–131.

Petermann, E., Orta, M.L., Issaeva, N., Schultz, N., and Helleday, T. (2010). Hydroxyurea-stalled replication forks become progressively inactivated and require two different RAD51-mediated pathways for restart and repair. Mol. Cell *37*, 492–502.

Petersen, S., Casellas, R., Reina-San-Martin, B., Chen, H.T., Difilippantonio, M.J., Wilson, P.C., Hanitsch, L., Celeste, A., Muramatsu, M., Pilch, D.R., et al. (2001). AID is required to initiate Nbs1/gamma-H2AX focus formation and mutations at sites of class switching. Nature *414*, 660–665.

Raveendranathan, M., Chattopadhyay, S., Bolon, Y.T., Haworth, J., Clarke, D.J., and Bielinsky, A.K. (2006). Genome-wide replication profiles of S-phase checkpoint mutants reveal fragile sites in yeast. EMBO J. *25*, 3627–3639.

Robbiani, D.F., Bothmer, A., Callen, E., Reina-San-Martin, B., Dorsett, Y., Difilippantonio, S., Bolland, D.J., Chen, H.T., Corcoran, A.E., Nussenzweig, A., and Nussenzweig, M.C. (2008). AID is required for the chromosomal breaks in c-myc that lead to c-myc/IgH translocations. Cell *135*, 1028–1038.

Robbiani, D.F., Bunting, S., Feldhahn, N., Bothmer, A., Camps, J., Deroubaix, S., McBride, K.M., Klein, I.A., Stone, G., Eisenreich, T.R., et al. (2009). AID produces DNA double-strand breaks in non-Ig genes and mature B cell lymphomas with reciprocal chromosome translocations. Mol. Cell *36*, 631–641.

Schlacher, K., Wu, H., and Jasin, M. (2012). A distinct replication fork protection pathway connects Fanconi anemia tumor suppressors to RAD51-BRCA1/2. Cancer Cell *22*, 106–116.

Sekimata, M., Pérez-Melgosa, M., Miller, S.A., Weinmann, A.S., Sabo, P.J., Sandstrom, R., Dorschner, M.O., Stamatoyannopoulos, J.A., and Wilson, C.B. (2009). CCCTC-binding factor and the transcription factor T-bet orchestrate T helper 1 cell-specific structure and function at the interferon-gamma locus. Immunity *31*, 551–564.

Shechter, D., Costanzo, V., and Gautier, J. (2004). ATR and ATM regulate the timing of DNA replication origin firing. Nat. Cell Biol. *6*, 648–655.

Sonoda, E., Sasaki, M.S., Buerstedde, J.M., Bezzubova, O., Shinohara, A., Ogawa, H., Takata, M., Yamaguchi-Iwai, Y., and Takeda, S. (1998). Rad51-deficient vertebrate cells accumulate chromosomal breaks prior to cell death. EMBO J. *17*, 598–608.

Stamatoyannopoulos, J.A., Snyder, M., Hardison, R., Ren, B., Gingeras, T., Gilbert, D.M., Groudine, M., Bender, M., Kaul, R., Canfield, T., et al.; Mouse ENCODE Consortium. (2012). An encyclopedia of mouse DNA elements (Mouse ENCODE). Genome Biol. *13*, 418.

Staszewski, O., Baker, R.E., Ucher, A.J., Martier, R., Stavnezer, J., and Guikema, J.E. (2011). Activation-induced cytidine deaminase induces reproducible DNA breaks at many non-Ig Loci in activated B cells. Mol. Cell *41*, 232–242.

Stephan, A.K., Kliszczak, M., and Morrison, C.G. (2011). The Nse2/Mms21 SUMO ligase of the Smc5/6 complex in the maintenance of genome stability. FEBS Lett. *585*, 2907–2913.

Tanaka, T., and Nasmyth, K. (1998). Association of RPA with chromosomal replication origins requires an Mcm protein, and is regulated by Rad53, and cyclin- and Dbf4-dependent kinases. EMBO J. *17*, 5182–5191.

Toledo, L.I., Murga, M., Zur, R., Soria, R., Rodriguez, A., Martinez, S., Oyarzabal, J., Pastor, J., Bischoff, J.R., and Fernandez-Capetillo, O. (2011). A cell-based screen identifies ATR inhibitors with synthetic lethal properties for cancer-associated mutations. Nat. Struct. Mol. Biol. *18*, 721–727.

Tsai, A.G., Lu, H., Raghavan, S.C., Muschen, M., Hsieh, C.L., and Lieber, M.R. (2008). Human chromosomal translocations at CpG sites and a theoretical basis for their lineage and stage specificity. Cell *135*, 1130–1142.

Ward, I.M., and Chen, J. (2001). Histone H2AX is phosphorylated in an ATR-dependent manner in response to replicational stress. J. Biol. Chem. *276*, 47759–47762.

Ward, I.M., Reina-San-Martin, B., Olaru, A., Minn, K., Tamada, K., Lau, J.S., Cascalho, M., Chen, L., Nussenzweig, A., Livak, F., et al. (2004). 53BP1 is required for class switch recombination. J. Cell Biol. *165*, 459–464.

Yamane, A., Resch, W., Kuo, N., Kuchen, S., Li, Z., Sun, H.W., Robbiani, D.F., McBride, K., Nussenzweig, M.C., and Casellas, R. (2011). Deep-sequencing identification of the genomic targets of the cytidine deaminase AID and its cofactor RPA in B lymphocytes. Nat. Immunol. *12*, 62–69.

Yamane, A., Robbiani, D.F., Resch, W., Bothmer, A., Nakahashi, H., Oliveira, T., Rommel, P.C., Brown, E.J., Nussenzweig, A., Nussenzweig, M.C., et al. (2013). RPA accumulation during class switch recombination represents 5′-3′ DNA end resection during S-G2/M phase of the cell cycle. Cell Rep. Published January 02, 2013. http://dx.doi.org/10.1016/j.celrep.2012.12.006.

Zhang, J., MacLennan, I.C., Liu, Y.J., and Lane, P.J. (1988). Is rapid proliferation in B centroblasts linked to somatic mutation in memory B cell clones? Immunol. Lett. *18*, 297–299.

Zhang, J., Ding, L., Holmfeldt, L., Wu, G., Heatley, S.L., Payne-Turner, D., Easton, J., Chen, X., Wang, J., Rusch, M., et al. (2012a). The genetic basis of early T-cell precursor acute lymphoblastic leukaemia. Nature *481*, 157–163.

Zhang, Y., McCord, R.P., Ho, Y.J., Lajoie, B.R., Hildebrand, D.G., Simon, A.C., Becker, M.S., Alt, F.W., and Dekker, J. (2012b). Spatial organization of the mouse genome and its role in recurrent chromosomal translocations. Cell *148*, 908–921.

Rif1 Prevents Resection of DNA Breaks and Promotes Immunoglobulin Class Switching

Michela Di Virgilio *et al.*

Science **339**, 711 (2013);
DOI: 10.1126/science.1230624

higher numbers from colon contents than was the nitrate respiration–deficient mutant (Fig. 3H and fig. S8B). Collectively, these data suggested that nitrate respiration conferred a marked growth advantage on commensal *E. coli* in the lumen of the inflamed gut.

The picture emerging from this study is that nitrate generated as a by-product of the host inflammatory response can be used by *E. coli*, and likely by other commensal Enterobacteriaceae, to edge out competing microbes that rely on fermentation to generate energy for growth. Obligate anaerobic microbes in the intestine compete for nutrients that are available for fermentation but cannot use nonfermentable nutrients (such as fermentation end products). The ability to degrade nonfermentable substrates probably enables *E. coli* to sidestep this competition, which explains the fitness advantage conferred by nitrate respiration in the inflamed gut. Through this mechanism, inflammation contributes to a bloom of nitrate-respiration–proficient Enterobacteriaceae, providing a plausible explanation for the dysbiosis associated with intestinal inflammation (*3*–*12*). This general principle might also influence the dynamics of host-associated bacterial communities outside the large bowel, as nitrate respiration confers a fitness advantage in the oxygen-poor and nitrate-rich environment of the cystic fibrosis airway (*21*).

References and Notes

1. P. B. Eckburg *et al.*, *Science* **308**, 1635 (2005).
2. R. E. Ley *et al.*, *Proc. Natl. Acad. Sci. U.S.A.* **102**, 11070 (2005).
3. A. Krook, B. Lindström, J. Kjellander, G. Järnerot, L. Bodin, *J. Clin. Pathol.* **34**, 645 (1981).
4. M. H. Giaffer, C. D. Holdsworth, B. I. Duerden, *J. Med. Microbiol.* **35**, 238 (1991).
5. P. Seksik *et al.*, *Gut* **52**, 237 (2003).
6. U. Gophna, K. Sommerfeld, S. Gophna, W. F. Doolittle, S. J. Veldhuyzen van Zanten, *J. Clin. Microbiol.* **44**, 4136 (2006).
7. D. N. Frank *et al.*, *Proc. Natl. Acad. Sci. U.S.A.* **104**, 13780 (2007).
8. M. M. Heimesaat *et al.*, *PLoS ONE* **2**, e662 (2007).
9. C. Lupp *et al.*, *Cell Host Microbe* **2**, 119 (2007).
10. B. Stecher *et al.*, *PLoS Biol.* **5**, e244 (2007).
11. M. Barman *et al.*, *Infect. Immun.* **76**, 907 (2008).
12. W. S. Garrett *et al.*, *Cell Host Microbe* **8**, 292 (2010).
13. J. O. N. Lundberg, J. M. Lundberg, K. Alving, P. M. Hellström, *Lancet* **344**, 1673 (1994).
14. I. I. Singer *et al.*, *Gastroenterology* **111**, 871 (1996).
15. A. Enocksson, J. Lundberg, E. Weitzberg, A. Norrby-Teglund, B. Svenungsson, *Clin. Diagn. Lab. Immunol.* **11**, 250 (2004).
16. C. Szabó, H. Ischiropoulos, R. Radi, *Nat. Rev. Drug Discov.* **6**, 662 (2007).
17. C. Schöneich, *Biochim. Biophys. Acta* **1703**, 111 (2005).
18. B. Balagam, D. E. Richardson, *Inorg. Chem.* **47**, 1173 (2008).
19. R. B. Gennis, V. Stewart, in Escherichia coli *and* Salmonella. *Cellular and Molecular Biology*, F. C. Neidhardt *et al.*, Eds. (ASM Press, Washington, DC, 1996), vol. 1, pp. 217–261.
20. M. C. Pils *et al.*, *Inflamm. Bowel Dis.* **17**, 2038 (2011).
21. L. R. Hoffman *et al.*, *PLoS Pathog.* **6**, e1000712 (2010).

Acknowledgments: We thank W. Müller for providing *Il10*$^{flox/flox}$ *Cd4-cre* mice and E. Romao for technical assistance. The data reported in the manuscript are tabulated in the main paper and in the supplementary materials. This work was supported by the California Agricultural Experiment Station (I.E.P. and S.J.P.) and Public Health Service grants AI090387 (R.M.T), AI076246 (L.G.A and A.J.B.), and AI088122 (A.J.B.). P.T. was supported by a scholarship from the Faculty of Medicine, Chiang Mai University, Thailand.

Supplementary Materials

www.sciencemag.org/cgi/content/full/339/6120/708/DC1
Materials and Methods
Figs. S1 to S11
Tables S1 and S2
References (*22*–*39*)

7 November 2012; accepted 5 December 2012
10.1126/science.1232467

Rif1 Prevents Resection of DNA Breaks and Promotes Immunoglobulin Class Switching

Michela Di Virgilio,[1] Elsa Callen,[3]* Arito Yamane,[4]* Wenzhu Zhang,[5]* Mila Jankovic,[1] Alexander D. Gitlin,[1] Niklas Feldhahn,[1] Wolfgang Resch,[4] Thiago Y. Oliveira,[1,6,7] Brian T. Chait,[5] André Nussenzweig,[3] Rafael Casellas,[4] Davide F. Robbiani,[1] Michel C. Nussenzweig[1,2]†

DNA double-strand breaks (DSBs) represent a threat to the genome because they can lead to the loss of genetic information and chromosome rearrangements. The DNA repair protein p53 binding protein 1 (53BP1) protects the genome by limiting nucleolytic processing of DSBs by a mechanism that requires its phosphorylation, but whether 53BP1 does so directly is not known. Here, we identify Rap1-interacting factor 1 (Rif1) as an ATM (ataxia-telangiectasia mutated) phosphorylation-dependent interactor of 53BP1 and show that absence of Rif1 results in 5′-3′ DNA-end resection in mice. Consistent with enhanced DNA resection, Rif1 deficiency impairs DNA repair in the G_1 and S phases of the cell cycle, interferes with class switch recombination in B lymphocytes, and leads to accumulation of chromosome DSBs.

The DNA damage response factor p53 binding protein 1 (53BP1) is a multidomain protein containing a chromatin-binding tudor domain, an oligomerization domain, tandem breast cancer 1 (BRCA1) C-terminal (BRCT) domains, and an N-terminal domain with 28 SQ/TQ potential phosphorylation sites for phosphatidylinositol 3-kinase–related kinases [PIKKs, ataxia-telangiectasia mutated (ATM)/ATM and Rad3-related/DNA-dependent protein kinase catalytic subunit (DNA-PKcs)] (*1*–*3*). 53BP1 contributes to DNA repair in several ways: This protein facilitates joining between intrachromosomal double-strand breaks (DSBs) at a distance (synapsis) (*4*–*7*), it enables heterochromatic DNA repair through relaxation of nucleosome compaction (*2*, *3*), and it protects DNA ends from resection and thereby favors repair of DSBs that occur in G_1 phase by nonhomologous end joining (NHEJ) (*4*, *5*, *8*). Consistent with its role in DNA-end protection, 53BP1 is essential for class switch recombination (CSR) in B lymphocytes (*9*, *10*).

Structure-function studies indicate that, besides the recruitment of 53BP1 to DNA ends, protection requires 53BP1 phosphorylation (*4*), but how this protective effect is mediated is unknown. To identify phosphorylation-dependent interactors of 53BP1, we applied stable isotope labeling by amino acids in cell culture (SILAC). *Trp53bp1*$^{-/-}$ (*Trp53bp1* encodes 53BP1) B cells were infected with retroviruses encoding a C-terminal deleted version of 53BP1 (53BP1^{DB}) or a phosphomutant in which all 28 N-terminal potential PIKK phosphorylation sites were mutated to alanine (53BP1^{DB28A}) (*4*), in media containing isotopically heavy (53BP1^{DB}) or light (53BP1^{DB28A}) lysine and arginine (fig. S1, A to C) (*11*).

Most proteins coprecipitating with 53BP1^{DB} and 53BP1^{DB28A} displayed a $H/(H+L)$ ratio of ~0.5 (H, heavy; L, light), which is characteristic of phospho-independent association (average of 0.57 ± 0.09, peptide count: at least four) (Fig. 1 and table S1). Many of these proteins are nonspecific contaminants, but others such as KRAB-associated protein 1 (KAP-1), dynein light chain LC8-type 1 (Dynll1), Nijmegen breakage syndrome 1 (Nbs1), and H2AX represent authentic phospho-independent 53BP1-interacting proteins (fig. S1D). Three proteins displayed an abundance ratio that was more than four standard deviations (SDs) above the mean, indicating that these proteins interact specifically

[1]Laboratory of Molecular Immunology, The Rockefeller University, New York, NY 10065, USA. [2]Howard Hughes Medical Institute (HHMI), The Rockefeller University, New York, NY 10065, USA. [3]Laboratory of Genome Integrity and Center for Cancer Research, National Cancer Institute (NCI), National Institutes of Health (NIH), Bethesda, MD 20892, USA. [4]Genomics and Immunity and National Institute of Arthritis and Musculoskeletal and Skin Diseases (NIAMS), NCI, NIH, Bethesda, MD 20892, USA. [5]Laboratory of Mass Spectrometry and Gaseous Ion Chemistry, The Rockefeller University, New York, NY 10065, USA. [6]Department of Genetics, Faculty of Medicine, University of São Paulo, Ribeirão Preto, Brazil. [7]National Institute of Science and Technology for Stem Cells and Cell Therapy, Ribeirão Preto, Brazil.

*These authors contributed equally to this work.
†To whom correspondence should be addressed. E-mail: nussen@rockefeller.edu

with phosphorylated 53BP1: Pax interaction with transcription-activation domain protein-1 (Paxip1, or PTIP; 0.95), PTIP-associated protein 1 (Pa1; 0.97), and Rap1-interacting factor 1 (Rif1) (0.96) (Fig. 1 and figs. S1D and S2). PTIP was known to interact with 53BP1 in a phospho-dependent manner (*12*), whereas Pa1 and Rif1 were not.

Rif1 was originally identified in budding yeast as a protein with a key role in telomere length maintenance (*13*). However, in mammalian cells, Rif1 is not essential for telomere homeostasis, but has been assigned a number of different roles in maintaining genome stability, including participation in the DNA damage response (*14*–*16*), repair of S-phase DNA damage (*17*, *18*), and regulation of origin firing during DNA replication (*19*, *20*). However, the mechanism by which Rif1 might contribute to DNA repair and maintenance of genome stability is not known.

To confirm that Rif1 interaction with 53BP1 is dependent on phosphorylation, we performed Western blot analysis of Flag immunoprecipitates from lysates of irradiated *Trp53bp1*$^{-/-}$ B cells infected with retroviruses encoding 53BP1^{DB} or 53BP1^{DB28A}. Whereas Dynll1, a phospho-independent 53BP1 interactor (SILAC ratio: 0.55) (fig. S1D), coimmunoprecipitated with 53BP1^{DB} and 53BP1^{DB28A} to a similar extent (Fig. 2A), only 53BP1^{DB} coimmunoprecipitated with Rif1. We conclude that the interaction between 53BP1 and Rif1 is dependent on phosphorylation of 53BP1.

Ataxia-telangiectasia mutated phosphorylates 53BP1 in response to DSBs (*1*, *3*). To determine whether ATM induces DNA damage–dependent association between Rif1 and 53BP1, we compared irradiated and nonirradiated B cells in coimmunoprecipitation experiments. Although we detected small amounts of Rif1 in 53BP1^{DB} immunoprecipitates from unirradiated cells, this was increased by a factor of >3 after irradiation, and the increase was abrogated by treatment with the ATM inhibitor KU55933 (Fig. 2B). We conclude that Rif1 preferentially interacts with phosphorylated 53BP1 in a DNA damage- and ATM-dependent manner.

Rif1 is recruited to DNA damage foci by 53BP1 (*15*). To determine whether 53BP1 phosphorylation is required for Rif1 focus formation, we tested Rif1 foci in irradiated *Trp53bp1*$^{-/-}$ immortalized mouse embryonic fibroblasts (iMEFs), which were stably transduced with either 53BP1^{DB} or 53BP1^{DB28A}. Rif1 foci were readily detected and colocalized with 53BP1^{DB} (Fig. 2C). In contrast, although 53BP1^{DB28A} formed normal-appearing foci, Rif1 foci were rare and did not colocalize with 53BP1 (Fig. 2C). Furthermore, Rif1 recruitment to ionizing radiation–induced foci (IRIF) and colocalization with 53BP1 were abrogated in ATM-deficient but not DNA-PKcs–deficient iMEFs (fig. S3) (*15*). We conclude that Rif1 recruitment to DNA damage response foci is dependent on ATM-mediated 53BP1 phosphorylation.

The phosphorylation of 53BP1 is essential for CSR (*4*). To examine the role of Rif1 in joining DSBs during CSR, we conditionally ablated Rif1 in B cells using CD19^{Cre}, which is expressed specifically in B cells (*Rif1*$^{F/F}$*Cd19*$^{Cre/+}$ mice) (fig. S4, A to C). To induce CSR, B cells were activated with lipopolysaccharide (LPS) and interleukin-4 (IL-4) in vitro, and switching to immunoglobulin G1 (IgG1) or IgG3 was measured by flow cytometry. CSR to IgG1 and IgG3 was markedly reduced in *Rif1*$^{F/F}$*Cd19*$^{Cre/+}$ B cells, but less so than in *Trp53bp1*$^{-/-}$ controls (Fig. 3, A and B, and fig. S5). Switch junctions from *Rif1*$^{F/F}$*Cd19*$^{Cre/+}$ B cells were comparable to those from *Trp53bp1*$^{-/-}$ and wild-type controls (fig. S6) (*7*), which indicates that, similar to 53BP1 deficiency, absence of Rif1 does not alter the nature of productive CSR joining events.

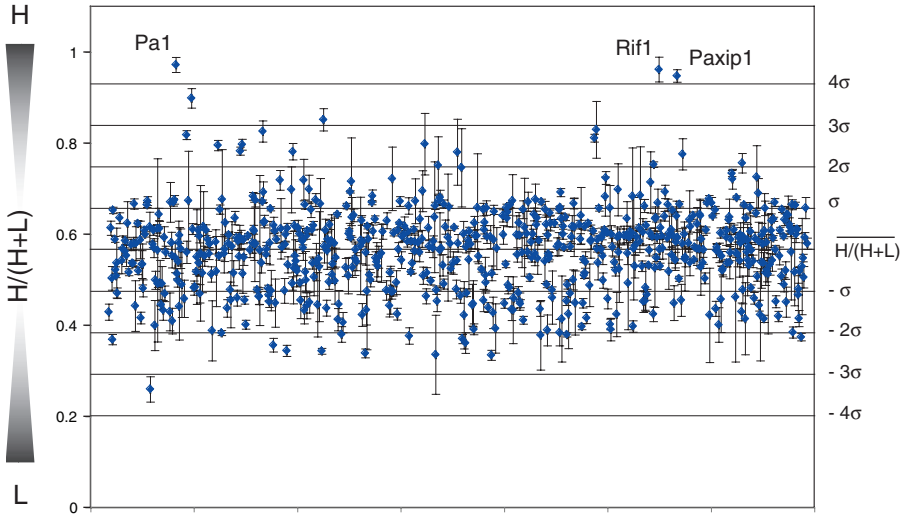

Fig. 1. Identification of phospho-dependent 53BP1 interactors. The graph shows the $H/(H + L)$ ratio distribution of proteins identified by SILAC. Error bars represent the SD of the $H/(H + L)$ mean value for all of the peptides identified for each individual protein (only proteins with at least four peptides were included). $\overline{H/(H + L)}$ and σ are the mean (0.57) and SD (0.09) of the distribution, respectively.

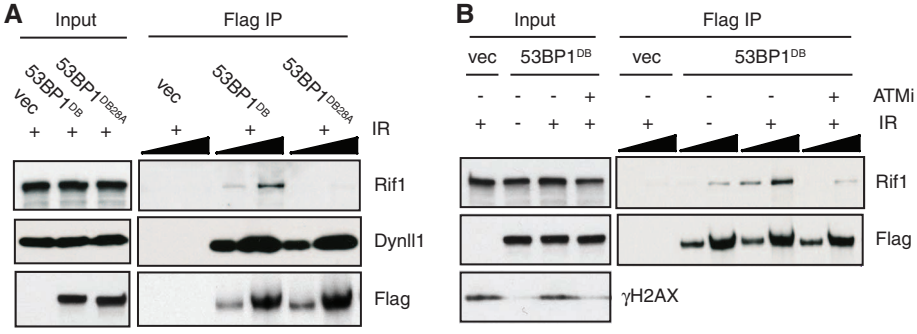

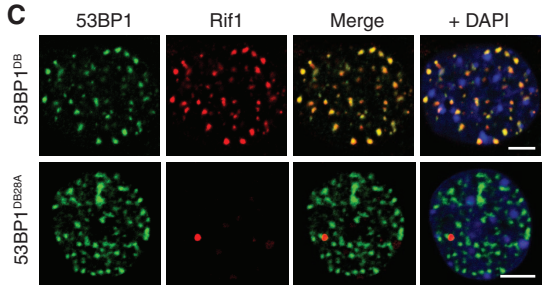

Fig. 2. Rif1 interaction with 53BP1 is dependent on phosphorylation, DNA damage, and ATM. (**A**) Western blot analysis of anti-Flag immunoprecipitates (IP) from irradiated (IR) *Trp53bp1*$^{-/-}$ B lymphocytes infected with empty vector (vec), 53BP1^{DB}, or 53BP1^{DB28A} virus. Triangles indicate threefold dilution. Data are representative of two independent experiments. (**B**) Western blot analysis of anti-Flag immunoprecipitates from *Trp53bp1*$^{-/-}$ B cells infected with empty vector or 53BP1^{DB}. Cells were either left untreated or irradiated [50 gray (Gy), 45-min recovery] in the presence or absence of the ATM kinase inhibitor KU55933 (ATMi). Triangles indicate threefold dilution. Data are representative of two independent experiments. (**C**) Immunofluorescent staining for 53BP1 (Flag) and Rif1 in irradiated *Trp53bp1*$^{-/-}$ iMEFs reconstituted with 53BP1^{DB} or 53BP1^{DB28A} retroviruses (*4*). Magnification, 100×; scale bars, 5 μm. Data are representative of two independent experiments. DAPI, 4′,6-diamidino-2-phenylindole.

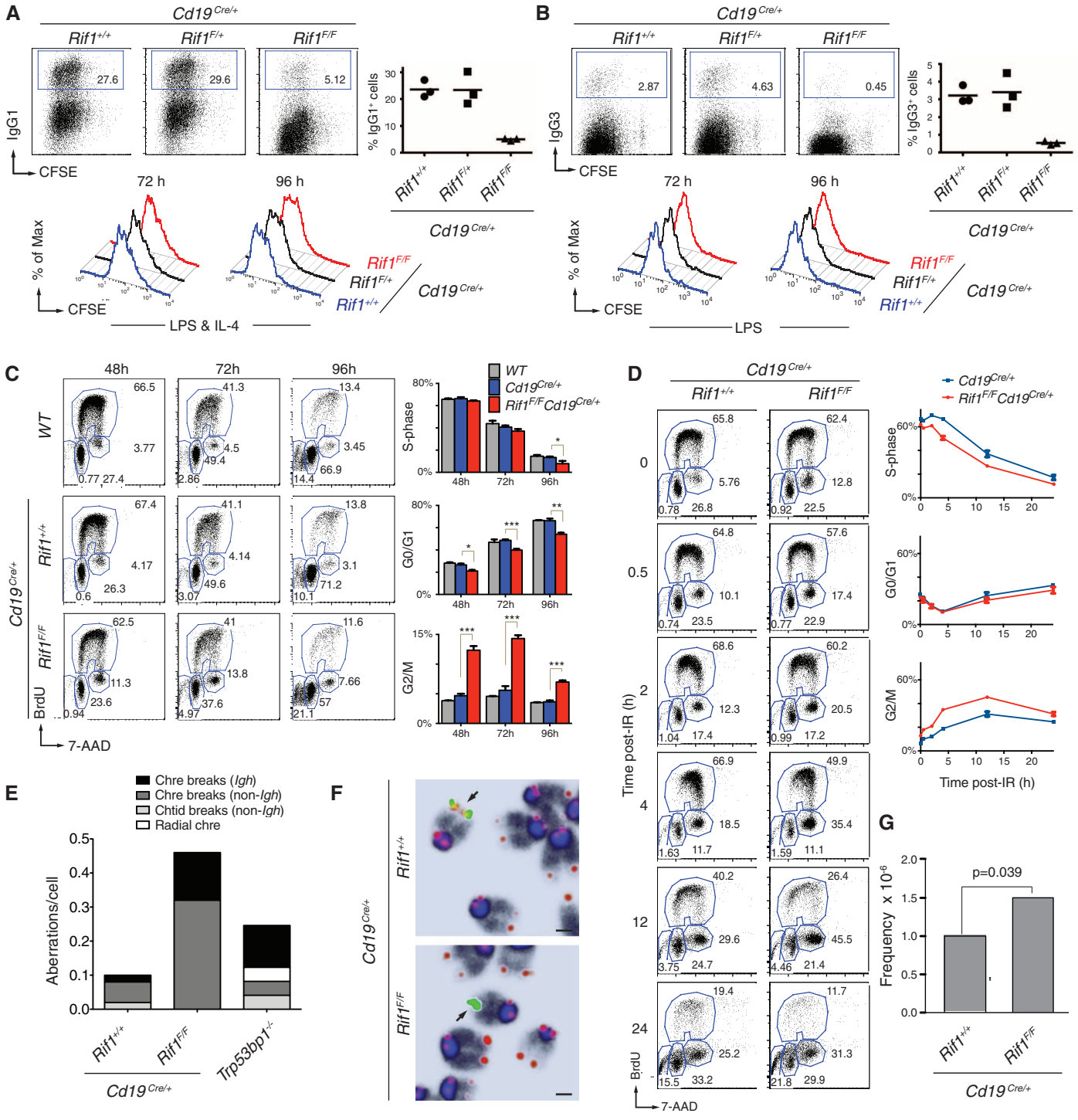

Fig. 3. Rif1 deficiency impairs CSR and causes *Igh* and genome instability in primary B cells. (**A**) (Left) CSR to IgG1 96 hours after stimulation of B lymphocytes with LPS and IL-4. (Right) Summary dot plot for three independent experiments (n = three mice per genotype). Mean values are: 23.6% for $Cd19^{Cre/+}$, 23.4% for $Rif1^{F/+}Cd19^{Cre/+}$, and 5.0% for $Rif1^{F/F}Cd19^{Cre/+}$ ($P < 0.008$ with the paired Student's t test). (Bottom) B cell proliferation by carboxyfluorescein succinimidyl ester (CFSE) dilution. Data are representative of three independent experiments. (**B**) Same as in (A) but for CSR to IgG3 after stimulation with LPS alone. Mean values are: 3.2% for $Cd19^{Cre/+}$, 3.4% for $Rif1^{F/+}Cd19^{Cre/+}$, and 0.5% for $Rif1^{F/F}Cd19^{Cre/+}$ ($P < 0.008$). (**C**) (Left) Cell cycle analysis of primary B cells after stimulation with LPS and IL-4. BrdU, 5-bromo-2′-deoxyuridine; 7-AAD, 7-amino-actinomycin D. (Right) Summary histograms for S, G_0/G_1, and G_2/M phase cells from two independent experiments (n = four mice per genotype). Error bars indicate SEM. * $0.01 < P < 0.05$, ** $0.001 < P < 0.01$, *** $P < 0.001$. WT, wild type. (**D**) (Left) Cell cycle analysis of LPS- and IL-4–stimulated splenocytes at the indicated times after irradiation (6 Gy). (Right) Summary graphs for S, G_0/G_1, and G_2/M phase cells from two independent experiments (n = three mice per genotype). Error bars indicate SD. (**E**) Analysis of genomic instability in metaphases from B cell cultures. Chtid, chromatid; Chre, chromosome. Data are representative of two independent experiments (n = 50 metaphases analyzed per genotype per experiment). (**F**) Examples of *Igh*-associated aberrations in $Rif1^{F/F}Cd19^{Cre/+}$ B cells. Chromosomes were hybridized with an *Igh* Cα probe (green; centromeric of Cγ1) and a telomere sequence-specific probe (red) and were counterstained with DAPI (dark blue/black). Arrows indicate *Igh* Cα/telomeric signal on chromosome 12. Magnification, 63×; scale bars, 1 μm. (**G**) Frequency of *c-myc/Igh* translocations in activated B cells. The graph shows combined results from three mice per genotype.

A similar CSR defect was also obtained by conditionally deleting Rif1 with 4-hydroxytamoxifen (4HT) in *Rif1*$^{F/F}$*ROSA26*$^{Cre\text{-}ERT2/+}$ B cells (fig. S7). Finally, short hairpin RNA–mediated partial down-regulation of CtBP-interacting protein (CtIP), which interacts with Rif1 (fig. S8C) and has been implicated in processing of DNA ends (*21*, *22*), resulted in a very small but reproducible increase in CSR (fig. S8, A and B). Thus, Rif1 is essential for normal CSR, and CtIP may not be the only factor that contributes to end processing in Rif1-deficient B cells.

Class switch recombination requires cell division, activation-induced cytidine deaminase (AID) expression, and *Igh* germline transcription (*23*). There are conflicting reports that Rif1 is required for proliferation in MEFs, but not in DT40 B cells (*17*, *18*). We found that cell division profiles of *Rif1*$^{F/F}$*Cd19*$^{Cre/+}$ and 4HT-treated *Rif1*$^{F/F}$*ROSA26*$^{Cre\text{-}ERT2/+}$ B cells were indistinguishable from controls (Fig. 3, A and B; and fig. S7, A, C, E, and G), indicating that Rif1 is dispensable for B cell proliferation in vitro. Finally, AID mRNA and protein expression and *Igh* germline transcription were not affected by Rif1 deletion (fig. S4, B and D).

We next examined the role of Rif1 in cell cycle progression in primary B cells. We found no major differences in the percentage of cells in G_0/G_1 and S phases (Fig. 3C). However, the number of cells in G_2/M phase was increased approximately twofold in the absence of Rif1 (2.64-, 2.56-, and 1.91-fold at 48, 72, and 96 hours, respectively) (Fig. 3C). We obtained similar results with the use of *Rif1*$^{F/F}$*ROSA26*$^{Cre\text{-}ERT2/+}$ B cells treated with 4HT (fig. S7, H and I).

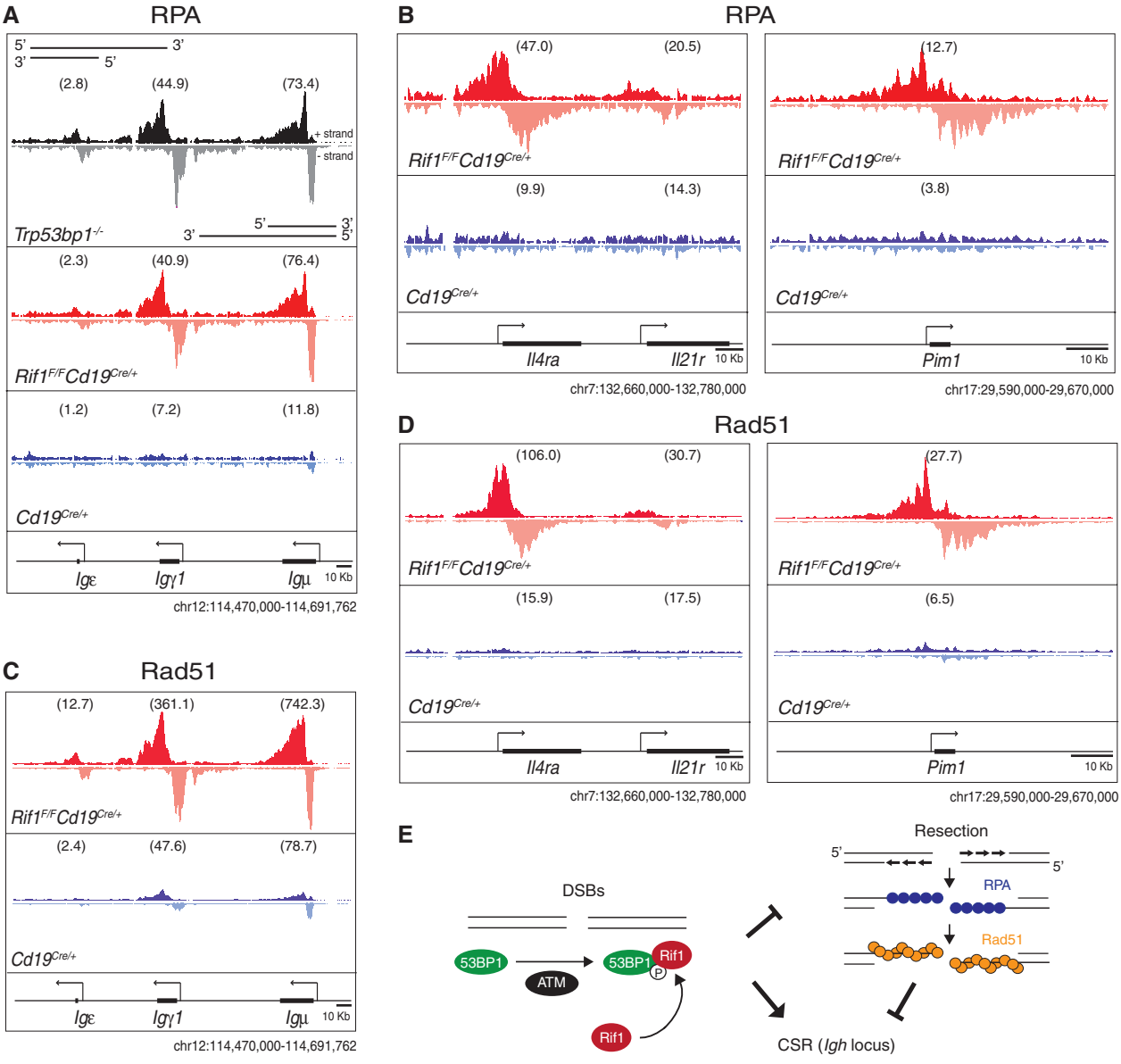

Fig. 4. Rif1 prevents resection of DNA ends at sites of AID-induced DNA damage. (**A** to **D**) RPA and Rad51 occupancy at the *Igh* locus (A and C) and at non-*Igh* AID targets genes (B and D) in B cells activated to undergo class switching. ChIP-seq libraries were resolved into upper (+) and lower (-) DNA strands to show RPA and Rad51 association with sense and antisense strands. Within a specified genomic window, graphs have the same scale and show tag density. Deep-sequencing samples were normalized per library size, and tags per million values were calculated for each genic region, as indicated in the supplementary materials and methods and shown in parenthesis. Data are representative of two independent experiments for RPA ChIP-seq and one for Rad51. (**E**) Model of Rif1 recruitment and DNA-end protection at DSBs. DNA damage activates ATM, which phosphorylates many targets, including 53BP1. This event recruits Rif1 to 53BP1 at the DSB, where it inhibits DNA resection. The extensive resection in the absence of Rif1 impairs CSR at the *Igh* locus. P, phosphate.

Furthermore, irradiation increases the accumulation of $Rif1^{F/F}Cd19^{Cre/+}$ B cells in G2/M phase (Fig. 3D). In addition, $Trp53bp1^{-/-}$ iMEFs expressing $53BP1^{DB28A}$, which did not recruit Rif1 to IRIF (Fig. 2C), exhibited delayed progression through S phase following DNA damage with accumulation of cells in G_2 phase after irradiation (fig. S9).

Accumulation of cells in G_2/M phase may reflect the persistence of unrepaired DNA damage in a fraction of Rif1-deficient cells. To investigate this possibility, we analyzed metaphase spreads from B cells dividing in response to LPS and IL-4 in vitro. These cells express AID, which produces DSBs in *Igh* and, less frequently at off-target sites throughout the genome, in the G_1 phase of the cell cycle (*24*–*26*). Chromosomal aberrations were increased in $Rif1^{F/F}Cd19^{Cre/+}$ B cells compared to controls (Fig. 3E), with many localized to the *Igh* locus (Fig. 3E). Consistent with the observation that *Igh* is targeted by AID in the G_1 phase of the cell cycle, all of the *Igh* breaks were chromosome breaks (Fig. 3, E and F). Interestingly, the frequency of *c-myc/Igh* translocations is moderately increased in $Rif1^{F/F}Cd19^{Cre/+}$ B cells; however, the breakpoint distribution was similar to the $Cd19^{Cre/+}$ control (1.5×10^{-6} versus 1.0×10^{-6} in the control; $P = 0.039$) (Fig. 3G and fig. S10). We conclude that in the absence of Rif1, DSBs fail to be resolved efficiently in the G_1, S, or G_2 phases, which leads to increased levels of genomic instability, including chromosome breaks at *Igh* and translocations in dividing B cells.

In the absence of 53BP1, DSBs produced by AID at the *Igh* locus accumulate the single-stranded DNA-binding replication protein A complex (RPA) as a result of increased DNA-end resection (*24*). To determine if Rif1 is required for DNA-end protection by 53BP1, we performed RPA–chromatin immunoprecipitation followed by massive parallel sequencing (ChIP-seq) experiments on $Rif1^{F/F}Cd19^{Cre/+}$ and control B cells. Ablation of Rif1 was indistinguishable from the loss of 53BP1 in that in its absence, RPA decorates the *Igh* locus asymmetrically, in a manner consistent with 5′-3′ resection (Fig. 4A) (*27*). In addition, absence of Rif1 also results in RPA accumulation at non-*Igh* genes, such as *Il4ra* and *Pim1*, that are damaged by AID in G_1 phase (Fig. 4B) (*24*, *25*). Rad51 is the recombinase that mediates repair of DSBs by homologous recombination in S/G_2/M phase (*22*). To confirm that Rif1 prevents resection that takes place in S phase, we monitored Rad51 accumulation in activated B cells by ChIP-seq. Loss of Rif1 was indistinguishable from the loss of 53BP1 (*27*), in that it led to asymmetric Rad51 accumulation at sites of AID-inflicted DNA damage (Fig. 4, C and D). We conclude that in the absence of Rif1, AID-induced DSBs incurred in G_1 phase persist and undergo extensive 5′-3′ DNA-end resection in S/G_2/M phase, as measured by RPA and Rad51 accumulation.

A role for Rif1 in maintenance of genome stability and protection of DNA ends against resection is consistent with its phosphorylation-dependent recruitment to the N-terminal domain of 53BP1 (*4*). 53BP1 facilitates DNA repair and prevents DNA-end resection during CSR. In the absence of 53BP1, AID-induced DSBs are resolved inefficiently in G_1 phase, leading to chromosome breaks, *Igh* instability, and resolution by alternative NHEJ or homologous recombination instead of classical NHEJ (*4*, *8*, *27*). Our experiments show that in the absence of Rif1, 53BP1 is insufficient to promote genomic stability or mediate efficient *Igh* repair, DNA-end protection, or CSR. Thus, these 53BP1 activities require Rif1 recruitment to the phosphorylated N terminus of 53BP1. Rif1 is likely to have additional functions beyond 53BP1, CSR, and DNA-end protection because although $Trp53bp1^{-/-}$ mice are viable, Rif1 deletion is lethal (*17*). Indeed, Rif1 is believed to play a role in the repair of S-phase DNA damage (*17*, *18*), as well as in the regulation of replication timing (*19*, *20*, *28*). Analogously, additional CSR factor(s) may exist downstream of 53BP1, as class switching in Rif1-deficienct B cells is significantly higher than in $Trp53bp1^{-/-}$.

In summary, our data are consistent with a model in which ATM-mediated phosphorylation of 53BP1 recruits Rif1 to sites of DNA damage, where it facilitates DNA repair in part by protecting DNA ends from resection (Fig. 4E). In the absence of Rif1, DNA breaks incurred in G_1 phase fail to be repaired by NHEJ and undergo extensive 5′-3′ end resection, resulting in the accumulation of chromosome breaks and genome instability.

References and Notes

1. M. M. Adams, P. B. Carpenter, *Cell Div.* **1**, 19 (2006).
2. J. Lukas, C. Lukas, J. Bartek, *Nat. Cell Biol.* **13**, 1161 (2011).
3. A. T. Noon, A. A. Goodarzi, *DNA Repair* **10**, 1071 (2011).
4. A. Bothmer *et al.*, *Mol. Cell* **42**, 319 (2011).
5. S. Difilippantonio *et al.*, *Nature* **456**, 529 (2008).
6. N. Dimitrova, Y. C. Chen, D. L. Spector, T. de Lange, *Nature* **456**, 524 (2008).
7. B. Reina-San-Martin, J. Chen, A. Nussenzweig, M. C. Nussenzweig, *Eur. J. Immunol.* **37**, 235 (2007).
8. A. Bothmer *et al.*, *J. Exp. Med.* **207**, 855 (2010).
9. J. P. Manis *et al.*, *Nat. Immunol.* **5**, 481 (2004).
10. I. M. Ward *et al.*, *J. Cell Biol.* **165**, 459 (2004).
11. Materials and methods are available as supplementary materials on *Science* Online.
12. I. A. Manke, D. M. Lowery, A. Nguyen, M. B. Yaffe, *Science* **302**, 636 (2003).
13. C. F. Hardy, L. Sussel, D. Shore, *Genes Dev.* **6**, 801 (1992).
14. S. Kumar *et al.*, *Cell Cycle* **11**, 1183 (2012).
15. J. Silverman, H. Takai, S. B. Buonomo, F. Eisenhaber, T. de Lange, *Genes Dev.* **18**, 2108 (2004).
16. L. Xu, E. H. Blackburn, *J. Cell Biol.* **167**, 819 (2004).
17. S. B. Buonomo, Y. Wu, D. Ferguson, T. de Lange, *J. Cell Biol.* **187**, 385 (2009).
18. D. Xu *et al.*, *EMBO J.* **29**, 3140 (2010).
19. D. Cornacchia *et al.*, *EMBO J.* **31**, 3678 (2012).
20. S. Yamazaki *et al.*, *EMBO J.* **31**, 3667 (2012).
21. A. A. Sartori *et al.*, *Nature* **450**, 509 (2007).
22. L. S. Symington, J. Gautier, *Annu. Rev. Genet.* **45**, 247 (2011).
23. R. Pavri, M. C. Nussenzweig, *Adv. Immunol.* **110**, 1 (2011).
24. O. Hakim *et al.*, *Nature* **484**, 69 (2012).
25. S. Petersen *et al.*, *Nature* **414**, 660 (2001).
26. A. Yamane *et al.*, *Nat. Immunol.* **12**, 62 (2011).
27. A. Yamane *et al.*, *Cell Rep.* 10.1016/j.celrep.2012.12.006 (2013).
28. M. Hayano *et al.*, *Genes Dev.* **26**, 137 (2012).

Acknowledgments: We thank all members of the Nussenzweig laboratory for discussion, D. Bosque and T. Eisenreich for help in managing mouse colonies, A. Gazumyan for assistance with *Igh* germline and AID transcript levels analysis, and K. Yao for help with genotyping. We thank T. de Lange (The Rockefeller University, New York) for $Rif1^{F/F}$ mice; S. Buonomo (European Molecular Biology Laboratory Mouse Biology Unit, Monterotondo, Italy) for the anti-mouse Rif1 serum #1240; G. Gutierrez (NIAMS, NIH, Bethesda, MD) for Illumina sequencing; N. Zampieri (Columbia University, New York) for assistance with immunofluorescence image processing, and M. P. Rout, J. LaCava, S. Obado, and L. Hough (The Rockefeller University) for invaluable help, discussions, and protocols for cryolysis and magnetic bead-mediated immunoisolation. The data presented in the manuscript are tabulated in the main text and in the supplementary materials. Sequence data shown in Fig. 4 have been deposited in the Gene Expression Omnibus database (accession number GSE42298) at www.ncbi.nlm.nih.gov/geo/. M.D.V. was a Fellow of the American Italian Cancer Foundation, and A.D.G. was supported by NIH Medical Scientist Training Program grant GM007739. This work was supported in part by NIH grants AI037526 (M.C.N.), RR022220 (B.T.C.), RR00862 (B.T.C.), and GM103314 (B.T.C.); and by the intramural program of NIAMS at the NIH (R.C.); and the intramural research program of NCI at the NIH and Center for Cancer Research (A.N. and E.C.). M.C.N. is an HHMI Investigator.

Supplementary Materials

www.sciencemag.org/cgi/content/full/science.1230624/DC1
Materials and Methods
Figs. S1 to S10
Table S1
References (*29*–*49*)

24 September 2012; accepted 16 November 2012
Published online 10 January 2013;
10.1126/science.1230624

Molecular Cell
Article

BRCA1 Functions Independently of Homologous Recombination in DNA Interstrand Crosslink Repair

Samuel F. Bunting,[1,5] Elsa Callén,[1,5] Marina L. Kozak,[1] Jung Min Kim,[3] Nancy Wong,[1] Andrés J. López-Contreras,[4] Thomas Ludwig,[2] Richard Baer,[2] Robert B. Faryabi,[1] Amy Malhowski,[1] Hua-Tang Chen,[1] Oscar Fernandez-Capetillo,[4] Alan D'Andrea,[3] and André Nussenzweig[1,*]

[1]Laboratory of Genome Integrity, National Cancer Institute, National Institutes of Health, 37 Convent Drive, Room 1108, Bethesda, MD 20892, USA
[2]Institute for Cancer Genetics, Columbia University Medical Center, Irving Cancer Research Center, Room 503A, 1130 Saint Nicholas Avenue, New York, NY 10032, USA
[3]Department of Radiation Oncology, Dana-Farber Cancer Institute, Harvard Medical School, 44 Binney Street, Boston, MA 02115, USA
[4]Genomic Instability Group, Spanish National Cancer Research Center, Madrid, Spain
[5]These authors contributed equally to this work
*Correspondence: andre_nussenzweig@nih.gov
DOI 10.1016/j.molcel.2012.02.015

SUMMARY

Brca1 is required for DNA repair by homologous recombination (HR) and normal embryonic development. Here we report that deletion of the DNA damage response factor 53BP1 overcomes embryonic lethality in *Brca1*-nullizygous mice and rescues HR deficiency, as measured by hypersensitivity to polyADP-ribose polymerase (PARP) inhibition. However, *Brca1,53BP1* double-deficient cells are hypersensitive to DNA interstrand crosslinks (ICLs), indicating that BRCA1 has an additional role in DNA crosslink repair that is distinct from HR. Disruption of the nonhomologous end-joining (NHEJ) factor, Ku, promotes DNA repair in *Brca1*-deficient cells; however deletion of either *Ku* or *53BP1* exacerbates genomic instability in cells lacking *FANCD2*, a mediator of the Fanconi anemia pathway for ICL repair. BRCA1 therefore has two separate roles in ICL repair that can be modulated by manipulating NHEJ, whereas FANCD2 provides a key activity that cannot be bypassed by ablation of 53BP1 or Ku.

INTRODUCTION

In mammalian cells, homologous recombination (HR) and nonhomologous end joining (NHEJ) are the two major pathways involved in the repair of DNA double-strand breaks (DSBs) (Kass and Jasin, 2010). HR is initiated by DNA end resection, which involves the production of recombinogenic 3′ single-stranded DNA by the action of several proteins, including BRCA1, Mre11, CtIP, Exo1, and Blm (Gravel et al., 2008; Sartori et al., 2007; Stracker and Petrini, 2011; Yun and Hiom, 2009). Following end resection, single-stranded DNA is stabilized by binding of replication protein A (RPA). Rad51 subsequently replaces RPA on single-stranded DNA, enabling strand invasion at an intact homologous DNA region, which is used as a template for repair (Kass and Jasin, 2010). In contrast to HR, NHEJ directly religates broken DNA. This process is initiated by the Ku70/Ku80 (Ku) heterodimer which binds directly to the break and recruits the catalytic subunit of the DNA-dependent protein kinase (DNA-PKcs), stabilizing and aligning the ends (Getts and Stamato, 1994; Rathmell and Chu, 1994; Taccioli et al., 1994). End rejoining is then completed by activities of the XRCC4/DNA ligase IV (Lig4) complex (Critchlow and Jackson, 1998).

The importance of double-strand break repair in mammalian cells is demonstrated by the tumor predisposition in humans and mice associated with mutation of the HR gene, *Brca1*. Rescue of homologous recombination in *Brca1*-deficient mice, which can be achieved by deletion of the DNA damage response factor, 53BP1, causes a significant reduction in genomic instability and tumor incidence (Bouwman et al., 2010; Bunting et al., 2010; Cao et al., 2009). Although 53BP1 is not a core NHEJ component, it is required for V(D)J recombination, class switch recombination, and fusion of uncapped telomeres, all of which are dependent on NHEJ (Difilippantonio et al., 2008; Dimitrova et al., 2008; Manis et al., 2004; Ward et al., 2003). Rescue of homologous recombination in *Brca1*-deficient cells by deletion of 53BP1 correlates with a significant increase in exonuclease-mediated resection of DNA double-strand breaks (Bothmer et al., 2011; Bunting et al., 2010), highlighting the importance of regulation of DNA end resection in determining DSB repair pathway choice.

Besides its essential role in repairing DSBs that occur spontaneously during DNA replication, HR is also important for repair of DSBs that arise during processing of DNA interstrand crosslinks (ICLs) (Kee and D'Andrea, 2010). ICLs, which are produced by the reaction of certain metabolites and drugs with DNA, activate a repair pathway comprising at least 15 gene products. Mutation of any of these genes causes the human disease Fanconi anemia (FA), which is associated with pancytopenia, tumor predisposition, and hypersensitivity to DNA crosslinking agents (Kee and D'Andrea, 2010; Wang et al., 2007). Several recent reports have indicated that genomic instability in FA cells is dependent on the activity of NHEJ factors (Adamo et al., 2010; Pace et al., 2010). For example, it

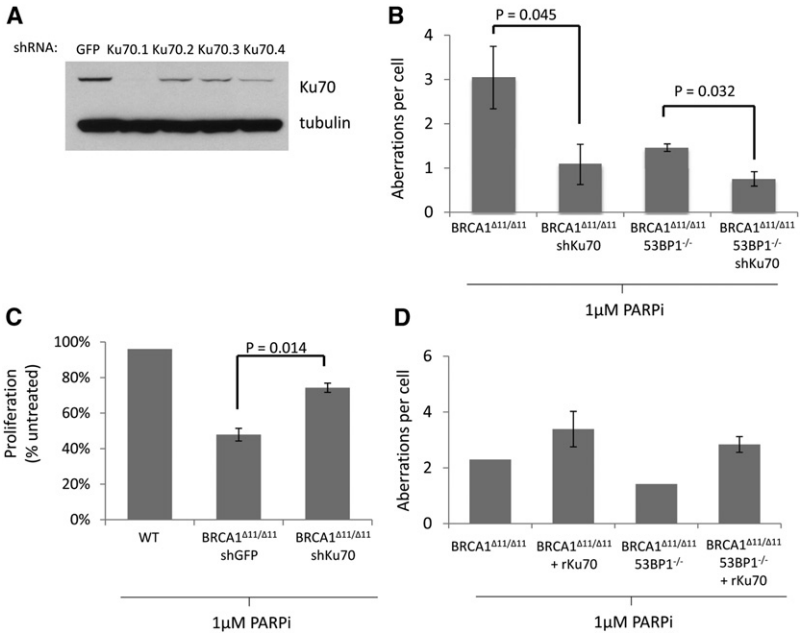

Figure 1. Ku Expression Correlates with Genomic Instability and Reduced Proliferation in *Brca1*-Deficient Cells Treated with PARP Inhibitor

(A) Ku70 expression in cells expressing Ku70 shRNAs. First lane (GFP) shows expression of Ku70 in cells expressing a control shRNA specific for GFP. The GFP and KU70.1 shRNAs were selected for integration into $Brca1^{\Delta11/\Delta11}$ MEFs.

(B) Average genomic instability observed in metaphase spreads from MEF cells treated overnight with 1 μM PARP inhibitor (PARPi).

(C) Proliferation of MEFs growing in the presence of 1 μM PARP inhibitor, relative to untreated cells.

(D) Genomic instability in metaphases from MEFs overexpressing rat Ku70. Error bars show standard deviation in each case. See also Figure S1.

was reported that loss of Ku in *FANCC* mutant chicken or human cells relieved their sensitivity to agents that cause ICLs. Furthermore, the activity of NHEJ has been shown to negatively affect DNA repair in cells lacking the HR factor BRCA2 (Patel et al., 2011).

To gain further insight into how DNA repair involving BRCA1 or factors of the FA pathway is affected by the activity of NHEJ proteins, we have tested the effects of deleting *Ku* or *53BP1* in *Brca1*- and *FANCD2*-deficient mice. Surprisingly, we find that *53BP1* deletion does not affect the sensitivity of *Brca1*-deficient cells to DNA crosslinking agents, despite the previous finding that HR is restored in *Brca1,53BP1* double-deficient cells (Bouwman et al., 2010; Bunting et al., 2010). By contrast, Ku depletion reduces—but does not abrogate—the sensitivity of *Brca1*-deficient cells to both polyADP-ribose polymerase (PARP) inhibitor and cisplatin, suggesting important differences in the roles of Ku70/80 and 53BP1 in response to ICLs. Contrary to the case with *Brca1*-deficient cells, we find that deletion of either *Ku80* or *53BP1* causes an increase in the sensitivity of $FANCD2^{-/-}$ cells to DNA crosslinking drugs. Thus, loss of NHEJ proteins can either cause additive repair defects or suppression of repair defects in response to ICLs.

RESULTS

Genomic Instability and Cell Death in *Brca1*-Deficient Cells after PARP Inhibitor Treatment Is Dependent on Ku and 53BP1

To investigate how Ku contributes to genomic instability in *Brca1*-deficient cells, we knocked down Ku70 in $Brca1^{\Delta11/\Delta11}$ mouse embryonic fibroblasts (MEFs). The $Brca1^{\Delta11}$ allele encodes a mutant isoform of *Brca1* lacking exon 11, which encodes ~50% of the WT protein (Xu et al., 1999b). As we found previously in primary $Brca1^{\Delta11/\Delta11}$ lymphocytes, $Brca1^{\Delta11/\Delta11}$ MEFs are highly sensitive to PARP inhibitor, an agent that is toxic to cells deficient in HR (Bunting et al., 2010) (Figure S1A). We identified a shRNA (Ku70.1) that significantly ablated Ku70 expression in $Brca1^{\Delta11/\Delta11}$ MEFs, as determined by western blotting (Figure 1A). We found that in $Brca1^{\Delta11/\Delta11}$ cells, knockdown of Ku70 caused a significant decrease in the level of genomic instability (chromosome and chromatid breaks, radial chromosomes, and translocations) induced by PARP inhibitor treatment (Figure 1B) and improved proliferation relative to cells expressing a control shRNA (Figure 1C). To further test the importance of Ku70 in modulating the degree of genomic instability in *Brca1*-deficient cells, we prepared cells carrying a stably integrated retroviral construct expressing rat Ku70 (rKu70). Overexpression of Ku70 in these cells led to an increase in genomic instability in $Brca1^{\Delta11/\Delta11}$ and $Brca1^{\Delta11/\Delta11}53BP1^{-/-}$ MEFs (Figures 1D and S1B). Altogether, these results suggest that Ku contributes to genomic instability in $Brca1^{\Delta11/\Delta11}$ cells.

As reported previously, deletion of *53BP1* reduced the level of genomic instability in $Brca1^{\Delta11/\Delta11}$ cells (Figure 1B) and significantly increased the proliferation of these cells in the presence of PARP inhibitor (Figure S1A). Knockdown of Ku70 further reduced the number of chromosome aberrations observed in $Brca1^{\Delta11/\Delta11}53BP1^{-/-}$ cells (Figure 1B), indicating that both Ku70 and 53BP1 contribute to genomic instability in *Brca1*-deficient cells.

$Brca1^{\Delta11/\Delta11}$ and *Brca1*-null mice die in utero (Ludwig et al., 1997; Xu et al., 1999b). However, embryonic lethality in $Brca1^{\Delta11/\Delta11}$ mice can be overcome by additional deletion of *53BP1* (Cao et al., 2009). To test whether deletion of *Ku* could enable an equivalent rescue of embryonic lethality in $Brca1^{\Delta11/\Delta11}$ mice, we bred $Brca1^{\Delta11/+}$ mice to $Ku80^{+/-}$ animals. Whereas we were able to obtain $Brca1^{+/+}Ku80^{-/-}$ and $Brca1^{\Delta11/+}Ku80^{-/-}$ pups, we found that $Brca1^{\Delta11/\Delta11}Ku80^{-/-}$ double-deficient mice did not survive to birth (Table 1). We were also unable to obtain $Brca1^{\Delta11/\Delta11}Ku80^{-/-}$ embryos at E13.5 (Table 1). Thus, in contrast to deletion of *53BP1*, targeting of Ku is not sufficient to overcome the embryonic lethality phenotype seen in $Brca1^{\Delta11/\Delta11}$ mice.

Table 1. Impact of Deletion of Ku or 53BP1 on the Survival of Brca1$^{\Delta11/\Delta11}$ and Brca1-Null Embryos

Brca1$^{\Delta11/+}$ Ku80$^{+/-}$ × Brca1 $^{\Delta11/+}$ Ku80$^{+/-}$ Intercross:					
		Brca1$^{\Delta11/\Delta11}$Ku80$^{+/+}$ or Brca1$^{\Delta11/\Delta11}$Ku80$^{+/-}$	Brca1$^{+/+}$Ku80$^{-/-}$ or Brca1$^{\Delta11/+}$Ku80$^{-/-}$	Brca1$^{\Delta11/\Delta11}$Ku80$^{-/-}$	Other Genotypes
E13.5 embryos	Expected:	9	9	3	27
(48 screened)	Observed:	4	12	0	32
Live pups	Expected:	30	30	10	90
(160 screened)	Observed:	0	13	0	147
Brca1$^{+/-}$ 53BP1$^{+/-}$ × Brca1$^{+/-}$ 53BP1$^{+/-}$ Intercross:					
		Brca1$^{-/-}$ 53BP1$^{+/+}$ or Brca1$^{-/-}$ 53BP1$^{+/-}$	Brca1$^{+/+}$ 53BP1$^{-/-}$ or Brca1$^{+/-}$ 53BP1$^{-/-}$	Brca1$^{-/-}$ 53BP1$^{-/-}$	Other Genotypes
Live pups	Expected:	21.75	21.75	7.25	65.25
(116 screened)	Observed:	0	22	4	90
Brca1$^{+/-}$ 53BP1$^{-/-}$ × Brca1$^{+/-}$ 53BP1$^{-/-}$ Intercross:					
		Brca1$^{-/-}$ 53BP1$^{+/+}$ or Brca1$^{-/-}$ 53BP1$^{+/-}$	Brca1$^{+/+}$ 53BP1$^{-/-}$ or Brca1$^{+/-}$ 53BP1$^{-/-}$	Brca1$^{-/-}$ 53BP1$^{-/-}$	Other Genotypes
Live pups	Expected:	0	66	22	0
(88 screened)	Observed:	0	72	16	0

Frequency of embryos at day E13.5 and live-born pups of the indicated genotypes is shown. See also Table S1.

53BP1 Deletion Does Not Affect the Sensitivity of *Brca1*-Deficient Cells to Cisplatin

Platinum-based drugs such as cisplatin and carboplatin are clinically important agents for the treatment of breast cancer (Cobleigh, 2011). We tested *Brca1*$^{\Delta11/\Delta11}$ and *Brca1*$^{\Delta11/\Delta11}$ *53BP1*$^{-/-}$ cells to determine their sensitivity to cisplatin. Whereas *Brca1*$^{\Delta11/\Delta11}$*53BP1*$^{-/-}$ cells were resistant to PARP inhibitor (Figures 1B and S1A), we found that *Brca1*$^{\Delta11/\Delta11}$ *53BP1*$^{-/-}$ cells were just as sensitive as *Brca1*$^{\Delta11/\Delta11}$ to the effects of cisplatin. This equivalent sensitivity was seen by measurements of both genomic instability in lymphocyte metaphases and colony formation assays using MEFs (Figures 2A and 2B). The high sensitivity of *Brca1*$^{\Delta11/\Delta11}$*53BP1*$^{-/-}$ cells to cisplatin was unexpected, because HR is restored to near WT levels in these cells (Bunting et al., 2010).

Genomic instability in cells treated with cisplatin arises from the ability of cisplatin to form mutagenic intra- and interstrand DNA crosslinks (Kee and D'Andrea, 2010; Wang, 2007). To determine whether intra- or interstrand crosslinks were responsible for cisplatin toxicity in *Brca1*$^{\Delta11/\Delta11}$ and *Brca1*$^{\Delta11/\Delta11}$ *53BP1*$^{-/-}$ cells, we tested two additional agents that produce a high proportion of DNA interstrand crosslinks: nitrogen mustard and mitomycin C (Figures S2A and S2B). *Brca1*$^{\Delta11/\Delta11}$ cells were hypersensitive to both of these drugs, and *53BP1* deletion did not affect sensitivity in either case (Figures S2A and S2B). Thus, even though HR proceeds efficiently, *Brca1*$^{\Delta11/\Delta11}$*53BP1*$^{-/-}$ cells are hypersensitive to a variety of drugs that induce DNA interstrand crosslinks.

The sensitivity of *Brca1*$^{\Delta11/\Delta11}$*53BP1*$^{-/-}$ cells to ICLs indicates that BRCA1 has a function in ICL repair that is separate from its known role in HR. To examine this further, we measured the assembly of nuclear Rad51 foci in cells treated with MMC. Rad51 nucleoprotein assembly is considered to be an essential step in DNA repair by HR (Kass and Jasin, 2010). We observed that, as is the case with ionizing radiation, *Brca1*$^{\Delta11/\Delta11}$ cells showed defective Rad51 foci formation after MMC treatment, but *Brca1*$^{\Delta11/\Delta11}$*53BP1*$^{-/-}$ cells showed Rad51 foci formation at close to wild-type levels (Figure S2C). As *Brca1*$^{\Delta11/\Delta11}$*53BP1*$^{-/-}$ cells are nonetheless highly sensitive to DNA crosslinking agents (Figures 2A and 2B), these data indicate that BRCA1 has a role in DNA crosslink repair that is independent of its previously known role in mediating Rad51 loading at DNA break sites.

Rescue of Embryonic Lethality in *Brca1*-Null Mice by 53BP1 Deletion

To ensure that our results were not specific to cells with the hypomorphic *Brca1*$^{\Delta11}$ allele, we tested the effect of crosslinking drugs in *Brca1*-null cells. *Brca1* nullizygosity has a much more severe phenotype than the *Brca1*$^{\Delta11/\Delta11}$ mutation, with embryonic lethality at E5.5–E8.5 in *Brca1*$^{-/-}$ mice compared to E12.5–E18.5 in *Brca1*$^{\Delta11/\Delta11}$ homozygotes (Ludwig et al., 1997; Xu et al., 1999b). Furthermore, whereas *Brca1*$^{\Delta11/\Delta11}$*p53*$^{+/-}$ animals are viable, embryonic lethality in *Brca1*-null animals cannot be overcome by deletion of *p53* (Xu et al., 2001). Consistent with this, we found that it was not possible to generate *Brca1*$^{-/-}$*53BP1*$^{+/+}$ or *Brca1*$^{-/-}$*53BP1*$^{+/-}$ pups (Table 1). Strikingly, however, double-null *Brca1*$^{-/-}$*53BP1*$^{-/-}$ pups were obtained at a frequency only slightly lower than the expected Mendelian ratio (Table 1). *53BP1* deletion, in contrast to *p53* deletion, is therefore able to rescue embryonic lethality in mice that are null for *Brca1*.

Brca1$^{-/-}$*53BP1*$^{-/-}$ mice appeared normal in all respects except that males were sterile and had small testes (Figure S3A). As was the case with *Brca1*$^{\Delta11/\Delta11}$*53BP1*$^{-/-}$ cells, *Brca1*$^{-/-}$ *53BP1*$^{-/-}$ cells showed resistance to PARP inhibitor (Figure S3B) but were hypersensitive to cisplatin and mitomycin C (Figures S3C– S3F). Hypersensitivity to DNA crosslinking drugs is therefore a common feature of *Brca1*-null and *Brca1*$^{\Delta11/\Delta11}$ cells that cannot be rescued by 53BP1 deletion. Male-specific sterility in *Brca1*$^{-/-}$*53BP1*$^{-/-}$ mice further supports an HR-independent role for BRCA, in this case during spermatogenesis. Female

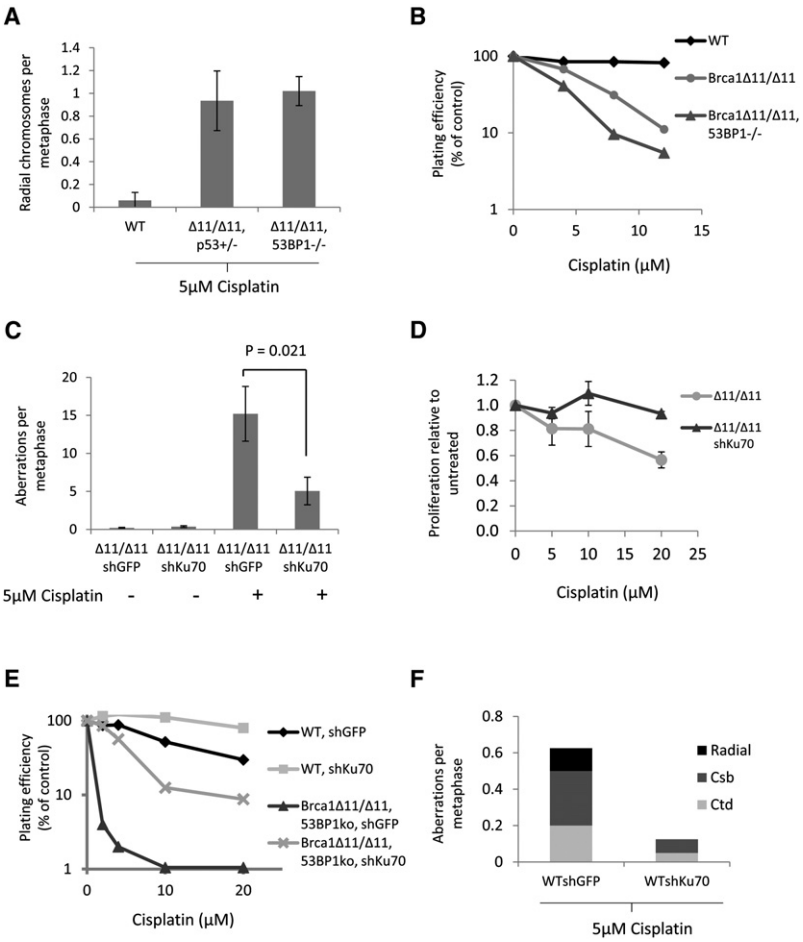

Figure 2. Reduced Genomic Instability and Increased Survival of *Brca1*-Deficient Cells with Ku70 Knockdown after Cisplatin Treatment

(A) Frequency of radial chromosome formation in lymphocytes of the indicated genotypes after overnight treatment with 5 μM cisplatin.

(B) Colony formation in MEFs treated for 2 hr with cisplatin.

(C) Genomic instability in MEFs expressing stably integrated shRNA against either GFP or Ku70, treated overnight with 5 μM cisplatin.

(D) Growth of BRCA1$^{\Delta 11/\Delta 11}$ cells with stably integrated Ku70 shRNA in the presence of cisplatin. Cisplatin was applied for 24 hr and growth assayed with CellTiter-Glo after a total of 5 days.

(E) Colony formation of MEF lines treated for 2 hr with cisplatin.

(F) Genomic instability in control (WTshGFP) or Ku70 knockdown MEFs after overnight treatment with 5 μM cisplatin. Error bars show standard deviation in each case. See also Figure S2.

mice, by contrast, showed normal ovaries and were fertile, suggesting a differential requirement for BRCA1 in male and female gametogenesis. Although *Brca1*-deficient mice were previously shown to have a defect in mammary development (Xu et al., 1999a), we observed no difference in mammary ductal morphogenesis in female WT, *53BP1*$^{-/-}$, or *Brca1*$^{-/-}$*53BP1*$^{-/-}$ mice at pregnancy day P8.5 (Figure S3G).

Cisplatin Cytotoxicity in *Brca1*-Deficient and WT Cells Is Dependent on Ku

As Ku depletion improved the survival of *Brca1*$^{\Delta 11/\Delta 11}$ cells treated with PARP inhibitor (Figure 1C), we tested whether Ku similarly modulated their sensitivity to ICLs. Unlike *53BP1* deletion, we found that Ku70 depletion reduced genomic instability in *Brca1*$^{\Delta 11/\Delta 11}$ MEFs treated with cisplatin and enhanced their proliferative ability in short-term growth assays as well as in long-term clonogenic colony formation assays (Figures 2C, 2D, and S2D). Ku70 depletion was also able to improve the growth of *Brca1*$^{\Delta 11/\Delta 11}$*53BP1*$^{-/-}$ MEFs treated with cisplatin, as measured by colony formation (Figure 2E). Interestingly, we noticed that Ku70 depletion also enabled WT cells to proliferate better after treatment with cisplatin (Figure 2E). This is consistent with a previous report, which showed that deletion of *Ku80* afforded increased survival in WT cells treated with cisplatin (Jensen and Glazer, 2004). Furthermore, improved growth in Ku70-deficient cells after cisplatin treatment correlated with reduced genomic instability (Figure 2F). These findings demonstrate that the presence of Ku sensitizes WT, *Brca1*$^{\Delta 11/\Delta 11}$, and *Brca1*$^{\Delta 11/\Delta 11}$*53BP1*$^{-/-}$ cells to the cytotoxic effects of cisplatin.

Ku Antagonizes HR without Significantly Affecting DSB Resection

Rad51 loading at sites of DNA double-strand breaks is a critical step in repair of DNA damage by HR, and deletion of *53BP1* in *Brca1*-deficient cells was previously shown to increase the proportion of cells with Rad51 foci following DNA damage (Bouwman et al., 2010; Bunting et al., 2010). To address the mechanism by which Ku depletion promotes genome integrity in *Brca1*$^{\Delta 11/\Delta 11}$ cells, we tested whether knockdown of Ku70 could cause an equivalent increase in irradiation-induced Rad51 foci. We found that, although Rad51 foci formation was reduced in *Brca1*$^{\Delta 11/\Delta 11}$ cells relative to WT, knocking down Ku70 caused a statistically significant ($p = 0.0005$) increase in Rad51 foci (Figure 3A), consistent with an increase in DNA repair by HR in the absence of Ku70 (Pierce et al., 2001). An increase in the proportion of irradiated cells exhibiting Rad51 foci after Ku knockdown was also seen in WT and *Brca1*$^{\Delta 11/\Delta 11}$*53BP1*$^{-/-}$ cells, although in these cases the increase did not reach the level of statistical significance.

Exonuclease resection of DNA double-strand breaks is considered to be a critical step in HR, because it generates single-stranded DNA that allows loading of RPA and Rad51 around the break site. To test the extent to which 53BP1 and Ku regulate resection of DNA double-strand breaks, we performed anti-RPA chromatin immunoprecipitation in B cells from WT, *53BP1*$^{-/-}$, and *Ku70*$^{-/-}$ mice. Stimulation of B cells with LPS and IL4 generates multiple DSBs centered around the immunoglobulin heavy chain (IgH) Sμ, Sγ1, Sγ3, and Sε switch regions (Nussenzweig and Nussenzweig, 2010). RPA

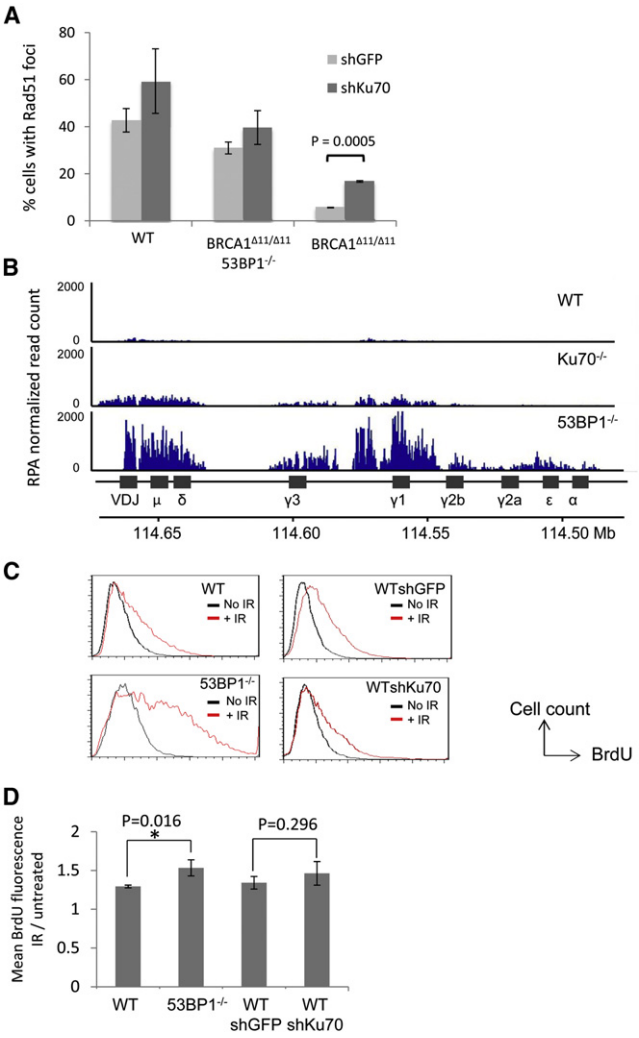

Figure 3. Effect of 53BP1 and Ku on Rad51 Foci and DSB Resection

(A) Quantification of Rad51 immunofluorescence in mouse embryonic fibroblasts of the indicated genotypes. Cells expressing either control shRNA against GFP or shRNA against Ku70 were irradiated (5 Gy, 4 hr recovery) and stained with anti-Rad51 antibody. The average percentages of cells (± standard deviation) with more than 5 nuclear foci from three experiments are shown.

(B) Anti-RPA ChIP-Seq in B cells. B cells were stimulated to undergo class switch recombination in vitro. Chromatin from B cells was harvested 48 hr poststimulation and used for RPA ChIP. RPA read count (normalized by the total library size per million) is shown at the IgH locus.

(C) Nondenaturing anti-BrdU immunofluorescence in MEFs treated with ionizing radiation (30 Gy, 2 hr recovery), measured by flow cytometry. Resection is measured by detection of exposed BrdU (x axis).

(D) Quantification of mean BrdU fluorescence intensity of the irradiated population shown in (C), normalized to the untreated population. Average ± standard deviation from five experiments. See also Figure S4.

loads at the site of DNA double-strand breaks following exonuclease resection, hence a greater enrichment of DNA sequences in the anti-RPA ChIP fraction indicates a greater amount of DSB resection (Yamane et al., 2011). *53BP1*$^{-/-}$ B cells showed a significantly increased extent of pull-down of IgH sequences in the anti-RPA ChIP fraction (Figure 3B), consistent with enhanced resection in these cells. This result is in accordance with previous reports, which suggested that loss of 53BP1 increases the extent of resection of DNA DSBs (Bothmer et al., 2010; Bunting et al., 2010; Difilippantonio et al., 2008). In comparison to *53BP1*$^{-/-}$ cells, however, *Ku70*$^{-/-}$ cells showed only a minor increase in resection relative to WT, as measured by RPA ChIP at IgH (Figure 3B).

To further test the role of NHEJ factors in the regulation of DSB resection, we pulsed WT, *53BP1*$^{-/-}$, and Ku70-depleted MEFs with 5-bromo-2′-deoxyuridine (BrdU) to enable the measurement of single-stranded DNA at ionizing radiation-induced DSBs. We adapted an existing nondenaturing BrdU immunofluorescence protocol for measurement of DSB resection (Sartori et al., 2007) to allow quantification of the amount of resection in a population of cells by flow cytometry (Figure 3C). Notably, we found that *53BP1*$^{-/-}$ cells showed a statistically significant increase in resection after irradiation compared to WT cells (Figures 3C and 3D). In contrast, Ku70-knockdown cells did not significantly increase resection compared to cells expressing a control shRNA. By staining for DNA content in the sample population, we observed that resection was significantly more extensive in cells in the S/G2 phases of the cell cycle (Figure S4A), consistent with previous findings (Huertas, 2010). Taken together, these results indicate that, whereas 53BP1 has a major role in regulating resection of DNA DSBs, Ku plays a more limited role in this process. The increase in Rad51-dependent HR seen in Ku-deficient cells after DNA damage therefore arises from a mechanism other than increased resection (see Discussion).

BRCA1 Mediates FANCD2 Foci Formation after Treatment with Crosslinking Agents

The sensitivity of *Brca1*$^{\Delta11/\Delta11}$*53BP1*$^{-/-}$ cells to DNA crosslinking agents (Figures 2A, 2B, S2A, and S2B) strongly suggests that BRCA1 provides an activity that is required for DNA crosslink repair that is separate from its function in HR. FANCD2 ubiquitylation and recruitment to sites of DNA crosslinks are considered to be essential steps in crosslink repair (Huang and D'Andrea, 2010; Knipscheer et al., 2009; Long et al., 2011). We therefore tested whether these steps are normal in *Brca1*$^{\Delta11/\Delta11}$ and *Brca1*$^{\Delta11/\Delta11}$*53BP1*$^{-/-}$ cells. BRCA1 was previously reported to be dispensable for FANCD2 ubiquitylation, but required for FANCD2 foci formation after DNA damage (Garcia-Higuera et al., 2001; Vandenberg et al., 2003). We found that FANCD2 ubiquitylation, as measured by western blotting, was not significantly altered in either *Brca1*$^{\Delta11/\Delta11}$ or *Brca1*$^{\Delta11/\Delta11}$ *53BP1*$^{-/-}$ cells (Figure 4A). By contrast, the number of cells showing FANCD2 foci after treatment with cisplatin or mitomycin C was reduced in both *Brca1*$^{\Delta11/\Delta11}$ and *Brca1*$^{\Delta11/\Delta11}$*53BP1*$^{-/-}$ cells (Figure 4B). Reduced FANCD2 foci in these cells was not caused by reduced growth rate, as *Brca1*$^{\Delta11/\Delta11}$, *Brca1*$^{\Delta11/\Delta11}$ *53BP1*$^{-/-}$, and WT controls showed a similar cell-cycle distribution (Figure S4B).

We found that depletion of Ku mitigates the toxic effects of DNA crosslinking agents (Figures 2C–2F). We therefore extended our approach by testing whether FANCD2 foci are affected by the presence of Ku70. We found that depletion of Ku70 restored the formation of FANCD2 foci after cisplatin or

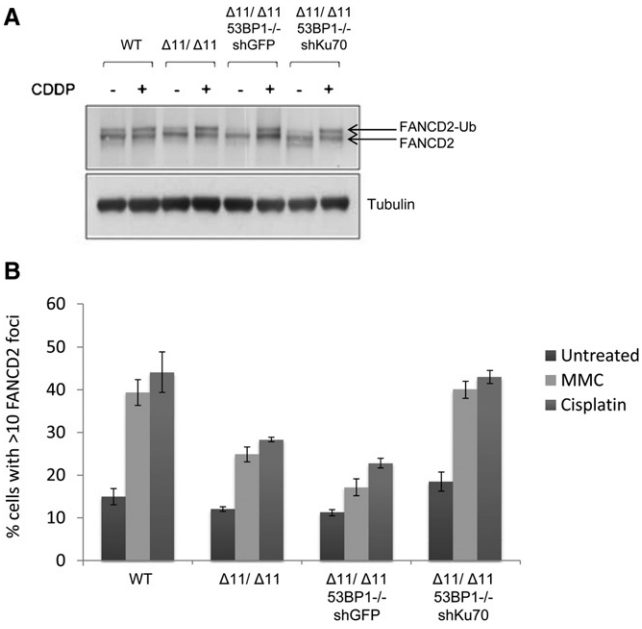

Figure 4. FANCD2 Ubiquitylation and Damage Foci in *Brca1*-Deficient Cells

(A) Western blot showing FANCD2 ubiquitylation in WT, *Brca1*$^{\Delta 11/\Delta 11}$, and *Brca1*$^{\Delta 11/\Delta 11}$*53BP1*$^{-/-}$ MEFs with and without cisplatin (CDDP) treatment. *Brca1*$^{\Delta 11/\Delta 11}$*53BP1*$^{-/-}$ MEFs expressed either control shRNA or shRNA against Ku70.

(B) FANCD2 foci analysis in MEFs treated with either cisplatin or mitomycin C. Cells with more than 10 FANCD2 foci were scored as positive. Mean ± SEM is shown. See also Figure S3.

MMC to a level equivalent to that seen in WT cells (Figure 4B). We conclude that Ku70/80 affects recruitment or retention of FANCD2 at sites of DNA crosslink repair.

Deletion of *53BP1* or *Ku* Exacerbates Genomic Instability in *FANCD2*-Deficient Cells

Hypersensitivity to DNA crosslinking agents is a key diagnostic test for genetic deficiency in components of the Fanconi anemia (FA) pathway (Wang, 2007). Cells from FA patients, or knockout mice with deficiencies in the FA pathway, are unable to repair DNA interstrand crosslinks and tend to accumulate genomic instability with an increased risk of tumorigenesis (Kee and D'Andrea, 2010; Wang, 2007). Recent studies have reported that hypersensitivity of human, nematode, and chicken DT40 cells to interstrand crosslinking agents can be rescued by knockdown, deletion, or inhibition of NHEJ factors such as Ku, Lig4, or DNA-PKcs (Adamo et al., 2010; Pace et al., 2010). To test whether it was possible to prevent genomic instability in FA cells by genetic ablation of DNA damage response factors, we bred mice that were double null for the key FA pathway component, *FANCD2* (Kee and D'Andrea, 2010; Wang, 2007), and either *53BP1* or *Ku80*. Consistent with the reported sensitivity of *FANCD2*$^{-/-}$ cells to DNA crosslinking agents (Houghtaling et al., 2003), cells from *FANCD2*$^{-/-}$ mice were hypersensitive to cisplatin and mitomycin C (Figures 5A and 5B). We found that 53BP1 deletion in *FANCD2*$^{-/-}$ cells led to increased sensitivity to cisplatin (Figure 5A). Similar results were observed with mitomycin C treatment, which induced higher levels of genomic instability in *FANCD2*$^{-/-}$ *53BP1*$^{-/-}$ cells relative to *FANCD2*$^{-/-}$ (Figure 5B). To examine the impact of *53BP1* loss in vivo we examined hematopoietic stem cells (HSCs). *FANCD2*$^{-/-}$ mice have hematopoietic defects, including a 50% reduction in the frequency of both HSCs and common lymphoid progenitors (CLPs) (Zhang et al., 2010). Quantification of HSC and CLP frequencies in double mutant mice revealed that these defects were equivalent in the combined absence of FANCD2 and 53BP1 (Figures S5A and S5B). Thus, loss of 53BP1 renders *FANCD2*-deficient cells more sensitive to DNA crosslinking agents and does not alleviate the severity of hematopoietic defects in mouse models of Fanconi anemia.

Although *Ku80*$^{-/-}$ and *FANCD2*$^{-/-}$ mice are viable, we were not able to obtain live mice that were double null for *FANCD2* and *Ku80* (n = 98 pups screened), suggesting that Ku deficiency also exacerbates developmental defects in the absence of *FANCD2*. This observation is consistent with a previous report, which showed that cells deficient in both *FANCD2* and the NHEJ factor *DNA-PKcs* had a diminished capacity to repair DNA damage compared to either single mutant (Houghtaling et al., 2005). Although we could not obtain double-null pups, we were able to isolate *FANCD2*$^{-/-}$*Ku80*$^{-/-}$ MEFs, and we tested these for their ability to repair interstrand crosslinks induced by cisplatin and mitomycin C. We found that, as compared to *FANCD2*$^{-/-}$ cells, *FANCD2*$^{-/-}$*Ku80*$^{-/-}$ double-knockout MEFs showed increased chromosomal damage in response to either cisplatin (Figure 5C) or mitomycin C (Figure 5D). Colony formation assays with *FANCD2*$^{-/-}$*Ku80*$^{-/-}$ MEFs revealed that these cells grew significantly worse than *FANCD2*$^{-/-}$ single-knockout cells after treatment with cisplatin or mitomycin C (Figures 5E and 5F). These results indicate that FANCD2 provides an essential activity for repair of interstrand crosslinks in murine cells that cannot be rescued by deletion of either *53BP1* or *Ku*. Indeed, the increased severity of the phenotypes observed after combining deficiency in *FANCD2* with loss of either *53BP1* or Ku suggests that NHEJ partially compensates for *FANCD2* deficiency in cisplatin-induced ICL repair.

DISCUSSION

Efficiency of ICL Repair Is Modified by BRCA1 and Ku70/80

Our study reveals that the requirements for BRCA1 in Rad51 nucleoprotein assembly (Bhattacharyya et al., 2000) and FANCD2 retention at DNA damage sites (Vandenberg et al., 2003) represent two distinct activities of the BRCA1 protein. We propose that during ICL repair, BRCA1 functions early at the crosslink excision step and, later, during HR. 53BP1 only affects the function of BRCA1 during the later HR stage. Deletion of 53BP1 therefore has no effect on the hypersensitivity of *Brca1*-deficient cells to agents that cause ICLs. In contrast, Ku affects both steps where BRCA1 is active, hence deletion of Ku reduces the hypersensitivity of *Brca1*-deficient cells to both PARP inhibitors and DNA crosslinking agents. We

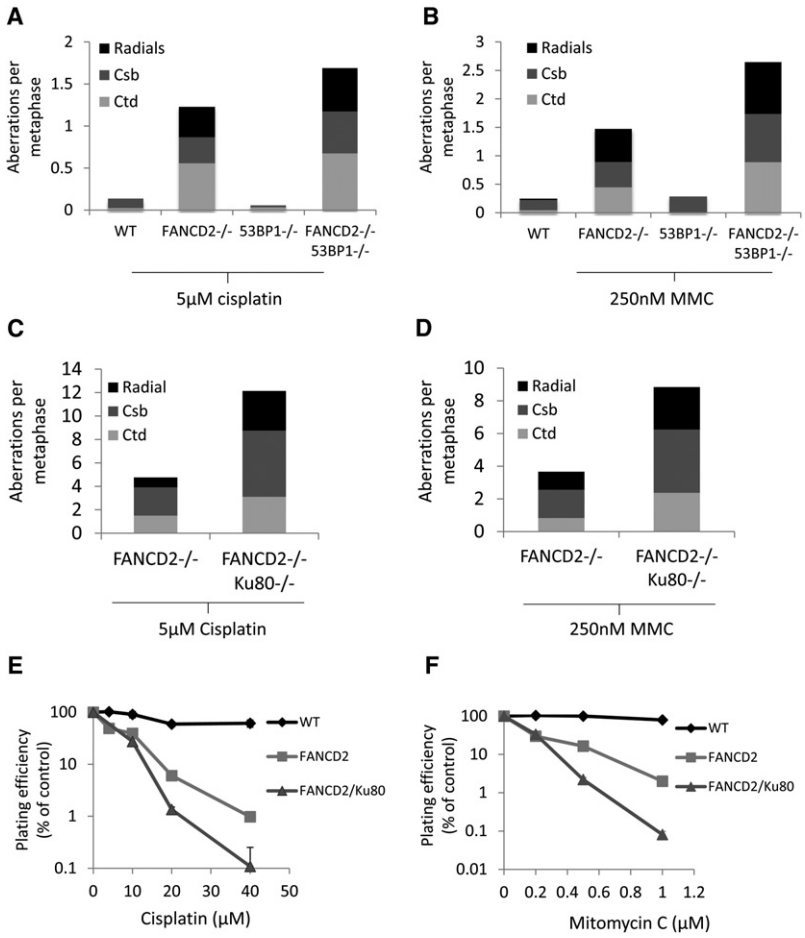

Figure 5. Genomic Instability in Metaphases from Cells Treated Overnight with Drugs to Induce DNA Interstrand Crosslinks

(A) Genomic instability in B cells from WT, *FANCD2*$^{-/-}$, and *FANCD2*$^{-/-}$*53BP1*$^{-/-}$ mice treated overnight with 5 μM cisplatin.

(B) Genomic instability in B cells from WT, *FANCD2*$^{-/-}$, and *FANCD2*$^{-/-}$*53BP1*$^{-/-}$ mice treated overnight with 250 nM mitomyin C (MMC).

(C) Total genomic aberrations in metaphases from *FANCD2*$^{-/-}$ and *FANCD2*$^{-/-}$*Ku80*$^{-/-}$ mouse embryonic fibroblast cells after overnight treatment with 5 μM cisplatin.

(D) Genomic instability in metaphases from *FANCD2*$^{-/-}$ and *FANCD2*$^{-/-}$*Ku80*$^{-/-}$ after overnight treatment with 250 nM MMC.

(E) Colony forming assay in WT, *FANCD2*$^{-/-}$, and *FANCD2*$^{-/-}$*Ku80*$^{-/-}$ MEFs treated with cisplatin.

(F) Colony forming assay WT, *FANCD2*$^{-/-}$, and *FANCD2,Ku80* double knockout MEFs treated with mitomycin C. (Mean ± standard deviation shown.) See also Figure S5.

summarize these results in a model showing the impact of BRCA1 and NHEJ factors in repairing different types of DNA damage (Figure 6).

Increased DSB Resection Associated with *53BP1* Deletion Does Not Improve ICL Repair

Treatment with PARP inhibitor stabilizes single-strand breaks (Figure 6, i), which are converted to double-strand breaks during DNA replication following collapse of the replication fork at a single-strand break (Bryant et al., 2005; Farmer et al., 2005). According to our model, the double-strand break formed by this process can be directed to either HR or NHEJ. The key rate-limiting step is resection of the DSB, which commits repair to HR (Figure 6, ii). *53BP1* deletion significantly increases resection; hence in the absence of 53BP1, error-free HR becomes the principal repair pathway (Figure 6, iii). Cisplatin or MMC treatment produces ICLs. These ICLs cause replication fork collapse, but in this case, the double-strand break is not immediately available for HR, because the homologous template must first be repaired by translesion synthesis (TLS) and nucleotide excision repair (NER) (Figures 6, vii–ix). Increased resection of DSBs mediated by ablation of 53BP1 may not be beneficial to ICL repair and, if so, only at a late stage when TLS and NER are complete. On the other hand, DSBs produced as a consequence of FANCD2-dependent endonuclease action at DNA crosslinks can be inappropriately joined to other DSBs present in the cell by the action of Ku-dependent NHEJ prior to commitment to HR (Figure 6, x). Deletion or knockdown of Ku therefore promotes error-free repair at the sites of ICLs by inhibiting potentially mutagenic repair by NHEJ.

Ku deletion does not rescue the embryonic lethality observed in *Brca1*-deficient mice. This also represents a significant difference compared to deletion of *53BP1*, which rescues the embryonic lethality of homozygous *Brca1*$^{\Delta 11/\Delta 11}$ or *Brca1*-null mice (Table S1) (Bunting et al., 2010). Failure of Ku deletion to rescue the embryonic lethality of *Brca1*-deficient mice correlates with the minor impact on DSB resection that is achieved by targeting Ku relative to *53BP1* (Figures 3B–3D). This difference in DSB resection likely reflects the distinct nature of the interaction between these repair factors and DNA. Whereas Ku binds directly to exposed DNA ends, 53BP1 binds to a histone mark that is present in the entire chromatin area around the double-strand break (Botuyan et al., 2006; Huyen et al., 2004). Any impact that Ku has on resection is therefore likely to be in the immediate vicinity of the DNA end, whereas 53BP1 is capable of impacting resection throughout a much larger chromatin domain. We hypothesize that the ability to bypass the requirement for BRCA1 in mammalian development requires a large extent of recombinogenic single-stranded DNA during replication, which is afforded by *53BP1* deletion, but not by Ku deficiency. In summary, although both Ku and 53BP1 antagonize HR, the impact of these factors in repairing various types of lesions is distinct, because *Ku* promotes mutagenic repair by NHEJ, whereas *53BP1* inhibits DNA end processing.

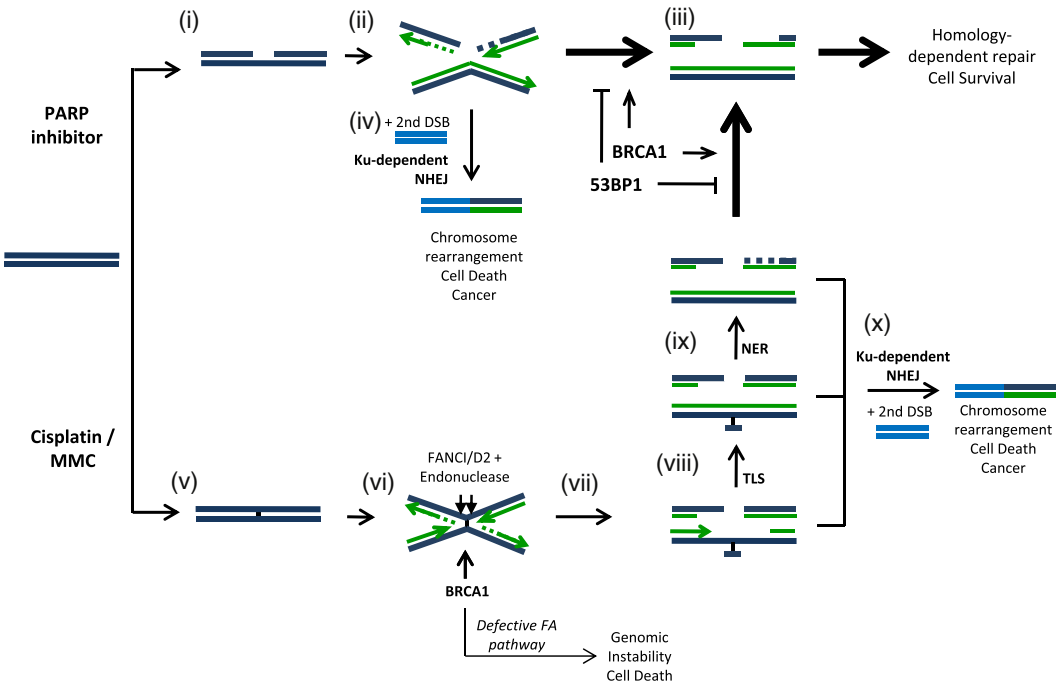

Figure 6. Model for Repair of DNA Double-Strand Breaks Induced by PARP Inhibitor or DNA Crosslinking Agents

In (i), treatment with PARP inhibitor stabilizes spontaneous DNA single-strand breaks, which are converted to double-strand breaks (DSBs) during DNA replication (Bryant et al., 2005; Farmer et al., 2005). In (ii), DNA DSBs can be repaired either by NHEJ or HR. In (iii), the 5′–3′ exonuclease resection commits repair to the error-free HR pathway. 53BP1 antagonizes double-strand break resection. In (iv), Ku70/80 can potentially join the DSB to a second DNA end present in the cells to cause chromosome rearrangements. In (v), treatment with cisplatin or MMC generates interstrand DNA crosslinks. In (vi), interstrand crosslinks cause replication fork stalling and collapse. Accumulation of FANCI/D2, dependent on BRCA1, recruits endonucleases that cut DNA on either side of the interstrand crosslink to generate a double-strand break (vii). Translesion synthesis (TLS) (viii) and nucleotide excision repair (NER) (ix) regenerate duplex DNA on one sister chromatid, enabling homology-dependent repair of the DNA DSB. In (x), aberrant joining mediated by Ku70/80 competes with normal repair and can potentially generate chromosome rearrangements leading to cancer or cell death.

Differing Requirements for BRCA1 and FANCD2 in Upstream ICL Repair

Our finding that *Brca1*$^{-/-}$*53BP1*$^{-/-}$ cells are HR competent but still hypersensitive to ICLs suggests that in addition to its established role in HR, BRCA1 has an upstream role in processing ICLs prior to DSB repair by HR (Figure 6, vi). BRCA1 has previously been reported to regulate the accumulation of FANCD2 into repair foci (Garcia-Higuera et al., 2001; Vandenberg et al., 2003). We found that FANCD2 foci are still impaired in Brca1$^{\Delta 11/\Delta 11}$53BP1$^{-/-}$ cells (Figure 4B), which may explain why loss of 53BP1 does not reduce the sensitivity of *Brca1*-deficient cells to DNA crosslinking agents. The requirement of BRCA1 for optimal retention of FANCD2 at the sites of ICL repair may be dependent on the reported ability of BRCA1 to promote chromatin unfolding (Ye et al., 2001), which may facilitate foci formation by monoubiquitylated FANCD2. Alternatively, BRCA1 may regulate signaling pathways downstream of DNA damage (such as ATR activation) (Yarden et al., 2002) or transcriptional events required for ICL repair (Aiyar et al., 2005; Zhu et al., 2011).

Depletion of Ku70/80 was able to reverse the defect in FANCD2 accumulation in *Brca1*-deficient cells (Figure 4B), suggesting that Ku70/80 and BRCA1 have antagonistic effects in regulating FANCD2 accumulation. Although the exact mechanism by which loss of Ku increases FANCD2 accumulation is unclear, one possibility is that Ku binding to DNA ends produced either by endonuclease excision of DNA crosslinks or by replication fork regression displaces FA gene products that are required for faithful repair at the crosslink site. Alternatively, Ku binding to DNA ends may prevent the action of a putative nuclease activity recently reported to be associated with FANCD2 (Pace et al., 2010).

Whereas *FANCD2*-deficient cells treated with DNA crosslinking agents accumulate additional genomic instability in the absence of Ku, *Brca1*-deficient cells show improved genomic stability and survival when Ku is depleted (Figures 2C–2E, 5C, and 5D). These data suggest that the role of BRCA1 in upstream ICL processing is not essential; BRCA1 rather has an accessory role in mediating optimal FANCD2 accumulation, as in the absence of BRCA1, FANCD2 foci after DNA crosslinking are reduced but not absent (Figure 4B). In contrast, FANCD2 is an essential player in ICL repair, and a deficiency in FANCD2 can therefore not be compensated by deletion of *53BP1* or *Ku.*

Two recent reports indicated that deletion of Ku promotes survival and restores genome integrity in cells deficient in the FA pathway (Adamo et al., 2010; Pace et al., 2010). Nevertheless, discordant results were obtained when testing the effects of various NHEJ mutants. For example, in chicken cells, it was

found that loss of DNA ligase IV (*Lig4*) in *FANCC* mutant cells caused additive repair defects, whereas loss of Ku suppressed the repair defects (Pace et al., 2010). The difference between our data and previously reported results may reflect the fact that DT40 cells used in earlier studies utilize HR for repair at a much higher frequency than other cell types, suggesting that different mechanisms could regulate DSB repair pathway choice in different model systems (Buerstedde and Takeda, 1991). Moreover, the function of FA proteins in mice and humans may be distinct, as several mouse models do not typically exhibit as severe congenital and hematopoietic abnormalities and cancer predisposition as in human patients. Nevertheless, based on our data on Ku deficiency and a corresponding study with *DNA-PKcs*$^{-/-}$ mice crossed with *FANCD2*$^{-/-}$ (Houghtaling et al., 2005) (Table S1), we do not believe it will be possible to relieve FA phenotypes by targeting NHEJ.

Secondary Mutations in *53BP1* and *Ku* as Potential Contributors to Chemoresistance

PARP inhibitors have shown considerable promise as targeted therapies for tumors with deficiencies in BRCA1 or BRCA2, and recent profiling of ovarian tumors has indicated that up to 50% of such cancer cases could be amenable to treatment with PARP inhibitors based on the presence of mutations that affect HR (Cancer Genome Atlas Research Network, 2011). Chemo resistance may arise in cancer cases treated with PARP inhibitor because of the presence of secondary mutations that reduce the sensitivity of HR-deficient tumor cells to PARP inhibition. We propose that mutations in *53BP1* and *Ku70/80* are candidates for altered drug sensitivity in HR-deficient tumors, and that characterization of the status of these genes is likely to have prognostic value in planning treatment with PARP inhibitors or platinum-based chemotherapy.

EXPERIMENTAL PROCEDURES

Mice

Mice carrying the *Brca1*$^{\Delta 11}$ allele were obtained from the NIH mouse repository. *Brca1*- and *Ku80*-null mice were obtained as described (Ludwig et al., 1997; Nussenzweig et al., 1996).

shRNA and Growth Assays

shRNA constructs were obtained from Open Biosystems. Twenty-four hours after lentiviral infection, stable integrants were selected with puromycin. Western blotting was performed using anti-Ku70 mouse monoclonal antibody (mab-Ku70, 3114-500, Abcam used at 1:500). For overexpression, rat Ku70 was subcloned (Yang et al., 1996) into the pMX retroviral vector for infection into passage-immortalized MEFs. For short-term growth assays, cells were grown continuously with PARP inhibitor or for 24 hr in the presence of cisplatin. Proliferation was assayed after 5 days with CellTiterGlo (Promega) according to the manufacturer's instructions. For colony formation, cells were grown for 14 days, then fixed with methanol and stained with crystal violet. Metaphase preparation and telomere FISH was as described (Callén et al., 2007). PARP inhibitor (KU58948) was obtained from Astra Zeneca.

Native BrdU Detection and RPA ChIP

Exponentially growing cells were pulsed with 1 μM BrdU (Sigma) for 36 hr, irradiated (30 Gy, 2 hr recovery at 37°C); then fixed with methanol at −20°C for 20 min. Cells were blocked in 3% BSA in PBS for 30 min, then stained with anti-BrdU monoclonal antibody for 1hr. Before analysis, propidium iodide was added to a final concentration of 20 μg/ml. RPA ChIP was performed as previously described (Yamane et al., 2011).

ACCESSION NUMBERS

GEO: ChIP-seq data for RPA, GSE35698.

SUPPLEMENTAL INFORMATION

Supplemental Information includes one table and five figures and can be found with this article online at doi:10.1016/j.molcel.2012.02.015.

ACKNOWLEDGMENTS

We thank Laura Niedernhofer, Jeremy Daniel, and Elise Kohn for helpful discussions and suggestions; Mark O'Connor for Parpi; and Michael Eckhaus and Mark Bryant for assistance with histology. The work was supported by the Intramural Research Program of the NIH, the National Cancer Institute, and the Center for Cancer Research, and by a Department of Defense grant to A.N. (BC102335) and a K99/R00 grant (1K99CA160574-01) to S.B. Research was conducted in compliance with the Animal Welfare Act Regulations and other federal statutes relating to animals and experiments involving animals and adheres to the principles set forth in the Guide for Care and Use of Laboratory Animals, National Research Council, 1996.

Received: September 9, 2011
Revised: January 13, 2012
Accepted: February 10, 2012
Published online: March 22, 2012

REFERENCES

Adamo, A., Collis, S.J., Adelman, C.A., Silva, N., Horejsi, Z., Ward, J.D., Martinez-Perez, E., Boulton, S.J., and La Volpe, A. (2010). Preventing nonhomologous end joining suppresses DNA repair defects of Fanconi anemia. Mol. Cell *39*, 25–35.

Aiyar, S., Sun, J.L., and Li, R. (2005). BRCA1: a locus-specific "liaison" in gene expression and genetic integrity. J. Cell. Biochem. *94*, 1103–1111.

Bhattacharyya, A., Ear, U.S., Koller, B.H., Weichselbaum, R.R., and Bishop, D.K. (2000). The breast cancer susceptibility gene BRCA1 is required for subnuclear assembly of Rad51 and survival following treatment with the DNA cross-linking agent cisplatin. J. Biol. Chem. *275*, 23899–23903.

Bothmer, A., Robbiani, D.F., Feldhahn, N., Gazumyan, A., Nussenzweig, A., and Nussenzweig, M.C. (2010). 53BP1 regulates DNA resection and the choice between classical and alternative end joining during class switch recombination. J. Exp. Med. *207*, 855–865.

Bothmer, A., Robbiani, D.F., Di Virgilio, M., Bunting, S.F., Klein, I.A., Feldhahn, N., Barlow, J., Chen, H.T., Bosque, D., Callen, E., et al. (2011). Regulation of DNA end joining, resection, and immunoglobulin class switch recombination by 53BP1. Mol. Cell *42*, 319–329.

Botuyan, M.V., Lee, J., Ward, I.M., Kim, J.E., Thompson, J.R., Chen, J., and Mer, G. (2006). Structural basis for the methylation state-specific recognition of histone H4-K20 by 53BP1 and Crb2 in DNA repair. Cell *127*, 1361–1373.

Bouwman, P., Aly, A., Escandell, J.M., Pieterse, M., Bartkova, J., van der Gulden, H., Hiddingh, S., Thanasoula, M., Kulkarni, A., Yang, Q., et al. (2010). 53BP1 loss rescues BRCA1 deficiency and is associated with triple-negative and BRCA-mutated breast cancers. Nat. Struct. Mol. Biol. *17*, 688–695.

Bryant, H.E., Schultz, N., Thomas, H.D., Parker, K.M., Flower, D., Lopez, E., Kyle, S., Meuth, M., Curtin, N.J., and Helleday, T. (2005). Specific killing of BRCA2-deficient tumours with inhibitors of poly(ADP-ribose) polymerase. Nature *434*, 913–917.

Buerstedde, J.M., and Takeda, S. (1991). Increased ratio of targeted to random integration after transfection of chicken B cell lines. Cell *67*, 179–188.

Bunting, S.F., Callén, E., Wong, N., Chen, H.T., Polato, F., Gunn, A., Bothmer, A., Feldhahn, N., Fernandez-Capetillo, O., Cao, L., et al. (2010). 53BP1 inhibits homologous recombination in Brca1-deficient cells by blocking resection of DNA breaks. Cell *141*, 243–254.

Callén, E., Jankovic, M., Difilippantonio, S., Daniel, J.A., Chen, H.T., Celeste, A., Pellegrini, M., McBride, K., Wangsa, D., Bredemeyer, A.L., et al. (2007). ATM prevents the persistence and propagation of chromosome breaks in lymphocytes. Cell *130*, 63–75.

Cancer Genome Atlas Research Network. (2011). Integrated genomic analyses of ovarian carcinoma. Nature *474*, 609–615.

Cao, L., Xu, X., Bunting, S.F., Liu, J., Wang, R.H., Cao, L.L., Wu, J.J., Peng, T.N., Chen, J., Nussenzweig, A., et al. (2009). A selective requirement for 53BP1 in the biological response to genomic instability induced by Brca1 deficiency. Mol. Cell *35*, 534–541.

Cobleigh, M.A. (2011). Other options in the treatment of advanced breast cancer. Semin. Oncol. *38* (*Suppl 2*), S11–S16.

Critchlow, S.E., and Jackson, S.P. (1998). DNA end-joining: from yeast to man. Trends Biochem. Sci. *23*, 394–398.

Difilippantonio, S., Gapud, E., Wong, N., Huang, C.Y., Mahowald, G., Chen, H.T., Kruhlak, M.J., Callen, E., Livak, F., Nussenzweig, M.C., et al. (2008). 53BP1 facilitates long-range DNA end-joining during V(D)J recombination. Nature *456*, 529–533.

Dimitrova, N., Chen, Y.C., Spector, D.L., and de Lange, T. (2008). 53BP1 promotes non-homologous end joining of telomeres by increasing chromatin mobility. Nature *456*, 524–528.

Farmer, H., McCabe, N., Lord, C.J., Tutt, A.N., Johnson, D.A., Richardson, T.B., Santarosa, M., Dillon, K.J., Hickson, I., Knights, C., et al. (2005). Targeting the DNA repair defect in BRCA mutant cells as a therapeutic strategy. Nature *434*, 917–921.

Garcia-Higuera, I., Taniguchi, T., Ganesan, S., Meyn, M.S., Timmers, C., Hejna, J., Grompe, M., and D'Andrea, A.D. (2001). Interaction of the Fanconi anemia proteins and BRCA1 in a common pathway. Mol. Cell *7*, 249–262.

Getts, R.C., and Stamato, T.D. (1994). Absence of a Ku-like DNA end binding activity in the xrs double-strand DNA repair-deficient mutant. J. Biol. Chem. *269*, 15981–15984.

Gravel, S., Chapman, J.R., Magill, C., and Jackson, S.P. (2008). DNA helicases Sgs1 and BLM promote DNA double-strand break resection. Genes Dev. *22*, 2767–2772.

Houghtaling, S., Timmers, C., Noll, M., Finegold, M.J., Jones, S.N., Meyn, M.S., and Grompe, M. (2003). Epithelial cancer in Fanconi anemia complementation group D2 (Fancd2) knockout mice. Genes Dev. *17*, 2021–2035.

Houghtaling, S., Newell, A., Akkari, Y., Taniguchi, T., Olson, S., and Grompe, M. (2005). Fancd2 functions in a double strand break repair pathway that is distinct from non-homologous end joining. Hum. Mol. Genet. *14*, 3027–3033.

Huang, M., and D'Andrea, A.D. (2010). A new nuclease member of the FAN club. Nat. Struct. Mol. Biol. *17*, 926–928.

Huertas, P. (2010). DNA resection in eukaryotes: deciding how to fix the break. Nat. Struct. Mol. Biol. *17*, 11–16.

Huyen, Y., Zgheib, O., Ditullio, R.A., Jr., Gorgoulis, V.G., Zacharatos, P., Petty, T.J., Sheston, E.A., Mellert, H.S., Stavridi, E.S., and Halazonetis, T.D. (2004). Methylated lysine 79 of histone H3 targets 53BP1 to DNA double-strand breaks. Nature *432*, 406–411.

Jensen, R., and Glazer, P.M. (2004). Cell-interdependent cisplatin killing by Ku/DNA-dependent protein kinase signaling transduced through gap junctions. Proc. Natl. Acad. Sci. USA *101*, 6134–6139.

Kass, E.M., and Jasin, M. (2010). Collaboration and competition between DNA double-strand break repair pathways. FEBS Lett. *584*, 3703–3708.

Kee, Y., and D'Andrea, A.D. (2010). Expanded roles of the Fanconi anemia pathway in preserving genomic stability. Genes Dev. *24*, 1680–1694.

Knipscheer, P., Räschle, M., Smogorzewska, A., Enoiu, M., Ho, T.V., Schärer, O.D., Elledge, S.J., and Walter, J.C. (2009). The Fanconi anemia pathway promotes replication-dependent DNA interstrand cross-link repair. Science *326*, 1698–1701.

Long, D.T., Räschle, M., Joukov, V., and Walter, J.C. (2011). Mechanism of RAD51-dependent DNA interstrand cross-link repair. Science *333*, 84–87.

Ludwig, T., Chapman, D.L., Papaioannou, V.E., and Efstratiadis, A. (1997). Targeted mutations of breast cancer susceptibility gene homologs in mice: lethal phenotypes of Brca1, Brca2, Brca1/Brca2, Brca1/p53, and Brca2/p53 nullizygous embryos. Genes Dev. *11*, 1226–1241.

Manis, J.P., Morales, J.C., Xia, Z., Kutok, J.L., Alt, F.W., and Carpenter, P.B. (2004). 53BP1 links DNA damage-response pathways to immunoglobulin heavy chain class-switch recombination. Nat. Immunol. *5*, 481–487.

Nussenzweig, A., and Nussenzweig, M.C. (2010). Origin of chromosomal translocations in lymphoid cancer. Cell *141*, 27–38.

Nussenzweig, A., Chen, C., da Costa Soares, V., Sanchez, M., Sokol, K., Nussenzweig, M.C., and Li, G.C. (1996). Requirement for Ku80 in growth and immunoglobulin V(D)J recombination. Nature *382*, 551–555.

Pace, P., Mosedale, G., Hodskinson, M.R., Rosado, I.V., Sivasubramaniam, M., and Patel, K.J. (2010). Ku70 corrupts DNA repair in the absence of the Fanconi anemia pathway. Science *329*, 219–223.

Patel, A.G., Sarkaria, J.N., and Kaufmann, S.H. (2011). Nonhomologous end joining drives poly(ADP-ribose) polymerase (PARP) inhibitor lethality in homologous recombination-deficient cells. Proc. Natl. Acad. Sci. USA *108*, 3406–3411.

Pierce, A.J., Hu, P., Han, M., Ellis, N., and Jasin, M. (2001). Ku DNA end-binding protein modulates homologous repair of double-strand breaks in mammalian cells. Genes Dev. *15*, 3237–3242.

Rathmell, W.K., and Chu, G. (1994). A DNA end-binding factor involved in double-strand break repair and V(D)J recombination. Mol. Cell. Biol. *14*, 4741–4748.

Sartori, A.A., Lukas, C., Coates, J., Mistrik, M., Fu, S., Bartek, J., Baer, R., Lukas, J., and Jackson, S.P. (2007). Human CtIP promotes DNA end resection. Nature *450*, 509–514.

Stracker, T.H., and Petrini, J.H. (2011). The MRE11 complex: starting from the ends. Nat. Rev. Mol. Cell Biol. *12*, 90–103.

Taccioli, G.E., Gottlieb, T.M., Blunt, T., Priestley, A., Demengeot, J., Mizuta, R., Lehmann, A.R., Alt, F.W., Jackson, S.P., and Jeggo, P.A. (1994). Ku80: product of the XRCC5 gene and its role in DNA repair and V(D)J recombination. Science *265*, 1442–1445.

Vandenberg, C.J., Gergely, F., Ong, C.Y., Pace, P., Mallery, D.L., Hiom, K., and Patel, K.J. (2003). BRCA1-independent ubiquitination of FANCD2. Mol. Cell *12*, 247–254.

Wang, W. (2007). Emergence of a DNA-damage response network consisting of Fanconi anaemia and BRCA proteins. Nat. Rev. Genet. *8*, 735–748.

Wang, B., Matsuoka, S., Ballif, B.A., Zhang, D., Smogorzewska, A., Gygi, S.P., and Elledge, S.J. (2007). Abraxas and RAP80 form a BRCA1 protein complex required for the DNA damage response. Science *316*, 1194–1198.

Ward, I.M., Minn, K., van Deursen, J., and Chen, J. (2003). p53 Binding protein 53BP1 is required for DNA damage responses and tumor suppression in mice. Mol. Cell. Biol. *23*, 2556–2563.

Xu, X., Wagner, K.U., Larson, D., Weaver, Z., Li, C., Ried, T., Hennighausen, L., Wynshaw-Boris, A., and Deng, C.X. (1999a). Conditional mutation of Brca1 in mammary epithelial cells results in blunted ductal morphogenesis and tumour formation. Nat. Genet. *22*, 37–43.

Xu, X., Weaver, Z., Linke, S.P., Li, C., Gotay, J., Wang, X.W., Harris, C.C., Ried, T., and Deng, C.X. (1999b). Centrosome amplification and a defective G2-M cell cycle checkpoint induce genetic instability in BRCA1 exon 11 isoform-deficient cells. Mol. Cell *3*, 389–395.

Xu, X., Qiao, W., Linke, S.P., Cao, L., Li, W.M., Furth, P.A., Harris, C.C., and Deng, C.X. (2001). Genetic interactions between tumor suppressors Brca1 and p53 in apoptosis, cell cycle and tumorigenesis. Nat. Genet. *28*, 266–271.

Yamane, A., Resch, W., Kuo, N., Kuchen, S., Li, Z., Sun, H.W., Robbiani, D.F., McBride, K., Nussenzweig, M.C., and Casellas, R. (2011). Deep-sequencing

identification of the genomic targets of the cytidine deaminase AID and its cofactor RPA in B lymphocytes. Nat. Immunol. *12*, 62–69.

Yang, S.H., Nussenzweig, A., Yang, W.H., Kim, D., and Li, G.C. (1996). Cloning and characterization of rat Ku70: involvement of Ku autoantigen in the heat-shock response. Radiat. Res. *146*, 603–611.

Yarden, R.I., Pardo-Reoyo, S., Sgagias, M., Cowan, K.H., and Brody, L.C. (2002). BRCA1 regulates the G2/M checkpoint by activating Chk1 kinase upon DNA damage. Nat. Genet. *30*, 285–289.

Ye, Q., Hu, Y.F., Zhong, H., Nye, A.C., Belmont, A.S., and Li, R. (2001). BRCA1-induced large-scale chromatin unfolding and allele-specific effects of cancer-predisposing mutations. J. Cell Biol. *155*, 911–921.

Yun, M.H., and Hiom, K. (2009). CtIP-BRCA1 modulates the choice of DNA double-strand-break repair pathway throughout the cell cycle. Nature *459*, 460–463.

Zhang, Q.S., Marquez-Loza, L., Eaton, L., Duncan, A.W., Goldman, D.C., Anur, P., Watanabe-Smith, K., Rathbun, R.K., Fleming, W.H., Bagby, G.C., and Grompe, M. (2010). Fancd2-/- mice have hematopoietic defects that can be partially corrected by resveratrol. Blood *116*, 5140–5148.

Zhu, Q., Pao, G.M., Huynh, A.M., Suh, H., Tonnu, N., Nederlof, P.M., Gage, F.H., and Verma, I.M. (2011). BRCA1 tumour suppression occurs via heterochromatin-mediated silencing. Nature *477*, 179–184.

Molecular Cell
Article

Regulation of DNA End Joining, Resection, and Immunoglobulin Class Switch Recombination by 53BP1

Anne Bothmer,[1,4] Davide F. Robbiani,[1,4] Michela Di Virgilio,[1] Samuel F. Bunting,[3] Isaac A. Klein,[1] Niklas Feldhahn,[1] Jacqueline Barlow,[3] Hua-Tang Chen,[3] David Bosque,[1] Elsa Callen,[3] André Nussenzweig,[3,5,*] and Michel C. Nussenzweig[1,2,5,*]
[1]Laboratory of Molecular Immunology
[2]Howard Hughes Medical Institute
The Rockefeller University, New York, NY 10065, USA
[3]Experimental Immunology Branch, National Cancer Institute, National Institutes of Health, Bethesda, MD 20892, USA
[4]These authors contributed equally to this work
[5]These authors contributed equally to this work
*Correspondence: nussenza@exchange.nih.gov (A.N.), nussen@mail.rockefeller.edu (M.C.N.)
DOI 10.1016/j.molcel.2011.03.019

SUMMARY

53BP1 is a DNA damage protein that forms phosphorylated H2AX (γ-H2AX) dependent foci in a 1 Mb region surrounding DNA double-strand breaks (DSBs). In addition, 53BP1 promotes genomic stability by regulating the metabolism of DNA ends. We have compared the joining rates of paired DSBs separated by 1.2 kb to 27 Mb on chromosome 12 in the presence or absence of 53BP1. 53BP1 facilitates joining of intrachromosomal DSBs but only at distances corresponding to γ-H2AX spreading. In contrast, DNA end protection by 53BP1 is distance independent. Furthermore, analysis of 53BP1 mutants shows that chromatin association, oligomerization, and N-terminal ATM phosphorylation are all required for DNA end protection and joining as measured by immunoglobulin class switch recombination. These data elucidate the molecular events that are required for 53BP1 to maintain genomic stability and point to a model wherein 53BP1 and H2AX cooperate to repress resection of DSBs.

INTRODUCTION

53BP1 is a DNA damage response protein that rapidly forms nuclear foci in response to DNA damage (Anderson et al., 2001; Rappold et al., 2001; Schultz et al., 2000). This process is dependent on PIKK- (ATM/ATR/DNA-PKcs) induced phosphorylation of histone H2AX (γ-H2AX) (Celeste et al., 2003; Fernandez-Capetillo et al., 2002; Ward et al., 2003; Yuan and Chen, 2010). γ-H2AX in turn recruits the E3 ubiquitin ligases RNF8 and RNF168 (Doil et al., 2009; Huen et al., 2007; Kolas et al., 2007; Mailand et al., 2007; Stewart et al., 2009), which promote histone ubiquitylation at sites of double-strand breaks (DSBs). The way in which ubiquitylation facilitates the accumulation of 53BP1 at sites of DSBs has not yet been defined, but one possible scenario is that ubiquitylation exposes constitutive chromatin marks, such as H4K20^{me2}, to which 53BP1 then binds via its tandem tudor domain (Botuyan et al., 2006; Mailand et al., 2007).

In addition to its chromatin-binding tudor domain, 53BP1 contains an oligomerization domain, tandem BRCA1 C-terminal (BRCT) domains, and numerous sites that can be modified post-translationally (Adams and Carpenter, 2006). Homo-oligomerization and interaction between the tudor domains and H4K20^{me2} are required for 53BP1 focus formation in response to DNA damage (Botuyan et al., 2006; Iwabuchi et al., 2003; Ward et al., 2003, 2006; Zgheib et al., 2009). In contrast, the C-terminal tandem BRCT domains are not essential for focus formation but mediate the interaction between 53BP1 and EXPAND1, a protein shown to promote chromatin changes after DNA damage and to facilitate repair (Huen et al., 2010; Ward et al., 2006). Finally, the N-terminal portion of 53BP1 lacks defined structural domains but contains multiple S/T-Q motifs, which are phosphorylation targets of ATM. Although mutating these residues to alanine alters the kinetics of resolution of DNA damage foci, it does not affect the formation of 53BP1 foci in response to DNA damage (DiTullio et al., 2002; Morales et al., 2003; Ward et al., 2006).

In addition to DNA damage-dependent focus formation, 53BP1 is required to protect DSBs from end resection (Bothmer et al., 2010; Bunting et al., 2010). The absence of 53BP1 facilitates resection, thereby relieving a block to homologous recombination in Brca1 mutant cells, promoting degradation of DNA ends during V(D)J recombination and promoting microhomology-mediated alternative NHEJ (A-NHEJ) during immunoglobulin class switch recombination (CSR) (Bothmer et al., 2010; Bunting et al., 2010; Difilippantonio et al., 2008). CSR is a B cell-specific antibody diversification reaction leading to the production of antibodies of different isotypes with altered effector functions (Manis et al., 2004; Ward et al., 2004). Mechanistically CSR is a deletional recombination reaction between paired DSBs in highly repetitive *Ig* switch regions (S regions) separated by 60–200 kb (Stavnezer et al., 2008). Each S region contains a characteristic repetitive sequence, which can also

serve as a substrate for proximal microhomology-mediated intraswitch repair by A-NHEJ at the expense of CSR (Boboila et al., 2010a, 2010b; Bothmer et al., 2010; Reina-San-Martin et al., 2007). Efficient rearrangements require synapsis and repair by classical-NHEJ (C-NHEJ). In addition to CSR, 53BP1 is also required for the joining of distal DSBs during V-J recombination at the TCRα locus (Difilippantonio et al., 2008), and for the fusion of deprotected telomeres (Dimitrova et al., 2008).

Several non-mutually exclusive models have been put forward to explain how 53BP1 helps maintain genome stability and contributes to CSR. One model proposes that 53BP1 facilitates distal DSB joining by synapsing paired DSBs, either by altering local chromatin structure or by increasing chromatin mobility (Difilippantonio et al., 2008; Dimitrova et al., 2008). 53BP1 may also favor CSR by protecting DSBs in Ig switch regions from resection, thereby limiting A-NHEJ mediated intraswitch recombination between homologous sequences while promoting productive interswitch rearrangements by C-NHEJ (Bothmer et al., 2010).

Here, we show that the effects of 53BP1 on joining depend on the distance between the broken ends while DNA end protection by 53BP1 is a distance independent function. We furthermore define the domains of 53BP1 that are required for CSR and DNA end protection.

RESULTS

Role of Distance in Joining of DSBs

During CSR, activation-induced cytidine deaminase (AID) produces tandem DSBs in Ig heavy chain (IgH) switch regions separated by 60–200 kb. 53BP1 is required for the efficient joining between IgH switch breaks and similarly facilitates the joining of I-SceI-induced DSBs separated by 96 kb (Bothmer et al., 2010). To determine how distance affects the joining efficiency of paired DSBs on the chromosome bearing the IgH locus, we produced additional knockin mice bearing I-SceI sites separated by 1.2 kb or 27 Mb on chromosome 12 ($IgH^{I\text{-}1k}$ and $IgH^{I\text{-}27M}$, respectively; Figures S1A and S1D available online). $IgH^{I\text{-}1k}$ and $IgH^{I\text{-}27M}$ showed normal B cell development and CSR to IgG1 upon stimulation with LPS and IL4 (Figures S1B and S1E).

To compare the joining efficiency of DSBs at different distances on the same chromosome, we infected $IgH^{I\text{-}1k/+}AID^{-/-}$ and $IgH^{I\text{-}27M/+}AID^{-/-}$ B cells with an I-SceI-expressing virus or an inactive I-SceI* control and measured recombination frequencies by sample dilution PCR (Figure S1C). Strikingly, the efficiency of joining DSBs separated by 27 Mb was >30-fold lower than that of DSBs separated by 1.2 kb (0.0048×10^{-2} versus 0.17×10^{-2}, $p < 0.0001$, gray bars in Figures 1E and 1B) or 96 kb (0.7×10^{-2}) (Bothmer et al., 2010). To determine how distal intrachromosomal repair compares with transchromosomal joining, we produced mice with paired I-SceI sites on chromosomes 12 and 15 (IgH^{I} and Myc^{I}, respectively) (Robbiani et al., 2008) and generated translocations by infecting cells with I-SceI viruses. The joining frequency of I-SceI-infected $IgH^{I/+}Myc^{I/+}AID^{-/-}$ B cells was 0.0027×10^{-2} per cell, which is comparable to the joining between I-SceI sites separated by 27 Mb in $IgH^{I\text{-}27M/+}AID^{-/-}$ (Figures 1E and 1H, gray bars). We conclude that the joining of proximal (1.2 or 96 kb) intrachromosomal DSBs is significantly more efficient than distal (27 Mb) intrachromosomal joining, and that the latter is similar to transchromosomal joining.

Loss of 53BP1 decreases the joining efficiency of I-SceI-induced DSBs separated by 96 kb at the IgH locus, although the effect is less pronounced than for AID-mediated CSR (Bothmer et al., 2010). To determine the role of 53BP1 in distal versus proximal repair of paired DSBs, we compared joining between I-SceI sites in 53BP1 deficient $IgH^{I\text{-}1k}$ (proximal), $IgH^{I\text{-}27M}$ (distal), and $IgH^{I}Myc^{I}$ (interchromosomal) B cells ($IgH^{I\text{-}1k/+}AID^{-/-}53BP1^{-/-}$, $IgH^{I\text{-}27M/+}AID^{-/-}53BP1^{-/-}$, and $Myc^{I/+}IgH^{I/+}AID^{-/-}53BP1^{-/-}$ B cells, respectively). In contrast to the joining of DSBs separated by 96 kb (Bothmer et al., 2010), the absence of 53BP1 did not reduce the frequency of joining between I-SceI sites separated by 1.2 kb or 27 Mb on the same chromosome or sites on different chromosomes. (Figures 1B, 1E, and 1H and Figures S1F–S1H). We conclude that in contrast to facilitating the joining of DSBs separated by 96 kb, the loss of 53BP1 does not alter the joining frequency of more proximal or distal DSBs.

The loss of 53BP1 results in increased DNA end resection (Bothmer et al., 2010). To determine whether this effect is dependent on distance, we measured end resection in $IgH^{I\text{-}1k/+}AID^{-/-}53BP1^{-/-}$ and $IgH^{I\text{-}27M/+}AID^{-/-}53BP1^{-/-}$ B cells and the respective 53BP1-proficient controls. Joins with deletions of more than 35 nt (indicative of extensive end processing) increased from 37.2% in $IgH^{I\text{-}1k/+}AID^{-/-}$ to 52.4% in $IgH^{I\text{-}1k/+}AID^{-/-}53BP1^{-/-}$ and from 55.5% in $IgH^{I\text{-}27M/+}AID^{-/-}$ to 75.5% in $IgH^{I\text{-}27M/+}AID^{-/-}53BP1^{-/-}$ (Figures 1C and 1F). We conclude that 53BP1's ability to prevent end resection is independent of the distance between paired DSBs.

In summary, 53BP1 has a distance-independent function in the prevention of DNA end resection and a distance-dependent function in facilitating the joining of DSBs.

BRCT Domains

To investigate the function of the BRCT domains of 53BP1 in CSR, we deleted the region corresponding to amino acids 1708–1969 from the mouse germline ($53BP1^{\Delta BRCT}$; Figure 2A and Figure S2A). Lymphocyte development and CSR were normal in $53BP1^{\Delta BRCT}$ mice, despite lower than wild-type levels of the mutant protein (Figures 2B and 2C and Figure S2B).

To determine whether the BRCT domains are required for DSB end protection, we produced $53BP1^{\Delta BRCT/-}IgH^{I\text{-}96k/+}$ mice and assayed the resection of paired I-SceI breaks. We found a minor increase in DNA end resection compared to controls, which is probably due to the decreased expression level of the mutant protein (Figures 2B and 2D). We conclude that the BRCT domains of 53BP1 are dispensable for CSR and the protection of DNA ends from resection.

53BP1 Chromatin Association

53BP1 binds to $H4K20^{me2}$, a constitutive histone modification, and forms nuclear foci in response to DNA damage (Botuyan et al., 2006; Schultz et al., 2000). To determine whether 53BP1 is chromatin associated in B cells, we fractionated unstimulated B cells before or after treatment with ionizing radiation (IR). We found that a portion of the total cellular 53BP1 is chromatin associated in the steady-state even in the absence of DNA damage (Figure 3A). This is consistent with the finding that 53BP1

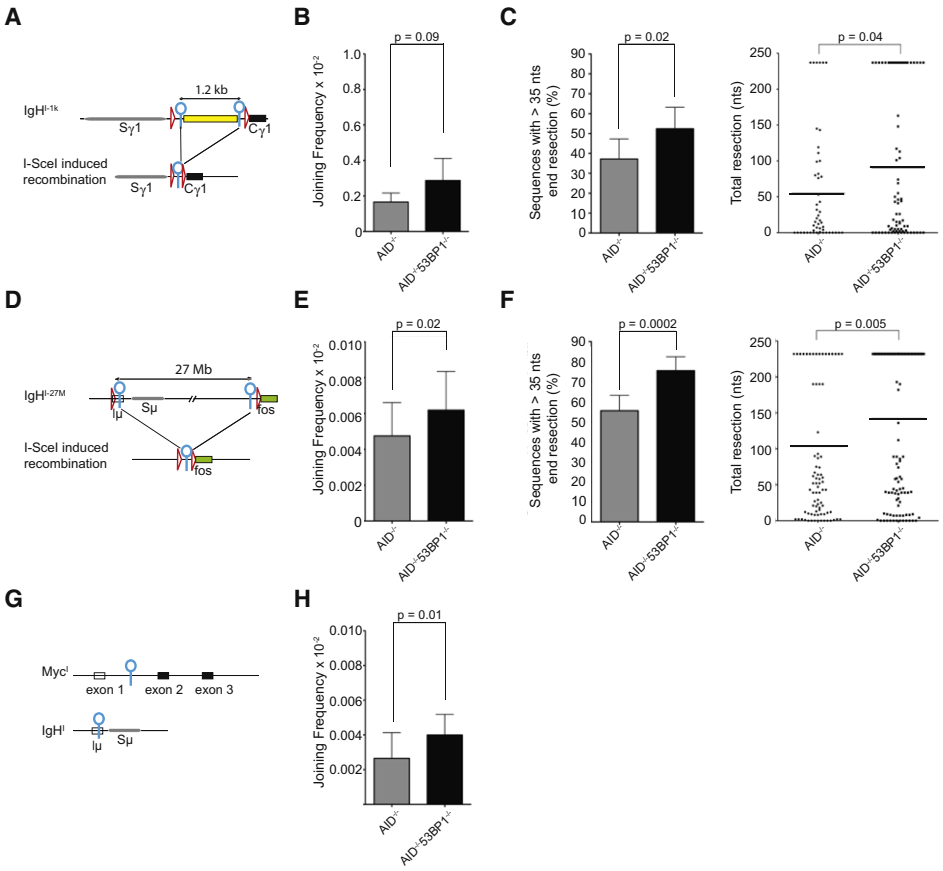

Figure 1. 53BP1 Effects on Joining of Proximal or Distal DSBs

(A) Schematic representation of IgH$^{I\text{-}1k}$ allele before (top) and after (bottom) I-SceI-induced recombination. I-SceI sites are indicated as blue circles and loxP sites as red triangles. Spacer sequence of 1.2 kb is indicated as yellow rectangle.

(B) Bar graph shows I-SceI-induced recombination frequency of IgH$^{I\text{-}1k/+}$AID$^{-/-}$ B cells in the presence or absence of 53BP1. p value was calculated with a paired two-tailed Student's t test. See also Figure S1F.

(C) Left: Bar graph showing the frequency of I-SceI-induced recombination products with more than 35 nt end processing for IgH$^{I\text{-}1k/+}$AID$^{-/-}$ and IgH$^{I\text{-}1k/+}$AID$^{-/-}$ 53BP1$^{-/-}$ B cells. Right: Dot plot showing resection in sequences from I-SceI-infected IgH$^{I\text{-}1k/+}$AID$^{-/-}$ and IgH$^{I\text{-}1k/+}$AID$^{-/-}$53BP1$^{-/-}$ B cells, with each dot representing one cloned sequence.

(D) Schematic representation of IgH$^{I\text{-}27M}$ allele before (top) and after (bottom) I-SceI-induced recombination.

(E) As in (B) for IgH$^{I\text{-}27M/+}$AID$^{-/-}$ and IgH$^{I\text{-}27M/+}$AID$^{-/-}$53BP1$^{-/-}$ B cells. See also Figure S1G.

(F) As in (C) for IgH$^{I\text{-}27M/+}$AID$^{-/-}$ and IgH$^{I\text{-}27M/+}$AID$^{-/-}$53BP1$^{-/-}$ B cells.

(G) Schematic representation of the Myc^{I} and IgH^{I} alleles.

(H) As in (B and E) for IgH$^{I/+}$Myc$^{I/+}$AID$^{-/-}$ B cells in the presence and absence of 53BP1. See also Figure S1H.

Horizontal lines in dot plots indicate the means. Error bars indicate standard deviations. p values were calculated using a two-tailed Student's t test, unless otherwise indicated. All graphs represent data from at least three independent experiments, unless specified. See also Figure S1.

constitutively associates with chromatin in a manner independent of RNF8 (Santos et al., 2010). Furthermore, chromatin association did not increase significantly after irradiation.

Residue D1521 in the tudor domain of 53BP1 is required for binding to H4K20^{me2} (Botuyan et al., 2006). To test the role of this interaction in CSR and DNA resection, we produced D1518R mutant mice (53BP1^{DR}) bearing a single amino acid substitution that is equivalent to D1521R in humans (Figure 3B and Figure S3A). Lymphocyte development was similar to the wild-type in 53BP1^{DR} mice (Figure S3B), and the mutant 53BP1^{DR} protein was normally phosphorylated at Ser^{25} upon IR (Figure S3C). In agreement with previous studies, 53BP1^{DR} failed to form IR-induced foci and showed only faint accumulation at sites of laser scissor damage in mouse embryonic fibroblasts (MEFs; Figure 3C and Figure S3D) (Botuyan et al., 2006; Huyen et al., 2004). In addition, 53BP1^{DR} was not chromatin associated in B cells (Figure 3D). We conclude that 53BP1 binds to chromatin constitutively through residue D1518 and that chromatin association is not required for 53BP1 phosphorylation.

To determine whether chromatin association is required for CSR, we stimulated 53BP1^{DR} B cells in vitro. Mutant B cells switched at about 10% of wild-type levels, phenocopying 53BP1$^{-/-}$ (Figure 3E). Loss of chromatin association also resulted in an increase in DNA end resection in 53BP1^{DR}IgH$^{I\text{-}96k/+}$ comparable to 53BP1$^{-/-}$IgH$^{I\text{-}96k/+}$ controls (Figure 3F). We conclude that 53BP1 is constitutively chromatin associated and

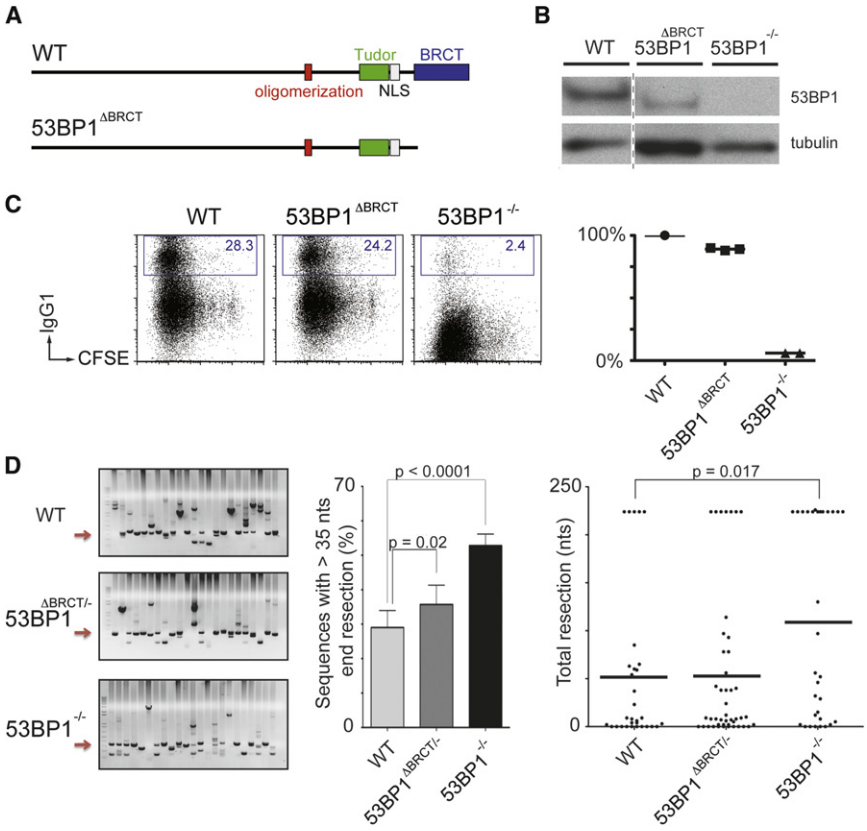

Figure 2. The BRCT Domains Are Dispensable for CSR and DNA End Protection

(A) Schematic representation of wild-type (WT) 53BP1 protein (top) and 53BP1 lacking the BRCT domains (bottom).

(B) Western blot showing 53BP1 expression levels in WT and 53BP1$^{\Delta BRCT}$ B cells.

(C) Left: Representative flow cytometry plots measuring CSR after stimulation of WT, 53BP1$^{\Delta BRCT}$ and 53BP1$^{-/-}$ B cells. Numbers indicate the percentage of IgG1 switched cells. CFSE dye tracks cell division. Right: Summary dot plot indicating CSR as a percentage of WT value within the same experiment. Each dot represents an independent experiment.

(D) Left: Representative ethidium bromide stained agarose gels showing PCR products obtained after I-SceI-induced recombination in IgH$^{I\text{-}96k/+}$, IgH$^{I\text{-}96k/+}$53BP1$^{\Delta BRCT/-}$, and IgH$^{I\text{-}96k}$53BP1$^{-/-}$ B cells. Middle: Bar graph quantitating the frequency of I-SceI-induced recombination products with more than 35 nt end processing. Error bars indicate standard deviation. Right: Dot plot showing resection with each dot representing one sequence. Two independent experiments.

See also Figure S2.

that this association is required for CSR and for the protection of DNA ends from resection.

H2AX Protects DNA Ends from Resection

H2AX is required for stable 53BP1 DNA damage focus formation, and its deficiency impairs CSR, but to a lesser extent than absence of 53BP1 (Celeste et al., 2002; Fernandez-Capetillo et al., 2002; Reina-San-Martin et al., 2003). Moreover, 53BP1 was reported to interact with H2AX (Ward et al., 2003). To determine whether the chromatin association of 53BP1 depends on this histone variant, we assayed H2AX-deficient B cells. Although H2AX is required for 53BP1 foci, we found that H2AX is dispensable for 53BP1 chromatin association (Figure 4A). To determine whether H2AX is required to prevent DNA resection, we assayed IgH$^{I\text{-}96k/+}$AID$^{-/-}$ H2AX$^{-/-}$ B cells. We found that resection was increased in the absence of H2AX to levels comparable to 53BP1$^{-/-}$ (51.7% compared to 35.8% in IgH$^{I\text{-}96k}$AID$^{-/-}$ control, Figure 4B). Interestingly, while allowing for resection, absence of H2AX does not reverse radial fusions that are observed in PARP inhibitor- (KU58948) treated Brca1 mutant cells (Figure 4C). Thus, although 53BP1 can be constitutively chromatin associated in the absence of H2AX, this alone is not sufficient to prevent the extensive resection.

The Oligomerization Domain of 53BP1 Is Required for CSR

The central region of 53BP1 is required for 53BP1 oligomerization (Ward et al., 2006; Zgheib et al., 2009) and contains residues that are phosphorylated by ATM (S1219) (Lee et al., 2009), ubiquitylated by Rad18 (K1268) (Watanabe et al., 2009), and methylated by PRMT1 (R1398, R1400, R1401) (Boisvert et al., 2005). To determine the role of this region in vivo, we produced mice that express a mutant form of 53BP1 lacking this region (Figure 5A and Figure S4A). 53BP1$^{\Delta 1210-1447}$ protein was expressed at normal levels, and lymphocyte development in 53BP1$^{\Delta 1210\text{-}1447}$ mice was similar to wild-type (Figures S4B and S4C).

However, 53BP1$^{\Delta 1210-1447}$ B cells are similar to null mutant cells in CSR (Figure 5B). To confirm this result and identify the responsible activity, we produced four region-specific mutant retroviruses and assayed them for their ability to rescue IgG1 switching in 53BP1$^{-/-}$ B cells (Figure 5C and 5D and Figure S4D; since full-length 53BP1 cannot be expressed by retroviruses, deletion of the BRCT domain, which is similar to wild-type [see Figure 2] can be used for retroviral expression). 53BP1$^{\Delta 1231-1270}$, which lacks the oligomerization domain, was the only mutant that failed to rescue CSR, despite partially retaining the ability to bind chromatin (Figure 5D and 5E) (Zgheib et al., 2009). We conclude that the oligomerization domain in 53BP1 is required for class switch recombination but that residues S1219, K1268, and R1398/R1400/R1401 are not.

Residues 1052 to 1710 of 53BP1 include the tudor and oligomerization domains, which are sufficient for chromatin binding and DNA damage focus formation (Figure 5F) (Ward et al., 2003; Zgheib et al., 2009). However, retrovirally expressed 53BP1$^{1052-1710}$ was unable to rescue CSR (Figure 5G and Figure S4E). We conclude that chromatin binding, oligomerization, and focus formation are insufficient to promote CSR, suggesting that the N terminus of 53BP1 may play an important role in this reaction.

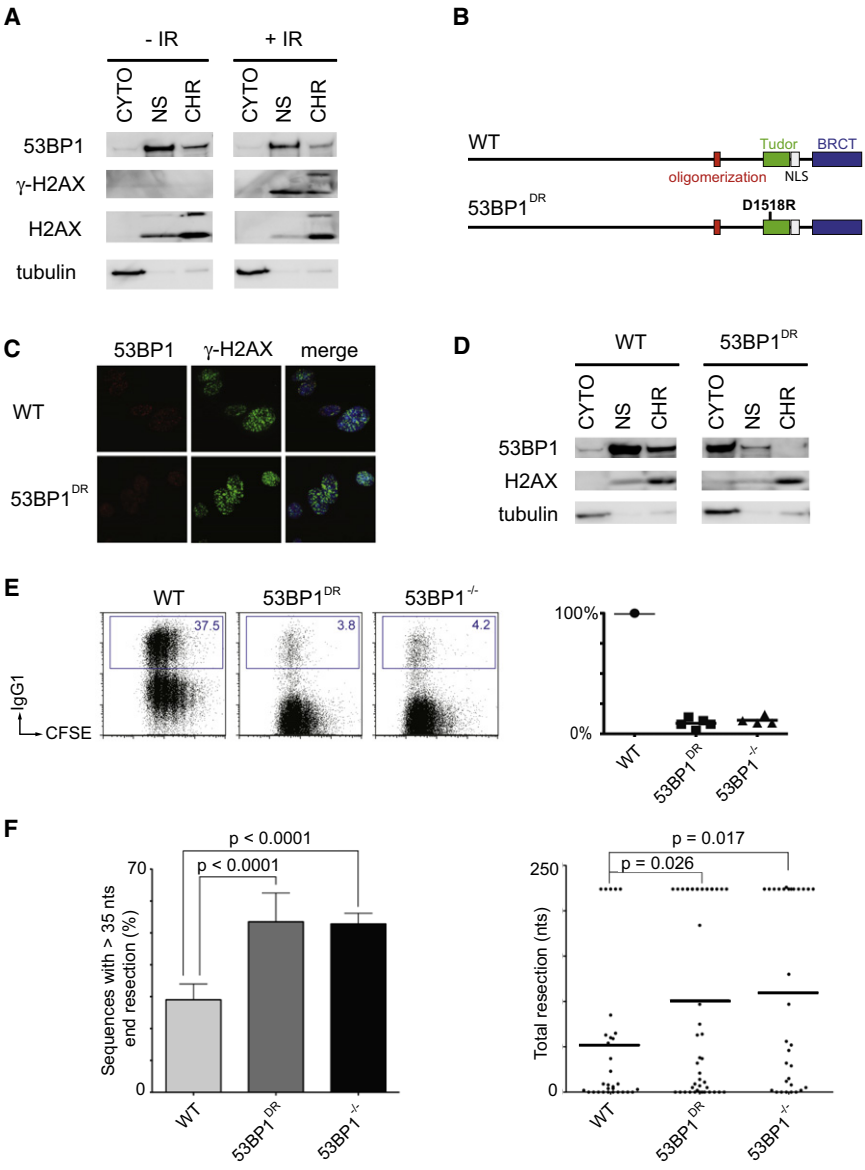

Figure 3. 53BP1 Tudor Domains Are Required for CSR and for the Protection of DNA Ends

(A) Western blots of fractionated WT B cells ± 10 Gy of IR. CYTO, cytoplasmic fraction; NS, nuclear soluble fraction; CHR, chromatin fraction.

(B) Schematic representation of WT 53BP1 (top) and 53BP1 with tudor domain mutation D1518R (bottom).

(C) 53BP1 and γ-H2AX IRIF in WT and 53BP1^{DR} MEFs after IR.

(D) Western blots of unstimulated, fractionated WT, and 53BP1^{DR} B cells.

(E) Left: Representative flow cytometry plots measuring CSR to IgG1 after stimulation of WT, 53BP1^{DR}, and 53BP1$^{-/-}$ B cells. Right: Summary dot plot indicating CSR as a percentage of WT. Each dot represents an independent experiment.

(F) As in Figure 1C for WT, 53BP1^{DR}, and 53BP1$^{-/-}$ B cells. Error bars indicate standard deviation. Two independent experiments.

See also Figure S3.

Phosphorylation Sites at the N Terminus of 53BP1

To examine the role of the N terminus of 53BP1 in CSR, we produced and tested additional mutants, including (1) smaller N-terminal deletions (53BP1$^{901–1710}$ and 53BP1$^{459–1710}$), (2) internal deletions corresponding to the amino acids encoded by exons 3–12 (53BP1$^{\Delta 61–901}$), 7–12 (53BP1$^{\Delta 216–901}$), and 12 alone (53BP1$^{\Delta 459–901}$), and (3) alanine substitution mutants of S/T-Q consensus sites for ATM phosphorylation (53BP1^{8A}, 53BP1^{7A}, 53BP1^{15A}, 53BP1^{28A}) (Morales et al., 2003; Ward et al., 2006). We found that all of the deletion mutants were unable to rescue CSR (Figures S5A and S5B). The alanine substitution mutants 53BP1^{8A}, 53BP1^{7A}, 53BP1^{15A}, and 53BP1^{28A} displayed a phenotype that correlated with the number of substitutions. 53BP1^{8A} showed 90% of WT CSR, whereas 53BP1^{28A} was similar to the null mutant (Figures 6A and 6B and Figure S5C). Despite its inability to rescue CSR, 53BP1^{28A} bound to chromatin and formed IR foci (Figures 6C and 6D). We conclude that multiple S/T-Q target sites for ATM phosphorylation at the N terminus of 53BP1 are required for CSR.

The Oligomerization Domain and N-Terminal Phosphorylation Sites in 53BP1 Protect DNA Ends from Processing

Loss of 53BP1 rescues homologous recombination in Brca1 mutant cells by facilitating the processing of DNA ends (Bunting et al., 2010). To determine which domains of 53BP1 are required for DNA end protection in Brca1 mutant cells, we infected Brca1$^{\Delta 11/\Delta 11}$53BP1$^{-/-}$ B cells with 53BP1 mutant retroviruses and measured the frequency of radial chromosome structures upon treatment with the PARP inhibitor (Bunting et al., 2010). Whereas 12 radial structures were found among 100 metaphases in Brca1$^{\Delta 11/\Delta 11}$53BP1$^{-/-}$ B cells infected with a negative control virus, 54 were present upon infection with 53BP1$^{1–1710}$ (average of two independent experiments, Figure 7A and Figure S6). Confirming our previous finding with 53BP1^{DR} B cells showing that chromatin binding is required for protection from DNA resection, a 53BP1^{D1521R} virus did not rescue radial formation (7/100 metaphases), nor did 53BP1$^{1052–1710}$ (10/100 metaphases), the oligomerization mutant 53BP1$^{\Delta 1231–1270}$ (12/100 metaphases), nor the alanine mutant 53BP1^{28A} (14/100 metaphases; Figure 7A). We conclude that the tudor and oligomerization domains and the S/T-Q sites at the N terminus of 53BP1 are required for end protection and contribute to 53BP1-mediated toxicity in Brca1 mutant cells.

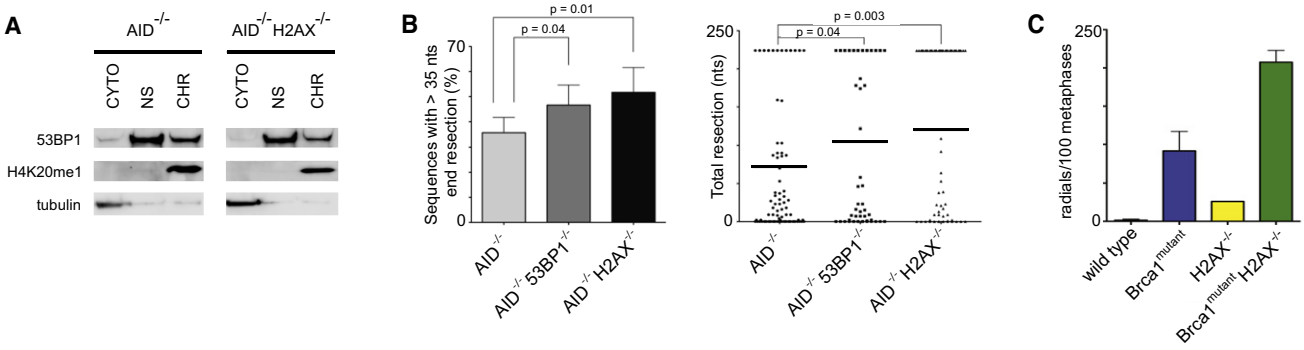

Figure 4. 53BP1 Chromatin Association in the Absence of H2AX Is Not Sufficient to Prevent End Resection

(A) Western blots of fractionated $AID^{-/-}$ and $AID^{-/-}H2AX^{-/-}$ B cells.

(B) Left: Bar graph showing the frequency of I-SceI-induced recombination products with more than 35 nt end processing for $IgH^{I\text{-}96k/+}AID^{-/-}$, $IgH^{I\text{-}96k/+}AID^{-/-}53BP1^{-/-}$, and $IgH^{I\text{-}96k/+}AID^{-/-}H2AX^{-/-}$ B cells. Right: Dot plot showing resection in sequences from I-SceI-infected $IgH^{I\text{-}96k/+}AID^{-/-}$, $IgH^{I\text{-}96k/+}AID^{-/-}53BP1^{-/-}$, and $IgH^{I\text{-}96k/+}AID^{-/-}H2AX^{-/-}$ B cells. Error bars indicate standard error of the mean. Two independent experiments.

(C) Histogram with number of radial structures in metaphases from PARP inhibitor-treated $Brca1^{lox/lox}CD19^{cre/+}$ ($Brca1^{mutant}$) B cells either proficient or deficient for H2AX. Error bars indicate standard error of the mean. Two independent experiments.

DISCUSSION

DNA breaks jeopardize genomic integrity, yet they occur as byproducts of DNA replication, oxidative metabolism, ionizing radiation, and antigen receptor diversification reactions in lymphocytes (Hoeijmakers, 2009; Lieber, 2010; Nussenzweig and Nussenzweig, 2010). Joining of paired DNA breaks on disparate chromosomes leads to translocations, while joining of paired intrachromosomal breaks produces deletions that result in loss of genetic information. Translocations and deletions are commonly observed in cancer, where they are often recurrent and contribute to malignant transformation (Futreal et al., 2004).

HO, I-SceI, and zinc-finger nucleases that produce unique DSBs in yeast and mammalian genomes have been used to explore the biology of chromosome translocations. However, much less is known about the role of DNA repair factors in protecting cells against intrachromosomal deletions. In the absence of a sister chromatid, DSBs are repaired by either C-NHEJ or A-NHEJ. The C-NHEJ pathway requires DNA ligase IV, XRCC4, Ku70, and Ku80, and is necessary for efficient repair of intrachromosomal DSBs as evidenced by reduced CSR when C-NHEJ is impaired (Boboila et al., 2010a; Boboila et al., 2010b). Contrary to its role in promoting intrachromosomal DSB repair, the C-NHEJ pathway inhibits chromosome translocations, which often harbor microhomologies at the translocation breakpoint indicative of joining by the A-NHEJ pathway (reviewed in Kass and Jasin, 2010, and Zhang et al., 2010; Ramiro et al., 2006) To study the role of distance and DNA damage response factors in repair of tandem intrachromosomal DSBs in mammalian cells, we compared joining between I-SceI-induced DSBs on chromosome 12 spaced by 1.2 kb, 96 kb, and 27 Mb. Our analysis reveals that DSBs 1.2 kb or 96 kb apart are more likely to join than those separated by 27 Mb. Indeed, when DSBs are separated by 27 Mb on chromosome 12 the rate of paired end joining in *cis* is similar to transchromosomal joining between *IgH* and *c-myc* on chromosome 15.

53BP1 facilitates end joining in *cis* (Bothmer et al., 2010); however, this effect is limited to DSBs separated by 96 kb, as loss of 53BP1 does not reduce the joining frequency of proximal, very distal, or transchromosomal DSBs. The selective effect of 53BP1 on joining paired breaks separated by 96 kb suggests a role for DNA damage factors that spread along the chromosome in response to DSBs in an H2AX/RNF8-dependent manner (Bekker-Jensen et al., 2006; Savic et al., 2009). Indeed, the extent of γ-H2AX spreading from an I-SceI-induced DSBs at the IgH locus is confined to ~1 Mb surrounding the break (Figure S1I).

The new results are consistent with the finding that 53BP1 allows for a higher probability of interactions between DNA elements 28–172 kb apart during rearrangements of the TCRα locus (Difilippantonio et al., 2008). Since DSBs produced during CSR are separated by 60–200 kb, our findings support a model in which 53BP1 and possibly other focus forming factors promote the synapsis of DSBs if they fall within the range of spread of the H2AX/RNF8-dependent DNA damage response. Interestingly, loss of 53BP1 does not affect recombination efficiency mediated by Cre/loxP, which is independent of the DNA damage response (Bothmer et al., 2010; Guo et al., 1997). This indicates that indeed 53BP1 acts downstream of a DSB, mediating synapsis of broken ends as part of the DNA damage response.

In addition to forming repair foci at DNA ends 53BP1 also protects DNA ends from resection and thereby favors repair by C-NHEJ while preventing A-NHEJ (a pathway with extensive processing and microhomology) and HR (Bothmer et al., 2010; Bunting et al., 2010). This may be particularly important during CSR in lymphocytes because switch regions are highly repetitive. Since 53BP1 protects ends from resection, its absence would favor microhomology-mediated intraswitch joining as opposed to productive switch recombination between different switch regions (Bothmer et al., 2010). However, end protection is not sufficient to explain the effects of 53BP1 on CSR since H2AX deficiency promotes extensive end resection (Figure 4B) and yet produces a milder CSR defect (Reina-San-Martin

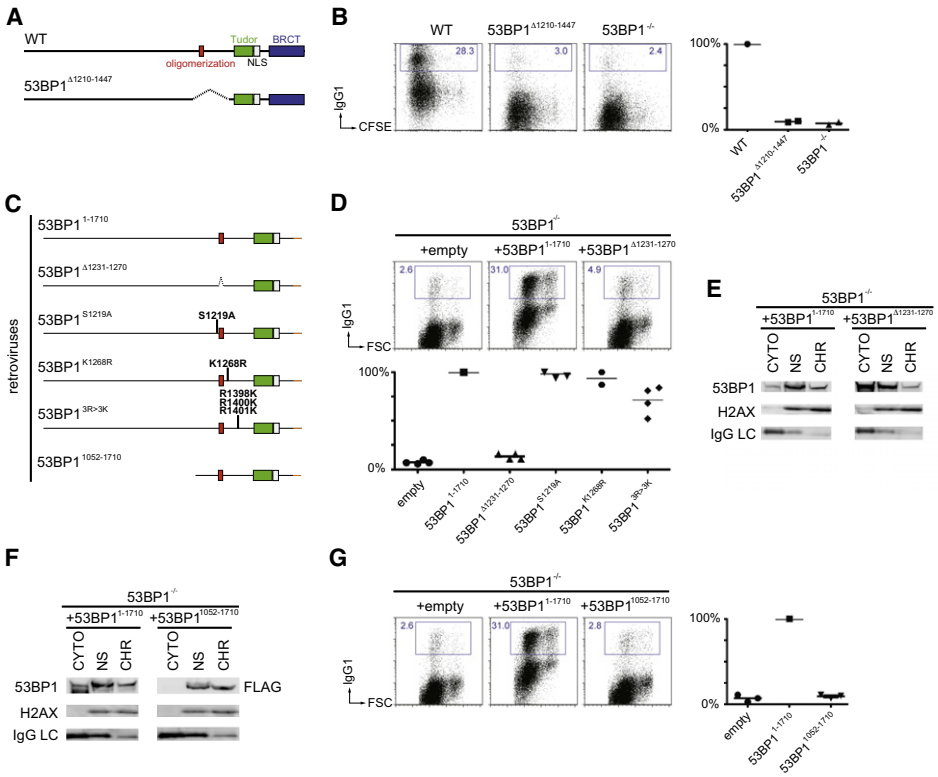

Figure 5. The Oligomerization Domain of 53BP1 in Chromatin Association and CSR

(A) Schematic representation of WT 53BP1 (top) and 53BP1 lacking amino acids 1210–1447 (bottom).

(B) As in Figure 2C for WT, 53BP1$^{\Delta 1210–1447}$, and 53BP1$^{-/-}$ B cells.

(C) Diagram of 53BP1 retroviral constructs with the indicated mutations and deletions.

(D) As in Figure 2C after infection of 53BP1$^{-/-}$ B cells with empty retrovirus, or retrovirus expressing 53BP1$^{1–1710}$, or the oligomerization mutant 53BP1$^{\Delta 1231–1270}$, or the other mutants listed in (C).

(E) Western blots of fractionated 53BP1$^{-/-}$ B cells stimulated and infected with 53BP1$^{1–1710}$ or 53BP1$^{\Delta 1231–1270}$.

(F) Western blots of fractionated 53BP1$^{-/-}$ B cells stimulated and infected with 53BP1$^{1–1710}$ or 53BP1$^{1052–1710}$.

(G) As in Figure 2C after infection of 53BP1$^{-/-}$ B cells with empty retrovirus, or retroviruses expressing 53BP1$^{1–1710}$ or the N-terminal deleted mutant 53BP1$^{1052–1710}$.

See also Figure S4.

et al., 2003). Of note, all joining experiments were performed in the absence of AID, and we cannot exclude the possibility that AID, in addition to 53BP1, influences the repair pathway choice.

The way in which 53BP1 mediates end protection and facilitates joining was investigated by analyzing the contribution of the structural domains of 53BP1 to DNA end protection and class switching in B lymphocytes. Human 53BP1 binds to the histone mark H4K20^{me2} via its tudor domain, and mutation of amino acid D1521 in the tudor domain abrogates 53BP1's ability to form DNA damage foci in response to IR (Botuyan et al., 2006; Huyen et al., 2004). We find that 53BP1 is chromatin associated even in the absence of DNA damage or H2AX, which is consistent with previous reports showing that H4K20^{me2} is a constitutive chromatin modification (Botuyan et al., 2006; Sanders et al., 2004) and that 53BP1 chromatin association is RNF8 independent (Santos et al., 2010). These studies suggest that even in the context of undamaged chromatin, this modification is accessible to 53BP1. Furthermore, a knockin mutant of the tudor domain (53BP1^{DR}) that fails to form foci in response to DNA damage also fails to associate with chromatin in nonirradiated cells. Therefore, an intact tudor domain is required for both constitutive binding to chromatin and DNA damage-induced focus formation. As predicted from its inability to bind chromatin or form DNA damage foci, 53BP1^{DR} was unable to protect DNA ends from resection or to support CSR.

The absence of 53BP1's oligomerization domain and deficiency in H2AX both impair the formation of stable DNA damage foci (Celeste et al., 2003; Fernandez-Capetillo et al., 2002; Ward et al., 2003; Yuan and Chen, 2010). In contrast, we find that neither the oligomerization domain of 53BP1 nor H2AX is required for 53BP1 binding to chromatin. However, DNA end protection and CSR are impaired in the absence of either. Thus, the ability to bind constitutively to chromatin appears to be necessary but not sufficient for end protection or CSR. Consistent with this idea, a fragment of 53BP1, which binds chromatin and forms DNA damage-inducible foci (53BP1$^{1052–1710}$), is unable to support either end protection or CSR. Interestingly, and unlike 53BP1, H2AX deficiency does not rescue the

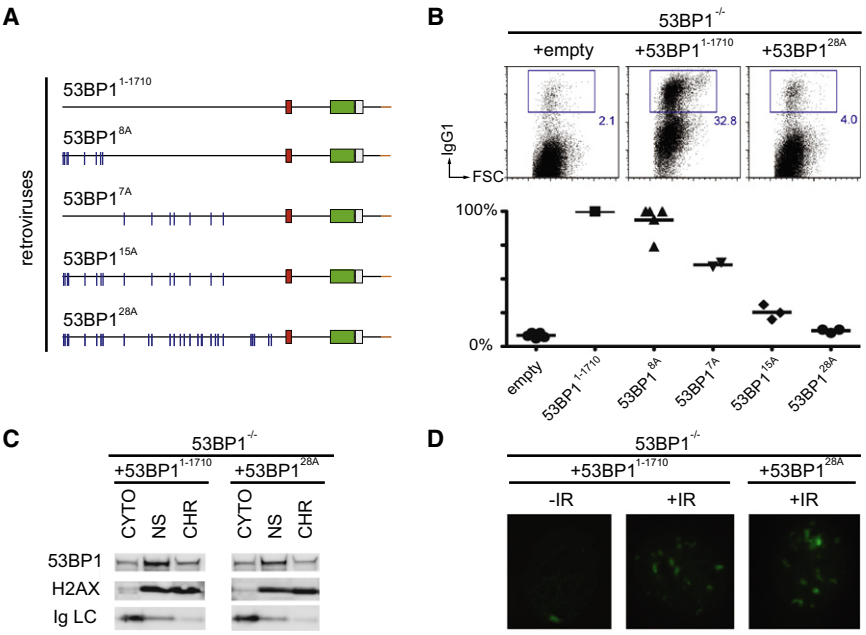

Figure 6. N-Terminal Phosphorylation of 53BP1 in DNA Damage and CSR

(A) Diagram of 53BP1 retroviral constructs with the indicated mutations.

(B) As in Figure 2C after infection of 53BP1$^{-/-}$ B cells with empty retrovirus, or retroviruses expressing 53BP1$^{1-1710}$, or the N-terminal mutant 53BP1^{28A}, or the other mutants listed in (A).

(C) Western blots of fractionated 53BP1$^{-/-}$ B cells stimulated and infected with 53BP1$^{1-1710}$ or 53BP1^{28A}.

(D) 53BP1 IRIF in 53BP1$^{-/-}$ MEFs reconstituted with 53BP1$^{1-1710}$ and 53BP1^{28A} after 10 Gy.

See also Figure S5.

formation of radial fusions observed in PARP inhibitor treated Brca1 mutant B cells (Figure 4C). Although deficiency in both H2AX and 53BP1 leads to increased end resection (Bothmer et al., 2010; Bunting et al., 2010; Helmink et al., 2011; Zha et al., 2011), H2AX—in contrast to 53BP1—probably plays additional roles in HR and NHEJ that may be essential in Brca1-deficient cells. Similar to H2AX, RNF8 and RNF168 are required for stable 53BP1 focus formation upon IR (Doil et al., 2009; Huen et al., 2007; Kolas et al., 2007; Mailand et al., 2007; Stewart et al., 2009; Yuan and Chen, 2010). In this context, it will be interesting to test the effect of RNF8/RNF168 deficiency on PARP inhibitor-induced chromosome abnormalities in Brca1$^{\Delta 11/\Delta 11}$ cells, as these ubiquitin ligases lie downstream of H2AX and upstream of 53BP1.

Our analysis of tandem BRCT domain-mutant B cells (53BP1$^{\Delta BRCT}$) showed that the C terminus is dispensable for both CSR and the protection of ends from processing, which suggests a role for the N terminus in these processes. The N terminus of 53BP1 lacks known structural domains but contains S/T-Q consensus target sites for ATM phosphorylation that are implicated in promoting the resolution of γ-H2AX foci upon IR (DiTullio et al., 2002; Morales et al., 2003; Ward et al., 2006). We find that the putative ATM phosphorylation sites are also required to prevent DNA resection and to support CSR, suggesting that N-terminally phosphorylated 53BP1 may recruit additional factors to regulate DNA repair. In summary (Figure 7B), out of all the 53BP1 functional domains tested, the ability to protect DNA ends from resection is the only parameter that correlates with CSR. Chromatin association, focus formation, oligomerization, and intact N-terminal ATM phosporylation sites are all essential but by themselves not sufficient to prevent DNA end processing or to support CSR. Therefore, end protection and CSR may not simply be mediated by direct physical association of 53BP1 with DNA ends but appear to require the assembly of a complex composed of H2AX, 53BP1, and possibly additional yet-to-be defined proteins.

EXPERIMENTAL PROCEDURES

Mice

IgH$^{I\text{-}1k/+}$, IgH$^{I\text{-}27M/+}$, 53BP1$^{\Delta BRCT/+}$, 53BP1$^{DR/+}$, and 53BP1$^{\Delta 1210\text{–}1447/+}$ mice were generated by homologous recombination in C57BL/6 albino embryonic stem cells (ESCs). Details of the targeting vectors, screening by Southern blot, and genotyping PCR are provided in the legends to Figures S1–S4. IgH$^{I\text{-}96k/+}$ (Bothmer et al., 2010), IgH$^{I/+}$ and Myc$^{I/+}$ (Robbiani et al., 2008), AID$^{-/-}$ (Muramatsu et al., 2000), 53BP1$^{-/-}$ (Ward et al., 2004), H2AX$^{-/-}$ (Celeste et al., 2002), Brca1$^{lox/lox}$ (Xu et al., 1999), Brca1$^{\Delta 11/\Delta 11}$ (Xu et al., 2001), and CD19^{cre} mice (Rickert et al., 1997) were previously described. Unless otherwise indicated, experiments were performed with mice homozygous for the indicated alleles. All experiments were performed in accordance with protocols approved by the Rockefeller University and National Institutes of Health (NIH) Institutional Animal Care and Use Committee.

Joining and Resection Analysis

The assay was performed as previously described (Bothmer et al., 2010). For details, see the Supplemental Experimental Procedures.

B Cell Cultures and Retroviral Infection

Resting B lymphocytes were isolated and stimulated for CSR as previously described (Robbiani et al., 2008). For analysis of radial structures, the PARP inhibitor KU58948 (1 μM) was added 16 hr before, and Colcemid (100 ng/ml, Roche) 1 hr before preparation of metaphase spreads (Bunting et al., 2010). For infection experiments, retroviral supernatants were prepared and administered as previously described (Robbiani et al., 2008). B cells were analyzed at 96 hr from the beginning of their culture.

Retroviruses

pMX-IRES-GFP based retroviruses encoding for I-SceI and catalytic mutant I-SceI* were previously described (Robbiani et al., 2008). Coding sequences of the human 53BP1 mutants were cloned into a modified pMX plasmid with deleted IRES-GFP (courtesy of Silvia Boscardin) to allow for proper packaging of this large protein. Therefore, in each experiment infection efficiency was monitored by western blot (see Figures S4–S6). 53BP1^{8A} encoded for the following alanine substitutions: S6A, S13A, S25A, S29A, S105A, S166A, S176A, and S178A. 53BP1^{7A} encoded for T302A, S452A, S523A, S543A, S625A, S784A, and S892A. 53BP1^{15A} encoded for the same alanine substitutions as in both 53BP1^{8A} and 53BP1^{7A}. In addition to these, 53BP1^{28A} also had S437A, S580A, S674A, T696A, S698A, S831A, T855A, S1068A, S1086A, S1104A, S1148A, T1171A, and S1219A. Unless otherwise noted, mutants bore a C-terminal HA-FLAG tag (in orange in Figures 5C and 6A and Figure S6).

A

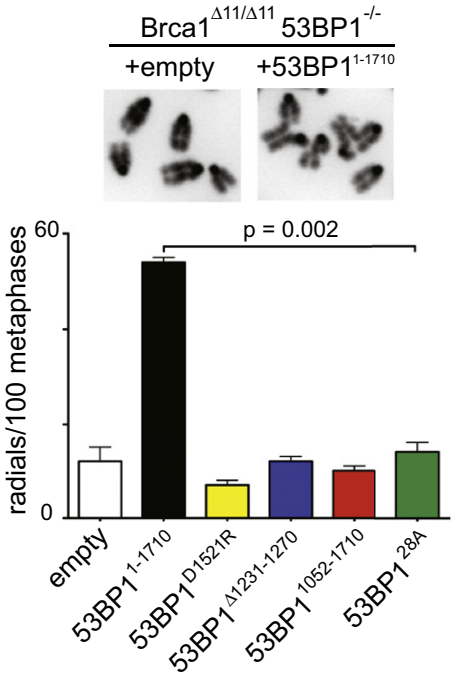

B

Domains of 53BP1	IRIF	Chromatin binding	CSR	Resection
BRCT	D	D	D	D
Tudor (D1518/D1521)	R	R	R	R
Oligomerization	R	D	R	R
N-terminal Phosphorylations	D	D	R	R

D = dispensable R = required

Figure 7. Domains of 53BP1 Required for Preventing DNA End Resection

(A) Brca1$^{\Delta11/\Delta11}$53BP1$^{-/-}$ B cells reconstituted with 53BP1 mutant retroviruses. Top: Examples of normal metaphases (+empty) or metaphases containing radial chromosome structures (+53BP1$^{1-1710}$). Bottom: Histogram quantitating the number of radial structures upon infection with the indicated retroviruses. Error bars indicate standard error of the mean. Two independent experiments.

(B) Table summarizing which functional domains of 53BP1 are required (R) or dispensable (D) for IRIF, chromatin binding, CSR, and protection of DNA ends from resection.

See also Figure S6.

Cell Fractionation and Western Blot

The cytoplasmic fraction from 5 Mio purified mutant splenic B cells (treated or not with 10 Gy IR and allowed 90 min recovery) was separated from the nuclei with the ProteoJET Cytoplasmic and Nuclear Protein Extraction Kit (Fermentas) according to the manufacturer's instructions. To separate nuclear-soluble and chromatin fractions, the manufacturer's nuclei lysis buffer was supplemented with the provided Nuclei Lysis reagent and with 30 mM EDTA, 2 mM EGTA, and 10 mM dithiothreitol. The nuclear extract was centrifuged at 1700 g for 20 min at 4°C; the supernatant was saved at −80°C as the "nuclear-soluble fraction," and the chromatin pellet was washed twice in 250 μl of 3 mM EDTA, 0.2 mM EGTA, 1 mM dithiothreitol, and protease inhibitors (Roche). Chromatin was resuspended in 30 μl of 10 mM HEPES, 10 mM KCl, 1 mM $MgCl_2$, 10% glycerol, 1 mM $CaCl_2$, 1 mM EDTA, 1× protease inhibitors (Roche), and 5 U micrococcal nuclease (New England Biolabs) and then incubated for 45 min at 37°C. The reaction was stopped by the addition of EGTA to 1 mM, and the digested pellet was stored at −80°C as the "chromatin-bound fraction." For retroviral reconstitution experiments, splenocytes were stimulated and fractionated on day 4. Expression of wild-type and mutant 53BP1 proteins was detected with antisera to 53BP1 (Bethyl), 53BP1 phosphorylated on Serine 25 (Bethyl), FLAG (SIGMA), or HA (Abcam) as indicated. Controls for DNA damage, cell fractionation, and loading were with antibodies to γ-H2AX (Millipore), H2AX (Bethyl), H4K20^{me1} (Abcam), IgG LC (Jackson Immunoresearch Laboratories), tubulin (Abcam), or actin (SIGMA).

Flow Cytometry

For fluorescence-activated cell sorting (FACS) analysis, spleen cell suspensions or cultures were stained with fluorochrome-conjugated anti-CD19, anti-CD3, anti-IgM, anti-IgD, and anti-IgG1 antibodies (PharMingen). Labeling for cell division was at 37°C for 10 min in 5 μM carboxyfluorescein succinimidyl esther (CFSE). Samples were acquired on a FACSCalibur instrument (Becton Dickinson) and analyzed with FlowJo software (Tree Star).

Ionizing Radiation Induced Foci and Laser Microirradiation

For IRIF, MEFs were grown overnight on glass coverslips in 30 mm culture dishes, then exposed to 5 Gy (53BP1 mutant MEFs) or 10 Gy (53BP1$^{-/-}$ MEFs reconstituted with mutant retroviruses) ionizing radiation and allowed to recover for 90 min. Cells were then fixed with 4% paraformaldehyde, followed by 0.5% Triton X-100 permeabilzation and processed for immunofluorescent staining at the indicated times after exposure. Images were acquired with an LSM 510 META microscope (Zeiss) or with DeltaVision (Applied Precision). For laser microirradiation, MEFs were grown in dye-free media. The DNA binding dye Hoechst 33258 was added at 10 mg/ml and incubated for 30 min at 37°C. After laser treatment, cells were allowed to recover for 30 min or 4 hr at 37°C and were subsequently fixed and processed for immunofluorescent staining as above. Primary antibodies used for immunofluorescence were rabbit anti-53BP1 (Novus Biologicals), mouse anti-γ-H2AX (Upstate Biotechnology), and mouse anti-FLAG-M2 (SIGMA). Secondary antibodies were Alexa568- and Alexa488-conjugated (Molecular Probes). DNA was counterstained with 4',6-diamidino-2-phenylindole (DAPI).

SUPPLEMENTAL INFORMATION

Supplemental Information includes Supplemental Experimental Procedures and six figures and can be found with this article online at doi:10.1016/j.molcel.2011.03.019.

ACKNOWLEDGMENTS

All members of the Nussenzweig labs for discussions. Thanos Halazonetis for wild type human 53BP1 plasmid and Philip Carpenter for plasmid with 53BP1 alanine substitutions. The Rockefeller University Gene Targeting Facility for the generation of mutant mice. The work was supported in part by a Fondazione Ettore e Valeria Rossi grant to D.F.R., by a NIH grant to M.C.N (AI037526), and a Department of Defense grant to A.N. (BC102335). A.N. and S.B. were supported by the Intramural Research Program of the NIH, the National Cancer Institute, and the Center for Cancer Research and I.A.K by NIH Medical Scientist Training Program grant GM07739. A.B. is a Predoctoral Fellow of the Cancer Research Institute, N.F. is and D.F.R. was a Fellow of the Leukemia and Lymphoma Society, M.D.V. is a Fellow of the American-Italian Cancer Foundation, and M.C.N. is a Howard Hughes Medical Institute Investigator.

Received: November 24, 2010
Revised: February 8, 2011
Accepted: March 28, 2011
Published: May 5, 2011

REFERENCES

Adams, M.M., and Carpenter, P.B. (2006). Tying the loose ends together in DNA double strand break repair with 53BP1. Cell Div. *1*, 19.

Anderson, L., Henderson, C., and Adachi, Y. (2001). Phosphorylation and rapid relocalization of 53BP1 to nuclear foci upon DNA damage. Mol. Cell. Biol. *21*, 1719–1729.

Bekker-Jensen, S., Lukas, C., Kitagawa, R., Melander, F., Kastan, M.B., Bartek, J., and Lukas, J. (2006). Spatial organization of the mammalian genome surveillance machinery in response to DNA strand breaks. J. Cell Biol. *173*, 195–206.

Boboila, C., Jankovic, M., Yan, C.T., Wang, J.H., Wesemann, D.R., Zhang, T., Fazeli, A., Feldman, L., Nussenzweig, A., Nussenzweig, M., and Alt, F.W. (2010a). Alternative end-joining catalyzes robust IgH locus deletions and translocations in the combined absence of ligase 4 and Ku70. Proc. Natl. Acad. Sci. USA *107*, 3034–3039.

Boboila, C., Yan, C., Wesemann, D.R., Jankovic, M., Wang, J.H., Manis, J., Nussenzweig, A., Nussenzweig, M., and Alt, F.W. (2010b). Alternative end-joining catalyzes class switch recombination in the absence of both Ku70 and DNA ligase 4. J. Exp. Med. *207*, 417–427.

Boisvert, F.M., Rhie, A., Richard, S., and Doherty, A.J. (2005). The GAR motif of 53BP1 is arginine methylated by PRMT1 and is necessary for 53BP1 DNA binding activity. Cell Cycle *4*, 1834–1841.

Bothmer, A., Robbiani, D.F., Feldhahn, N., Gazumyan, A., Nussenzweig, A., and Nussenzweig, M.C. (2010). 53BP1 regulates DNA resection and the choice between classical and alternative end joining during class switch recombination. J. Exp. Med. *207*, 855–865.

Botuyan, M.V., Lee, J., Ward, I.M., Kim, J.E., Thompson, J.R., Chen, J., and Mer, G. (2006). Structural basis for the methylation state-specific recognition of histone H4-K20 by 53BP1 and Crb2 in DNA repair. Cell *127*, 1361–1373.

Bunting, S.F., Callén, E., Wong, N., Chen, H.T., Polato, F., Gunn, A., Bothmer, A., Feldhahn, N., Fernandez-Capetillo, O., Cao, L., et al. (2010). 53BP1 inhibits homologous recombination in Brca1-deficient cells by blocking resection of DNA breaks. Cell *141*, 243–254.

Celeste, A., Petersen, S., Romanienko, P.J., Fernandez-Capetillo, O., Chen, H.T., Sedelnikova, O.A., Reina-San-Martin, B., Coppola, V., Meffre, E., Difilippantonio, M.J., et al. (2002). Genomic instability in mice lacking histone H2AX. Science *296*, 922–927.

Celeste, A., Fernandez-Capetillo, O., Kruhlak, M.J., Pilch, D.R., Staudt, D.W., Lee, A., Bonner, R.F., Bonner, W.M., and Nussenzweig, A. (2003). Histone H2AX phosphorylation is dispensable for the initial recognition of DNA breaks. Nat. Cell Biol. *5*, 675–679.

Difilippantonio, S., Gapud, E., Wong, N., Huang, C.Y., Mahowald, G., Chen, H.T., Kruhlak, M.J., Callen, E., Livak, F., Nussenzweig, M.C., et al. (2008). 53BP1 facilitates long-range DNA end-joining during V(D)J recombination. Nature *456*, 529–533.

Dimitrova, N., Chen, Y.C., Spector, D.L., and de Lange, T. (2008). 53BP1 promotes non-homologous end joining of telomeres by increasing chromatin mobility. Nature *456*, 524–528.

DiTullio, R.A., Jr., Mochan, T.A., Venere, M., Bartkova, J., Sehested, M., Bartek, J., and Halazonetis, T.D. (2002). 53BP1 functions in an ATM-dependent checkpoint pathway that is constitutively activated in human cancer. Nat. Cell Biol. *4*, 998–1002.

Doil, C., Mailand, N., Bekker-Jensen, S., Menard, P., Larsen, D.H., Pepperkok, R., Ellenberg, J., Panier, S., Durocher, D., Bartek, J., et al. (2009). RNF168 binds and amplifies ubiquitin conjugates on damaged chromosomes to allow accumulation of repair proteins. Cell *136*, 435–446.

Fernandez-Capetillo, O., Chen, H.T., Celeste, A., Ward, I., Romanienko, P.J., Morales, J.C., Naka, K., Xia, Z., Camerini-Otero, R.D., Motoyama, N., et al. (2002). DNA damage-induced G2-M checkpoint activation by histone H2AX and 53BP1. Nat. Cell Biol. *4*, 993–997.

Futreal, P.A., Coin, L., Marshall, M., Down, T., Hubbard, T., Wooster, R., Rahman, N., and Stratton, M.R. (2004). A census of human cancer genes. Nat. Rev. Cancer *4*, 177–183.

Guo, F., Gopaul, D.N., and van Duyne, G.D. (1997). Structure of Cre recombinase complexed with DNA in a site-specific recombination synapse. Nature *389*, 40–46.

Helmink, B.A., Tubbs, A.T., Dorsett, Y., Bednarski, J.J., Walker, L.M., Feng, Z., Sharma, G.G., McKinnon, P.J., Zhang, J., Bassing, C.H., and Sleckman, B.P. (2011). H2AX prevents CtIP-mediated DNA end resection and aberrant repair in G1-phase lymphocytes. Nature *469*, 245–249.

Hoeijmakers, J.H. (2009). DNA damage, aging, and cancer. N. Engl. J. Med. *361*, 1475–1485.

Huen, M.S., Grant, R., Manke, I., Minn, K., Yu, X., Yaffe, M.B., and Chen, J. (2007). RNF8 transduces the DNA-damage signal via histone ubiquitylation and checkpoint protein assembly. Cell *131*, 901–914.

Huen, M.S., Huang, J., Leung, J.W., Sy, S.M., Leung, K.M., Ching, Y.P., Tsao, S.W., and Chen, J. (2010). Regulation of chromatin architecture by the PWWP domain-containing DNA damage-responsive factor EXPAND1/MUM1. Mol. Cell *37*, 854–864.

Huyen, Y., Zgheib, O., Ditullio, R.A., Jr., Gorgoulis, V.G., Zacharatos, P., Petty, T.J., Sheston, E.A., Mellert, H.S., Stavridi, E.S., and Halazonetis, T.D. (2004). Methylated lysine 79 of histone H3 targets 53BP1 to DNA double-strand breaks. Nature *432*, 406–411.

Iwabuchi, K., Basu, B.P., Kysela, B., Kurihara, T., Shibata, M., Guan, D., Cao, Y., Hamada, T., Imamura, K., Jeggo, P.A., et al. (2003). Potential role for 53BP1 in DNA end-joining repair through direct interaction with DNA. J. Biol. Chem. *278*, 36487–36495.

Kass, E.M., and Jasin, M. (2010). Collaboration and competition between DNA double-strand break repair pathways. FEBS Lett. *584*, 3703–3708.

Kolas, N.K., Chapman, J.R., Nakada, S., Ylanko, J., Chahwan, R., Sweeney, F.D., Panier, S., Mendez, M., Wildenhain, J., Thomson, T.M., et al. (2007). Orchestration of the DNA-damage response by the RNF8 ubiquitin ligase. Science *318*, 1637–1640.

Lee, H., Kwak, H.J., Cho, I.T., Park, S.H., and Lee, C.H. (2009). S1219 residue of 53BP1 is phosphorylated by ATM kinase upon DNA damage and required for proper execution of DNA damage response. Biochem. Biophys. Res. Commun. *378*, 32–36.

Lieber, M.R. (2010). The mechanism of double-strand DNA break repair by the nonhomologous DNA end-joining pathway. Annu. Rev. Biochem. *79*, 181–211.

Mailand, N., Bekker-Jensen, S., Faustrup, H., Melander, F., Bartek, J., Lukas, C., and Lukas, J. (2007). RNF8 ubiquitylates histones at DNA double-strand breaks and promotes assembly of repair proteins. Cell *131*, 887–900.

Manis, J.P., Morales, J.C., Xia, Z., Kutok, J.L., Alt, F.W., and Carpenter, P.B. (2004). 53BP1 links DNA damage-response pathways to immunoglobulin heavy chain class-switch recombination. Nat. Immunol. *5*, 481–487.

Morales, J.C., Xia, Z., Lu, T., Aldrich, M.B., Wang, B., Rosales, C., Kellems, R.E., Hittelman, W.N., Elledge, S.J., and Carpenter, P.B. (2003). Role for the BRCA1 C-terminal repeats (BRCT) protein 53BP1 in maintaining genomic stability. J. Biol. Chem. *278*, 14971–14977.

Muramatsu, M., Kinoshita, K., Fagarasan, S., Yamada, S., Shinkai, Y., and Honjo, T. (2000). Class switch recombination and hypermutation require activation-induced cytidine deaminase (AID), a potential RNA editing enzyme. Cell *102*, 553–563.

Nussenzweig, A., and Nussenzweig, M.C. (2010). Origin of chromosomal translocations in lymphoid cancer. Cell *141*, 27–38.

Ramiro, A.R., Jankovic, M., Callen, E., Difilippantonio, S., Chen, H.T., McBride, K.M., Eisenreich, T.R., Chen, J., Dickins, R.A., Lowe, S.W., et al. (2006). Role of genomic instability and p53 in AID-induced c-myc-Igh translocations. Nature *440*, 105–109.

Rappold, I., Iwabuchi, K., Date, T., and Chen, J. (2001). Tumor suppressor p53 binding protein 1 (53BP1) is involved in DNA damage-signaling pathways. J. Cell Biol. *153*, 613–620.

Reina-San-Martin, B., Difilippantonio, S., Hanitsch, L., Masilamani, R.F., Nussenzweig, A., and Nussenzweig, M.C. (2003). H2AX is required for recombination between immunoglobulin switch regions but not for intra-switch region recombination or somatic hypermutation. J. Exp. Med. *197*, 1767–1778.

Reina-San-Martin, B., Chen, J., Nussenzweig, A., and Nussenzweig, M.C. (2007). Enhanced intra-switch region recombination during immunoglobulin class switch recombination in 53BP1-/- B cells. Eur. J. Immunol. *37*, 235–239.

Rickert, R.C., Roes, J., and Rajewsky, K. (1997). B lymphocyte-specific, Cre-mediated mutagenesis in mice. Nucleic Acids Res. *25*, 1317–1318.

Robbiani, D.F., Bothmer, A., Callen, E., Reina-San-Martin, B., Dorsett, Y., Difilippantonio, S., Bolland, D.J., Chen, H.T., Corcoran, A.E., Nussenzweig, A., and Nussenzweig, M.C. (2008). AID is required for the chromosomal breaks in c-myc that lead to c-myc/IgH translocations. Cell *135*, 1028–1038.

Sanders, S.L., Portoso, M., Mata, J., Bähler, J., Allshire, R.C., and Kouzarides, T. (2004). Methylation of histone H4 lysine 20 controls recruitment of Crb2 to sites of DNA damage. Cell *119*, 603–614.

Santos, M.A., Huen, M.S., Jankovic, M., Chen, H.T., López-Contreras, A.J., Klein, I.A., Wong, N., Barbancho, J.L., Fernandez-Capetillo, O., Nussenzweig, M.C., et al. (2010). Class switching and meiotic defects in mice lacking the E3 ubiquitin ligase RNF8. J. Exp. Med. *207*, 973–981.

Savic, V., Yin, B., Maas, N.L., Bredemeyer, A.L., Carpenter, A.C., Helmink, B.A., Yang-Iott, K.S., Sleckman, B.P., and Bassing, C.H. (2009). Formation of dynamic gamma-H2AX domains along broken DNA strands is distinctly regulated by ATM and MDC1 and dependent upon H2AX densities in chromatin. Mol. Cell *34*, 298–310.

Schultz, L.B., Chehab, N.H., Malikzay, A., and Halazonetis, T.D. (2000). p53 binding protein 1 (53BP1) is an early participant in the cellular response to DNA double-strand breaks. J. Cell Biol. *151*, 1381–1390.

Stavnezer, J., Guikema, J.E., and Schrader, C.E. (2008). Mechanism and regulation of class switch recombination. Annu. Rev. Immunol. *26*, 261–292.

Stewart, G.S., Panier, S., Townsend, K., Al-Hakim, A.K., Kolas, N.K., Miller, E.S., Nakada, S., Ylanko, J., Olivarius, S., Mendez, M., et al. (2009). The RIDDLE syndrome protein mediates a ubiquitin-dependent signaling cascade at sites of DNA damage. Cell *136*, 420–434.

Ward, I.M., Minn, K., Jorda, K.G., and Chen, J. (2003). Accumulation of checkpoint protein 53BP1 at DNA breaks involves its binding to phosphorylated histone H2AX. J. Biol. Chem. *278*, 19579–19582.

Ward, I.M., Reina-San-Martin, B., Olaru, A., Minn, K., Tamada, K., Lau, J.S., Cascalho, M., Chen, L., Nussenzweig, A., Livak, F., et al. (2004). 53BP1 is required for class switch recombination. J. Cell Biol. *165*, 459–464.

Ward, I., Kim, J.E., Minn, K., Chini, C.C., Mer, G., and Chen, J. (2006). The tandem BRCT domain of 53BP1 is not required for its repair function. J. Biol. Chem. *281*, 38472–38477.

Watanabe, K., Iwabuchi, K., Sun, J., Tsuji, Y., Tani, T., Tokunaga, K., Date, T., Hashimoto, M., Yamaizumi, M., and Tateishi, S. (2009). RAD18 promotes DNA double-strand break repair during G1 phase through chromatin retention of 53BP1. Nucleic Acids Res. *37*, 2176–2193.

Xu, X., Wagner, K.U., Larson, D., Weaver, Z., Li, C., Ried, T., Hennighausen, L., Wynshaw-Boris, A., and Deng, C.X. (1999). Conditional mutation of Brca1 in mammary epithelial cells results in blunted ductal morphogenesis and tumour formation. Nat. Genet. *22*, 37–43.

Xu, X., Qiao, W., Linke, S.P., Cao, L., Li, W.M., Furth, P.A., Harris, C.C., and Deng, C.X. (2001). Genetic interactions between tumor suppressors Brca1 and p53 in apoptosis, cell cycle and tumorigenesis. Nat. Genet. *28*, 266–271.

Yuan, J., and Chen, J. (2010). MRE11-RAD50-NBS1 complex dictates DNA repair independent of H2AX. J. Biol. Chem. *285*, 1097–1104.

Zgheib, O., Pataky, K., Brugger, J., and Halazonetis, T.D. (2009). An oligomerized 53BP1 tudor domain suffices for recognition of DNA double-strand breaks. Mol. Cell. Biol. *29*, 1050–1058.

Zha, S., Guo, C., Boboila, C., Oksenych, V., Cheng, H.L., Zhang, Y., Wesemann, D.R., Yuen, G., Patel, H., Goff, P.H., et al. (2011). ATM damage response and XLF repair factor are functionally redundant in joining DNA breaks. Nature *469*, 250–254.

Zhang, Y., Gostissa, M., Hildebrand, D.G., Becker, M.S., Boboila, C., Chiarle, R., Lewis, S., and Alt, F.W. (2010). The role of mechanistic factors in promoting chromosomal translocations found in lymphoid and other cancers. Adv. Immunol. *106*, 93–133.